NASA-TM-86371 19850021614

NASA Technical Memorandum 86371

High Reynolds Number Tests of a NASA SC(3)-0712(B) Airfoil in the Langley 0.3-Meter Transonic Cryogenic Tunnel

William G. Johnson, Jr., Acquilla S. Hill,
and Otto Eichmann

JUNE 1985

NASA

NASA Technical Memorandum 86371

High Reynolds Number Tests of a NASA SC(3)-0712(B) Airfoil in the Langley 0.3-Meter Transonic Cryogenic Tunnel

William G. Johnson, Jr., Acquilla S. Hill,
and Otto Eichmann
Langley Research Center
Hampton, Virginia

National Aeronautics
and Space Administration
**Scientific and Technical
Information Branch**
1985

Contents

Summary 1
Introduction 1
Symbols 1
Wind Tunnel and Model 2
Test Apparatus and Procedures 3
Data Reduction and Quality 5
Presentation of Results 6
Discussion 7
Concluding Remarks 8
Appendixes 10
References 96
Tables 97
Figures 99

Summary

In a cooperative effort with U.S. manufacturers of large transport aircraft, NASA is conducting a systematic study of well-known conventional and advanced-technology airfoil concepts over a wide range of Reynolds number. This study, referred to as the Advanced Technology Airfoil Tests (ATAT) program, is being conducted in the two-dimensional test section of the Langley 0.3-Meter Transonic Cryogenic Tunnel (0.3-m TCT).

The results presented in this report are from the test of a NASA 12-percent-thick supercritical advanced-technology airfoil. This test was conducted as part of the ATAT program. Test temperature was varied from 220 K to 96 K at pressures ranging from about 122 kPa (1.2 atm) to 436 kPa (4.3 atm). Mach number was varied from 0.50 to 0.80. These variables provided a Reynolds number range (based on airfoil model chord) from 4.4×10^6 to 40.0×10^6.

The aerodynamic results are presented as integrated force and moment coefficients and pressure distributions. (The same pressure data are also published in plotted and tabulated formats in a separate companion report, NASA TM-86370.) The data show changes in the airfoil characteristics with increasing Mach number, such as increased normal-force slope, increased drag force, and increased nose-down pitching moment. These data also show that increasing the Reynolds number results in increased normal force, increased nose-down pitching moment, and generally decreased drag force. Additional data are included which show the effects of fixed transition. Model design, model structural integrity, and overall test experience are discussed.

Introduction

The National Aeronautics and Space Administration (NASA) is conducting a systematic study of well-known conventional and advanced-technology airfoil concepts over a wide range of Reynolds number. This study, described in detail in reference 1, is referred to as the Advanced Technology Airfoil Tests (ATAT) program and is being conducted in the Langley 0.3-Meter Transonic Cryogenic Tunnel (0.3-m TCT). A significant portion of the advanced-technology airfoil phase of the ATAT program is being carried out in cooperation with U.S. industry. Three U.S. manufacturers of large commercial transport aircraft (Boeing, Douglas, and Lockheed) are participating individually in this phase of the program by providing technical personnel, airfoil design concepts, and airfoil models. The overall objectives of the ATAT program are (1) to provide the industry participants with the opportunity to test and compare their advanced airfoils with the latest NASA airfoils at flight design Reynolds numbers in the same facility, (2) to provide industry with experience in cryogenic wind tunnel model design, construction, and testing techniques, (3) to expand the high Reynolds number airfoil data base, and (4) to provide each participant with the opportunity to evaluate their current level of airfoil technology. As part of the first objective, it is necessary to test some of the latest NASA designs in the same facility used by the industry participants.

The results presented in this report are from tests of a second model of the NASA SC(3)-0712 airfoil. The first model, designated NASA SC(3)-0712(A), distorted enough during its test to raise questions about the validity of the data. A second model, designated SC(3)-0712(B), was constructed with different material and fabrication procedures and is the subject model of this report. The tests were conducted in the Langley 0.3-m TCT with a two-dimensional, 20- by 60-cm (8- by 24-in.) test section installed. Reference 2 describes the operating envelope of this transonic cryogenic pressure tunnel. Test temperature was varied from 220 K to cryogenic temperatures (about 96 K) at pressures ranging from about 1.2 to 4.3 atm (1 atm = 101.3 kPa). Mach number was varied from 0.50 to 0.80. These variables provided a Reynolds number range (based on airfoil model chord) from 4.4×10^6 to 40.0×10^6. The aerodynamic results are presented herein as integrated force and moment coefficients and pressure distributions. (The same pressure data are also published in plotted and tabulated formats in ref. 3.) Included in this report are details of the model design and airfoil coordinates, details of the model fabrication techniques, and a discussion of the operational experience with the model.

Symbols

The measurements and calculations were made in U.S. Customary Units; however, the measurements are presented in the International System of Units (SI) with the U.S. Customary Units in parentheses. Factors relating these two systems of units can be found in reference 4.

AOA	angle of attack
b	airfoil model span, cm (in.)
c	airfoil model chord, cm (in.)
c_d	section drag force coefficient from wake measurements
c_m	section pitching-moment coefficient about model quarter-chord point

c_n	section normal-force coefficient from model pressures
C_p	pressure coefficient
M	free-stream Mach number
R	free-stream Reynolds number based on model chord
x	chordwise distance from leading edge of model (positive measured aft), cm (in.)
y	spanwise distance along model from centerline of tunnel and model (positive measured toward right-hand side), cm (in.)
z	vertical distance from model reference plane (positive measured up), cm (in.)
z_{design}	airfoil ordinate as designed, cm (in.)
z_{meas}	airfoil ordinate as measured, cm (in.)
α	uncorrected angle of attack (positive measured from tunnel centerline up to airfoil reference line), deg

Airfoil designation:

NASA SC(3)-0712(B)	supercritical (phase 3), 0.7 design lift coefficient, 12 percent thick, model construction technique B

Wind Tunnel and Model

Wind Tunnel

The tests were made in the 20- by 60-cm (8- by 24-in.) two-dimensional test section of the 0.3-m TCT. A photograph of the tunnel is shown in figure 1(a). A schematic drawing showing some physical characteristics of the tunnel is shown in figure 1(b). A photograph and sketch of the two-dimensional test section are shown in figure 2. In the photograph, figure 2(a), the plenum lid and test section ceiling have been removed to show model installation. The 0.3-m TCT is a continuous-flow, single-return, fan-driven transonic tunnel which uses nitrogen gas as the test medium. It is capable of operating at stagnation temperatures from about 80 K to about 327 K and stagnation pressures from slightly greater than 1 atm to 6 atm. Test section Mach number can be varied from near zero to 0.9. The ability to operate at cryogenic temperatures and 6 atm pressure provides an extremely high Reynolds number capability at relatively low model loadings.

The two-dimensional test section, which features a slotted floor and ceiling, contains computer-driven angle-of-attack and wake survey rake systems. The angle-of-attack system is capable of varying the angle of attack over a range of about 40°. The wake survey rake, located just downstream of the model (see fig. 2(a)), provides up to nine total-pressure measurements across half the width of the tunnel. These pressures are converted to drag levels and provide a convenient mechanism for determining the extent of two-dimensionality of the flow over the model. Additional design features and characteristics regarding the cryogenic concept in general and the 0.3-m TCT in particular are presented in references 5 and 6.

Model

The airfoil model used in this test is a 12-percent thick, advanced-technology supercritical airfoil designed by NASA for a Reynolds number of 30×10^6 and is designated the NASA SC(3)-0712(B). The model has a chord of 15.24 cm (6.0 in.) and was fabricated in accordance with NASA aerodynamic and structural requirements for the ATAT program models. The aerodynamic specifications require airfoil contour accuracies of ±0.0025 cm (±0.001 in.), surface finishes of 0.254 μm (0.00001 in.) or better, and a sufficient coverage of pressure orifices with diameters of about 0.025 cm (0.010 in.). The structural specifications included tolerance requirements for the model chord and span dimensions, a selection of material suitable for use at cryogenic temperatures, a safety factor of at least 3 at all operating conditions, Charpy impact strengths of at least 20.34 J (15.0 ft-lb) at 77 K, and compatibility with existing 0.3-m TCT sidewall turntables. A photograph of the model installed in the 0.3-m TCT test section is shown in figure 3. The model was equipped with 64 static pressure orifices, each having a diameter of 0.025 cm (0.010 in.). Figure 4 is a schematic drawing which indicates the general locations of the orifices and the general shape of the airfoil section. Table I lists the x/c and $y/(b/2)$ locations for each orifice.

Model stress analysis. The stress analysis used a design load of 6.4 kN (1440 lb) normal force. The analysis indicated a maximum bending stress level of 82 740 kN/m^2 (12 000 psi) along the row of orifices. Along the bond surface the maximum shear stress was found to be 2069 kN/m^2 (300 psi). These stress levels resulted in safety factors of 10 or better. Deflections along the model centerline and the decambering effect of the trailing edge under load were scaled-up calculations from a previously designed 6-percent supercritical airfoil model

subjected to the same design loads. The scaled centerline deflection for the model as a simply supported beam under uniform loading was 0.010 cm (0.004 in.). The scaled trailing-edge deflection was 0.0003 to 0.0005 cm (0.0001 to 0.0002 in.).

Model fabrication. The model was fabricated from 18-percent Ni alloy, maraging, grade 200 steel (VascoMax C-200, manufactured by Teledyne Vasco). The contouring was done in stages and the model was cryocycled (i.e., cooled to liquid-nitrogen temperature and warmed to ambient temperature) during the contouring phase to allow for material stabilization and reduce the possibility of model distortion during cryogenic testing. A "cover plate" type of construction was used. For this model, the cover plate was basically the bottom half of the model block from about 3.2 percent chord to 90.7 percent chord. Trenches were cut from the parting line into both halves of the model block, which had been machined to a slightly oversize contour for the aerodynamic surface. Holes were then drilled in the bottom of these trenches to within approximately 0.075 cm (0.030 in.) of the outside surface. Stainless steel tubing with a 0.152-cm (0.060-in.) outside diameter (o.d.) and a 0.102-cm (0.040-in.) inside diameter (i.d.) was then soldered into all holes except for the orifices, noted in table I, which had smaller diameter tubing in order to remain within the cambered contour at the model trailing edge. All undersized tubes were jumped to the largest size tube as soon as possible within the model. This procedure has been shown to improve the response time in measuring the model pressures. The pressure tubes were then routed along the trench and out a slot to the side of the model. The two halves of the model block were bonded together with a structural adhesive film and the outside model surfaces were machined to the final contour. The static-pressure orifices, 0.025 cm (0.010 in.) in diameter, were then drilled into the model surface to meet the soldered tubes.

Pretest checks of the pressure tubes indicated that orifices 4, 21, 24, 40, 63, and 64 were completely lost due to blockage or severe leakage. Four of the six lost orifices were plumbed in such a way as to require joints in the tubing inside the model, and these joints were very likely the source of the problems. This experience highlights the fact that extreme care should be used to insure the integrity of the pressure-measuring tubes located within the model since the area is no longer accessible once bonding is completed.

Model accuracy. Past experience has shown that many metals undergo drastic and irreversible changes in shape when exposed to a cryogenic environment. This has been very apparent in the current airfoil program. For example, the first version of this model, designated SC(3)-0712(A), was machined from Armco 15-5 PH stainless steel, and its posttest validation indicated about a 0.019-cm (0.008-in.) bow in the spanwise direction. Model construction procedures have since been established to alleviate this problem. It is now standard practice that all airfoil models intended for testing in the 0.3-m TCT be thermally cycled to cryogenic temperatures during the fabrication process so they can stabilize before the final model contour validation and testing. Final contour and pressure orifice locations on the model were checked with a Brown and Sharpe Validator 50 probe, which under ideal conditions has an accuracy of ± 0.0013 cm (± 0.0005 in.). The contour of the airfoil was checked at 50 chordwise stations at the centerline and at the ± 5.08-cm (± 2.0-in.) spanwise stations on both the upper and lower surfaces. Table II presents the design coordinates and the pretest measured coordinates for the centerline ($y = 0$) station. The differences between the design coordinates and measured coordinates are shown in figure 5 as a function of chordwise location. In general, the specified fabrication tolerance was maintained except on the high-curvature regions of the leading and trailing edges, which are recognized as the most difficult to manufacturer as well as to measure.

Test Apparatus and Procedures

Test Instrumentation and Apparatus

A detailed discussion of the instrumentation and procedures selected for the calibration and control of the 0.3-m TCT can be found in reference 7. For two-dimensional airfoil tests, the 0.3-m TCT is equipped to obtain static-pressure measurements on the airfoil model surface, total-pressure measurements in the model wake, and static-pressure measurements on the test section sidewalls, floor, and ceiling. The pressures are measured with individual transducers, except for the tunnel floor and ceiling pressures, which are measured with a scanning valve system capable of operating ten 48-port scanning valves. Because of the large changes in tunnel pressure over its operational range, commercially available, high-precision, variable-capacitance pressure transducers are used instead of conventional strain gauge pressure transducers.

Airfoil model pressures. The pressures on the airfoil model are measured by individual transducers connected by tubing to each orifice on the model. The pressure transducers are located adjacent to the

test section in order to reduce response time. To provide increased accuracy, the transducers are mounted on thermostatically controlled heater bases to maintain a constant temperature and on "shock" mounts to reduce possible vibration effects. The electrical outputs from the transducers are connected to individual signal conditioners located in the tunnel control room. The signal conditioners have autoranging capability and have seven ranges available. As a result of the autoranging capability, the analog electrical output to the data acquisition system is kept at a high level, even though the pressure transducer may be operating at the low end of its range. The maximum range of these differential transducers is about ± 6.8 atm, with an accuracy of ± 0.25 percent of the reading from -25 percent to $+100$ percent of full scale.

Wake pressures. A vertically traversing survey mechanism is located on the left sidewall of the two-dimensional test section downstream of the turntables (fig. 2). The purpose of this mechanism is to move a total-pressure probe rake through the airfoil wake to survey the total pressures within the wake. Details of this survey rake are shown in figure 6. The survey mechanism has a total traversing range of 25.4 cm (10 in.). The rake support can be located with the measurement plane of the rake at either of two tunnel stations, 21.0 cm (8.3 in.) or 26.0 cm (10.2 in.). For this test, the wake survey measurements were made at the 26.0-cm (10.2-in.) station, which placed the measurement plane about 1.2 chord lengths downstream of the airfoil trailing edge. The survey mechanism is driven by an electric stepper motor and is designed to operate at speeds from about 0.25 to about 15 cm/sec (0.1 to 6 in/sec). The stroke (that portion of the total traversing range used in a given survey) and speed of the survey mechanism can be controlled from the operator's panel in the control room to suit the research requirements. The vertical position of the rake is recorded using the output from a digital shaft encoder geared to the survey mechanism. The wake survey mechanism is synchronized with the scanning valves so that the rake is moved to a different vertical location each time the scanning valves are advanced to a new port. This continues until the scanning valves complete their stepping, at which time the rake continues to step at a predetermined rate through the remaining portion of the wake. Nine total-pressure probes are located on the survey rake. However, only five were used in this test because of blockage or leaks in the remaining four tubes. The five were located at the following spanwise locations: $y(b/2) = 0.0$, -0.125, -0.250, -0.375, and -0.500. Nine tunnel sidewall static-pressure taps are also provided in the measurement plane of the rake. Data from these are averaged for use in the determination of the momentum loss and, therefore, airfoil drag coefficient based on the method outlined in reference 8. The more sensitive individual differential pressure transducers, with a maximum range of ± 1.36 atm and of the type described previously, are used on each tube on the survey rake and for each of the sidewall taps.

Angle of attack. The angle-of-attack mechanism has a traversing range of $\pm 20°$, which can be offset from $0°$ in either direction at model installation. The mechanism is driven by an electric stepper motor, which is connected through a yoke to the perimeter of both turntables. This arrangement drives both ends of the model through the angle-of-attack range to eliminate possible model twisting. The angular position of the turntables, and therefore the angle of attack of the model, is recorded using the output from a digital shaft encoder geared to one of the turntables.

Test Program

Figure 7 shows the test program (R versus M) used in this investigation. The selection of test conditions was made in an effort to overlap experimental and theoretical work for some of the airfoils in the ATAT program. The extent of the effort to establish transition effects (fixed and free), Reynolds number effects, and Mach number effects can be seen in this figure.

Test Procedures

Pressure data. For the tests reported herein, 20 samples of the airfoil static pressure data were taken only while the rake was at its first position. Since there were individual transducers for each orifice on the model, each sample consisted of simultaneous static pressure readings from all orifices on the model. Likewise, 20 samples of total-pressure (wake rake) data were taken at the first rake position and then at each succeeding step (vertical position) of the rake. As the rake was stepped to each new position, a 1/2-sec delay was followed by the 1-sec averaging period. For each angle of attack at each combination of test conditions, the rake was stepped in 50 increments through the wake. As a result, only about 75 sec per data point were required to determine the wake defect (drag condition) and airfoil pressures.

Use of wake rake. To provide maximum definition of the model wake, the stroke of the rake (lower to upper limits) and the number of steps within the stroke can be changed for each test condition, such

as angle of attack or Mach number. For this test, the number of steps within the stroke was held constant at 50. However, the stroke was changed as required to scan the entire wake. An example of this stroke variation is shown in figure 8 for $M = 0.76$ and $M = 0.78$.

Transition. Transition strips located on both the upper and lower surfaces were used during a portion of the testing to evaluate their effect on the aerodynamic characteristics of the model. The transition strips were sized for chord Reynolds number of 4×10^6 and were located at the 5-percent chord line. The strips, which were approximately 1.6 mm (0.06 in.) wide, consisted of 0.041-mm (0.0016-in.) diameter glass beads that were applied using a clear acrylic spray. Figure 7 shows the test conditions for fixed transition.

Data Reduction and Quality

0.3-m TCT Data Acquisition System

Data were recorded on magnetic tape with a computer-controlled high-speed digital data acquisition system located in the control room of the 0.3-m TCT. This system has a total of 192 analog channels with five selectable ranges from 8.191 to 131 mV and a resolution of 1 part in 8191. All analog data were filtered with a 10-Hz low-pass filter. An operating and acquisition program is used by the computer to scan the data acquisition hardware and to write the raw data on tape.

Through the use of a separate "real-time" program, visual displays of Mach number, Reynolds number, stagnation pressure, and other flow and tunnel parameters are provided on LED readouts on the tunnel control panel and on a color CRT. This "real-time" program provides many on-line data reduction functions, such as correcting Mach number for real-gas effects and calculating the local pressure ratios and pressure coefficients, which are then integrated around the airfoil to determine values of c_n and c_m. Values of c_d are computed on-line by integrating the total head loss through the model wake. Local pressure coefficients, local pressure ratios, local Mach numbers, total head loss through the model wake, and model aerodynamic coefficients (c_n, c_d, and c_m) can be displayed graphically on an intelligent graphics terminal interfaced with the computer. This information can then be sent to a plotter/printer, which produces hard copies.

Data Reduction

The test Mach number is based on an average of the Mach number distributions measured as a function of Reynolds number at several longitudinal stations during the calibration of the "empty" test section. As mentioned in the previous section, Mach number is corrected for real-gas effects. Real-gas effects are included in the data reduction process through the use of the thermodynamic properties of nitrogen gas calculated from the Beattie-Bridgeman equation of state. This equation of state has been shown in reference 9 to give essentially the same thermodynamic properties and flow calculation results in the temperature-pressure regime of the 0.3-m TCT as are given by the more complicated Jacobsen equation of state. Detailed discussions of real-gas effects when testing in cryogenic nitrogen are contained in references 10 and 11.

Section normal-force and pitching-moment coefficients are calculated from numerical integration (based on the trapezoidal method) of the local surface pressure coefficient measured at each orifice multiplied by an appropriate weighting factor (incremental area). Drag coefficient is obtained from the wake survey pressures by computing an incremental or point drag coefficient by the method of reference 8 for each rake tube pressure at each rake position. These point drag coefficients are then numerically integrated across the model wake according to the trapezoidal method. Specifically, the point drag coefficients are compared one by one to a "threshold" value of drag coefficient, which accounts for a non-zero pressure decrement outside the model wake. This threshold is determined from several wake profiles early in the test as well as from past experience with similar tests. For this test, the threshold value was 0.0002. If, in the integrating process, the individual coefficient is greater than or equal to the threshold, the weighting factor (incremental area) is applied and the incremental drag is included in the running sum of the total drag. If the individual coefficient is less than the threshold, the weighting factor is set equal to zero and the incremental drag is not included in the running sum of the total drag. The results of this integration are total drag coefficients for each of the five rake pitot tubes. The data reduction program then provides a correction which subtracts that summed portion of the individual incremental drag coefficients within the wake which is attributable to the threshold level. These corrected values are the ones used for the discussion of the drag data. All drag data discussions, except for the discussion of the spanwise drag uniformity, use the data from the rake tube at $y/(b/2) = -0.125$. Normally, the tunnel centerline tube is used, but the data from this off-centerline tube were inadvertently plotted for this report. Examination of the data shows little dif-

ference in the comparisons except for the high Mach number, high-normal-force conditions.

Data Quality

Mach number fluctuations. In all wind tunnel testing, and especially in transonic testing, the steadiness of the tunnel flow conditions, such as Mach number, has direct bearing on the quality of the final aerodynamic data. With the use of individual pressure transducers on each of the model pressure orifices, and with all model data recorded at the time of the first rake step, Mach number fluctuations in the model data for any given point were essentially nonexistent. The possibility of Mach number fluctuations during the time required for the rake to complete the survey of the wake was checked for several angles of attack for a single set of tunnel test conditions, $M = 0.76$ and $R = 30.0 \times 10^6$. The mean value of Mach number $\bar{M}$ and the standard deviation σ for the selected angles of attack are as follows:

α, deg	$\bar{M}$	σ
−3	0.7616	0.0019
0	.7600	.0022
+3	.7633	.0025

This statistical sample of 102 values is based on two data points per α (from a hysteresis run) and 51 data frames per data point (50 rake steps plus step zero).

Repeatability of data. Two examples illustrating the degree of repeatability for the normal-force, pitching-moment, and axial-force coefficients at a Reynolds number of 30×10^6 are shown in figures 9 and 10. The repeatability shown in these figures is considered to be generally good.

Evaluation of hysteresis effects. An airfoil may exhibit substantially different aerodynamic characteristics at a given test condition, such as angle of attack, when the test condition is "approached" from different directions. A very brief attempt to develop hysteresis was made during this investigation, and the results obtained are plotted in figures 11 through 14. The hysteresis data points were obtained by increasing the model angle of attack until substantial separation occurred and then decreasing the angle of attack to the desired test condition before taking data. The data indicate an absence of hysteresis at the higher Reynolds number (30×10^6) for free transition and for all Reynolds numbers when transition was fixed. The effect of the transition location on hysteresis manifests itself in the low Reynolds number, free-transition drag data of figure 11 but is absent in the low Reynolds number, fixed-transition drag data of figure 13.

Presentation of Results

Because of the uncertainty in lift-induced interference effects and solid and wake blockage effects (particularly in the presence of local supercritical flow), no corrections for wall effects have been applied to the basic experimental data. Appendixes A through P contain plots of the pressure distributions. These pressure distribution plots and the associated tabulated pressure data are also contained in reference 3. An outline of the plotted aerodynamic coefficient data presented herein is given below, along with the applicable figure reference.

	Figure
Repeatability of data:	
$M \approx 0.76; R \approx 30.0 \times 10^6$; free transition	9
$M \approx 0.76; R \approx 30.0 \times 10^6$; fixed transition	10
Hysteresis of data:	
$M \approx 0.76; R \approx 7.0 \times 10^6$; free transition	11
$M \approx 0.76; R \approx 30.0 \times 10^6$; free transition	12
$M \approx 0.76; R \approx 7.0 \times 10^6$; fixed transition	13
$M \approx 0.76; R \approx 30.0 \times 10^6$; fixed transition	14
Spanwise drag for several Mach numbers:	
$R \approx 30.0 \times 10^6$; free transition	15
Spanwise drag for several Reynolds numbers:	
$M \approx 0.76$; free transition	16
Spanwise drag for free and fixed transition for several Reynolds numbers:	
$M \approx 0.76$	17
Effect of fixing transition on aerodynamic characteristics of airfoil:	
$M \approx 0.50; R \approx 4.4 \times 10^6$	18
$M \approx 0.50; R \approx 7.0 \times 10^6$	19
$M \approx 0.65; R \approx 7.0 \times 10^6$	20
$M \approx 0.65; R \approx 30.0 \times 10^6$	21
$M \approx 0.76; R \approx 4.4 \times 10^6$	22
$M \approx 0.76; R \approx 7.0 \times 10^6$	23
$M \approx 0.76; R \approx 10.0 \times 10^6$	24
$M \approx 0.76; R \approx 15.0 \times 10^6$	25
$M \approx 0.76; R \approx 30.0 \times 10^6$	26
$M \approx 0.76; R \approx 40.0 \times 10^6$	27
$M \approx 0.78; R \approx 4.4 \times 10^6$	28
$M \approx 0.78; R \approx 7.0 \times 10^6$	29
$M \approx 0.78; R \approx 10.0 \times 10^6$	30
$M \approx 0.78; R \approx 15.0 \times 10^6$	31
$M \approx 0.78; R \approx 30.0 \times 10^6$	32

Effect of Mach number on aerodynamic characteristics of airfoil with free transition:
$R \approx 4.4 \times 10^6$ 33
$R \approx 7.0 \times 10^6$ 34
$R \approx 10.0 \times 10^6$ 35
$R \approx 15.0 \times 10^6$ 36
$R \approx 30.0 \times 10^6$ 37
$R \approx 40.0 \times 10^6$ 38

Effect of Mach number on aerodynamic characteristics of airfoil with fixed transition:
$R \approx 4.4 \times 10^6$ 39
$R \approx 7.0 \times 10^6$ 40
$R \approx 10.0 \times 10^6$ 41
$R \approx 15.0 \times 10^6$ 42
$R \approx 30.0 \times 10^6$ 43
$R \approx 40.0 \times 10^6$ 44

Effect of Reynolds number on aerodynamic characteristics of airfoil with free transition:
$M \approx 0.50$ 45
$M \approx 0.60$ 46
$M \approx 0.65$ 47
$M \approx 0.70$ 48
$M \approx 0.72$ 49
$M \approx 0.74$ 50
$M \approx 0.75$ 51
$M \approx 0.76$ 52
$M \approx 0.77$ 53
$M \approx 0.78$ 54
$M \approx 0.79$ 55
$M \approx 0.80$ 56

Effect of Reynolds number on aerodynamic characteristics of airfoil with fixed transition:
$M \approx 0.50$ 57
$M \approx 0.65$ 58
$M \approx 0.76$ 59
$M \approx 0.78$ 60

Effect of Mach number on variation of section drag coefficient with Reynolds number . . . 61

Effect of Reynolds number on variation of section drag coefficient with Mach number 62

Discussion

Assessment of Two-Dimensionality of Flow

The wake survey rake, described in the "Test Apparatus and Procedures" section and shown in figure 6, is equipped with several spanwise total pressure probes which enable an assessment of the airfoil model drag levels across the tunnel and provide an indication of the two-dimensionality of the flow over the model. A sampling of these data is shown in figures 15 through 17. Figure 15 ($R \approx 30.0 \times 10^6$) shows that as long as the airfoil model was not significantly above a Mach number of about 0.76 or positioned at a high enough angle of attack to load the model to a normal-force coefficient greater than about 0.8, the flow had uniform spanwise drag characteristics. Beyond these conditions, separation effects on the tunnel sidewall and/or model began to occur and the uniformity deteriorated. The data shown in figure 16 were taken at $M = 0.76$ and show similar deterioration of the spanwise drag uniformity for conditions above a normal-force coefficient of about 0.8 at all Reynolds numbers. For those Reynolds number conditions less than 10.0×10^6, separation or changes in the chordwise transition location across the span produced a nonuniform distribution for all levels of normal-force coefficient. Figure 17 ($M \approx 0.76$) shows that when transition was fixed for the low Reynolds number conditions, a very uniform spanwise drag distribution then occurred for all Reynolds number conditions and at all c_n levels except those above the 0.8 level, as discussed previously.

Effect of Fixing Transition

The effect of fixing transition was examined over a Mach number range of 0.50 to 0.78 and a Reynolds number range of 4.4×10^6 to 40×10^6. Figures 18 through 32 show the results of these tests. For the $M = 0.50$ data (figs. 18 and 19), there are only slight differences in the free- and fixed-transition normal-force and pitching-moment data. The low Reynolds number free-transition drag data (fig. 18), however, show a characteristic similar to the "laminar bucket" of the NACA 6-series wing sections, on which there were extensive regions of laminar flow that persisted but decayed rapidly. When the Mach number was increased to 0.65 (figs. 20 and 21), the data obtained at a Reynolds number of 7×10^6 showed nearly constant differences in the aerodynamic characteristics between the free and fixed transition, and at $R = 30 \times 10^6$, these differences disappeared. The data for $M = 0.76$ (figs. 22 through 27) and $M = 0.78$ (figs. 28 through 32) exhibit differences between free and fixed transition which are sizable for $R = 4.4 \times 10^6$ and then decrease as Reynolds number increases up to about 15×10^6. Above this Reynolds number, the drag differences remain nearly constant and suggest penetration of the thinner boundary layer (due to the higher Reynolds number) by the transition strips and the resulting artificial transition drag. This is shown in the summary data of figure 61.

Effects of Mach Number and Reynolds Number on the Basic Aerodynamic Characteristics

Figures 33 through 44 show the effects of Mach number (for each test Reynolds number) on the basic aerodynamic characteristics of the model. The trends show higher normal-force slopes and more nose-down pitching moments as the Mach number was increased. The data show substantial increases in drag levels and noticeable changes in nose-down pitching moment slope in the mid-angle-of-attack range as the Mach number for drag divergence was approached. Figures 33 and 34 show sizable variations in the drag data through the low- and mid-angle-of-attack ranges. These variations probably result from changes in the natural transition location and do not improve significantly with increasing Mach number. In figure 33, the lack of agreement between the two sets of $M = 0.76$ drag data is unexplained. Since one run was made at the beginning and one at the end of the test, possible changes in the model surface roughness, as discussed in the next section, may be the cause.

In figures 45 through 60, the basic data presented earlier have been arranged and compared in a different format to show the effects of Reynolds number (at a given Mach number) on the basic aerodynamic characteristics of the model. In general, these results exhibit only slight increases in normal force with increasing Reynolds number, and the nose-down pitching moments typically became more negative as the Reynolds number was increased. The longitudinal stability parameter (dc_m/dc_n) appears to be relatively insensitive to Reynolds number changes. The drag data, with the exception of all free-transition 4.4×10^6 Reynolds number data and some free-transition 7.0×10^6 Reynolds number data, display reductions in drag levels with increasing Reynolds number. These reductions in drag level are summarized in figure 61 for several normal-force coefficients.

Figure 62 presents summary results illustrating the effect of Reynolds number on the variation of drag with Mach number. The increase in the drag coefficient versus Mach number curve which occurs just prior to the drag rise Mach number is frequently referred to as "drag creep." Drag creep is a complicated phenomenon which can occur as a result of several different causes and is highly dependent upon boundary layer conditions and the associated fluid shape of the airfoil. Drag creep is, therefore, a point of interest in high Reynolds number airfoil testing. In general, drag creep seems to exist over a wider range of Mach number as the normal-force coefficients increase. In addition, drag creep is more pronounced at the lower Reynolds numbers and diminishes in severity with increasing Reynolds number.

Model Assessment

Recent experience gained by NASA in airfoil model testing in the 0.3-m TCT has indicated that the dimensional stability of models tested at cryogenic temperature is a function of the material, the configuration design, and the overall processing procedures used during model fabrication. Model accuracies are a major consideration for the high Reynolds number boundary layer conditions provided by cryogenic pressure wind tunnels. Therefore, a thorough assessment of the accuracy of the model contours and a quantitative definition of the model surface finish both before and after the tests are considered to be essential parts of the overall research effort.

The results reported herein were obtained during 72 runs at pressures ranging from about 1.2 to 4.3 atm and temperatures ranging from 220 K to 96 K. In order to determine if the repeated mechanical and thermal cycling of the model had produced any permanent distortion, a posttest validation was conducted. As can be seen in figure 63, the posttest measurements were in reasonable agreement with those obtained in the pretest validation. The similarity in the shapes of the curves suggests that the differences in magnitude are a function of the precision of the measurements and are not due to a change in the airfoil shape during testing. The differences in magnitude illustrate the difficulty in repeat measurements of an airfoil model.

No structural problems were encountered with the load-carrying parts of the model. Posttest examinations of the model did not indicate any obvious distortions or structural failures in the cover plates or associated bond joints. It did appear, however, that some very slight deterioration of the surface finish occurred near the leading edge of the model. The exact cause of the surface finish deterioration is not known.

As discussed in the model fabrication section, pretest checks of the static pressure tubes found six tubes to be unusable. Posttest checks showed the six tubes to be still unusable, but no additional tubes became unusable as a result of the extensive tunnel testing. In general, the design and fabrication techniques used for the airfoil model were found to be suitable for models to be tested in a cryogenic environment.

Concluding Remarks

A wind tunnel investigation of a 12-percent thick, advanced-technology supercritical airfoil, designated

NASA SC(3)-0712(B), was conducted in the Langley 0.3-Meter Transonic Cryogenic Tunnel (TCT). This investigation represents another in the series of NASA/U.S. industry two-dimensional airfoil studies in the Advanced Technology Airfoil Tests program. This investigation was designed to (1) test a NASA advanced-technology airfoil from low to flight-equivalent Reynolds numbers, (2) provide experience in cryogenic wind tunnel model design and testing techniques, and (3) demonstrate the suitability of the 0.3-m TCT as an airfoil test facility.

All the objectives of this investigation were met. Limited analysis of the data indicated the following general conclusions.

1. Increasing Mach number resulted in increased normal-force slope, increased drag force, and increased nose-down pitching moment.
2. Increasing Reynolds number resulted in increased normal force, increased nose-down pitching moment, and generally decreased drag force. Likewise, increasing Reynolds number resulted in a diminished drag creep at a given normal-force coefficient.
3. A limited amount of data indicated that the repeatability of these data is good and the only apparent hysteresis effect was a change in transition location at the lowest Reynolds number.
4. The spanwise measurements of the wake behind the airfoil model appear to be uniform for unseparated flow conditions and indicate minimum tunnel sidewall effects. For high-angle-of-attack postseparation conditions, the flow became less uniform and less two-dimensional.
5. The boundary layer transition strips, which were sized for a chord Reynolds number of 4×10^6, satisfactorily tripped the flow at low Reynolds numbers with only a slight increase in drag at higher Reynolds numbers.
6. The design and fabrication techniques used for this model were found to be suitable for models to be tested in cryogenic wind tunnels. The model was structurally sound, dimensionally proper, and finished to an adequate tolerance.

NASA Langley Research Center
Hampton, VA 23665
February 20, 1985

Appendixes

The pressure data from this investigation are presented as pressure coefficient versus x/c location in these appendixes. Each appendix contains data for a given Mach number through the Reynolds number range. For each combination of Mach number and Reynolds number, the data are plotted for each angle of attack. The pressure data from the upper surface of the airfoil are plotted as open symbols and the lower-surface data are plotted as solid symbols. Since it is the intent of the authors to make these appendixes convenient for the user, similar angles of attack are always plotted at the same location on the page (e.g., $\alpha = 0$ is always at the page center). This arrangement should help the reader to follow a trend at a constant α even if data were not taken at some angles of attack. The list below indicates the parameters plotted in each appendix.

Appendix	Mach no.	Reynolds no. ($\times 10^{-6}$)	Page
Free Transition			
A	0.50	4.4, 7.0	11
B	0.60	7.0, 10.0, 15.0, 30.0	14
C	0.65	7.0, 30.0	19
D	0.70	4.4, 7.0, 10.0, 15.0, 30.0	22
E	0.72	7.0, 30.0	28
F	0.74	4.4, 7.0, 10.0, 15.0, 30.0, 40.0	31
G	0.75	10.0, 15.0, 30.0	38
H	0.76	[a]4.4, [b]7.0, 10.0, 15.0, [a,b]30.0, 40.0	42
I	0.77	10.0, 15.0, 30.0, 40.0	53
J	0.78	4.4, 7.0, 10.0, 15.0, 30.0, 40.0	58
K	0.79	10.0, 30.0	65
L	0.80	4.4, 7.0, 10.0, 15.0, 30.0	68
Fixed Transition			
M	0.50	4.4, 7.0	74
N	0.65	7.0, 30.0	77
O	0.76	4.4, [b]7.0, 10.0, 15.0, [a,b]30.0, 40.0	80
P	0.78	4.4, 7.0, 10.0, 15.0, 30.0	90

[a]Conditions for "repeat data" runs.
[b]Conditions for "hysteresis data" runs.

Appendix A

Pressure Data for $M = 0.50$; $R = 4.4 \times 10^6$ and 7.0×10^6; Free Transition

The pressure measurements made on the NASA SC(3)-0712(B) airfoil are presented in coefficient form in graphs in this appendix. The data are for a given Mach number through the Reynolds number range. The pressure data from the upper surface of the airfoil are plotted as open symbols and the lower-surface data are plotted as solid symbols.

TEST	167
RUN	17
MACH	.500
R	4.4 x 10^6

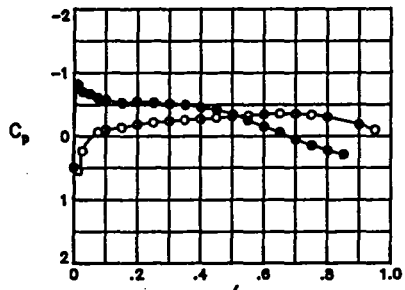

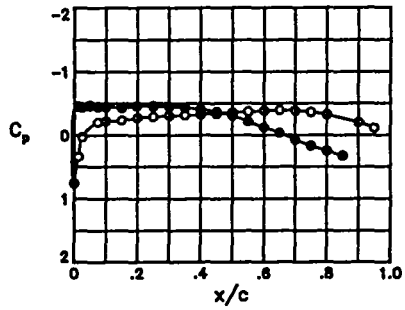

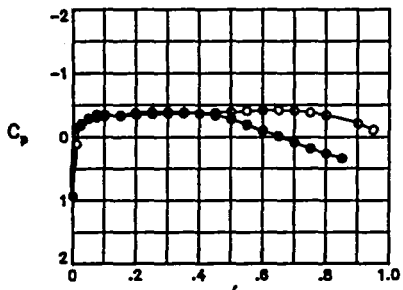

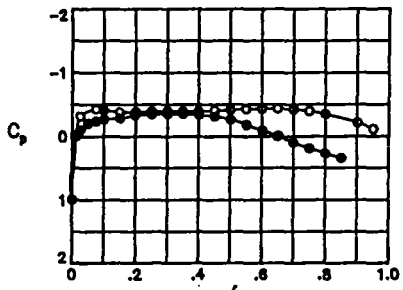

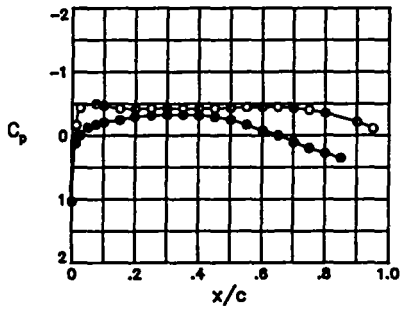

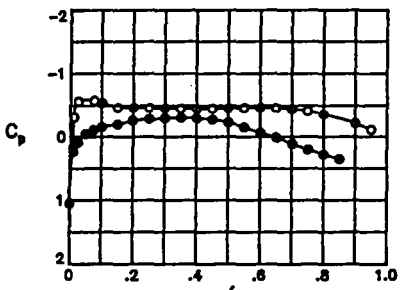

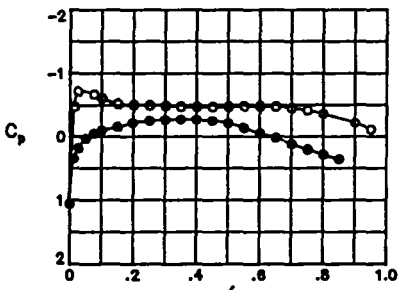

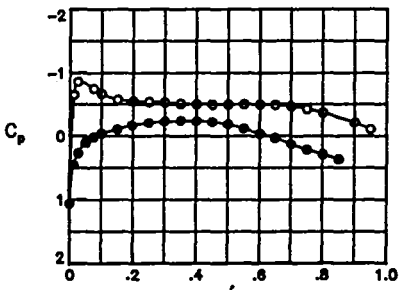

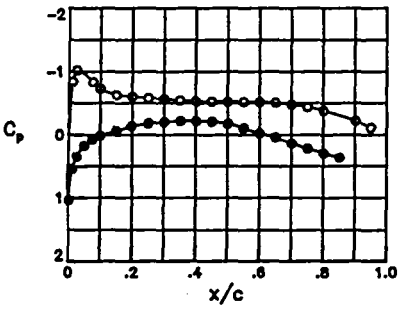

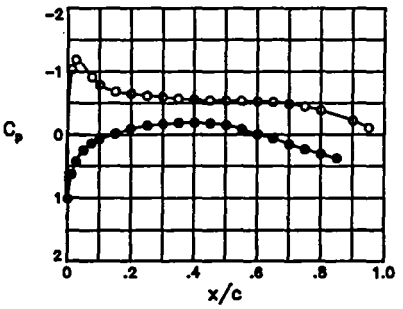

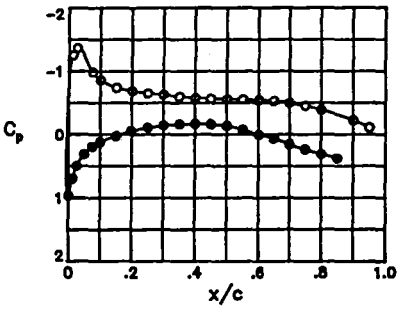

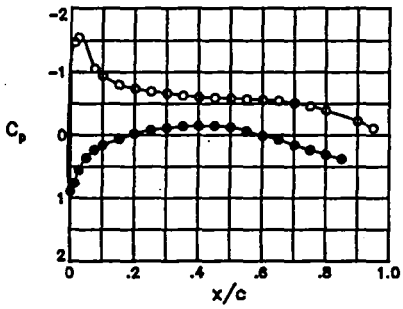

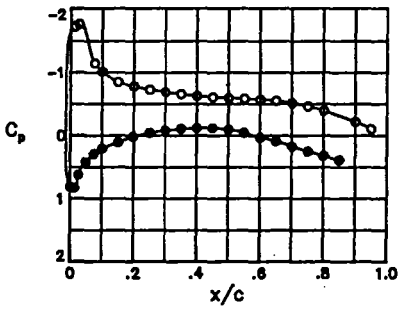

TEST 167
RUN 19
MACH .500
R 7.0 x 10^6

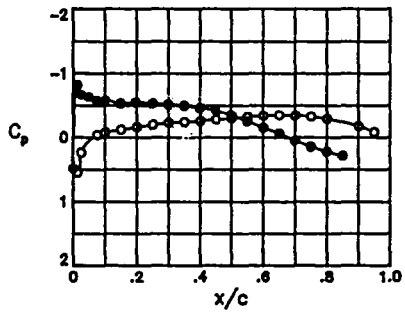

α=-4.00

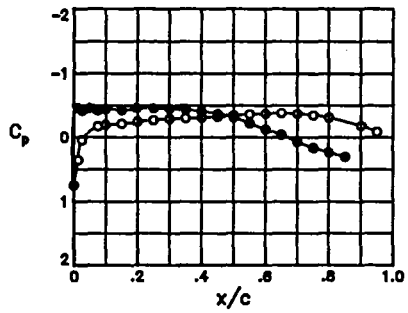

α=-2.98

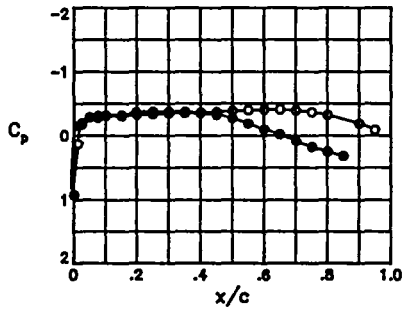

α=-2.00

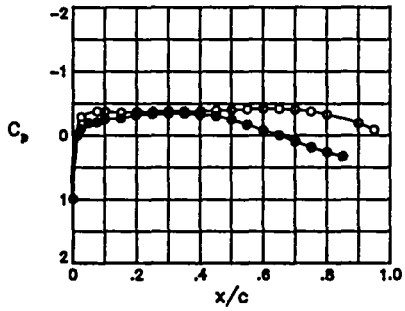

α=-1.51

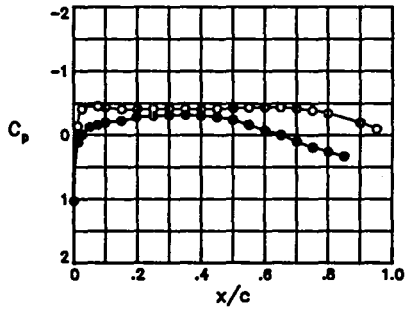

α=-1.01

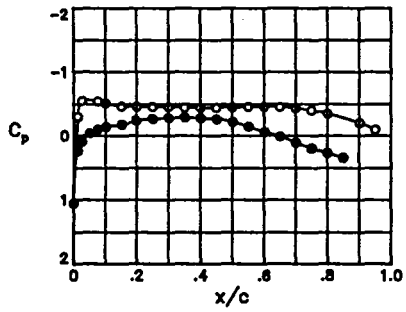

α=-.49

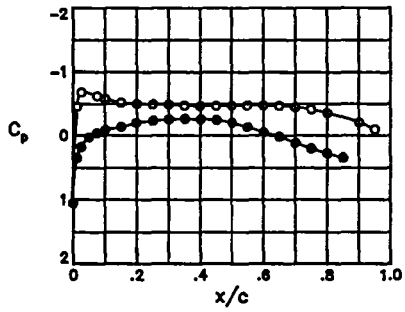

α=-.01

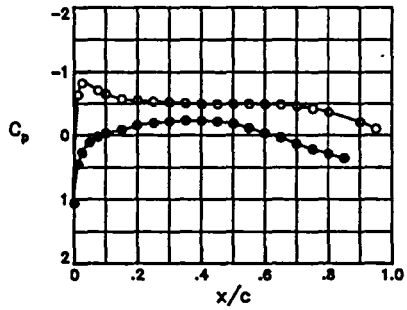

α=.51

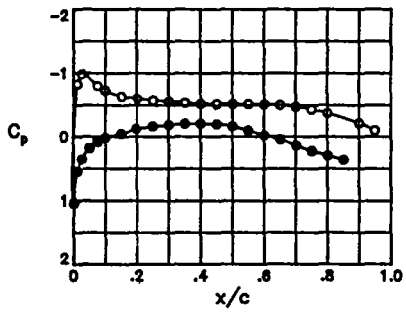

α=1.01

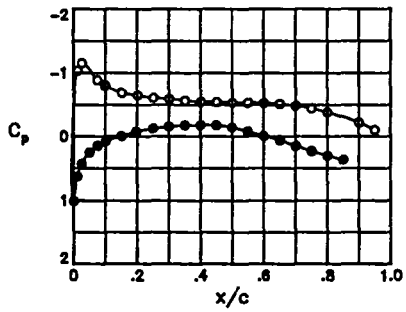

α=1.51

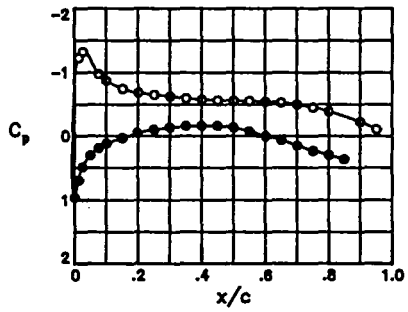

α=2.01

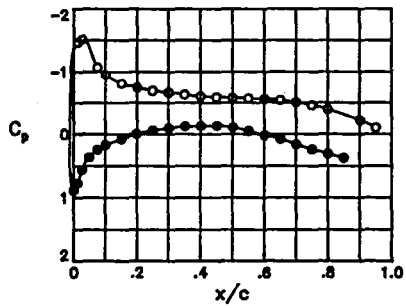

α=2.53

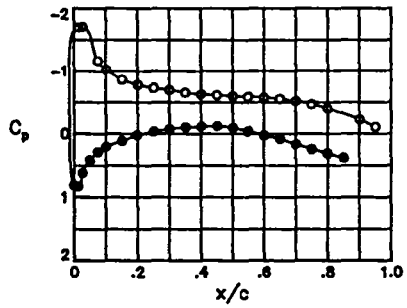

α=2.99

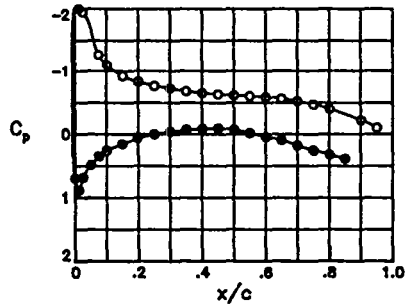

α=3.50

Appendix B

Pressure Data for $M = 0.60$; $R = 7.0 \times 10^6$, 10.0×10^6, 15.0×10^6, and 30.0×10^6; Free Transition

The pressure measurements made on the NASA SC(3)-0712(B) airfoil are presented in coefficient form in graphs in this appendix. The data are for a given Mach number through the Reynolds number range. The pressure data from the upper surface of the airfoil are plotted as open symbols and the lower-surface data are plotted as solid symbols.

TEST	167
RUN	18
MACH	.600
R	7.0 x 10^6

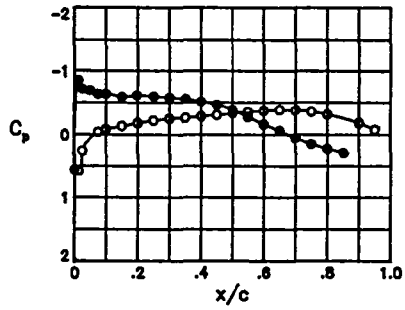

α=-3.99

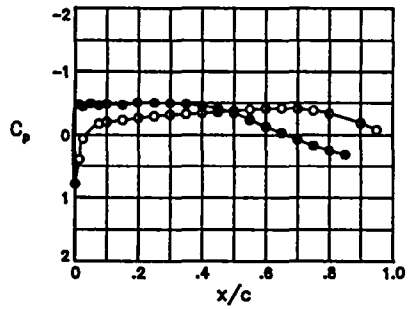

α=-3.00

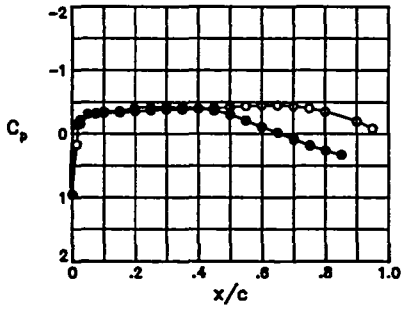

α=-2.00

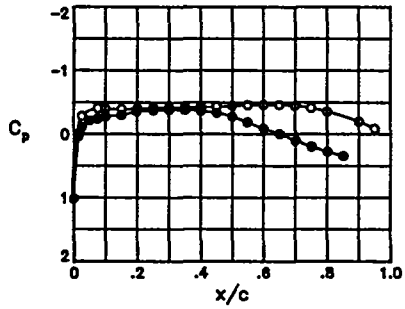

α=-1.49

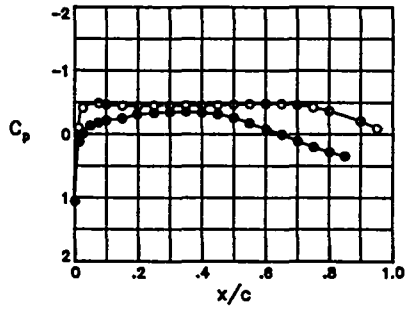

α=-.99

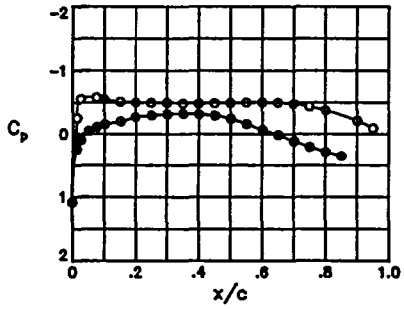

α=-.49

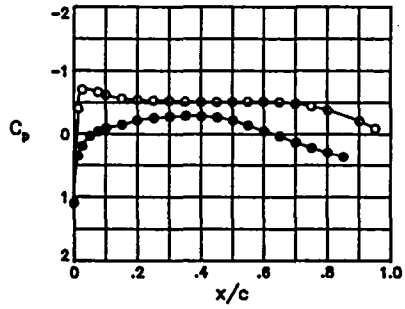

α=.01

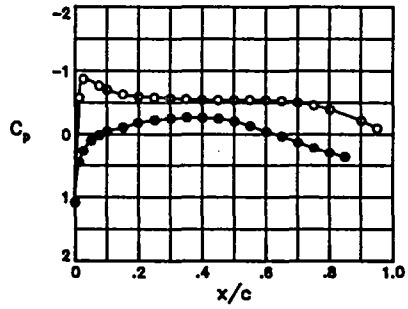

α=.51

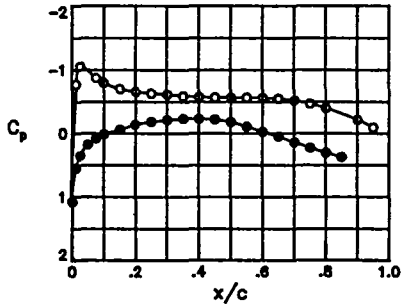

α=1.01

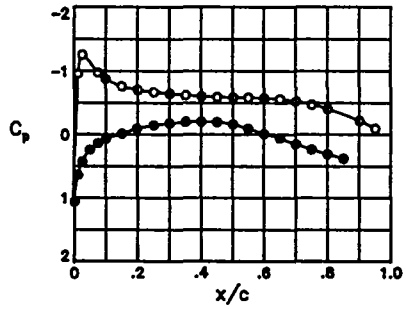

α=1.53

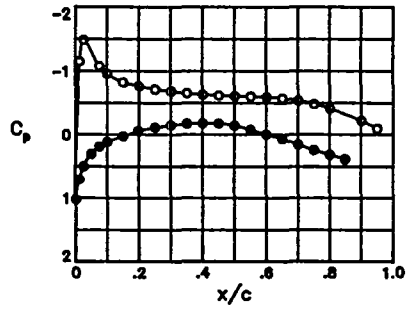

α=2.01

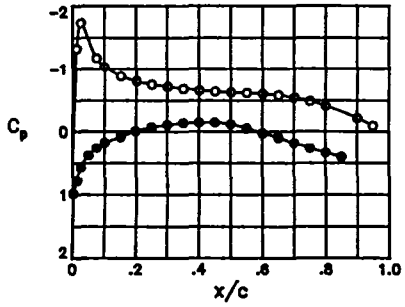

α=2.52

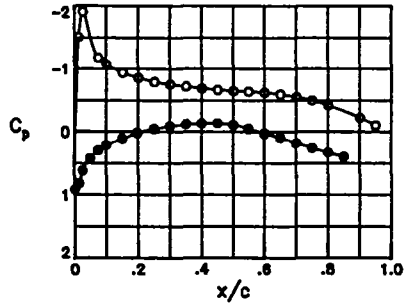

α=3.02

TEST	167
RUN	20
MACH	.600
R	10.0 x 10^6

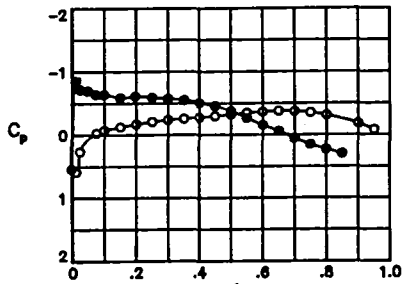

α=-4.01

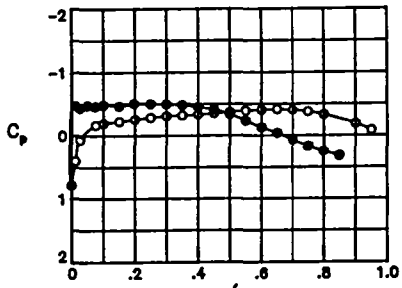

α=-2.98

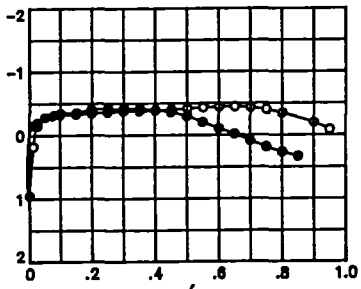

α=-2.00

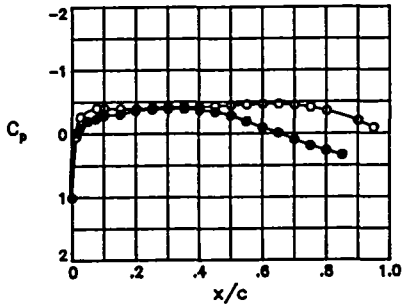

α=-1.50

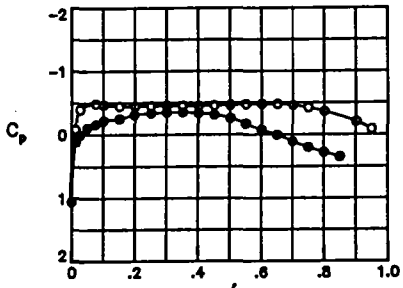

α=-1.00

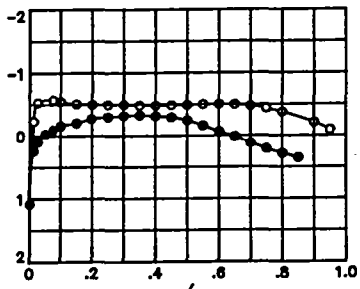

α=-.50

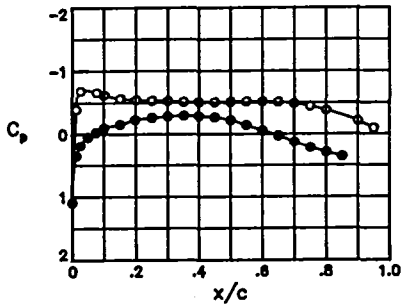

α=0.00

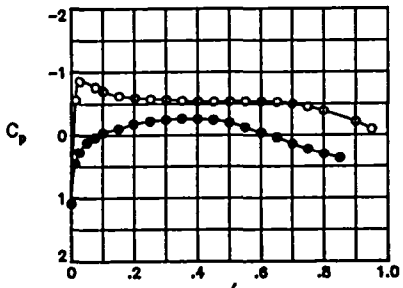

α=.51

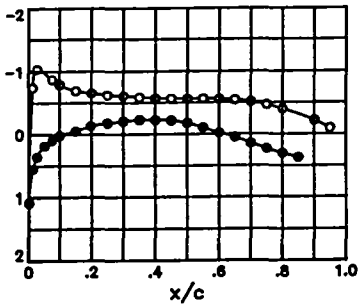

α=1.01

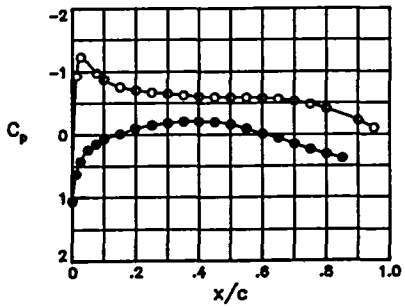

α=1.50

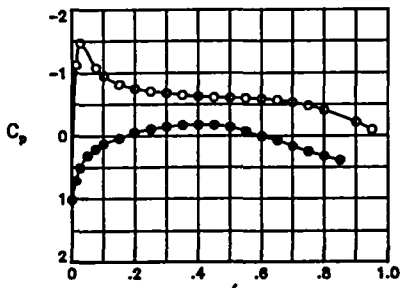

α=2.01

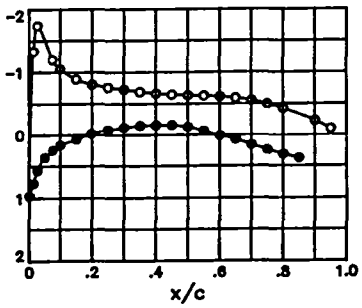

α=2.52

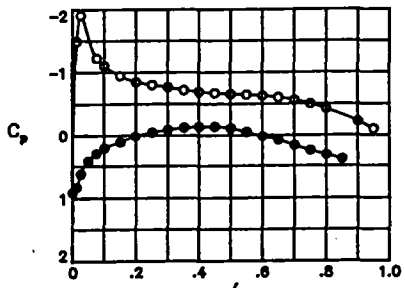

α=3.01

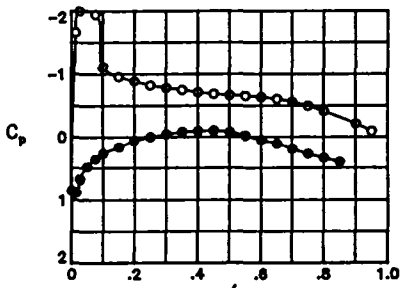

α=3.50

TEST	167
RUN	21
MACH	.600
R	15.0 x 10^6

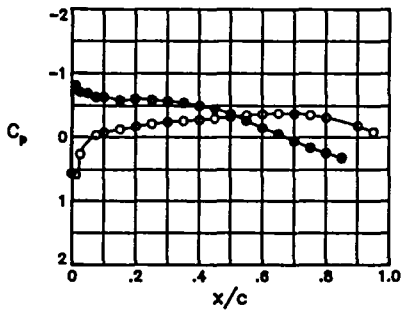

α=-3.98

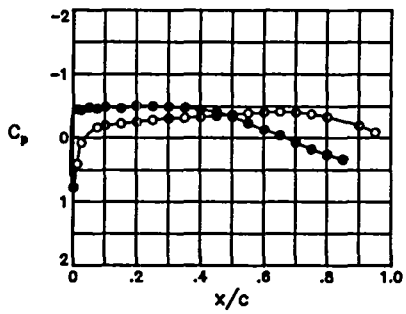

α=-2.99

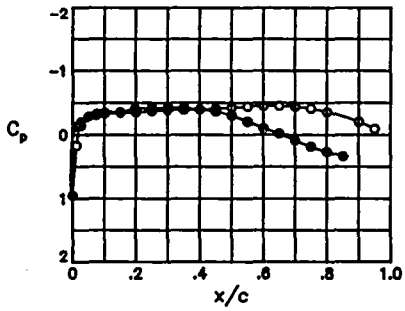

α=-2.00

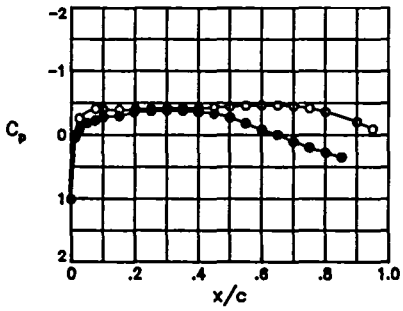

α=-1.49

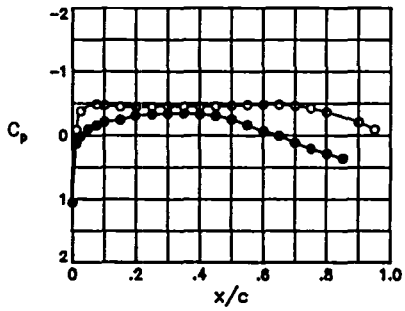

α=-1.00

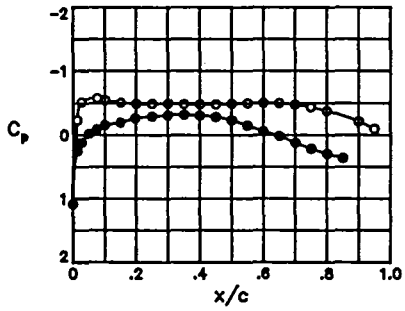

α=-.50

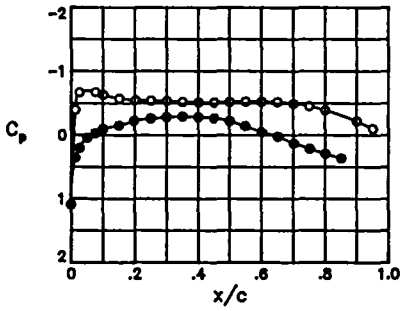

α=0.00

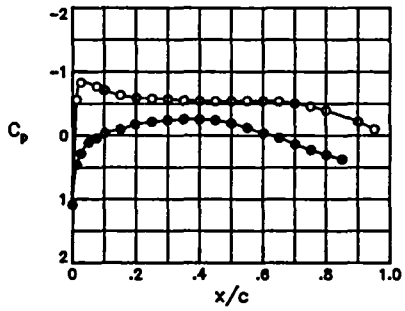

α=.50

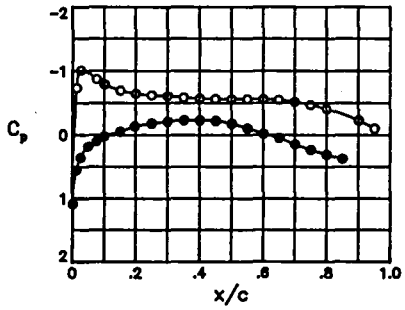

α=1.01

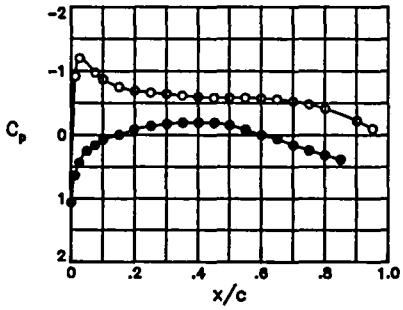

α=1.50

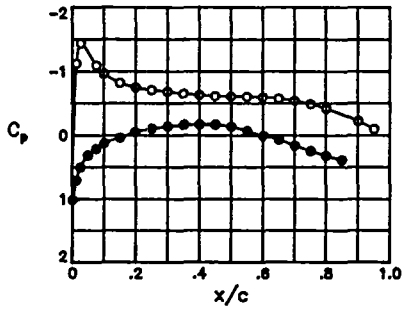

α=2.01

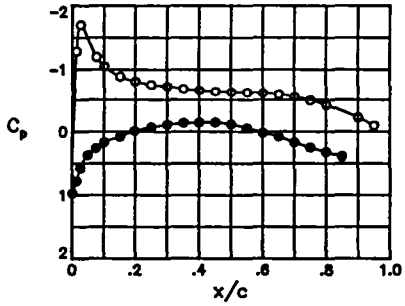

α=2.49

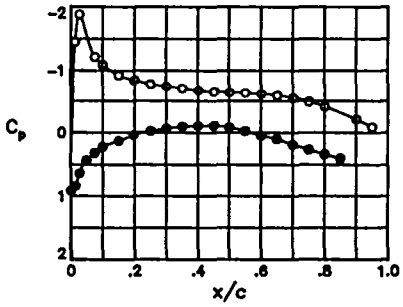

α=2.99

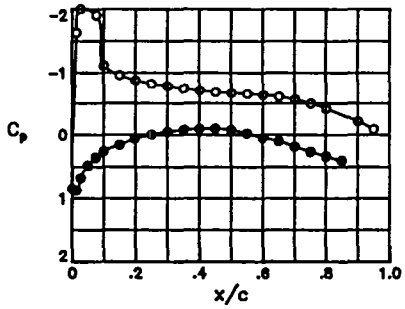

α=3.51

TEST	167
RUN	22
MACH	.600
R	30.0 x 10^6

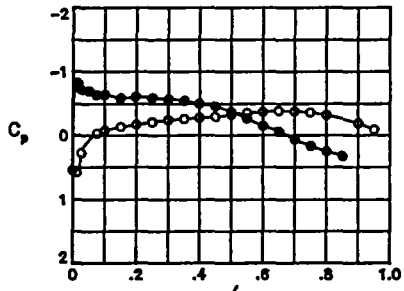

α= -4.00

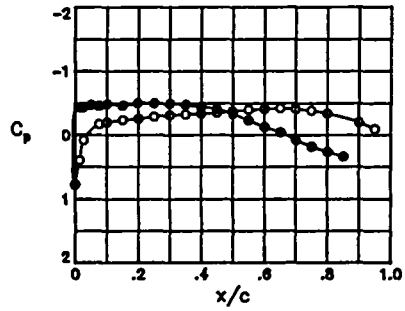

α= -3.00

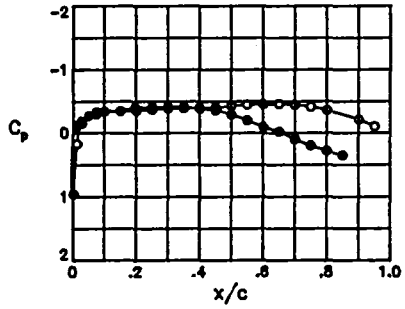

α= -1.99

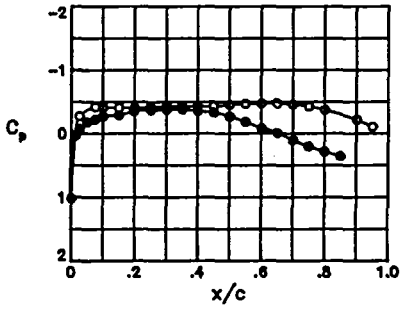

α= -1.49

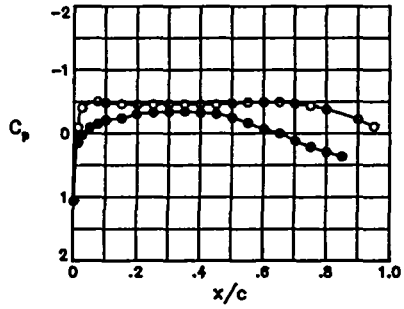

α= -1.00

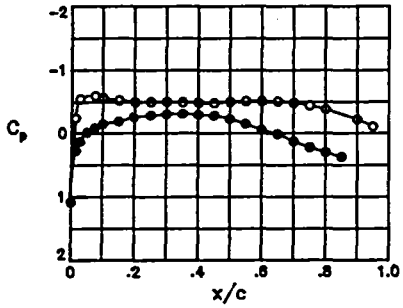

α= -.49

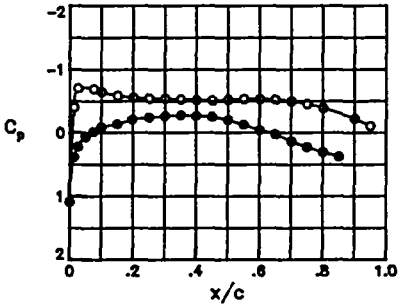

α= .01

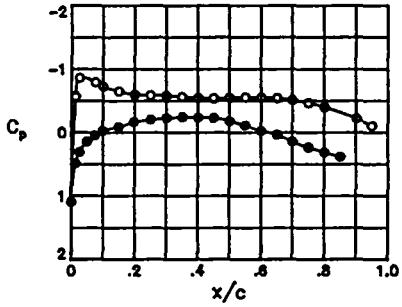

α= .51

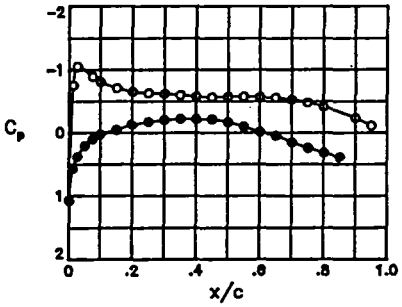

α= 1.01

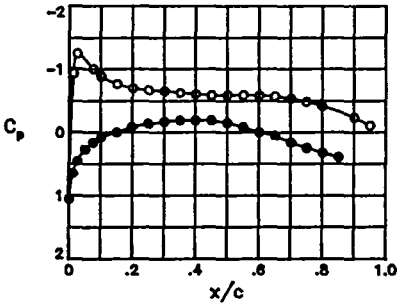

α= 1.52

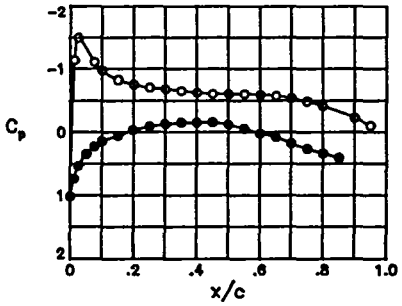

α= 2.02

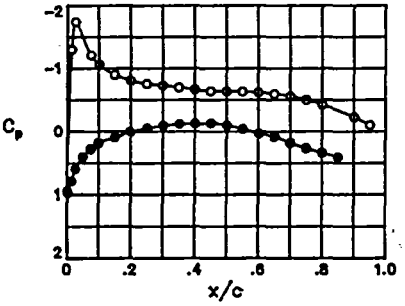

α= 2.53

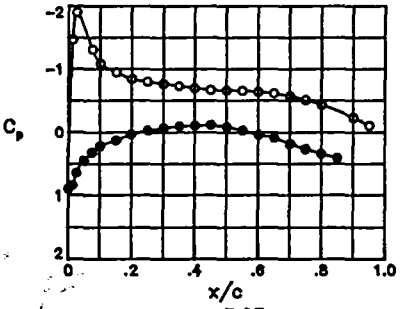

α= 3.03

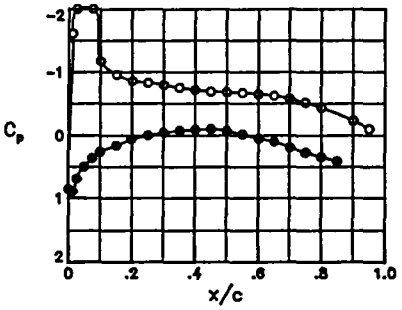

α= 3.42

Appendix C

Pressure Data for $M = 0.65$; $R = 7.0 \times 10^6$ and 30.0×10^6; Free Transition

The pressure measurements made on the NASA SC(3)-0712(B) airfoil are presented in coefficient form in graphs in this appendix. The data are for a given Mach number through the Reynolds number range. The pressure data from the upper surface of the airfoil are plotted as open symbols and the lower-surface data are plotted as solid symbols.

TEST	167
RUN	26
MACH	.650
R	7.0 x 10^6

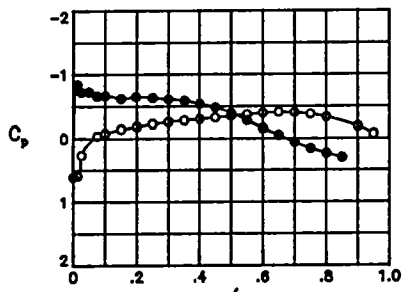

α= -3.95

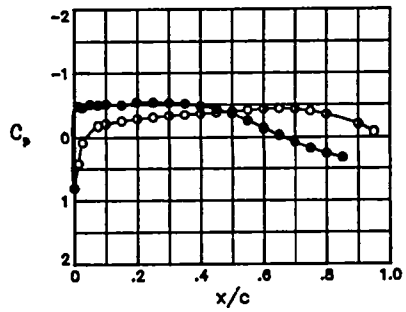

α= -3.01

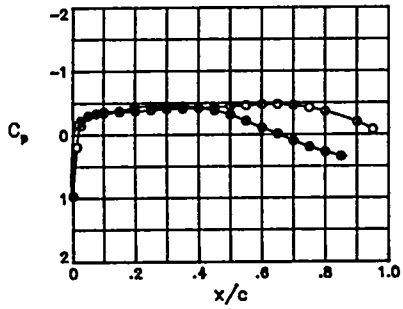

α= -2.00

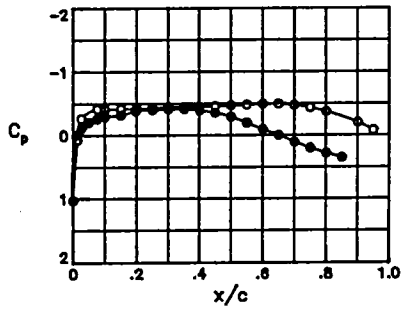

α= -1.50

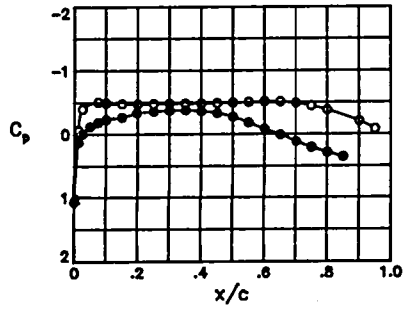

α= -1.00

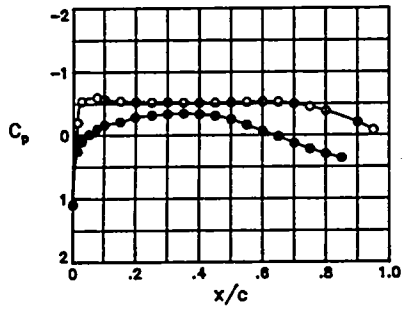

α= -.49

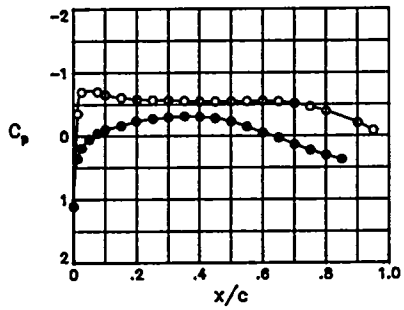

α= .01

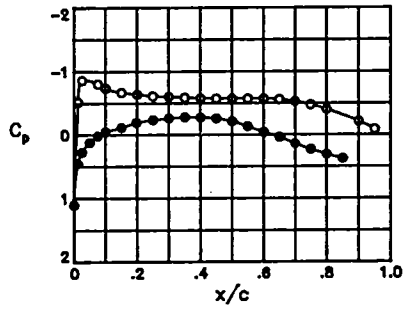

α= .50

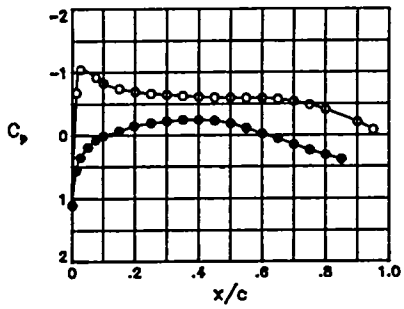

α= 1.00

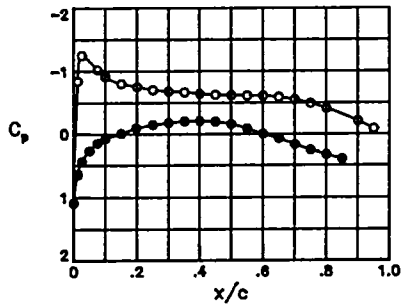

α= 1.51

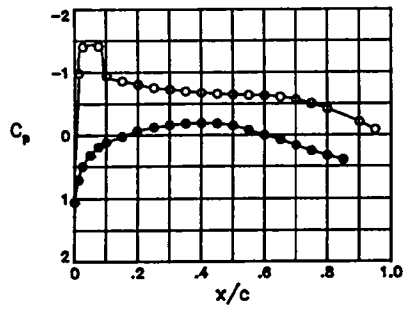

α= 2.02

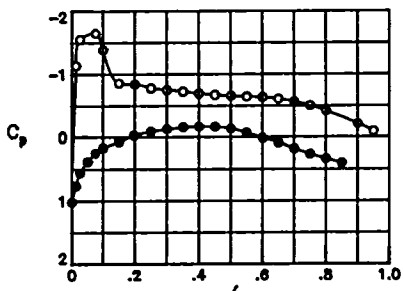

α= 2.50

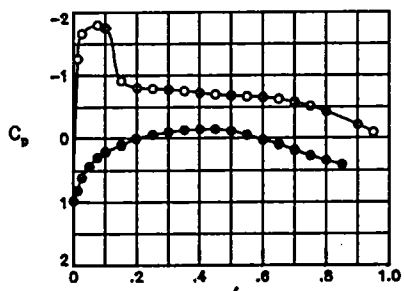

α= 3.01

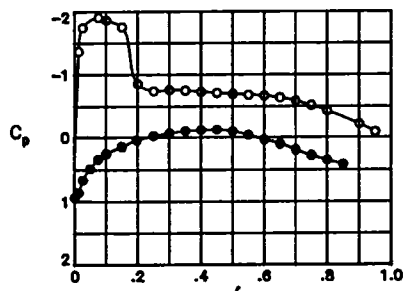

α= 3.50

TEST 167
RUN 23
MACH .650
R 30.0 x 10^6

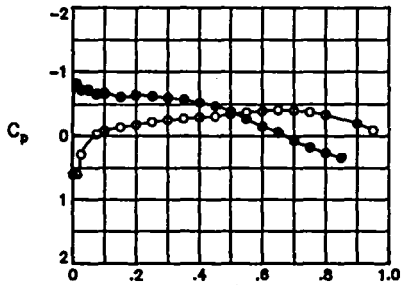

α=-4.01

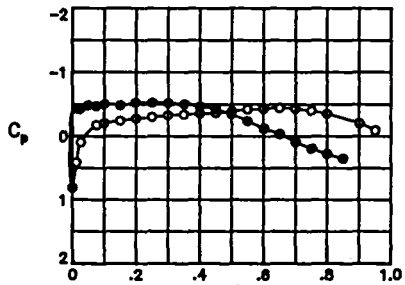

α=-2.98

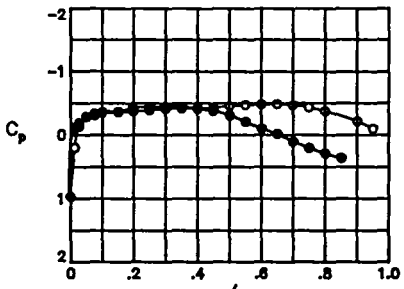

α=-1.99

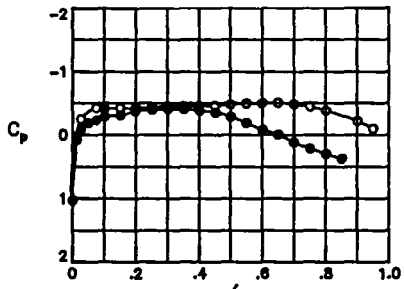

α=-1.49

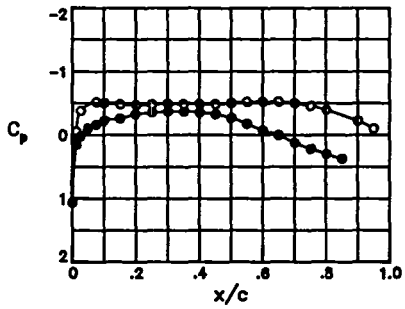

α=-1.00

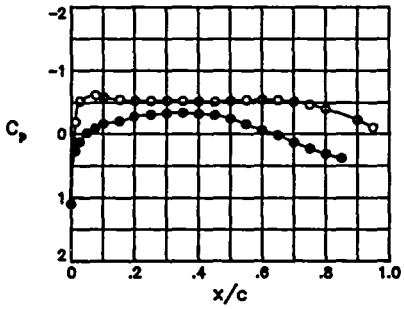

α=-.50

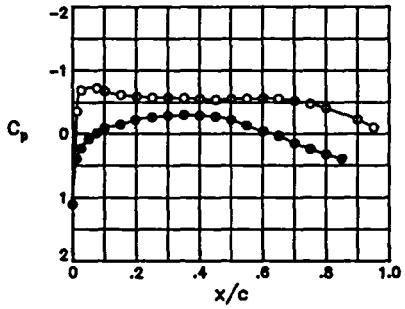

α=.02

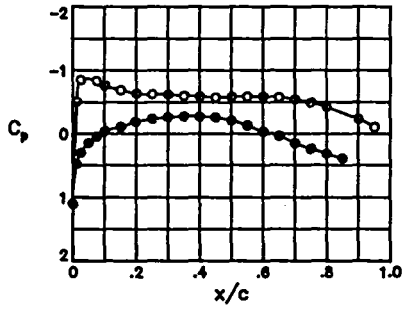

α=.52

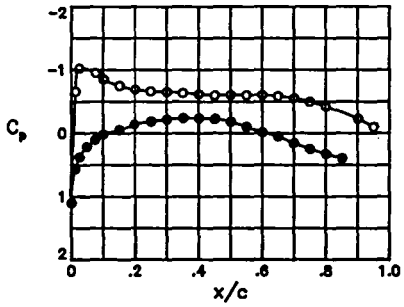

α=1.02

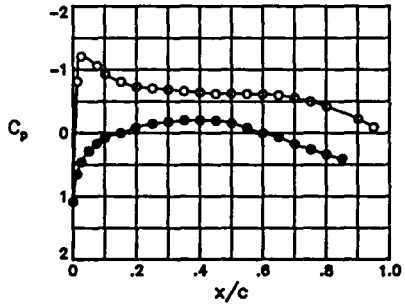

α=1.52

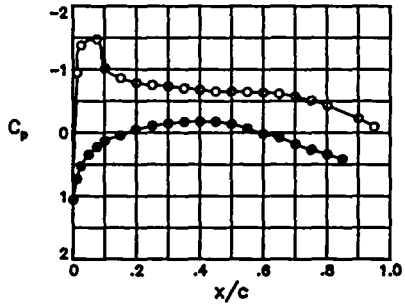

α=2.02

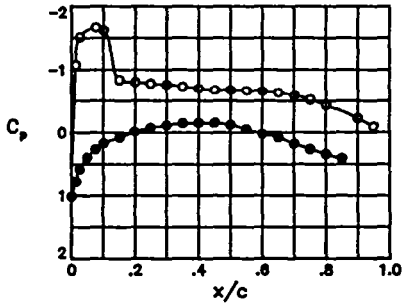

α=2.54

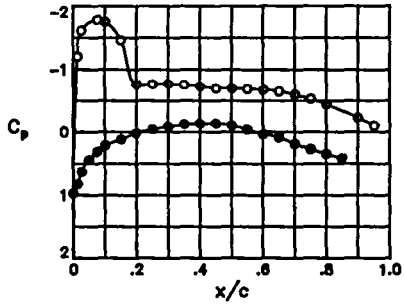

α=3.01

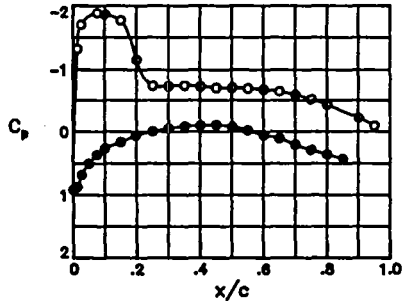

α=3.53

Appendix D

Pressure Data for $M = 0.70$; $R = 4.4 \times 10^6$, 7.0×10^6, 10.0×10^6, 15.0×10^6, and 30.0×10^6; Free Transition

The pressure measurements made on the NASA SC(3)-0712(B) airfoil are presented in coefficient form in graphs in this appendix. The data are for a given Mach number through the Reynolds number range. The pressure data from the upper surface of the airfoil are plotted as open symbols and the lower-surface data are plotted as solid symbols.

TEST	167
RUN	24
MACH	.700
R	4.4 x 10^6

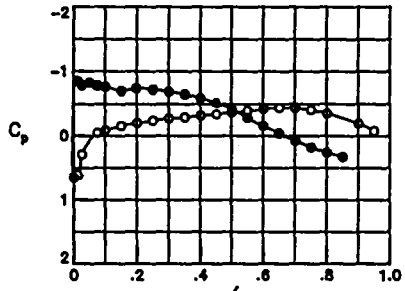

α= -4.00

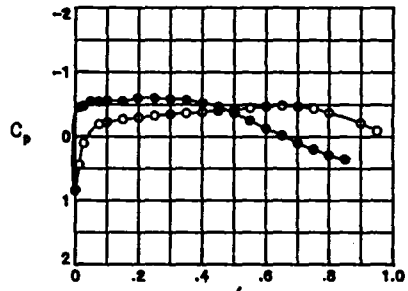

α= -2.99

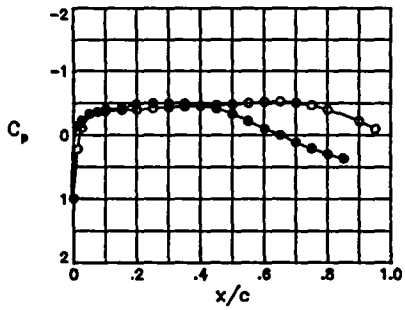

α= -2.00

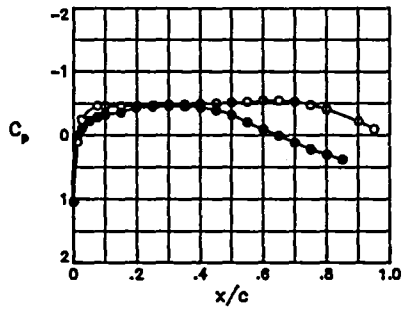

α= -1.49

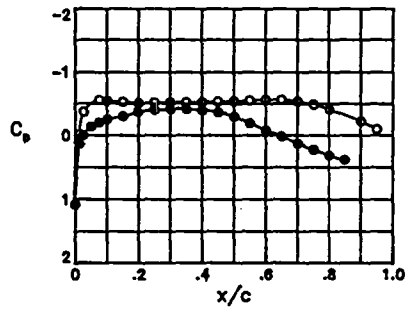

α= -.98

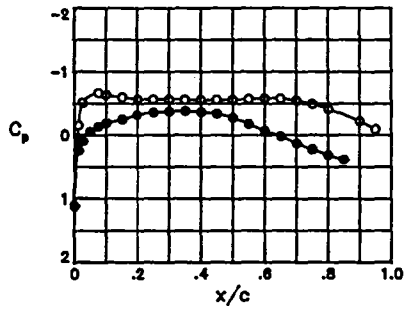

α= -.49

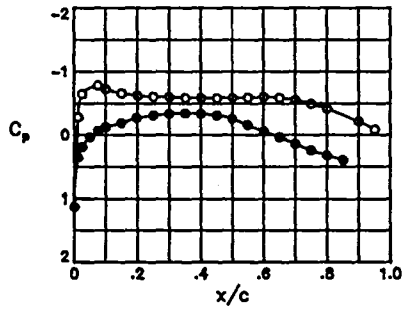

α= .02

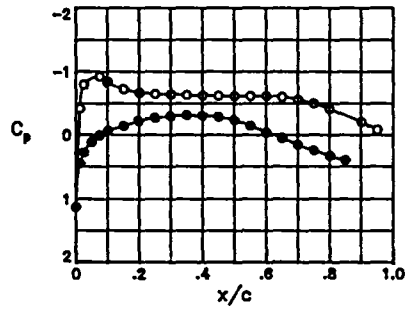

α= .52

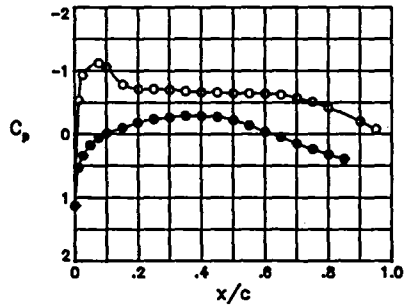

α= 1.02

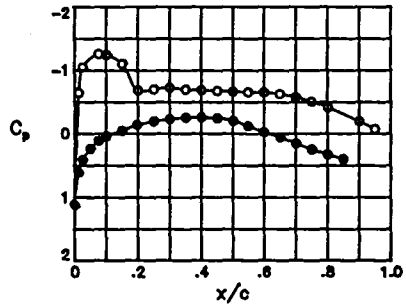

α= 1.50

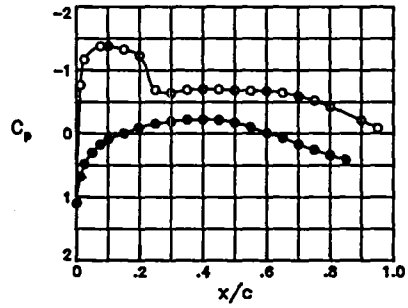

α= 2.03

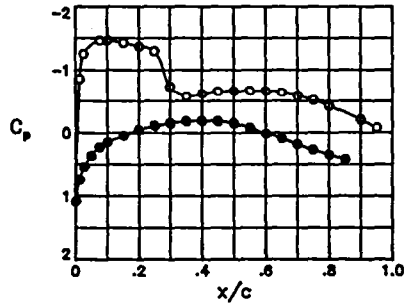

α= 2.50

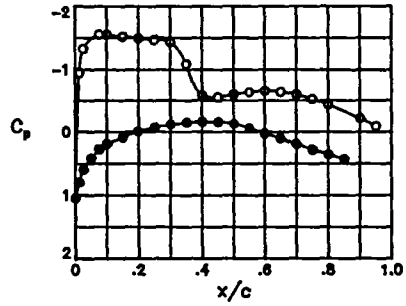

α= 3.01

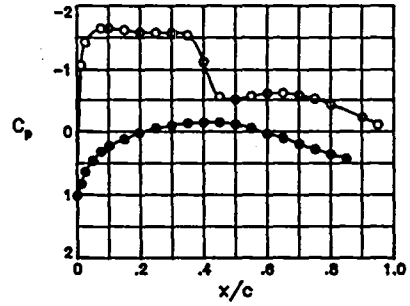

α= 3.52

TEST	167
RUN	25
MACH	.700
R	7.0 x 10^6

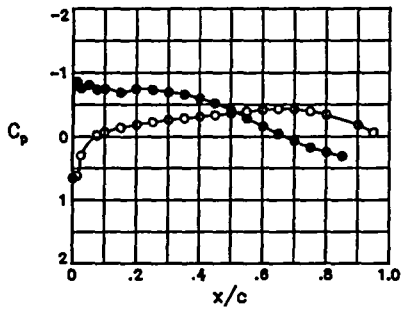

α=-3.98

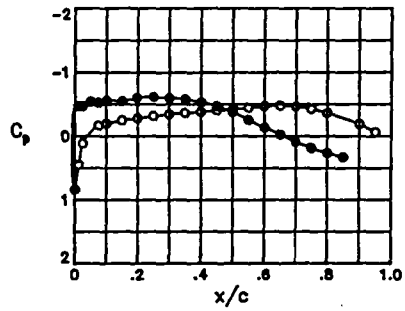

α=-2.99

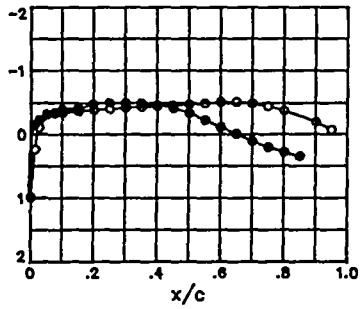

α=-2.00

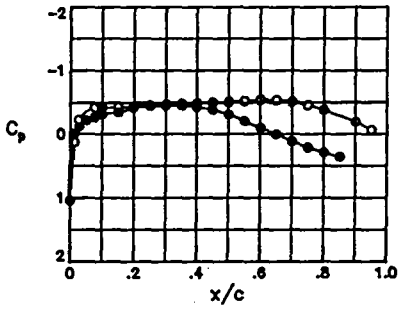

α=-1.49

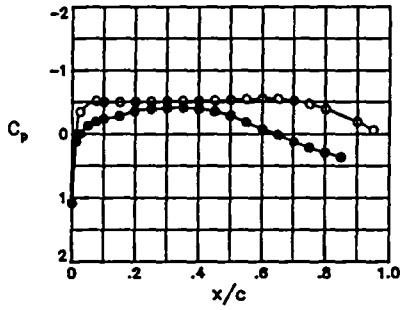

α=-1.00

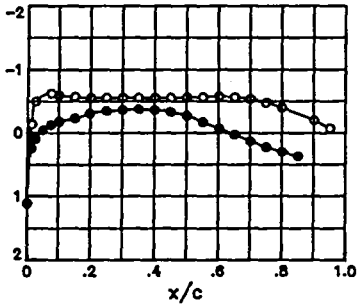

α=-.47

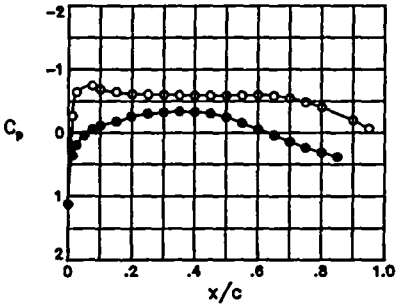

α=.02

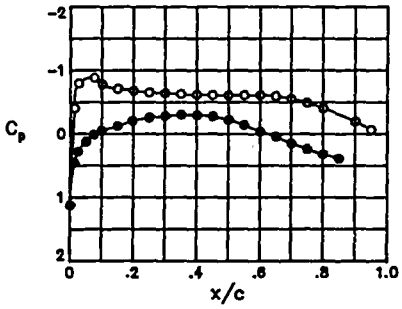

α=.51

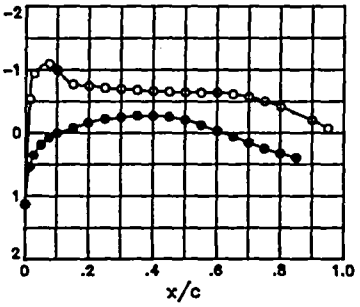

α=1.01

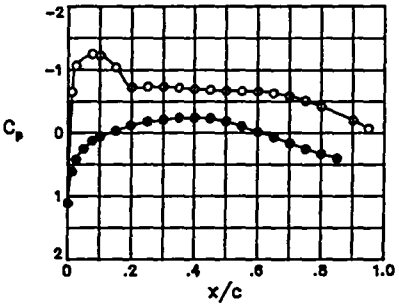

α=1.52

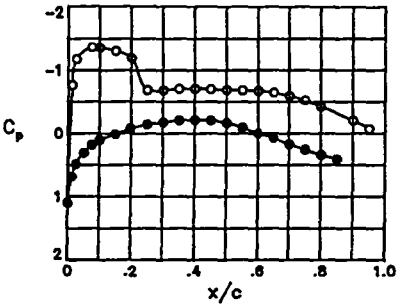

α=2.01

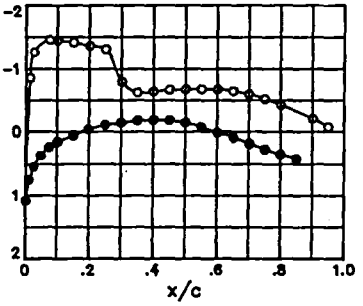

α=2.50

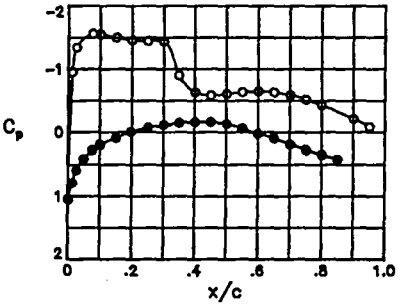

α=3.00

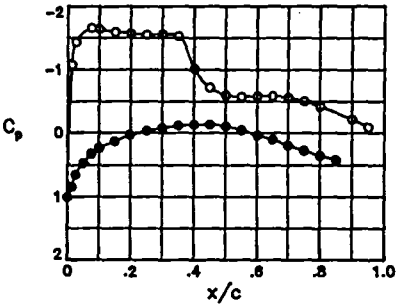

α=3.59

TEST 167
RUN 53
MACH .700
R 10.0 x 10^6

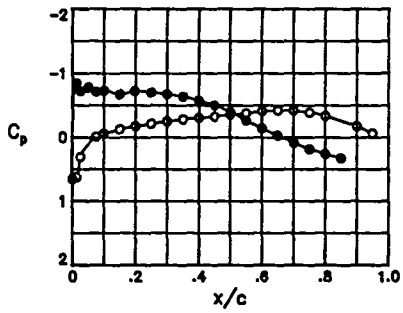

α=-3.99

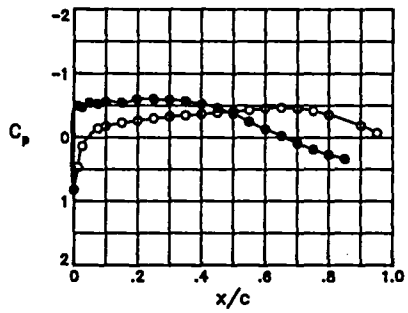

α=-3.07

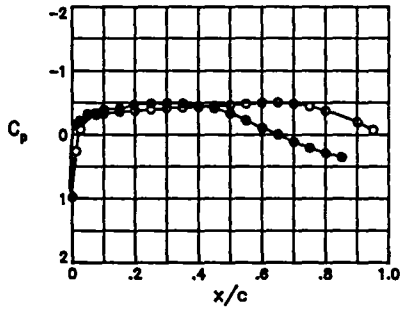

α=-2.04

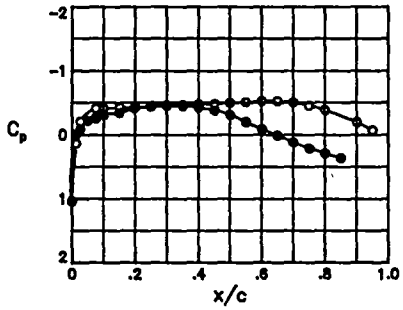

α=-1.50

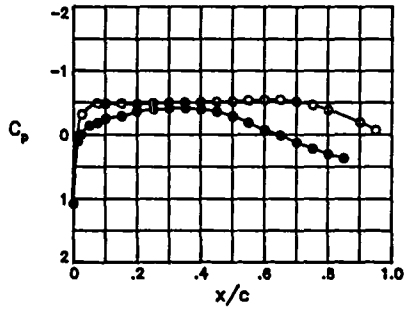

α=-1.05

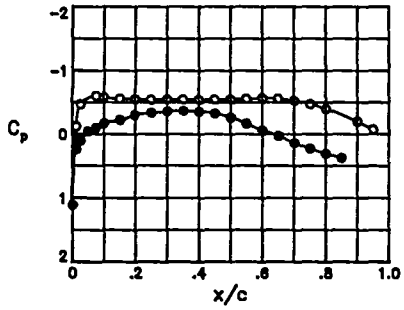

α=-.49

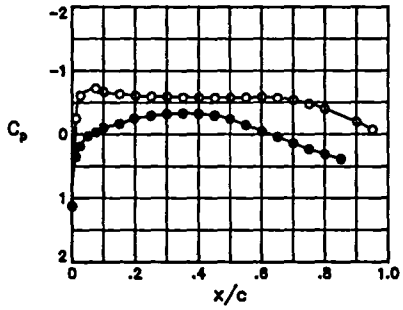

α=.01

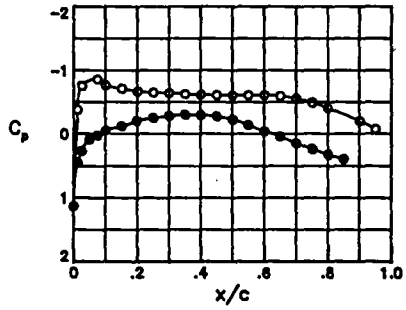

α=.52

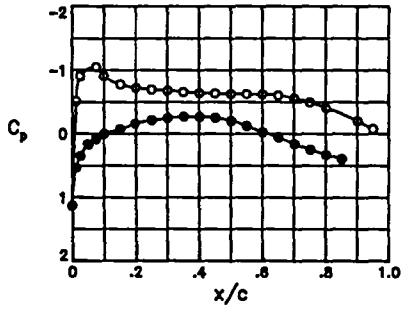

α=1.00

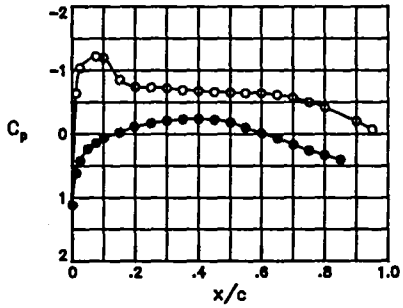

α=1.52

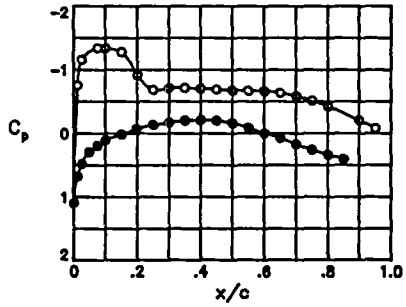

α=2.02

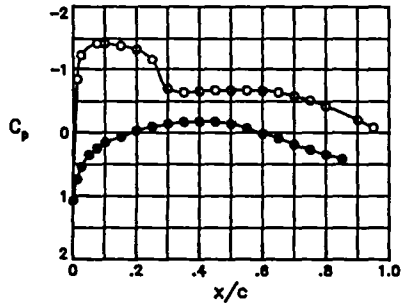

α=2.50

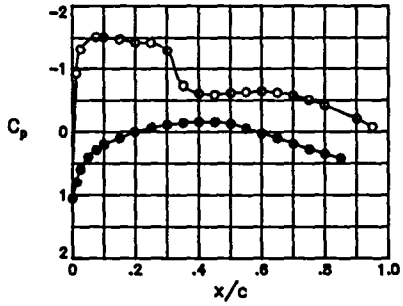

α=3.01

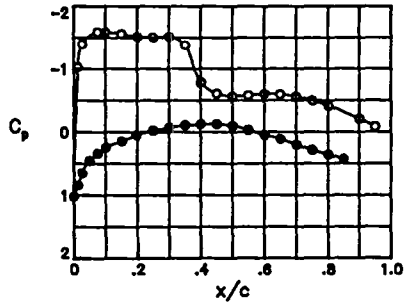

α=3.51

TEST	167
RUN	47
MACH	.700
R	15.0 x 10^6

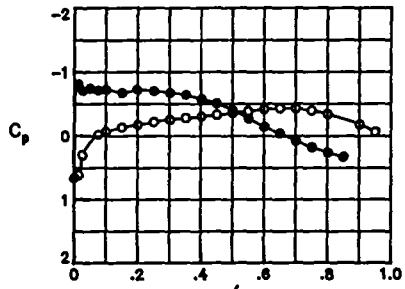

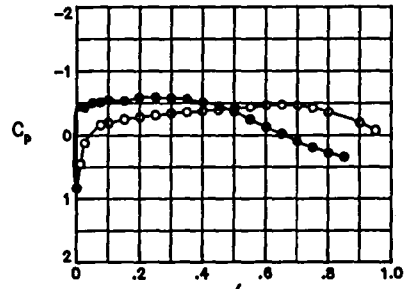

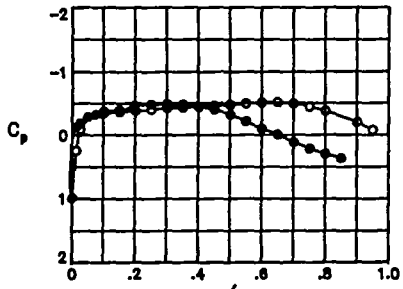

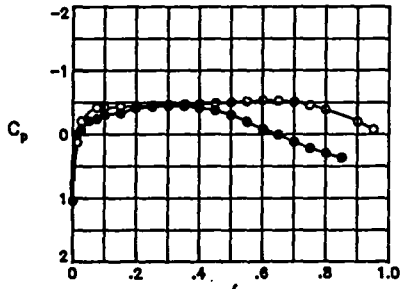

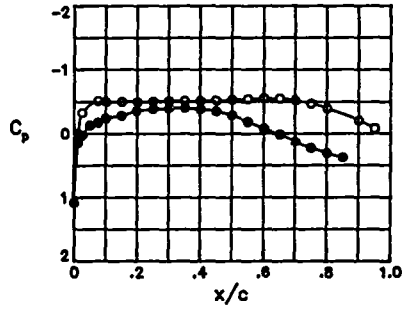

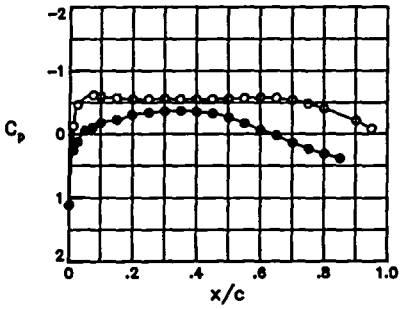

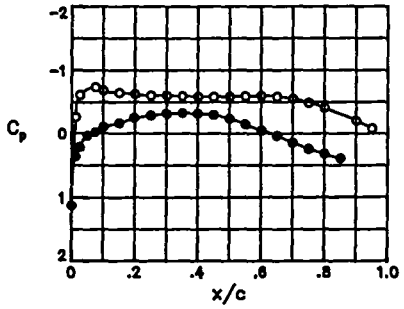

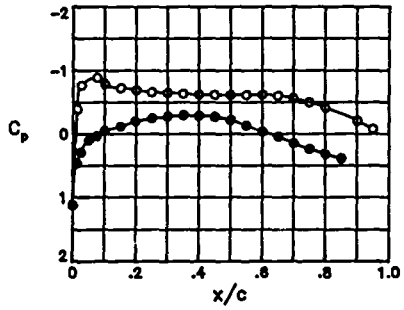

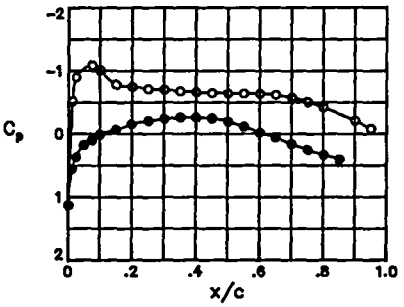

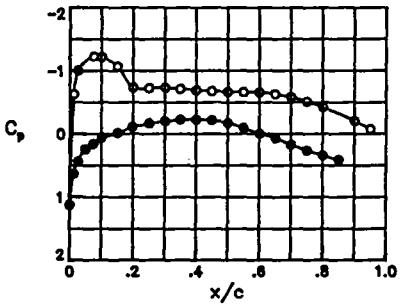

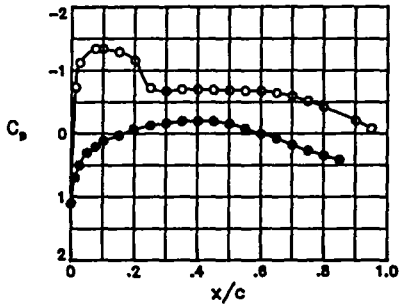

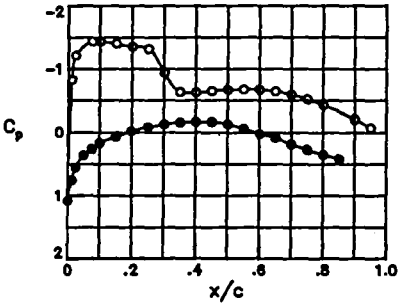

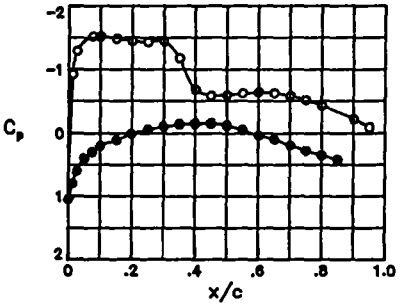

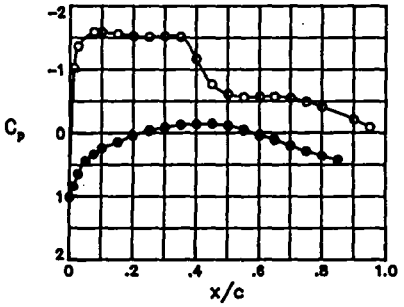

TEST	167
RUN	41
MACH	.700
R	30.0 x 10^6

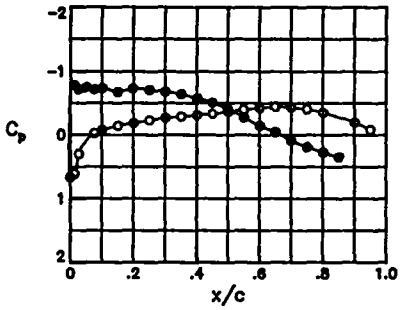

α=-3.99

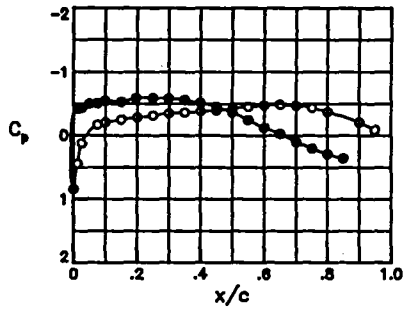

α=-2.99

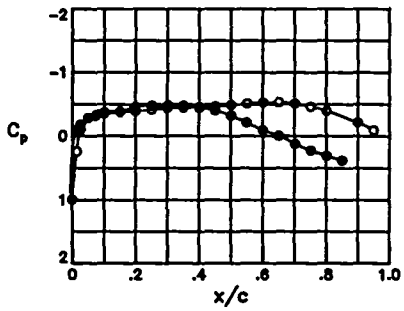

α=-2.00

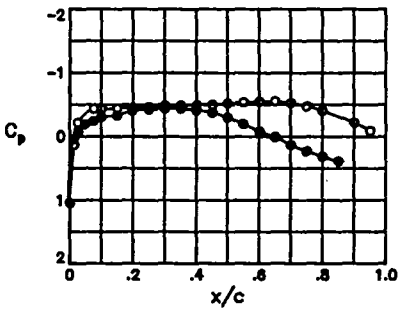

α=-1.51

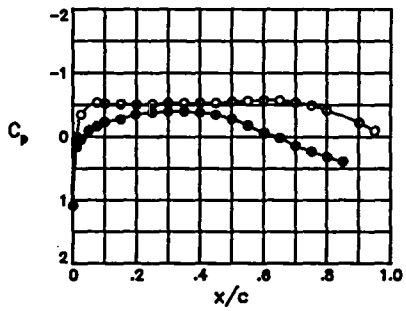

α=-1.00

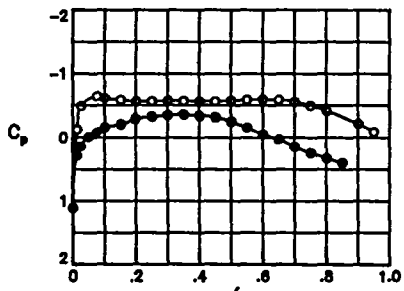

α=-.49

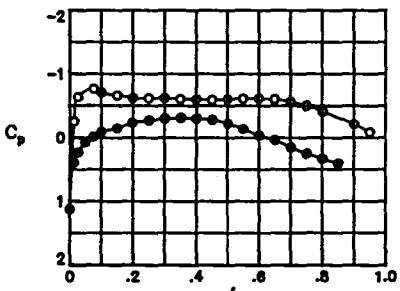

α=.01

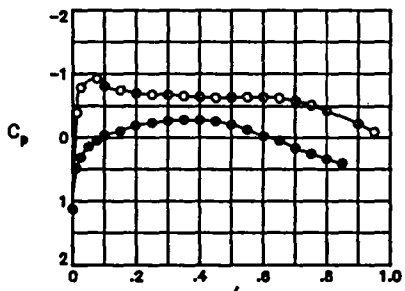

α=.51

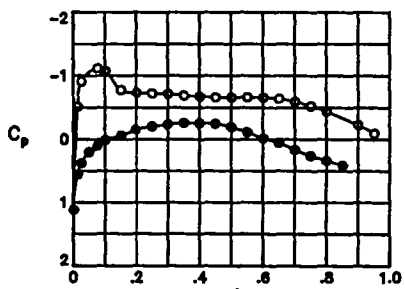

α=1.00

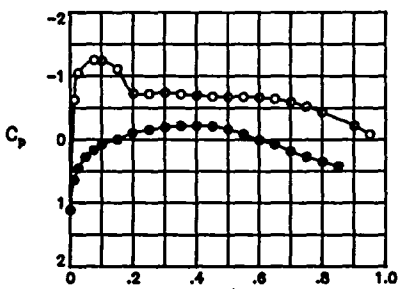

α=1.51

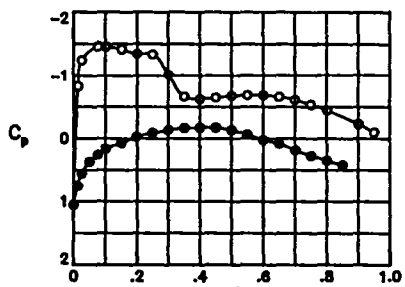

α=2.52

Appendix E

Pressure Data for $M = 0.72$; $R = 7.0 \times 10^6$ and 30.0×10^6; Free Transition

The pressure measurements made on the NASA SC(3)-0712(B) airfoil are presented in coefficient form in graphs in this appendix. The data are for a given Mach number through the Reynolds number range. The pressure data from the upper surface of the airfoil are plotted as open symbols and the lower-surface data are plotted as solid symbols.

TEST	167
RUN	54
MACH	.720
R	7.0 x 10^6

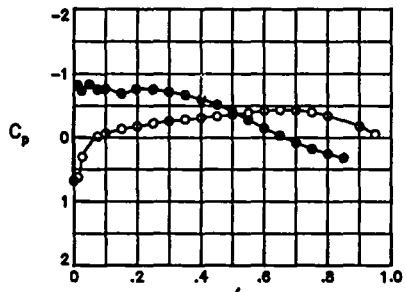

α=-3.98

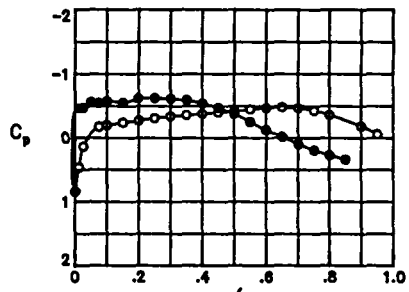

α=-2.99

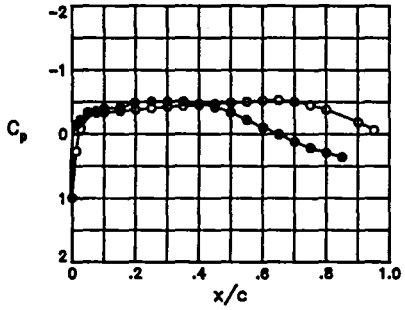

α=-1.99

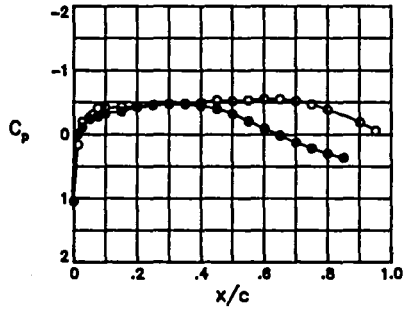

α=-1.49

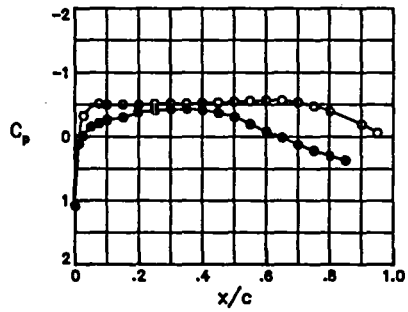

α=-1.00

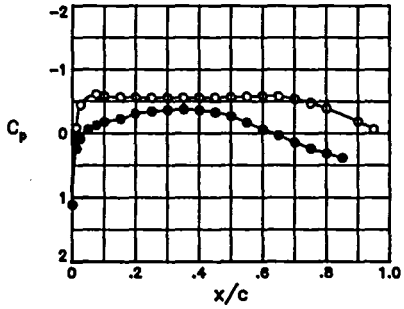

α=-.50

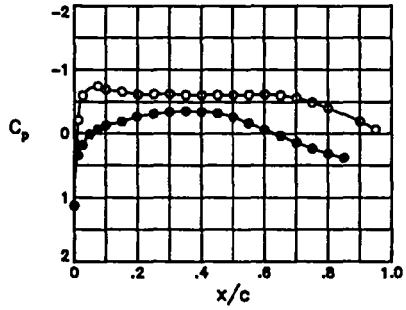

α=.01

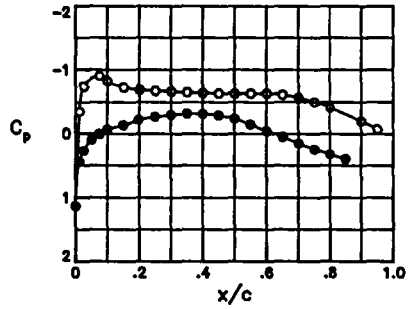

α=.51

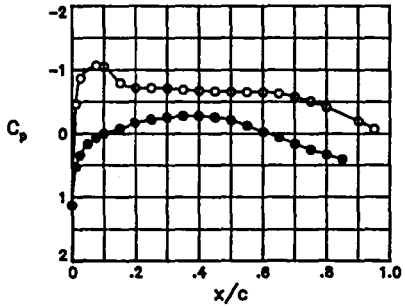

α=1.01

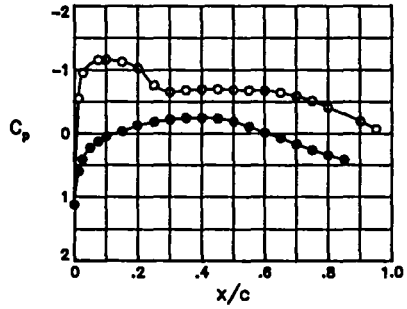

α=1.50

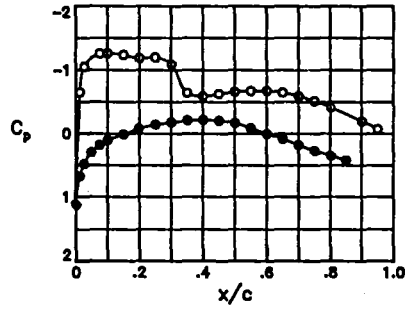

α=2.01

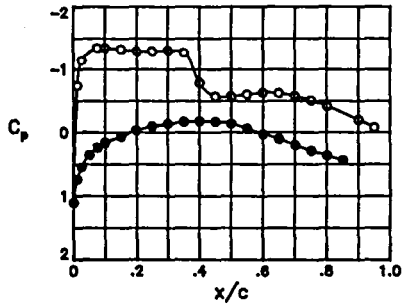

α=2.50

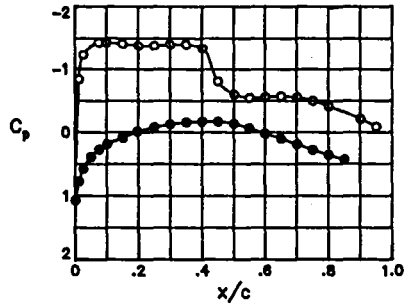

α=3.00

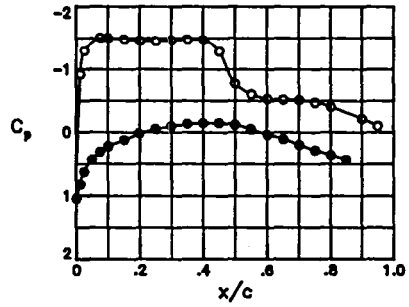

α=3.50

TEST	167
RUN	40
MACH	.720
R	30.0 x 10^6

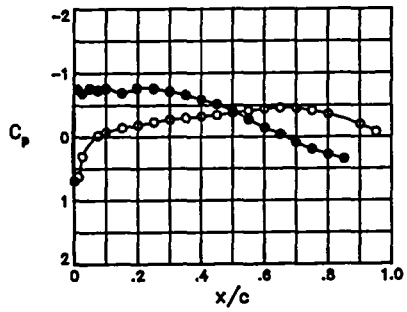

α=-3.99

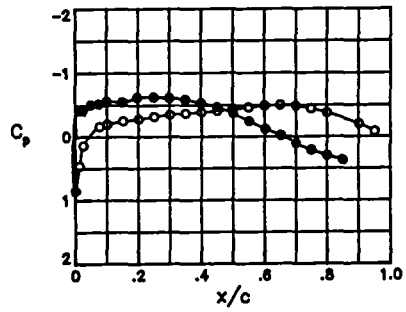

α=-3.01

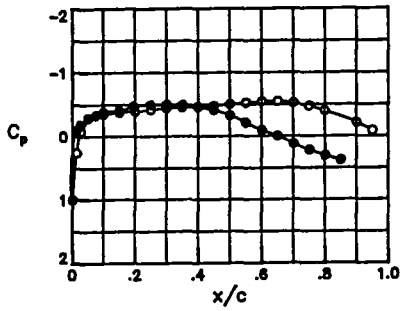

α=-2.01

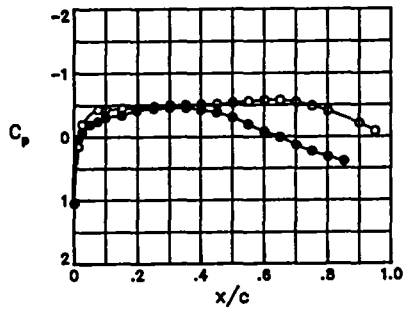

α=-1.51

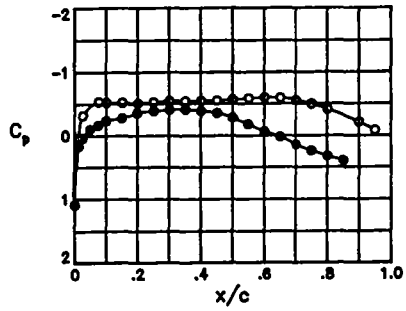

α=-1.01

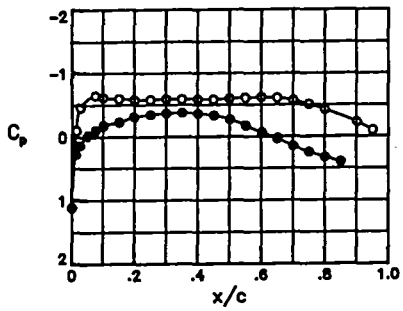

α=-.50

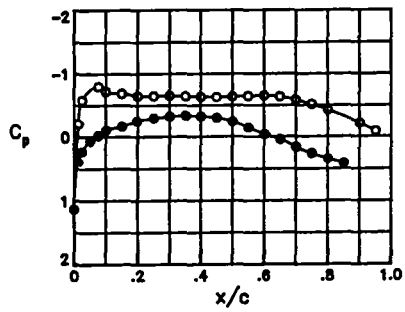

α=.02

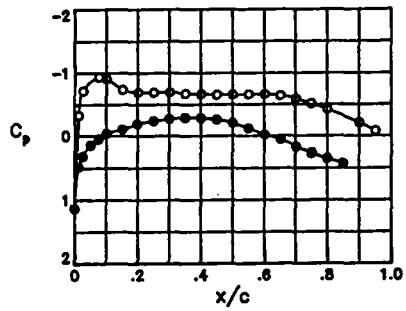

α=.52

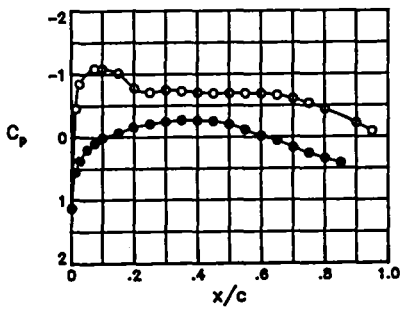

α=1.01

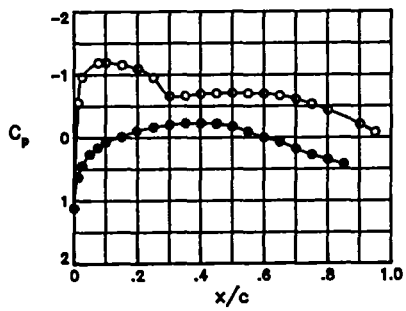

α=1.51

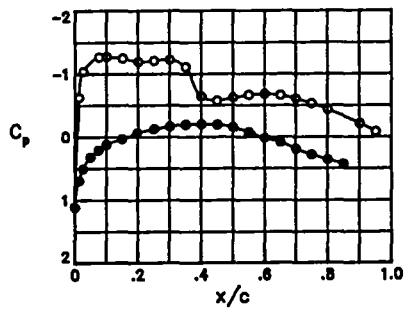

α=2.01

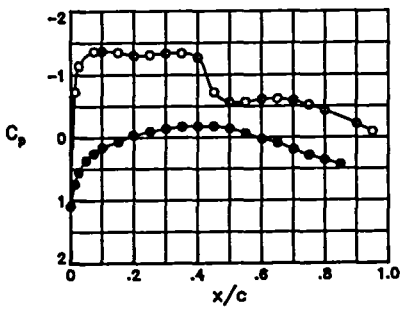

α=2.52

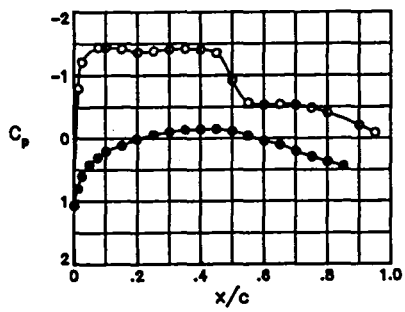

α=3.01

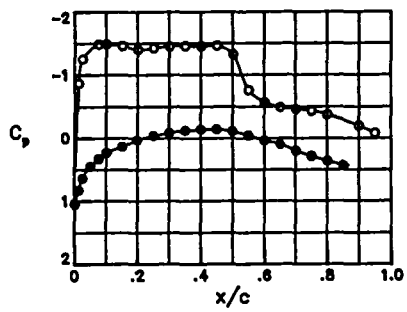

α=3.50

Appendix F

Pressure Data for $M = 0.74$; $R = 4.4 \times 10^6$, 7.0×10^6, 10.0×10^6, 15.0×10^6, 30.0×10^6, and 40.0×10^6; Free Transition

The pressure measurements made on the NASA SC(3)-0712(B) airfoil are presented in coefficient form in graphs in this appendix. The data are for a given Mach number through the Reynolds number range. The pressure data from the upper surface of the airfoil are plotted as open symbols and the lower-surface data are plotted as solid symbols.

TEST	167
RUN	11
MACH	.740
R	4.4 x 10^6

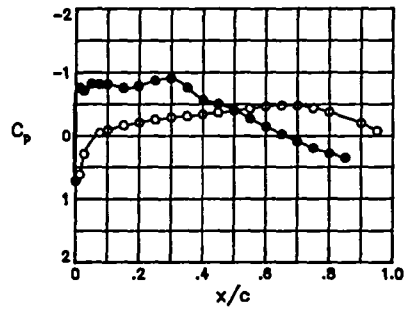

α=-4.00

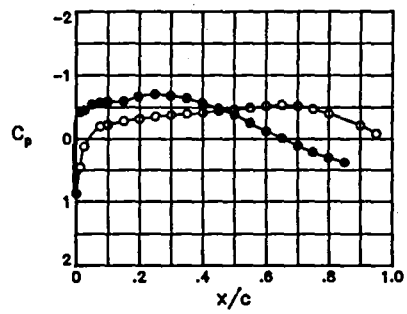

α=-3.00

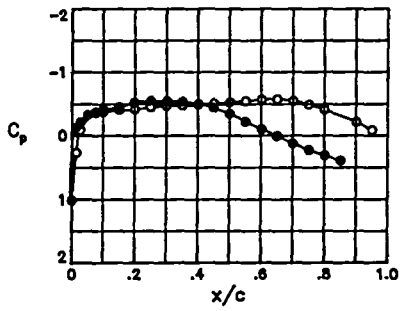

α=-2.00

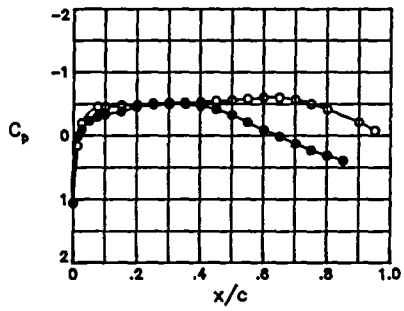

α=-1.49

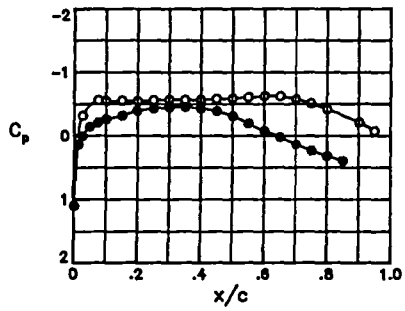

α=-.99

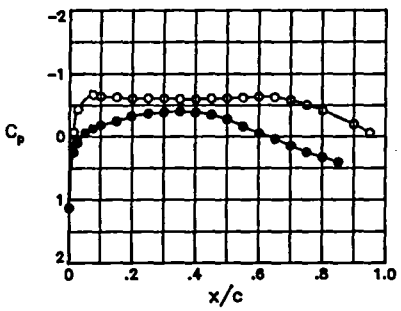

α=-.49

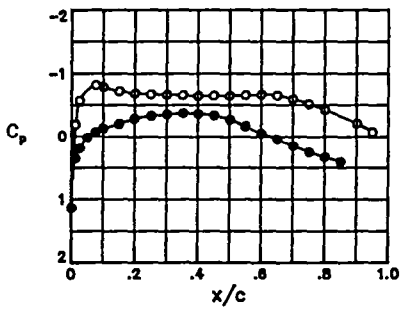

α=.03

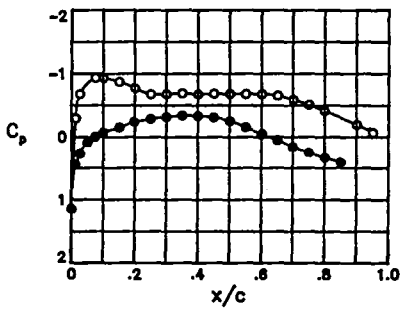

α=.53

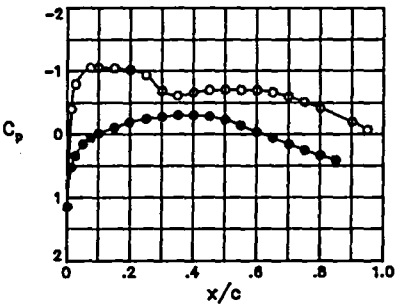

α=1.02

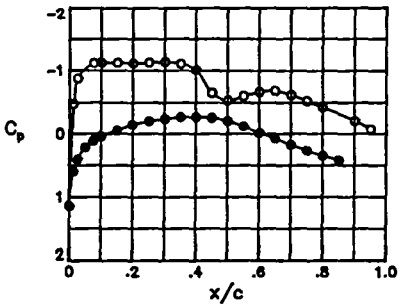

α=1.52

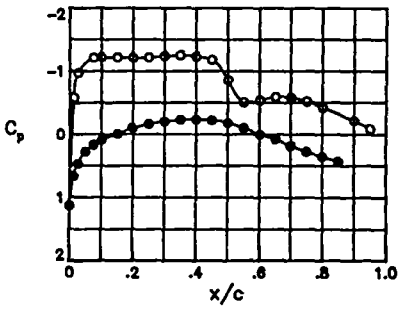

α=2.01

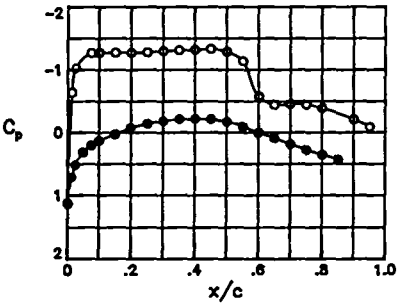

α=2.52

TEST 167
RUN 12
MACH .740
R 7.0 x 10^6

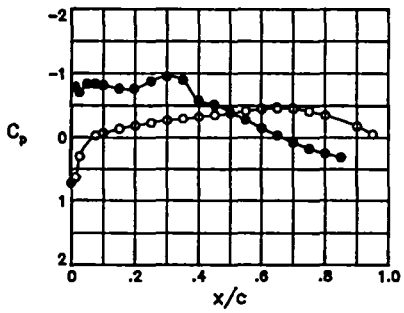

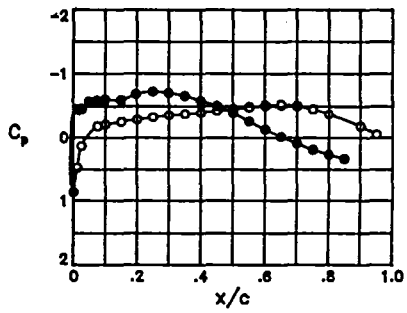

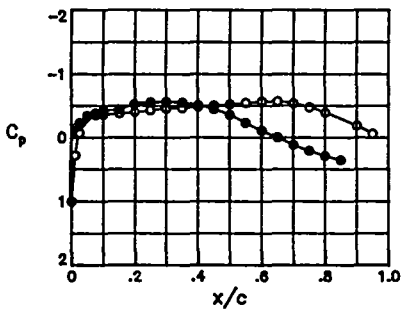

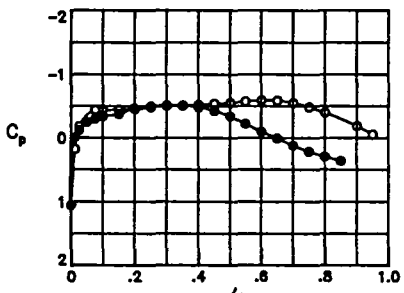

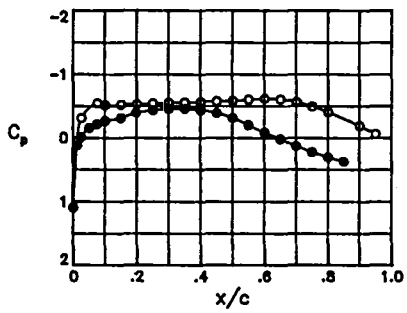

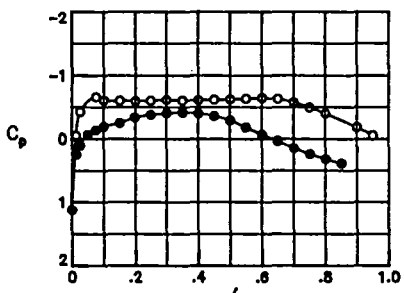

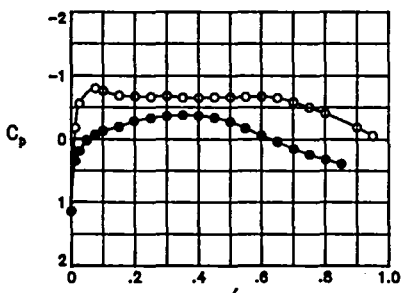

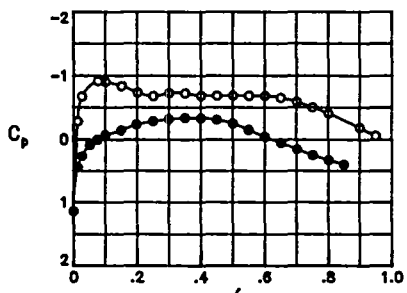

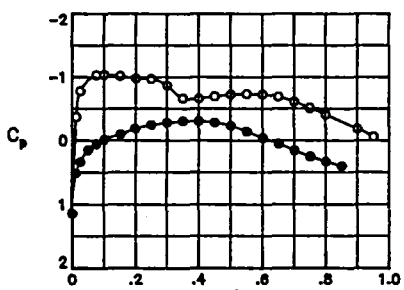

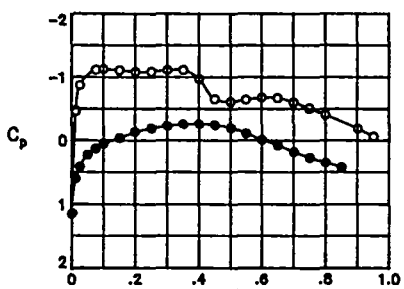

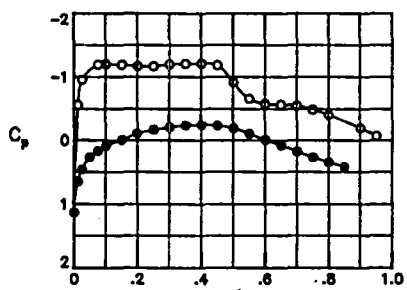

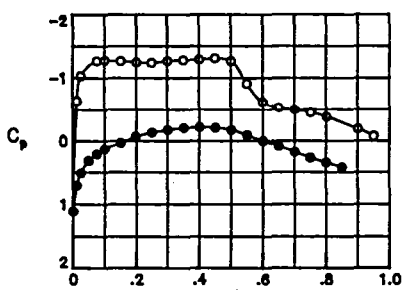

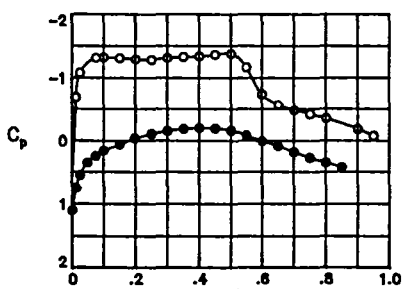

TEST	167
RUN	13
MACH	.740
R	10.0 x 10^6

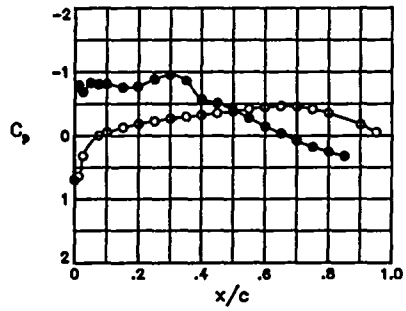

α=-4.03

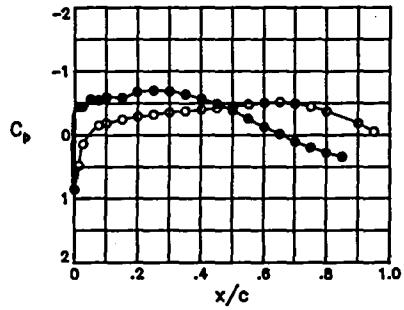

α=-3.01

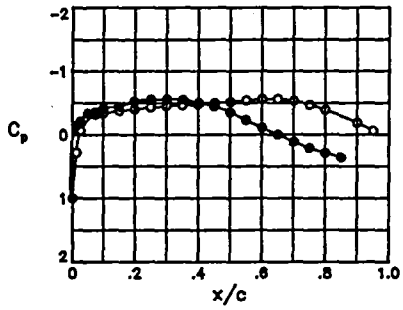

α=-2.00

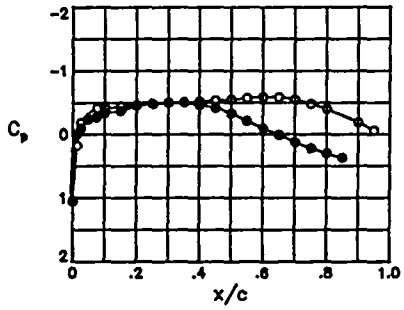

α=-1.49

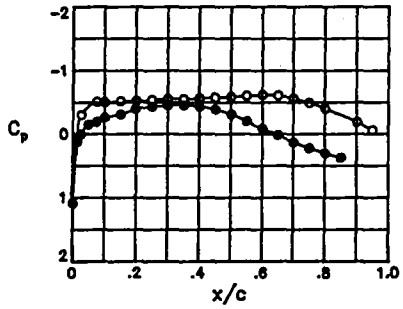

α=-1.00

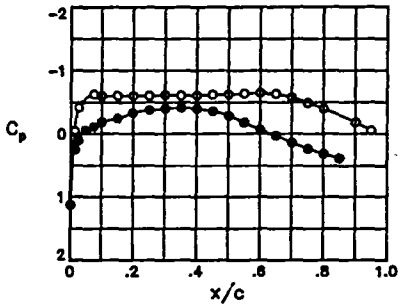

α=-.48

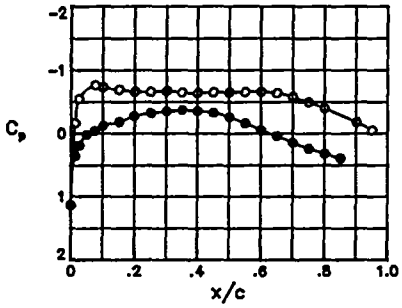

α=.02

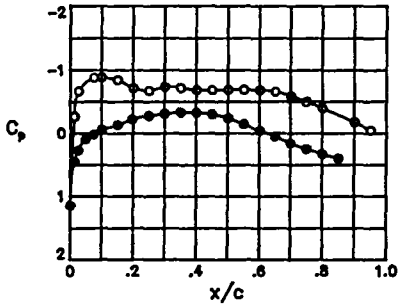

α=.51

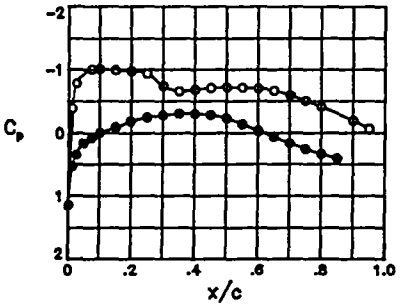

α=1.01

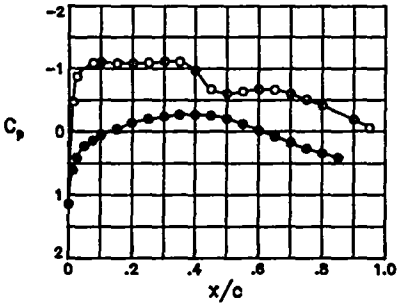

α=1.53

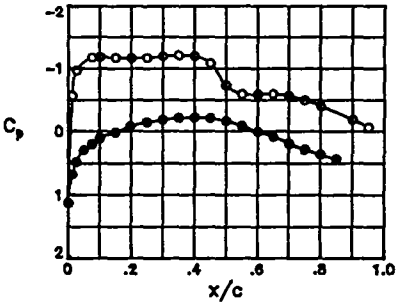

α=2.02

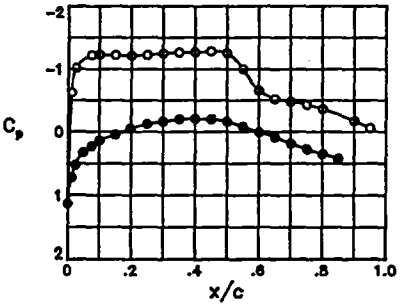

α=2.53

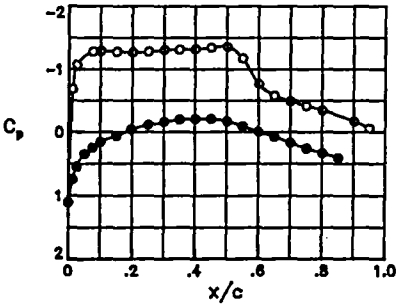

α=3.02

TEST	167
RUN	15
MACH	.740
R	15.0 x 10^6

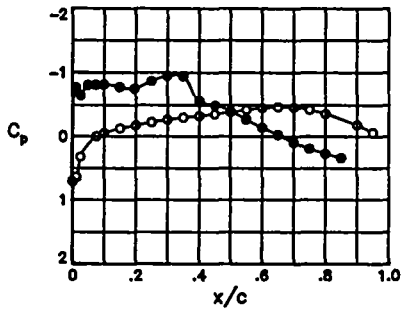

α=-4.04

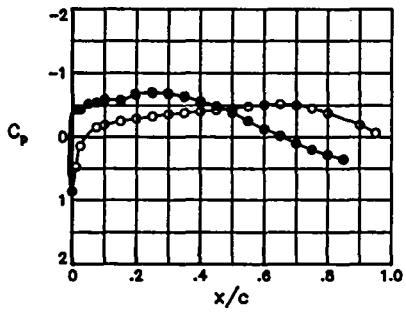

α=-2.99

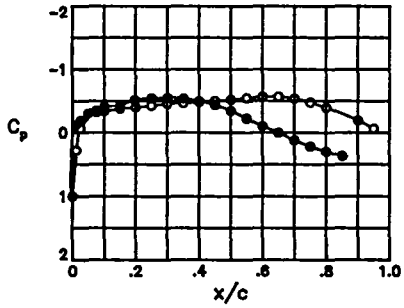

α=-1.98

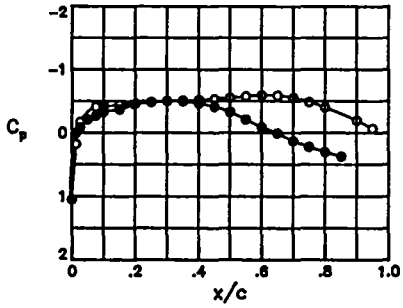

α=-1.50

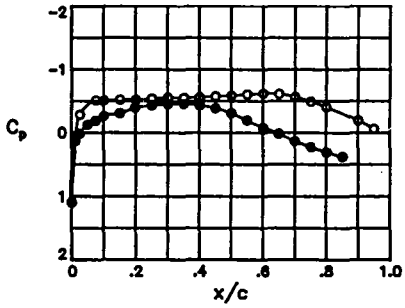

α=-1.00

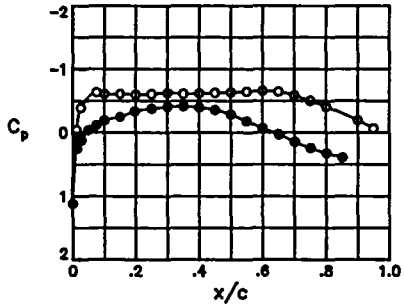

α=-.54

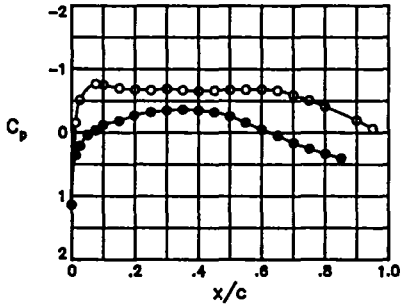

α=-.03

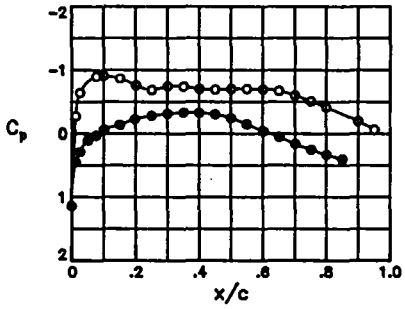

α=.52

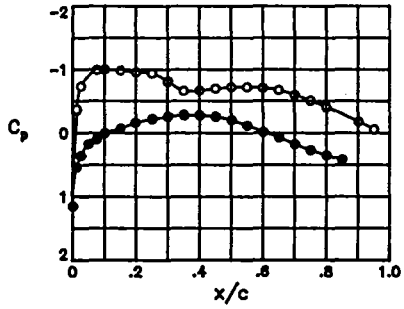

α=1.01

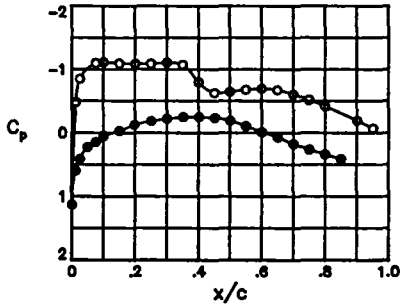

α=1.52

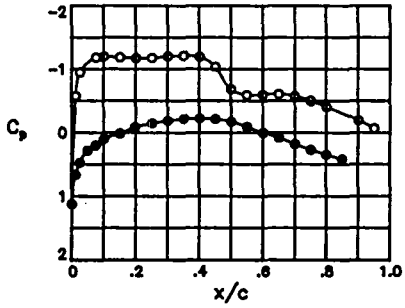

α=2.02

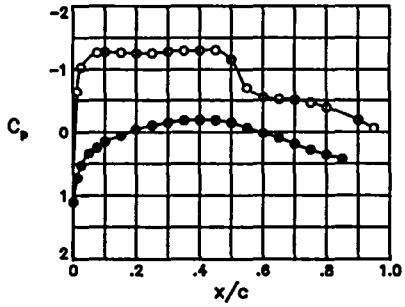

α=2.53

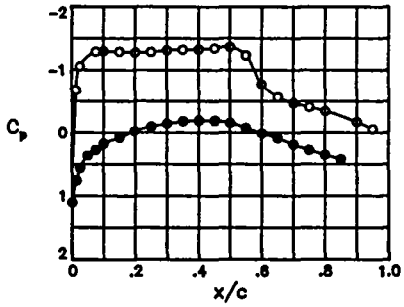

α=3.03

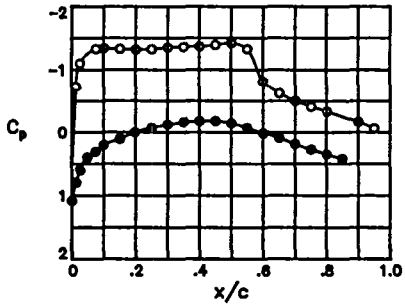

α=3.51

TEST	167
RUN	10
MACH	.740
R	30.0 x 10^6

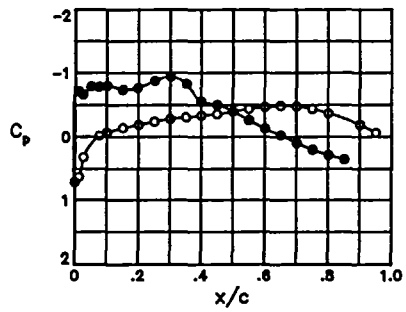

α=-3.99

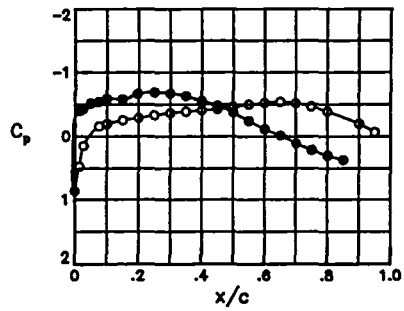

α=-2.99

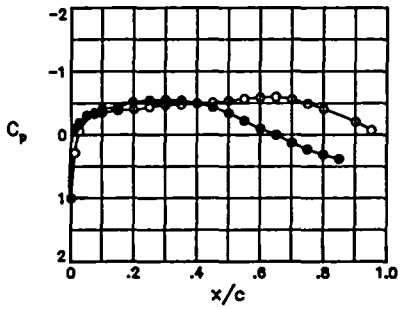

α=-2.01

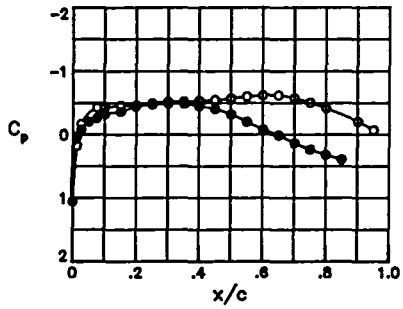

α=-1.51

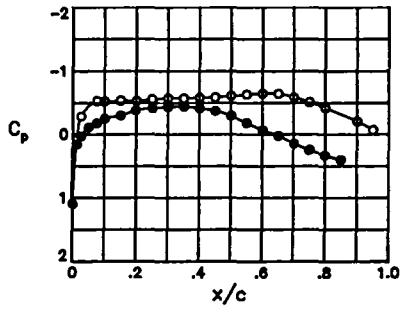

α=-1.00

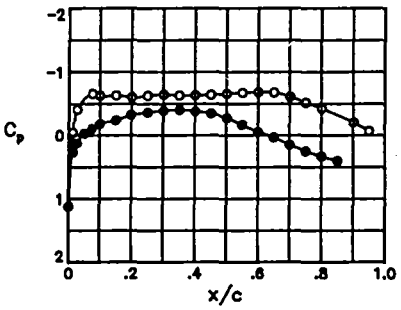

α=-.50

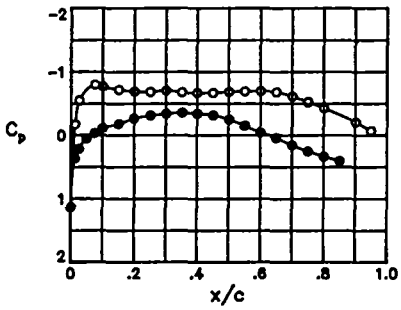

α=.01

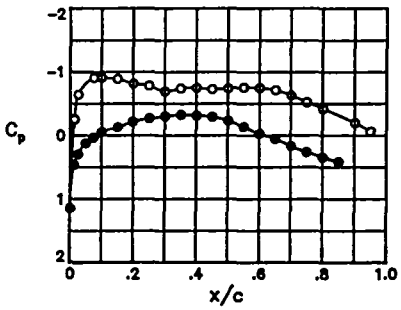

α=.52

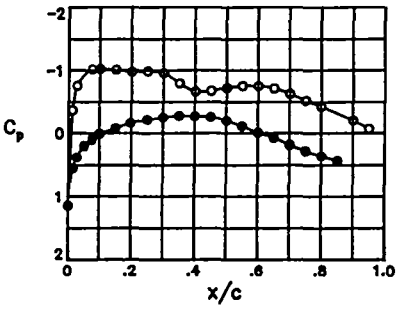

α=1.01

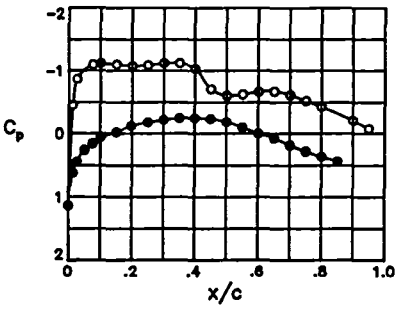

α=1.54

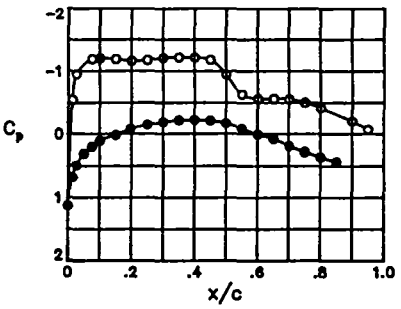

α=2.04

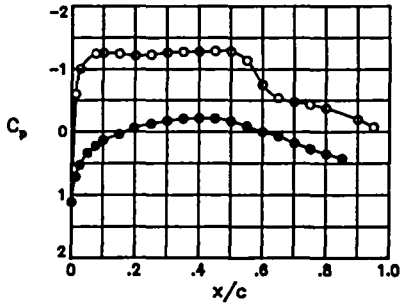

α=2.53

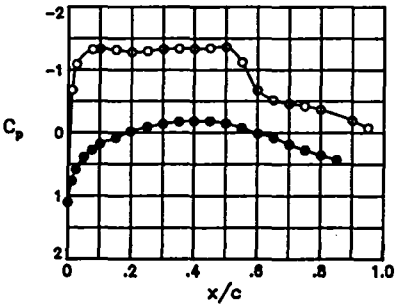

α=3.03

TEST	167
RUN	34
MACH	.740
R	40.0 x 10^6

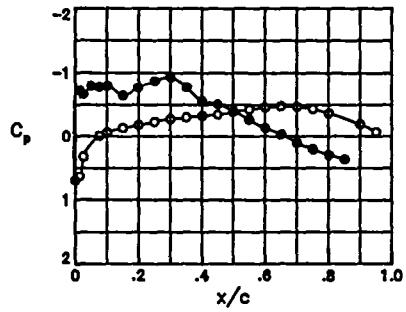

α=-4.01

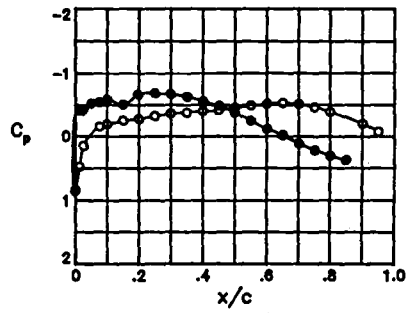

α=-3.01

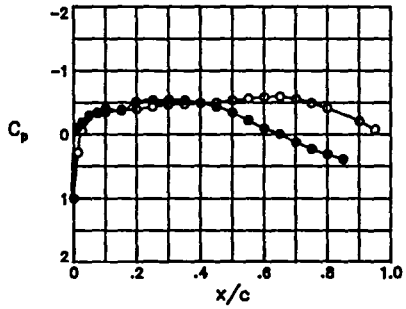

α=-2.00

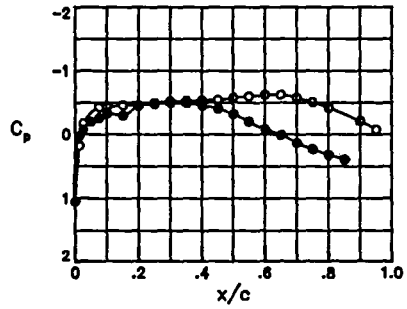

α=-1.50

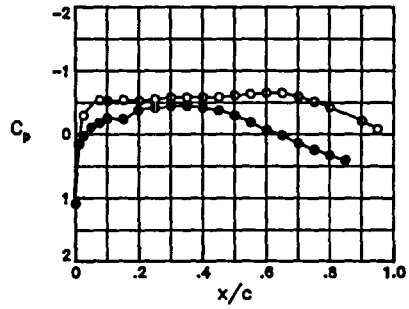

α=-.99

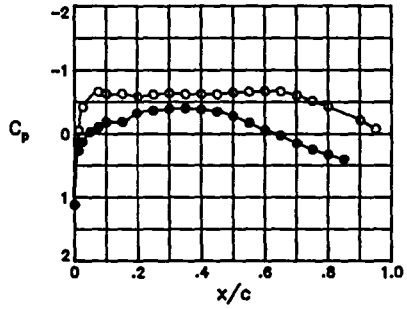

α=-.49

Appendix G

Pressure Data for $M = 0.75$; $R = 10.0 \times 10^6$, 15.0×10^6, and 30.0×10^6; Free Transition

The pressure measurements made on the NASA SC(3)-0712(B) airfoil are presented in coefficient form in graphs in this appendix. The data are for a given Mach number through the Reynolds number range. The pressure data from the upper surface of the airfoil are plotted as open symbols and the lower-surface data are plotted as solid symbols.

TEST	167
RUN	52
MACH	.750
R	10.0 x 10^6

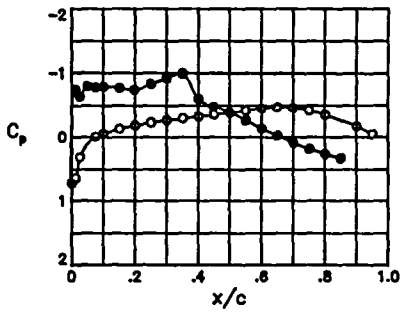

α=-3.98

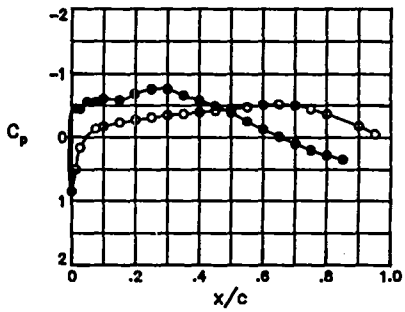

α=-3.06

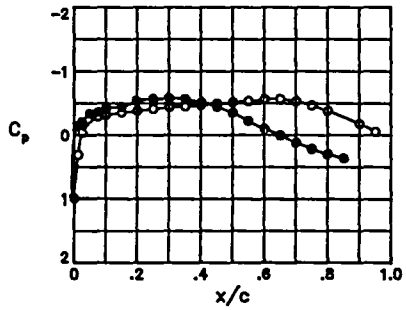

α=-2.05

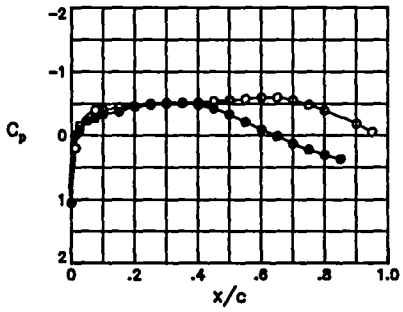

α=-1.49

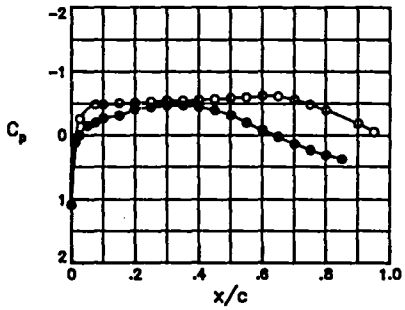

α=-1.03

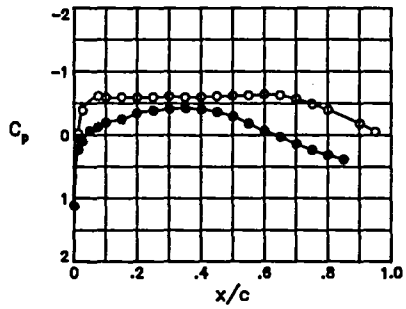

α=-.49

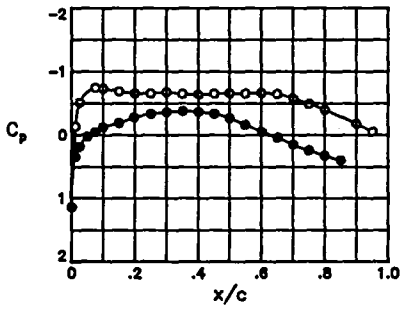

α=.01

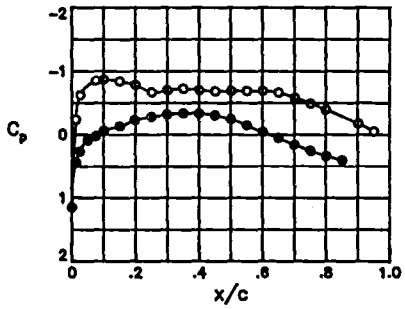

α=.52

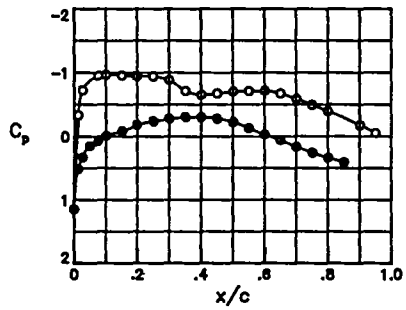

α=.99

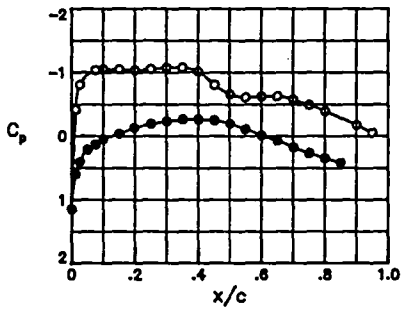

α=1.52

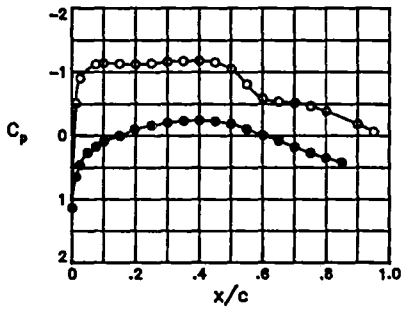

α=2.01

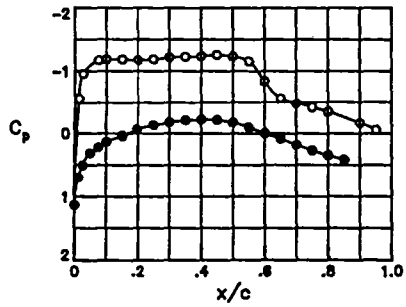

α=2.52

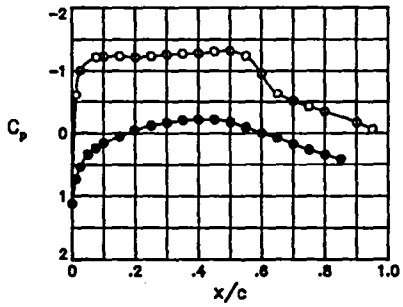

α=3.02

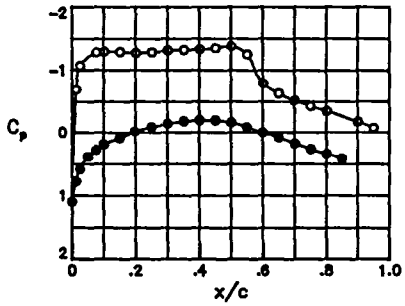

α=3.48

TEST	167
RUN	46
MACH	.750
R	15.0 x 10^6

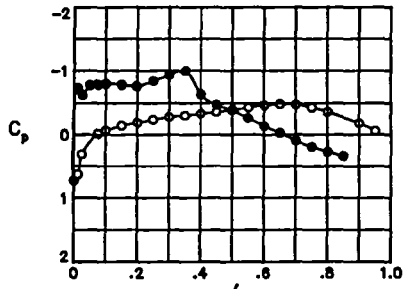

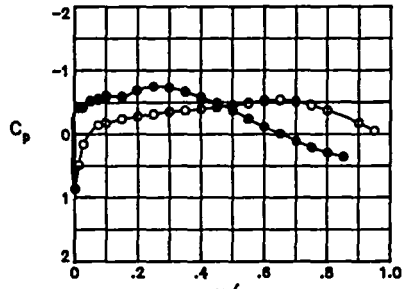

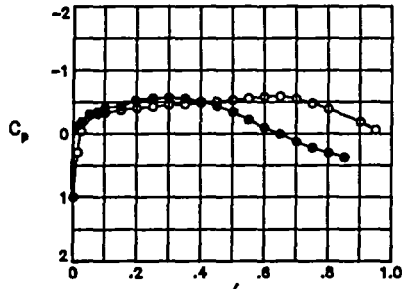

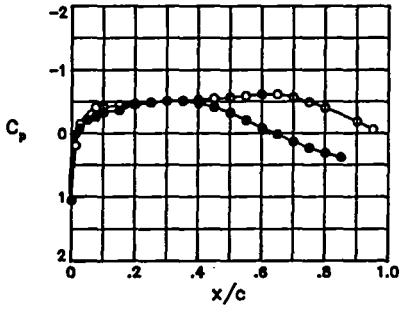

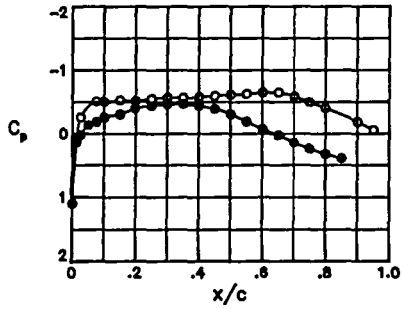

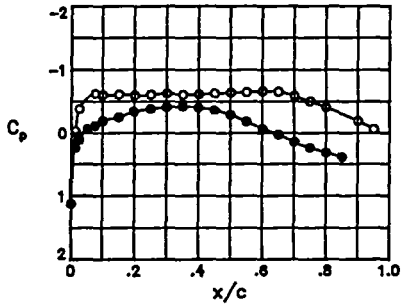

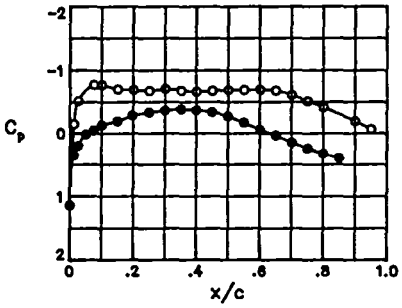

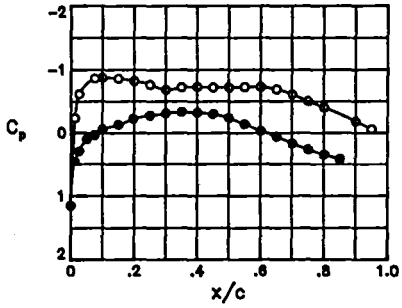

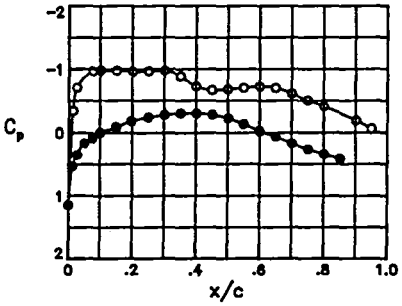

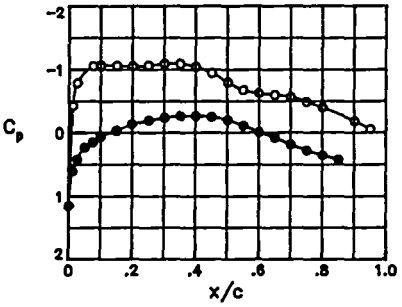

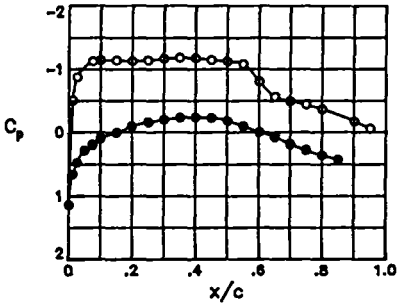

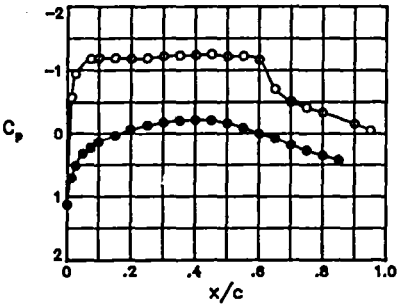

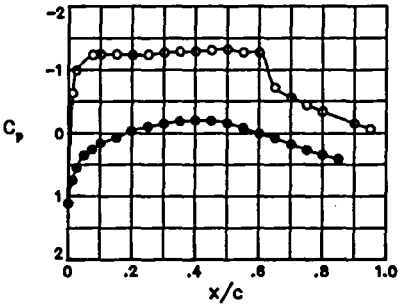

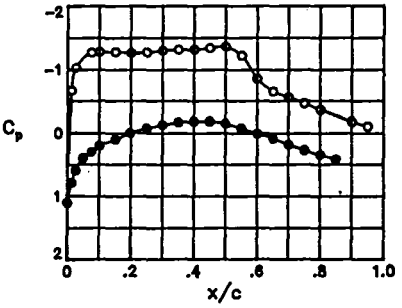

TEST	167
RUN	38
MACH	.750
R	30.0 x 10^6

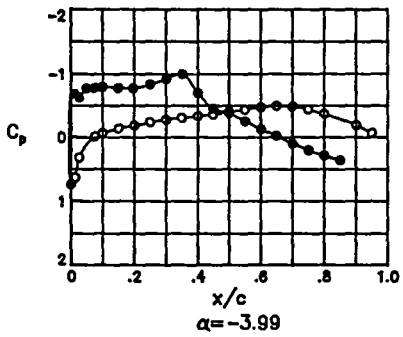

α=-3.99

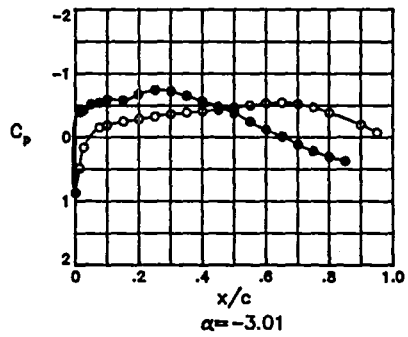

α=-3.01

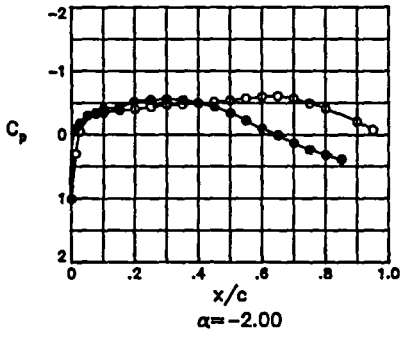

α=-2.00

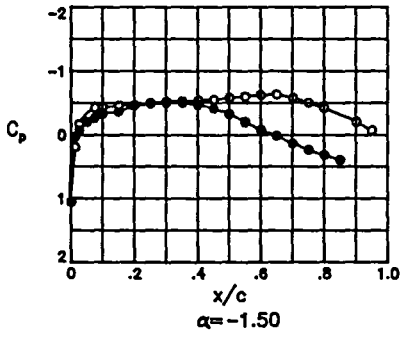

α=-1.50

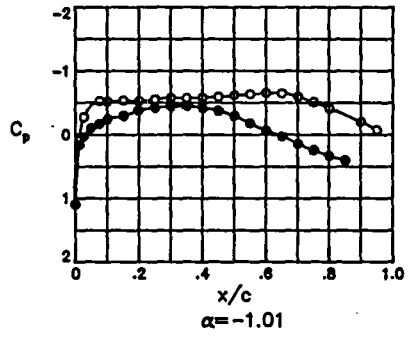

α=-1.01

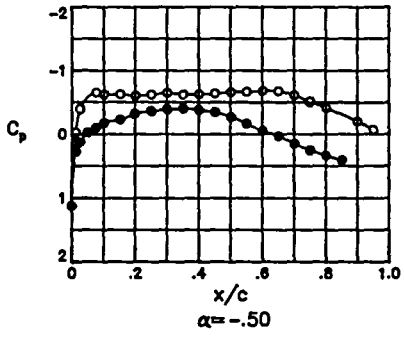

α=-.50

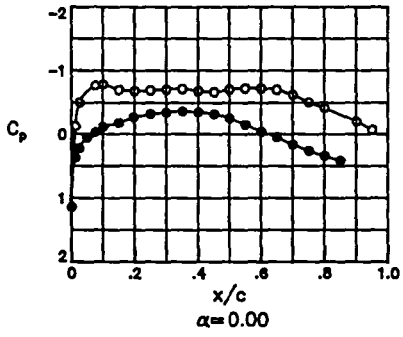

α=0.00

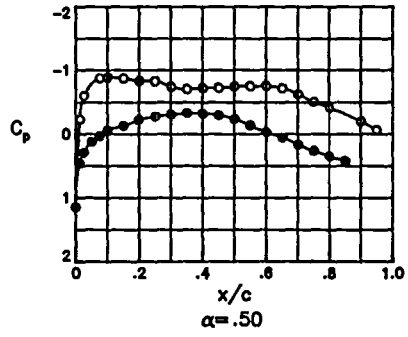

α=.50

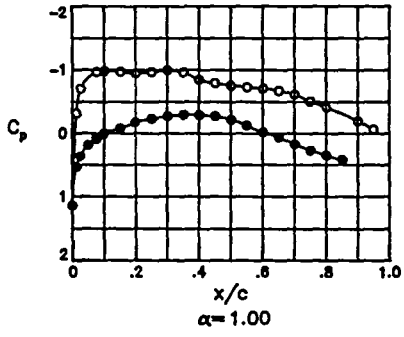

α=1.00

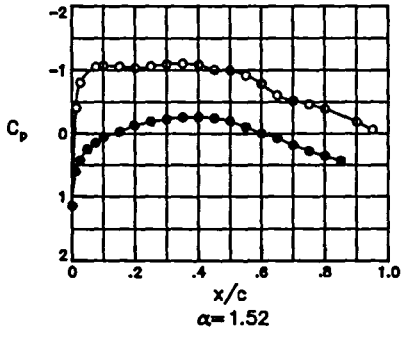

α=1.52

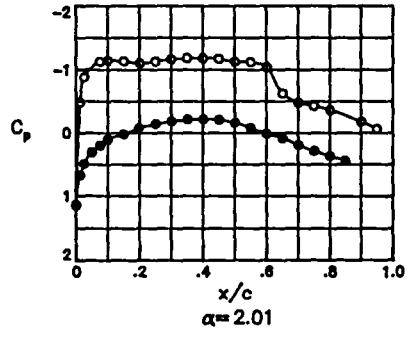

α=2.01

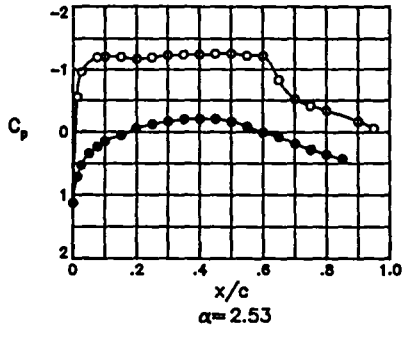

α=2.53

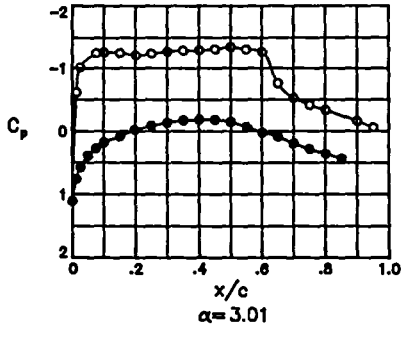

α=3.01

Appendix H

Pressure Data for $M = 0.76$; $R = 4.4 \times 10^6$, 7.0×10^6, 10.0×10^6, 15.0×10^6, 30.0×10^6, and 40.0×10^6; Free Transition

The pressure measurements made on the NASA SC(3)-0712(B) airfoil are presented in coefficient form in graphs in this appendix. The data are for a given Mach number through the Reynolds number range. The pressure data from the upper surface of the airfoil are plotted as open symbols and the lower-surface data are plotted as solid symbols.

TEST 167
RUN 1
MACH .760
R 4.4 x 10^6

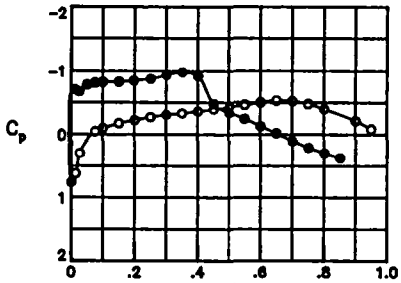

α=-4.01

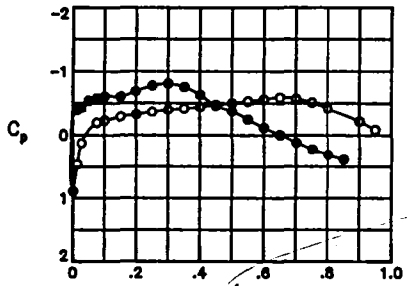

α=-2.98

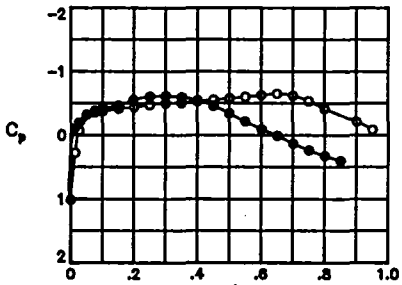

α=-1.99

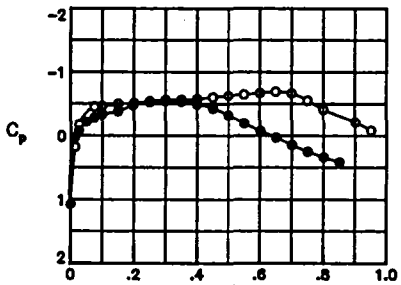

α=-1.49

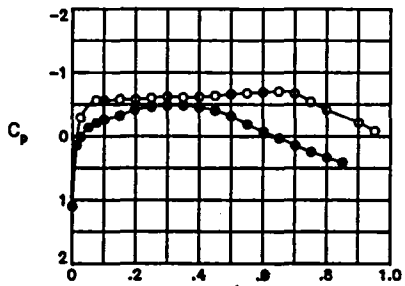

α=-1.00

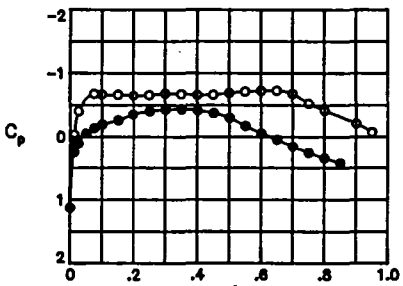

α=-.49

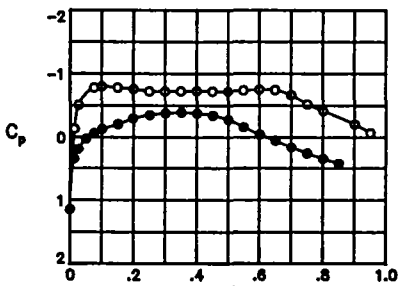

α=.02

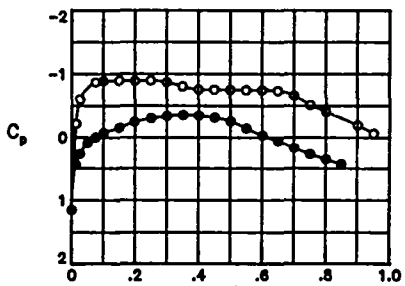

α=.52

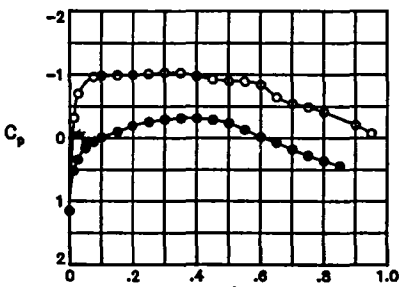

α=1.05

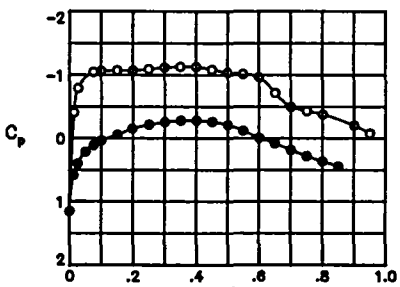

α=1.53

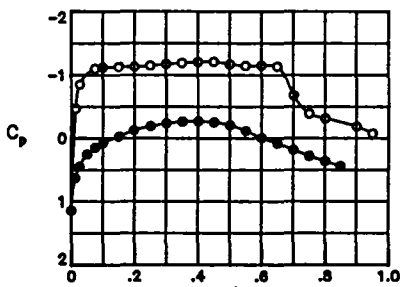

α=2.03

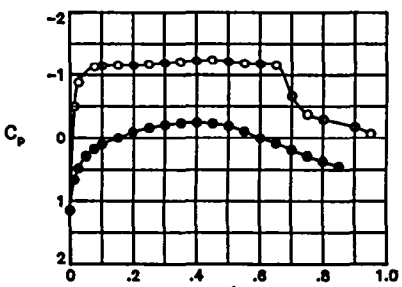

α=2.32

TEST	167
RUN	55
MACH	.760
R	4.4 x 10^6

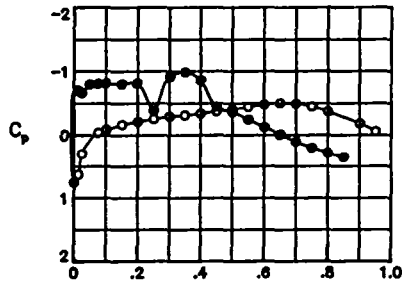

$\alpha = -4.00$

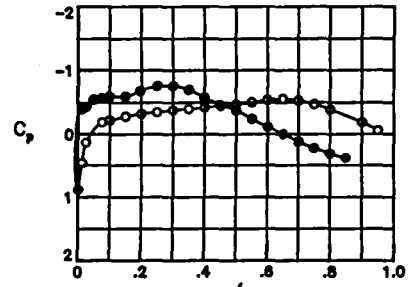

$\alpha = -2.96$

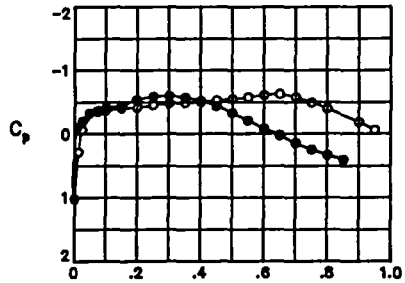

$\alpha = -2.00$

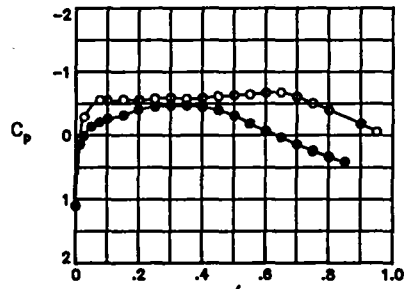

$\alpha = -1.00$

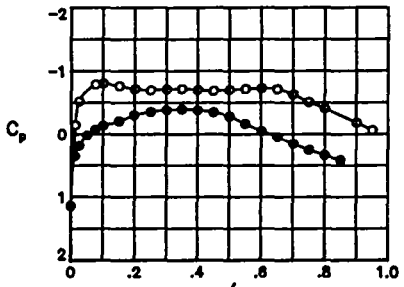

$\alpha = 0.00$

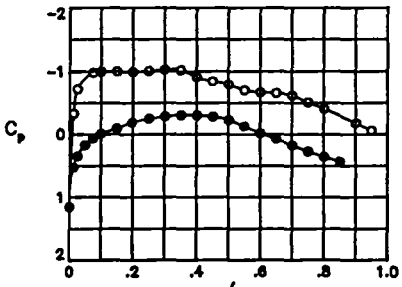

$\alpha = 1.01$

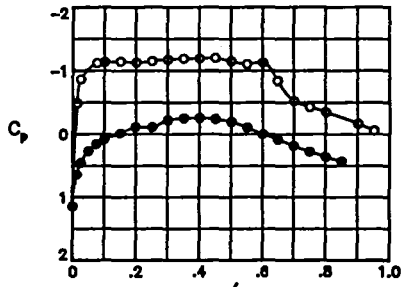

$\alpha = 2.00$

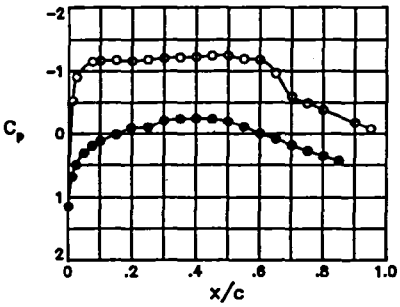

$\alpha = 2.50$

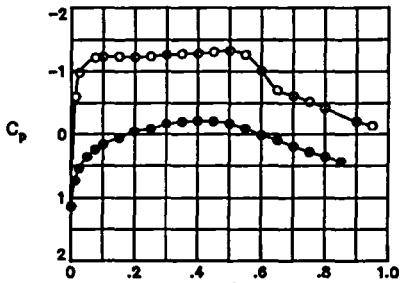

$\alpha = 3.00$

TEST	167
RUN	2
MACH	.760
R	7.0 x 10^6

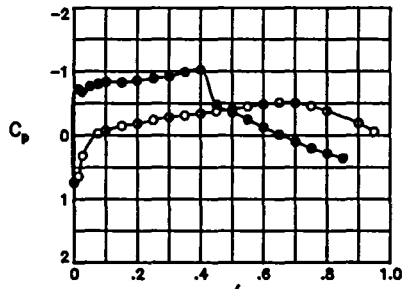

α=-4.06

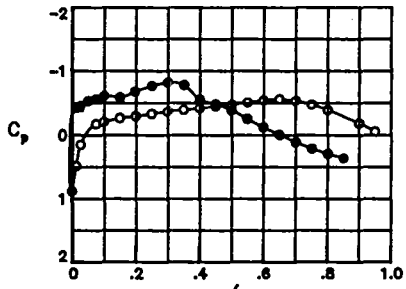

α=-3.01

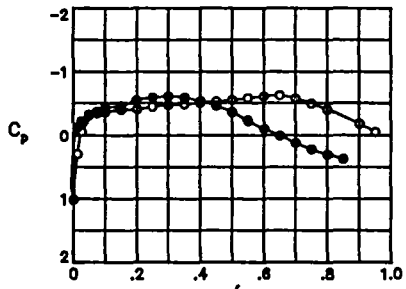

α=-1.98

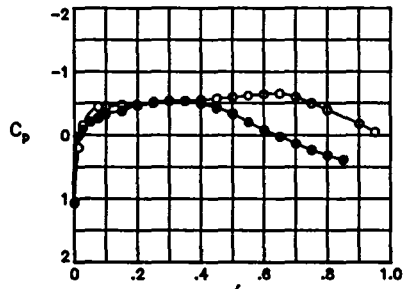

α=-1.48

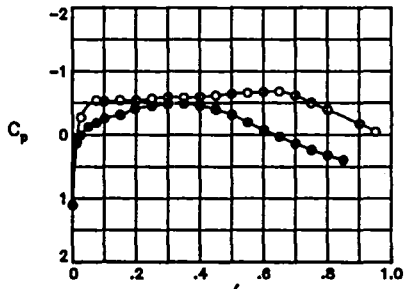

α=-.97

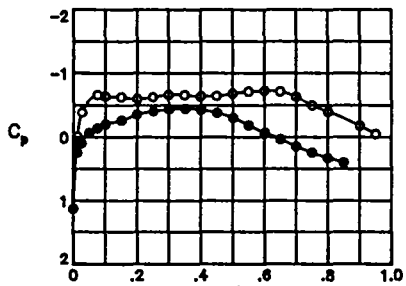

α=-.47

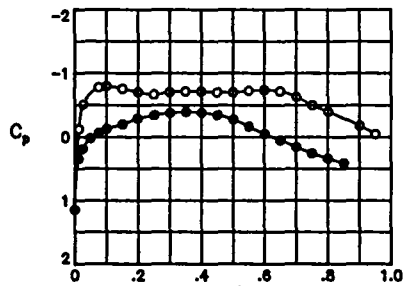

α=.04

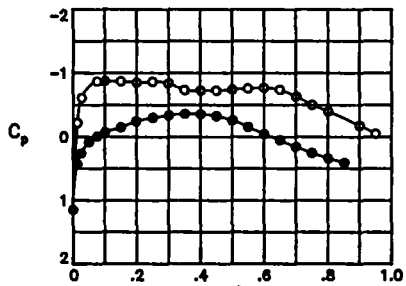

α=.52

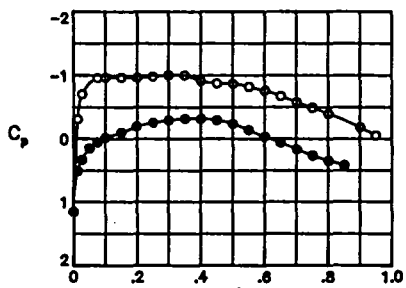

α=1.03

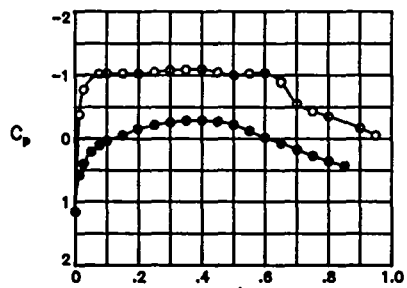

α=1.53

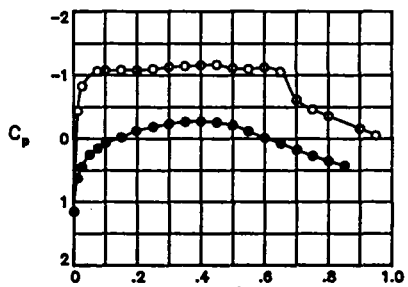

α=2.03

TEST	167
RUN	3
MACH	.760
R	7.0 x 10^6

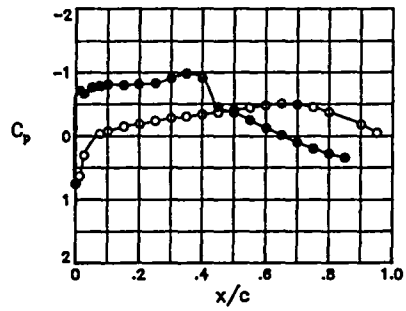

α=-4.01

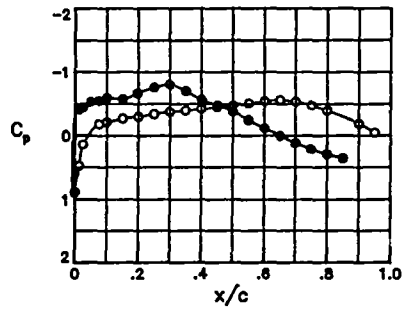

α=-2.99

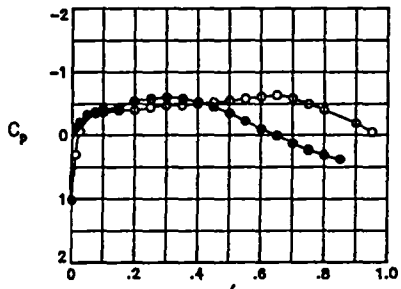

α=-2.00

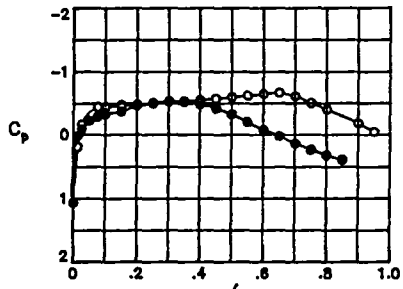

α=-1.49

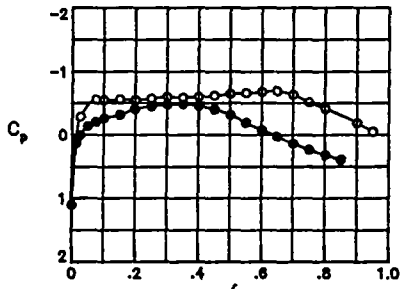

α=-.99

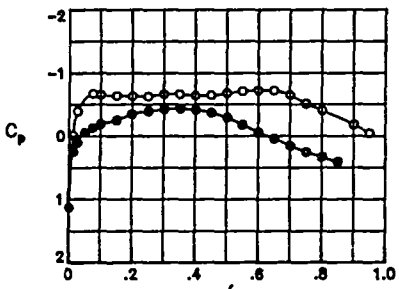

α=-.50

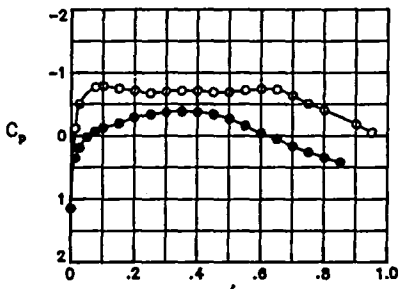

α=0.00

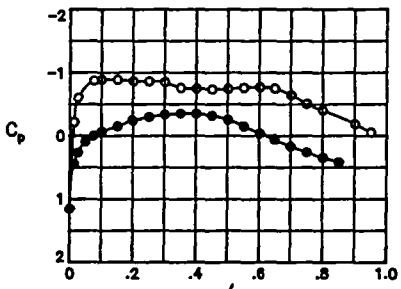

α=.50

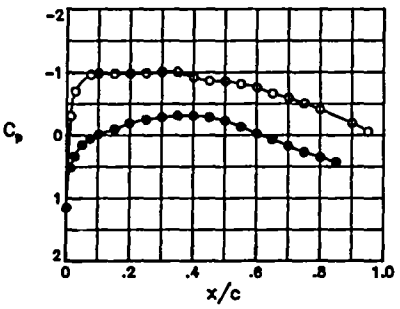

α=.99

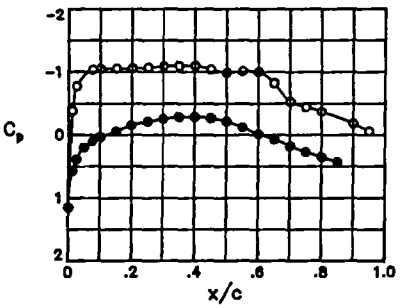

α=1.49

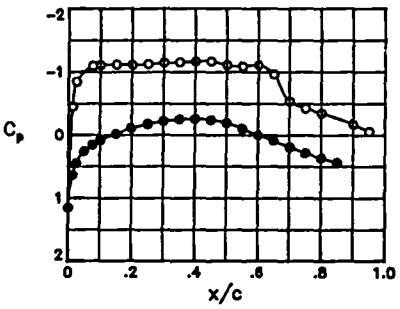

α=1.94

TEST 167
RUN 6
MACH .760
R 10.0 x 10^6

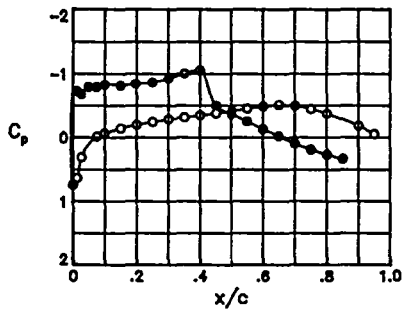

α=-4.01

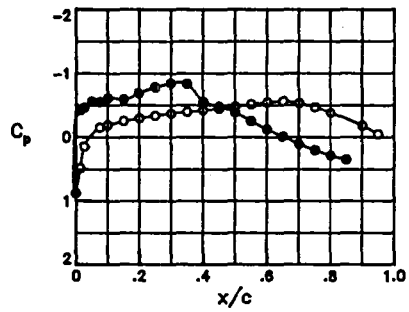

α=-2.99

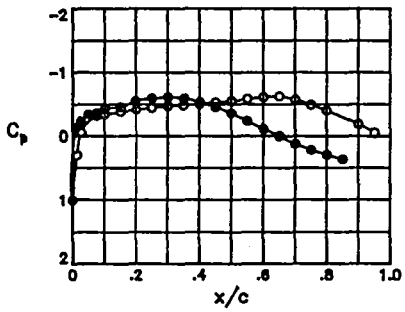

α=-2.00

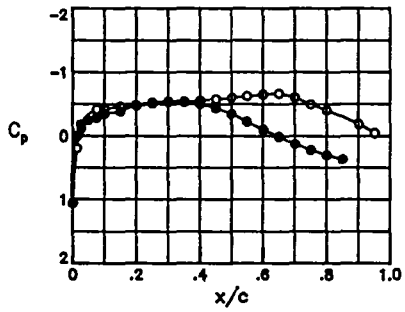

α=-1.49

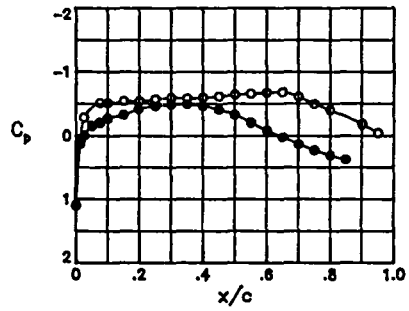

α=-.99

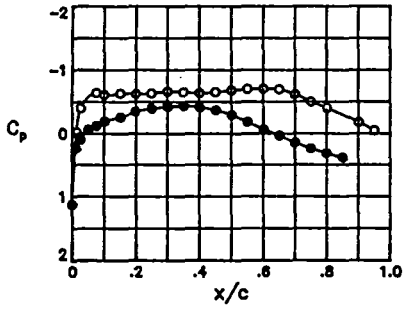

α=-.49

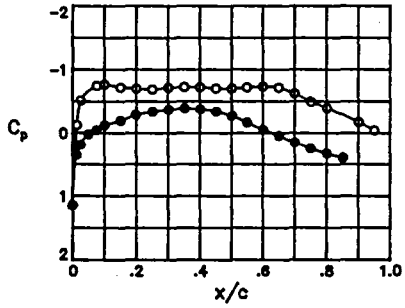

α=.02

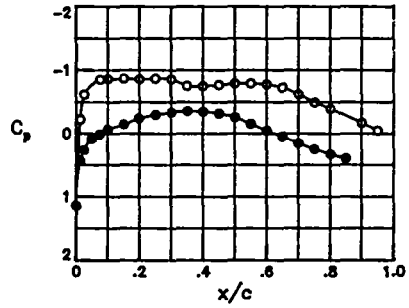

α=.52

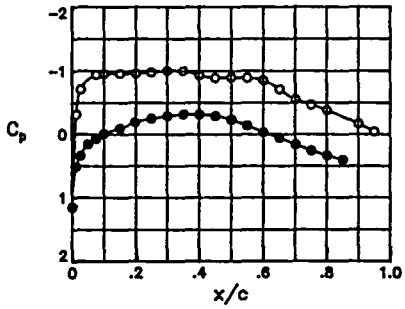

α=1.03

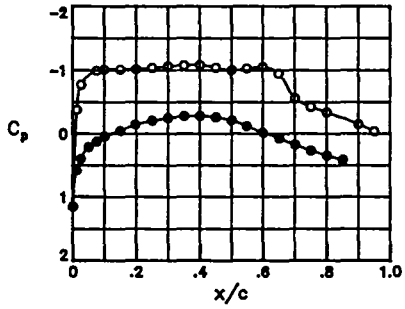

α=1.52

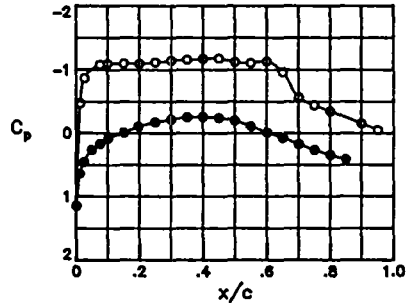

α=2.02

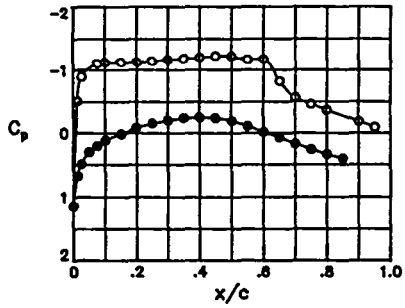

α=2.52

TEST	167
RUN	7
MACH	.760
R	15.0 x 10^6

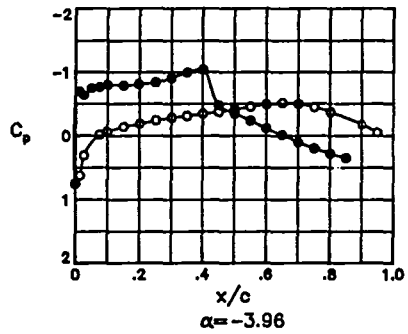

α=-3.96

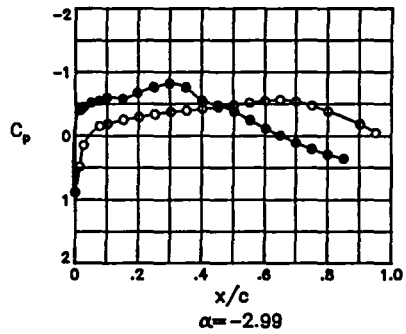

α=-2.99

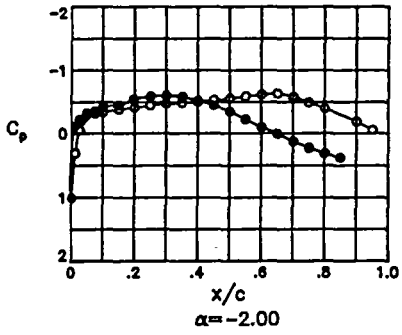

α=-2.00

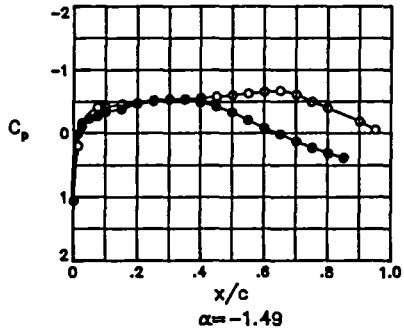

α=-1.49

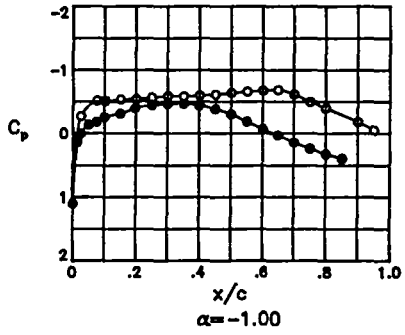

α=-1.00

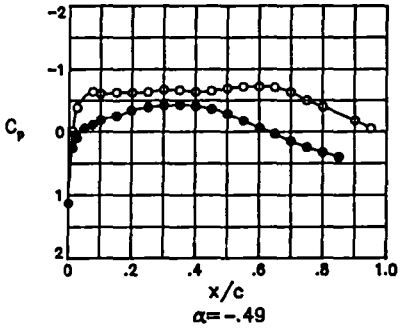

α=-.49

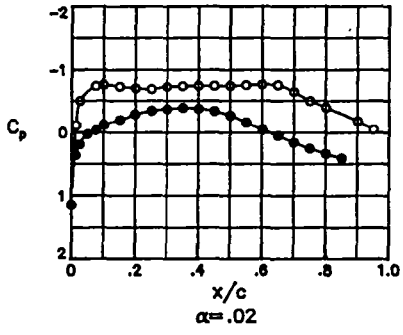

α=.02

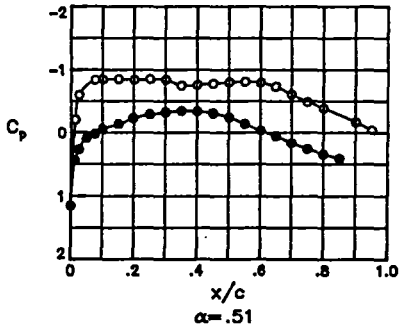

α=.51

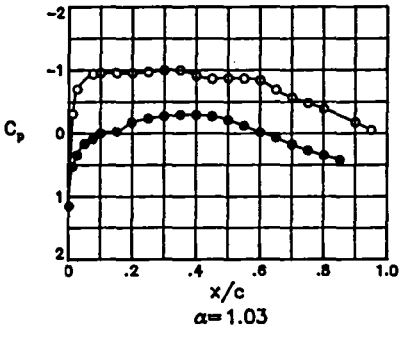

α=1.03

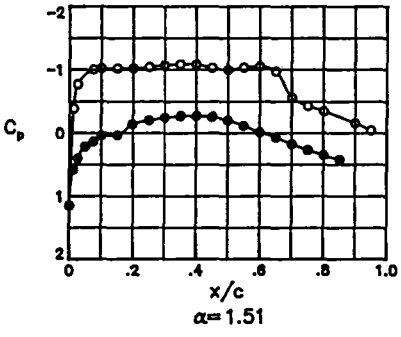

α=1.51

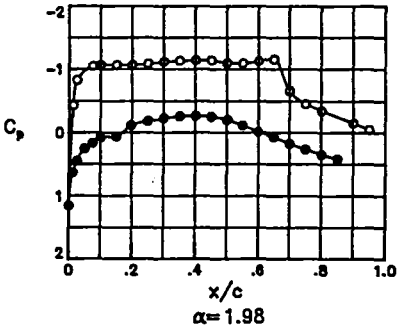

α=1.98

TEST	167
RUN	8
MACH	.760
R	30.0 x 10^6

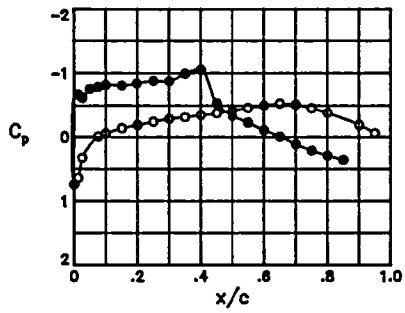

α=-4.02

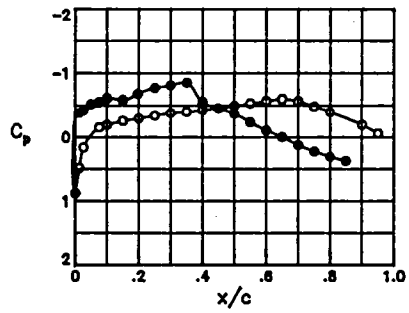

α=-2.99

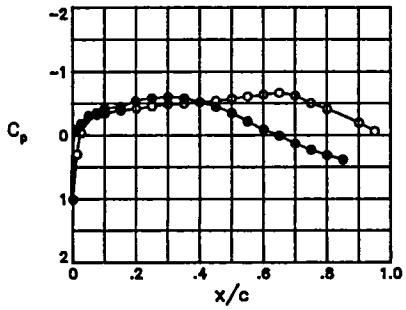

α=-1.99

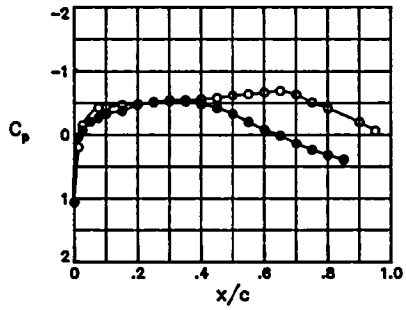

α=-1.49

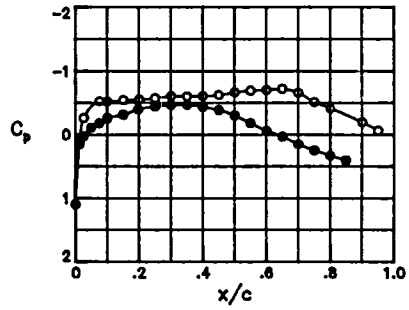

α=-1.00

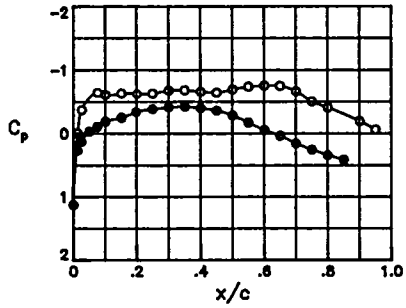

α=-.49

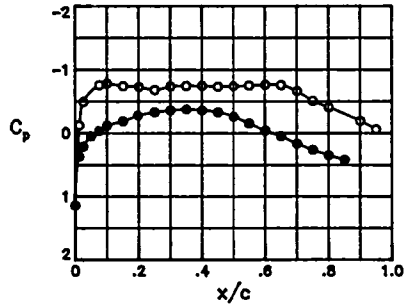

α=.04

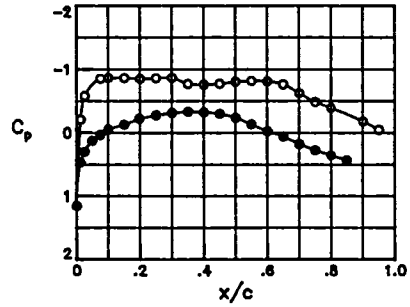

α=.53

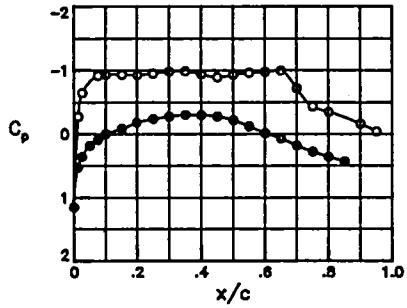

α=1.02

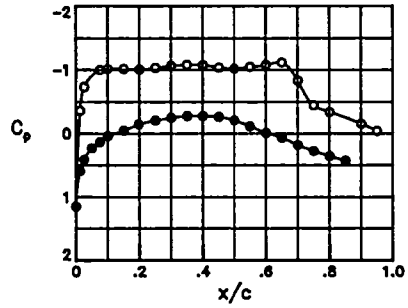

α=1.52

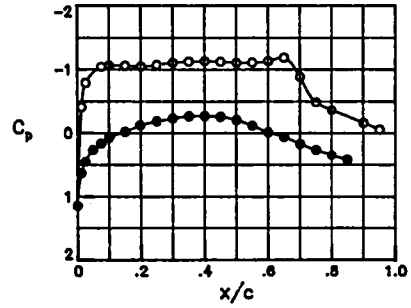

α=1.99

TEST	167
RUN	16
MACH	.760
R	30.0 x 10^6

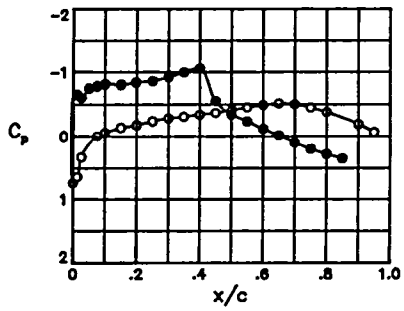

α=-4.00

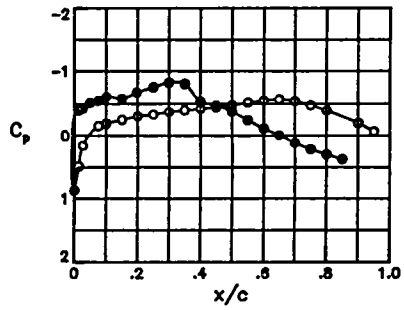

α=-2.99

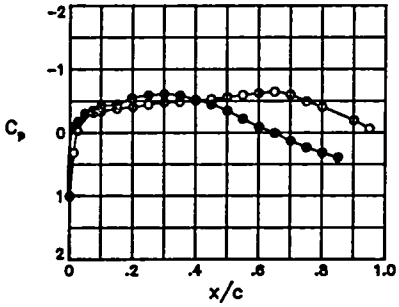

α=-1.99

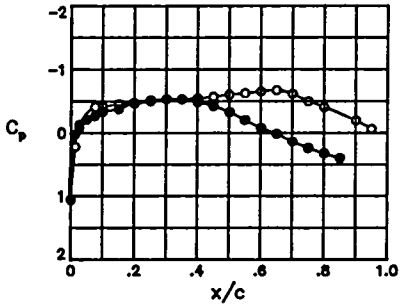

α=-1.49

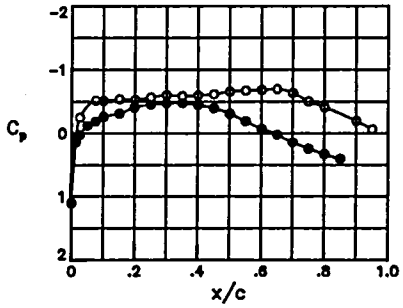

α=-.99

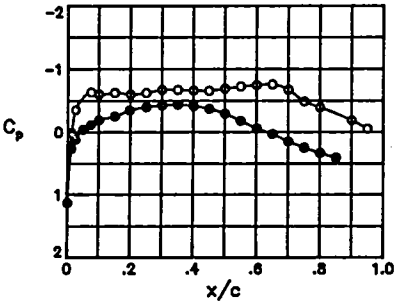

α=-.48

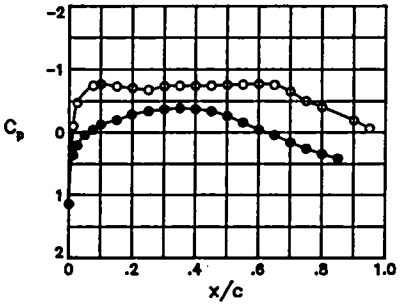

α=.03

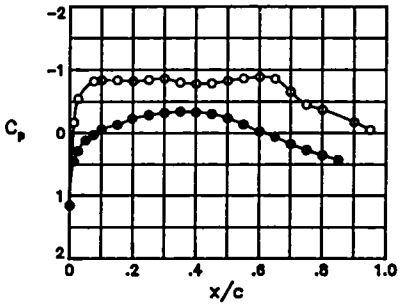

α=.52

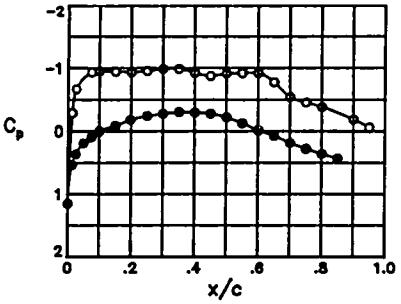

α=1.03

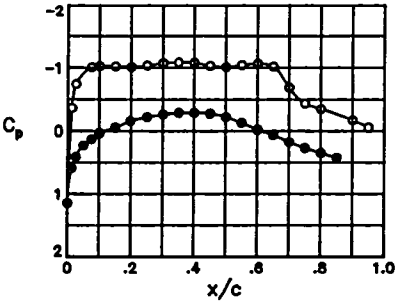

α=1.54

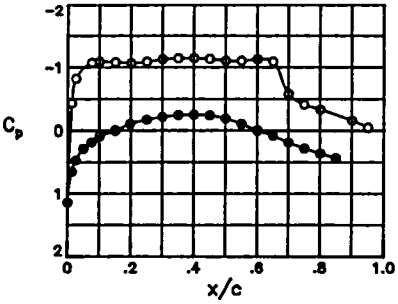

α=2.01

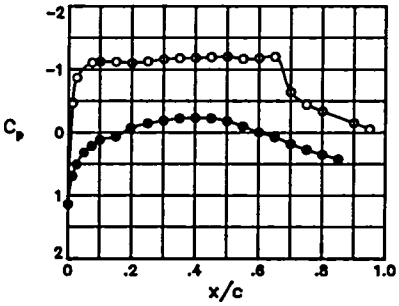

α=2.53

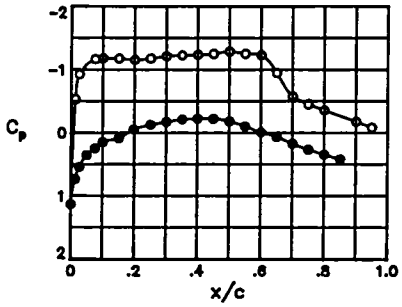

α=3.02

TEST	167
RUN	16
MACH	.760
R	30.0 x 10^6

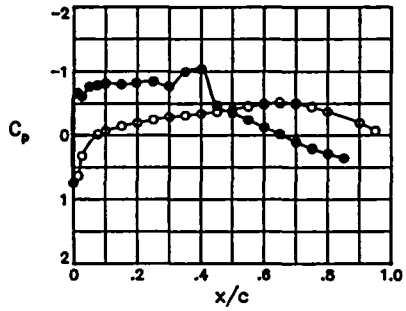

α=-3.99

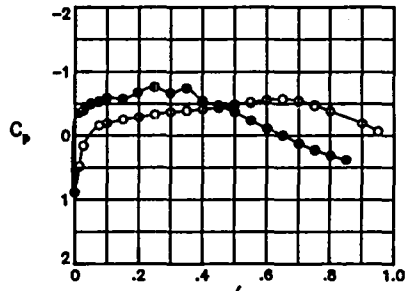

α=-2.98

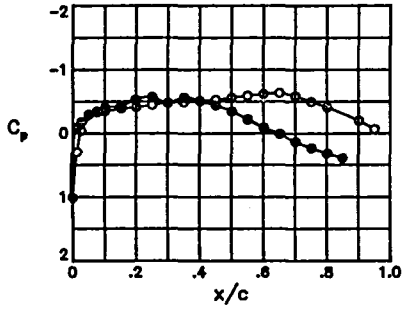

α=-1.99

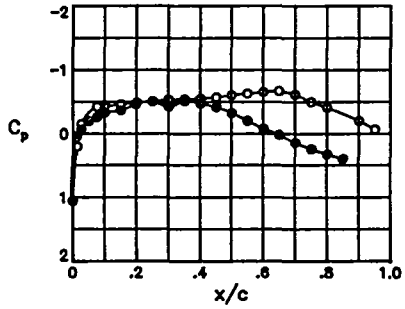

α=-1.49

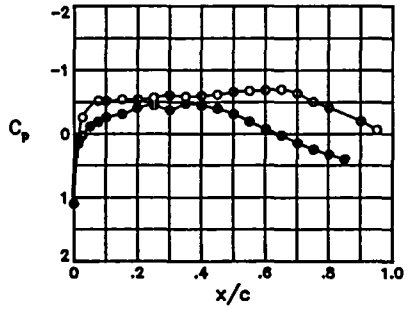

α=-1.01

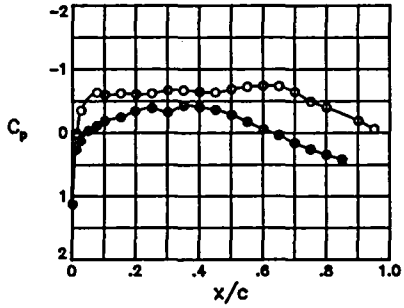

α=-.49

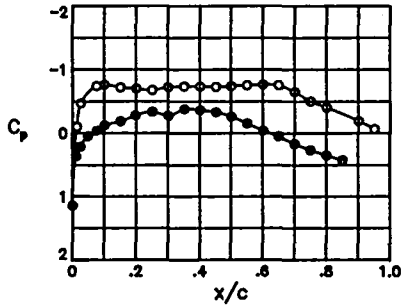

α=0.00

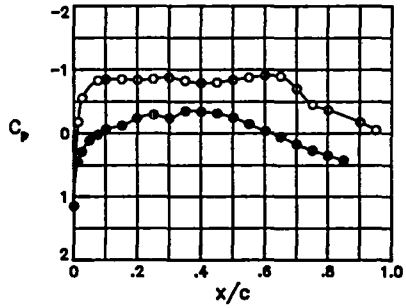

α=.55

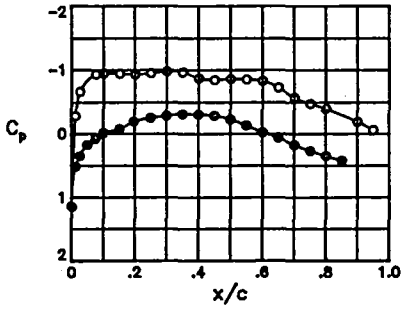

α=.95

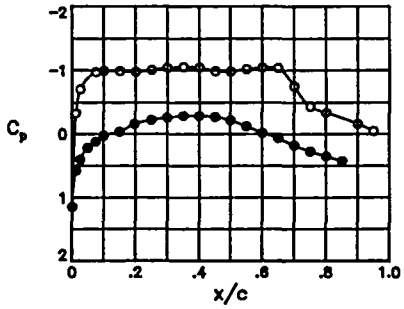

α=1.43

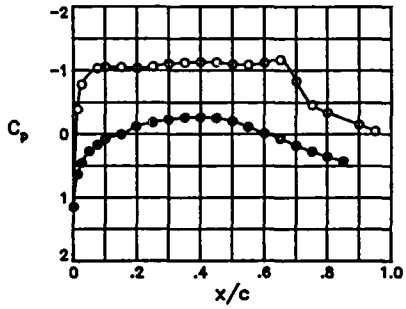

α=2.01

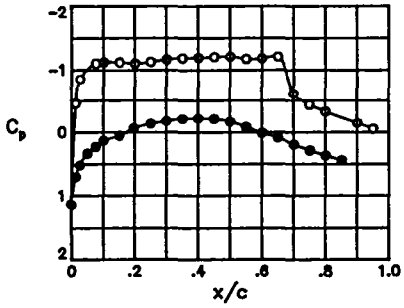

α=2.52

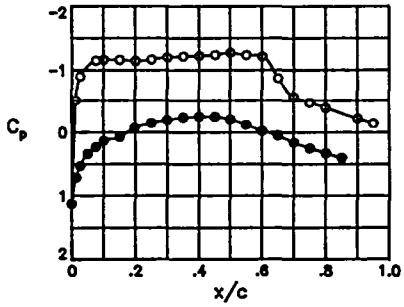

α=3.02

TEST	167
RUN	9
MACH	.760
R	40.0 x 10^6

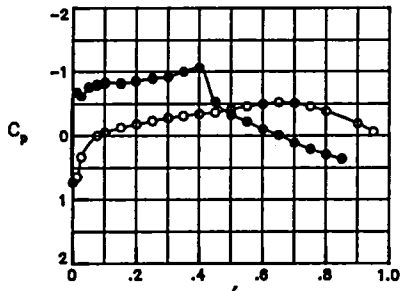

α=-4.10

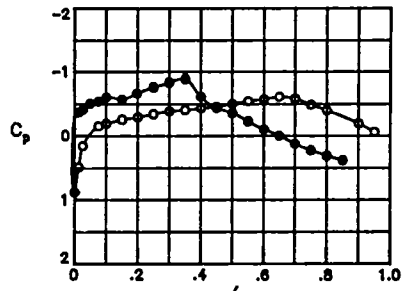

α=-2.99

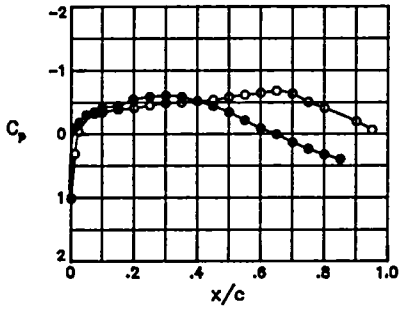

α=-2.02

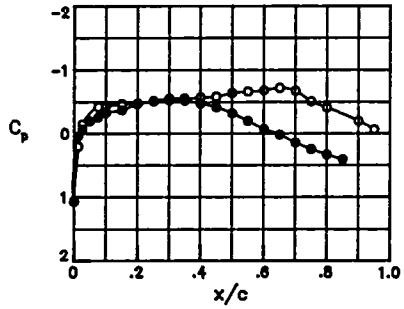

α=-1.49

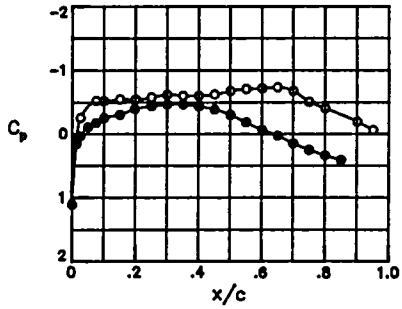

α=-.98

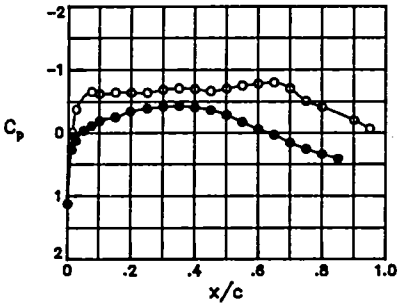

α=-.48

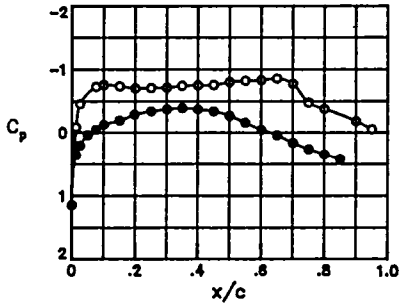

α=-.01

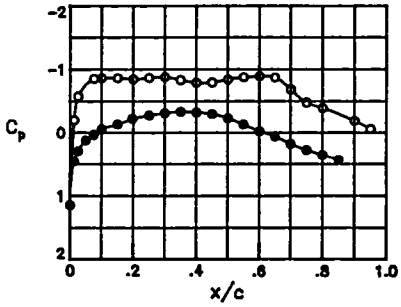

α=.52

Appendix I

Pressure Data for $M = 0.77$; $R = 10.0 \times 10^6$, 15.0×10^6, 30.0×10^6, and 40.0×10^6; Free Transition

The pressure measurements made on the NASA SC(3)-0712(B) airfoil are presented in coefficient form in graphs in this appendix. The data are for a given Mach number through the Reynolds number range. The pressure data from the upper surface of the airfoil are plotted as open symbols and the lower-surface data are plotted as solid symbols.

TEST	167
RUN	51
MACH	.770
R	10.0 x 10^6

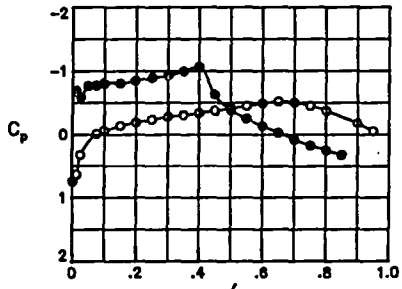

α=-3.99

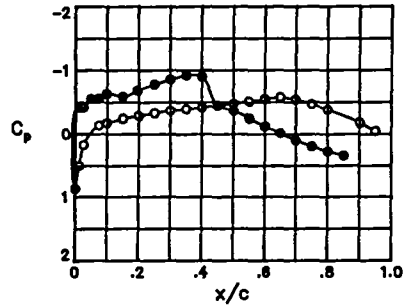

α=-2.99

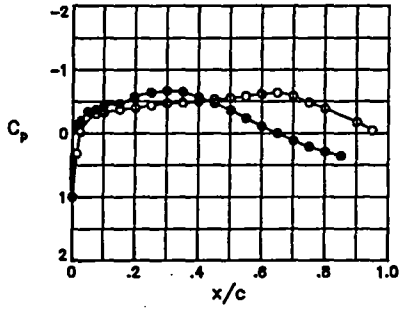

α=-1.97

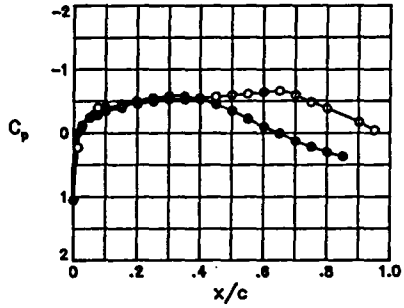

α=-1.49

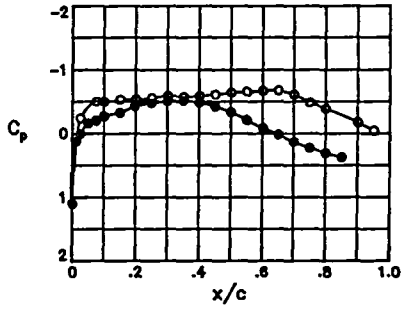

α=-.98

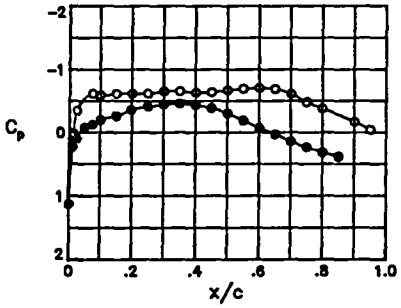

α=-.49

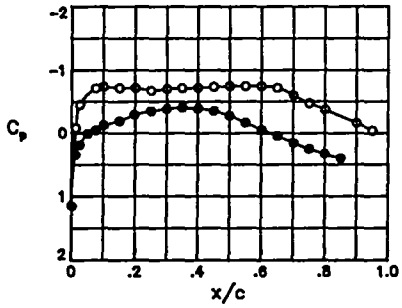

α=.04

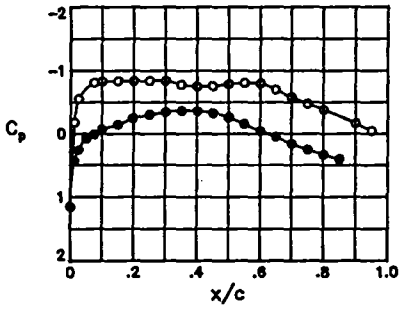

α=.52

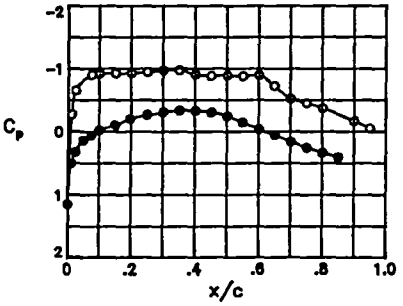

α=1.02

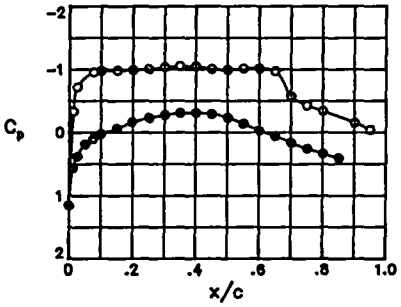

α=1.52

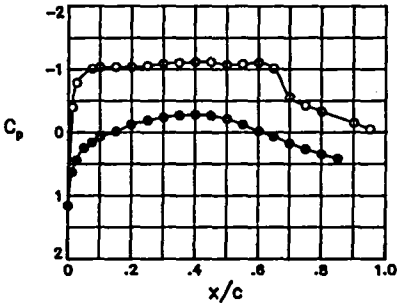

α=2.02

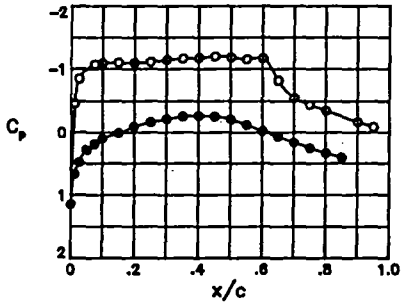

α=2.53

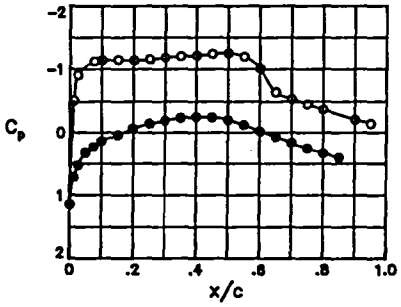

α=3.02

TEST	167
RUN	44
MACH	.770
R	15.0 x 10^6

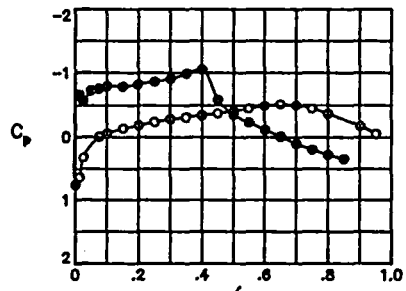

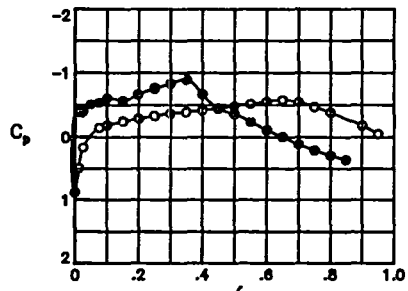

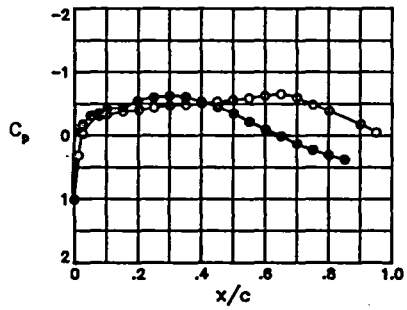

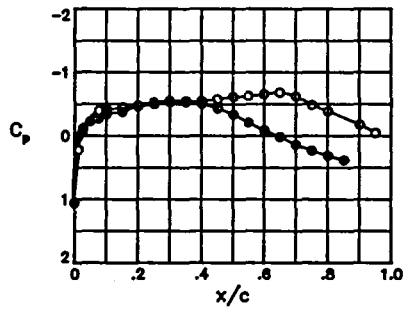

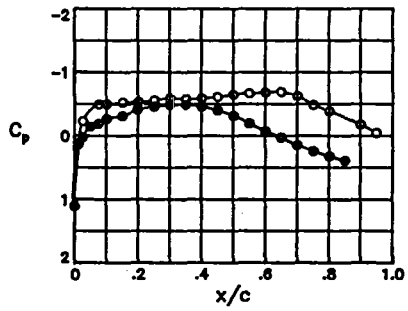

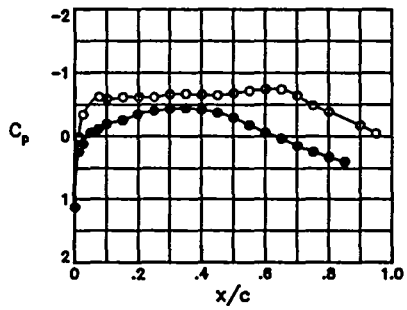

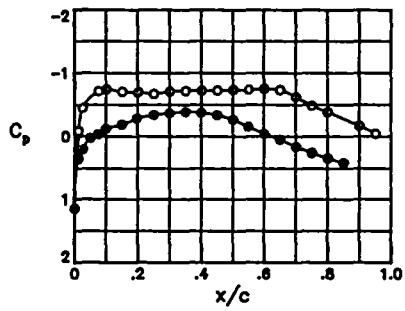

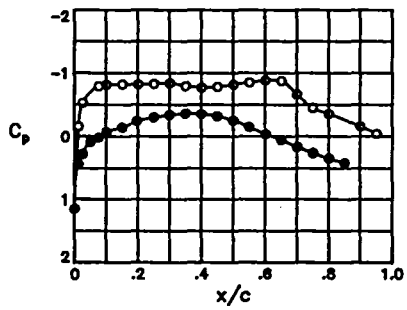

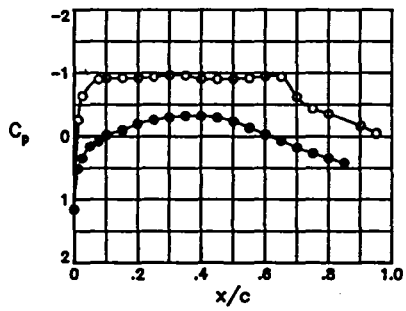

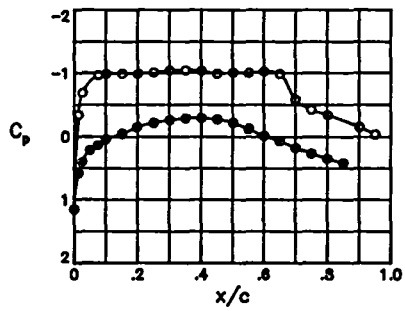

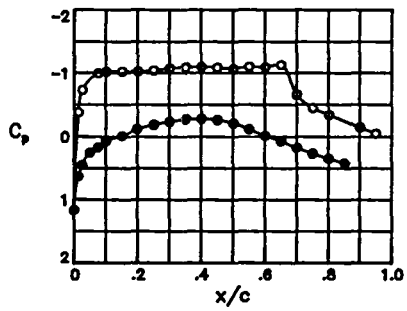

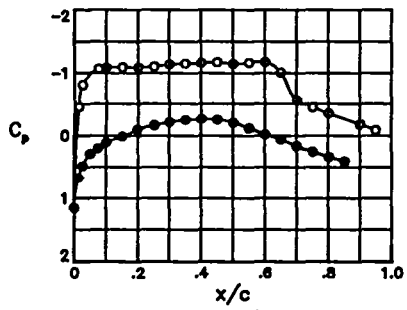

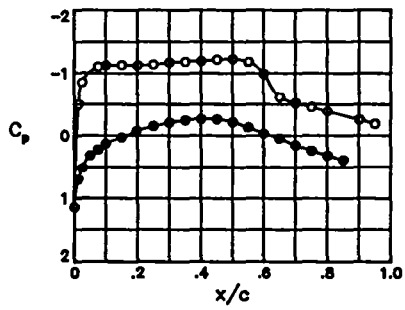

TEST	167
RUN	37
MACH	.770
R	30.0 x 10^6

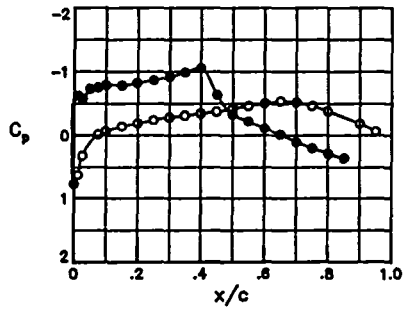

α=-3.98

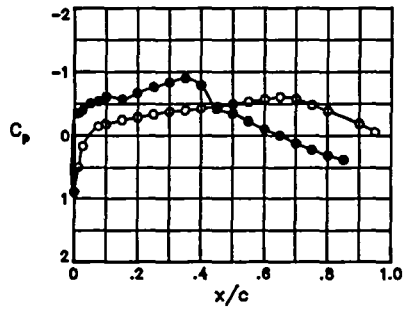

α=-2.99

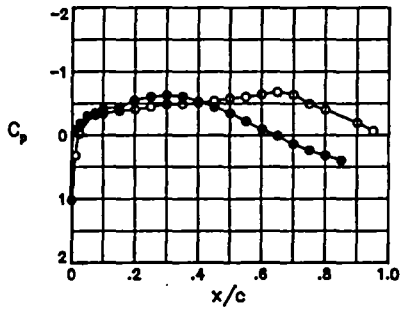

α=-2.00

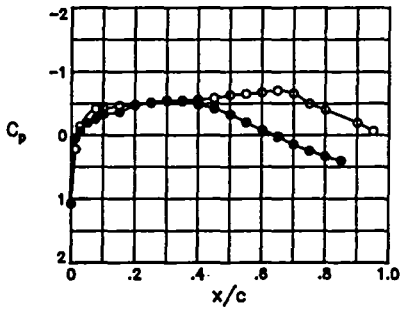

α=-1.48

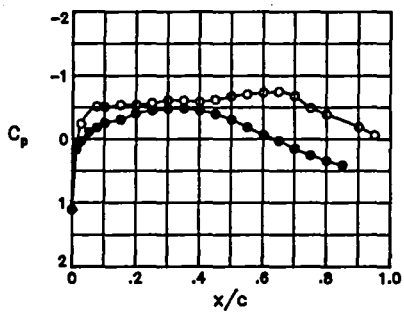

α=-1.00

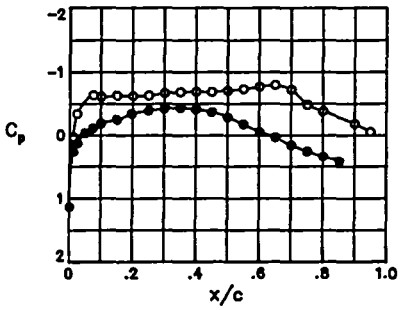

α=-.50

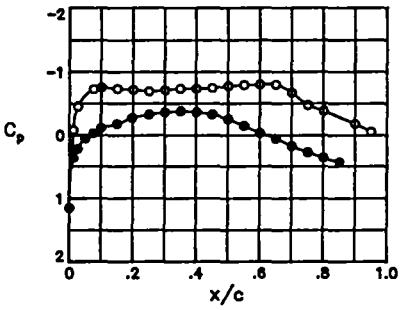

α=.02

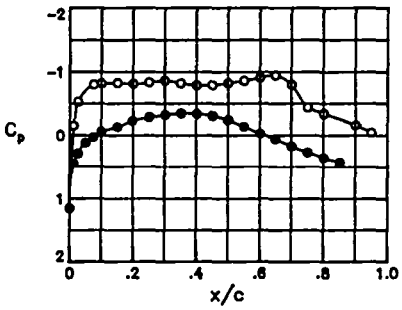

α=.52

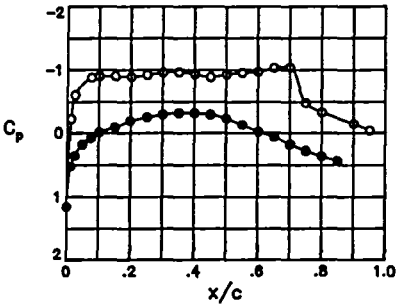

α=1.03

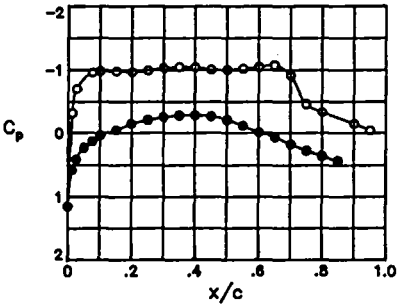

α=1.52

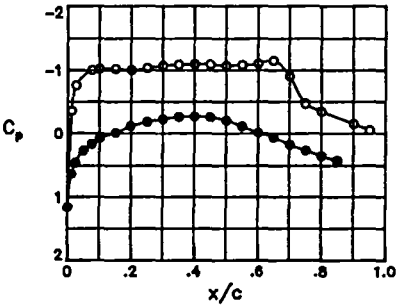

α=2.01

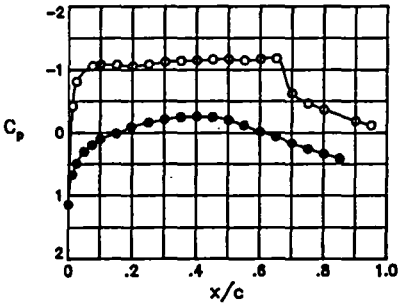

α=2.53

TEST	167
RUN	33
MACH	.770
R	40.0 x 10^6

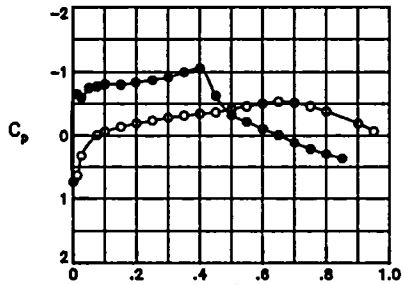

α=-4.00

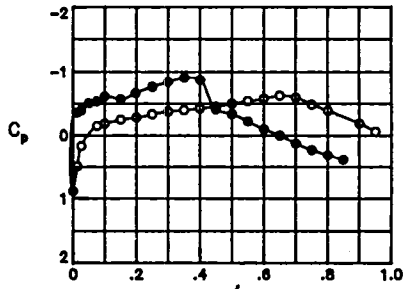

α=-2.97

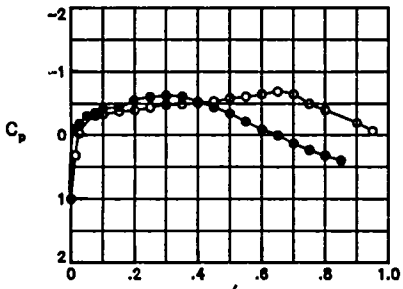

α=-2.03

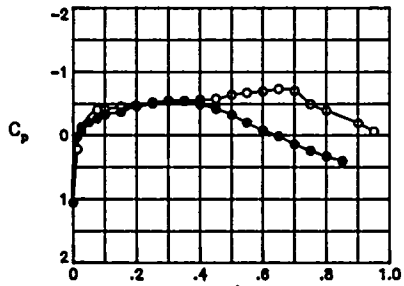

α=-1.51

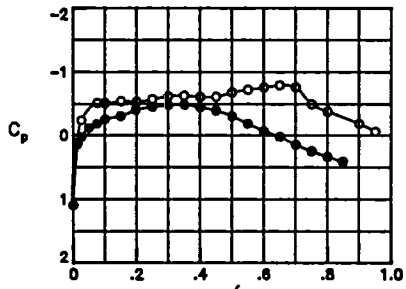

α=-.98

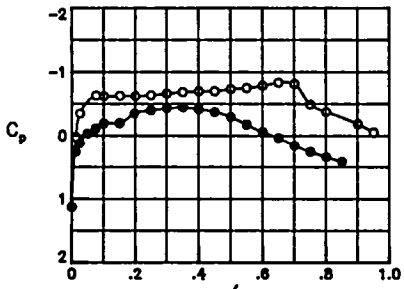

α=-.49

Appendix J

Pressure Data for $M = 0.78$; $R = 4.4 \times 10^6$, 7.0×10^6, 10.0×10^6, 15.0×10^6, 30.0×10^6, and 40.0×10^6; Free Transition

The pressure measurements made on the NASA SC(3)-0712(B) airfoil are presented in coefficient form in graphs in this appendix. The data are for a given Mach number through the Reynolds number range. The pressure data from the upper surface of the airfoil are plotted as open symbols and the lower-surface data are plotted as solid symbols.

TEST 167
RUN 56
MACH .780
R 4.4 x 10^6

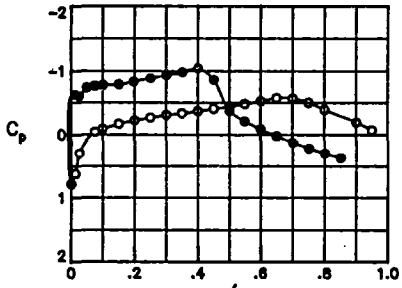

α=-3.99

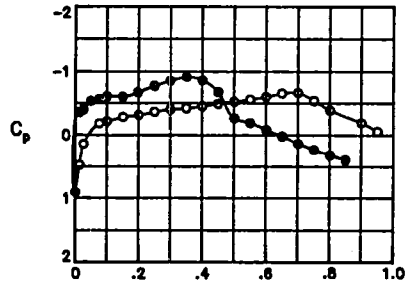

α=-2.99

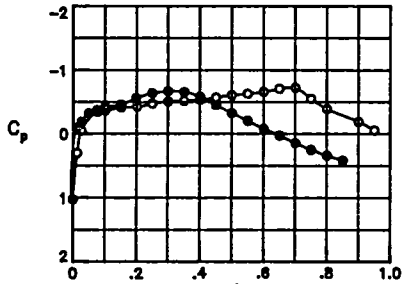

α=-2.00

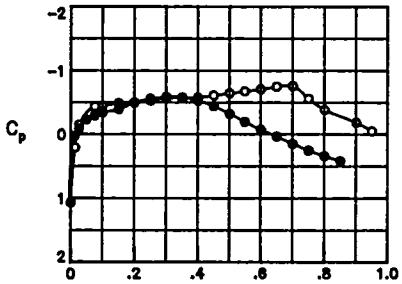

α=-1.52

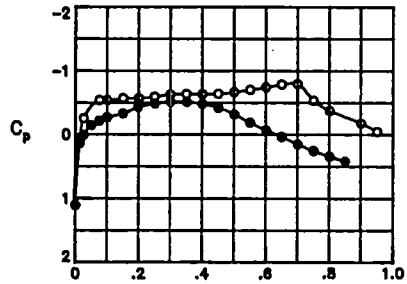

α=-1.01

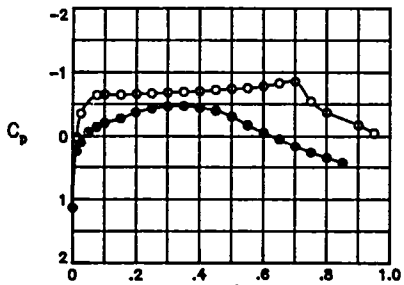

α=-.50

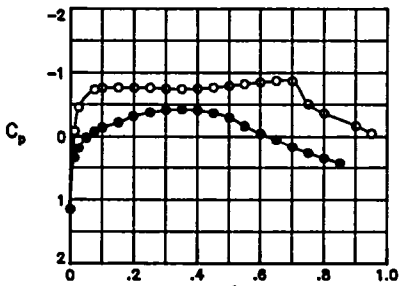

α=.01

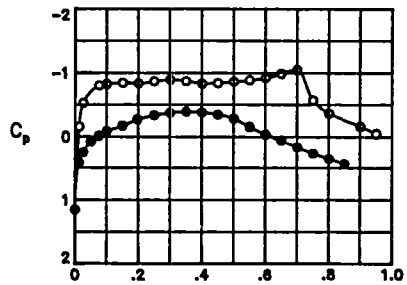

α=.52

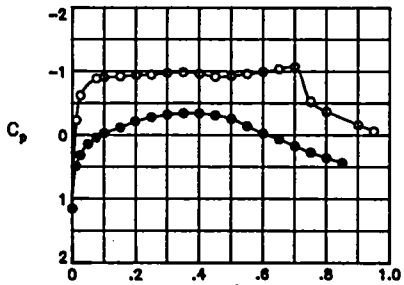

α=1.01

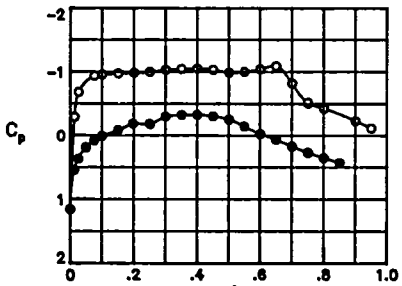

α=1.52

TEST	167
RUN	28
MACH	.780
R	7.0 x 10^6

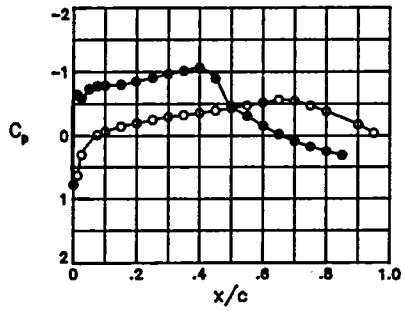

α= -4.04

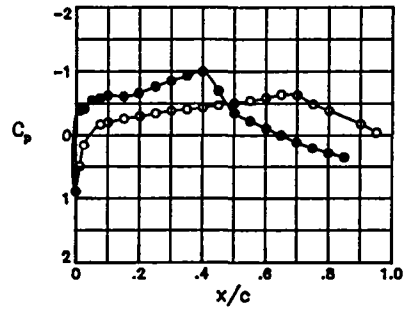

α= -3.01

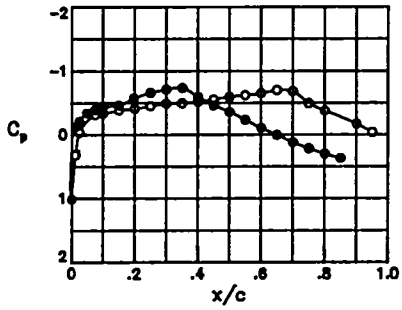

α= -1.98

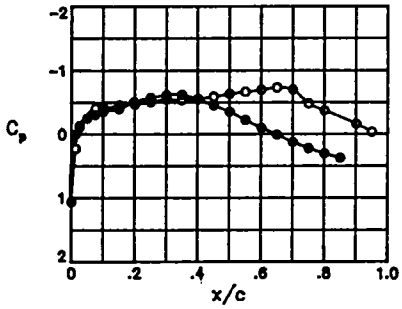

α= -1.49

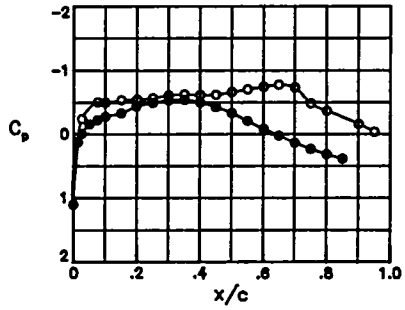

α= -.98

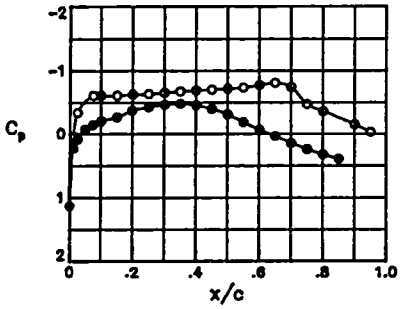

α= -.49

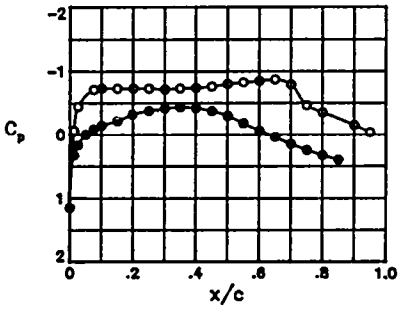

α= .03

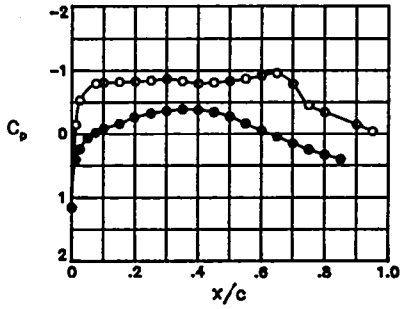

α= .52

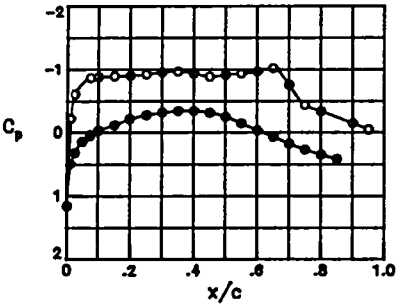

α= 1.02

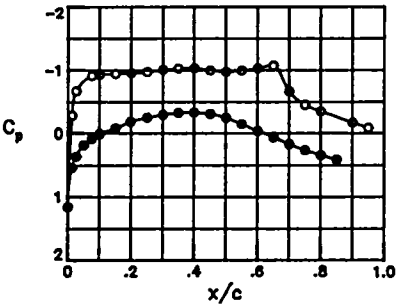

α= 1.53

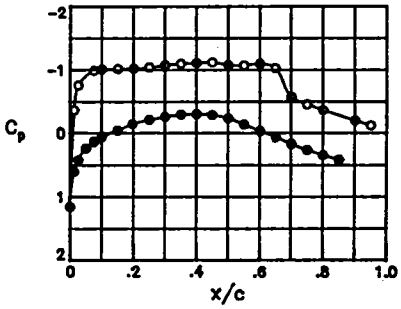

α= 2.03

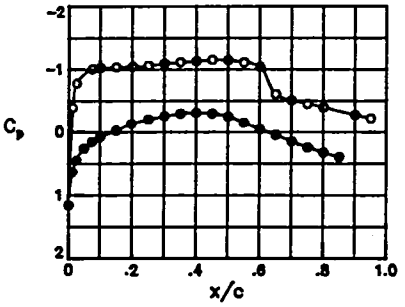

α= 2.53

TEST 167
RUN 29
MACH .780
R 10.0 x 10^6

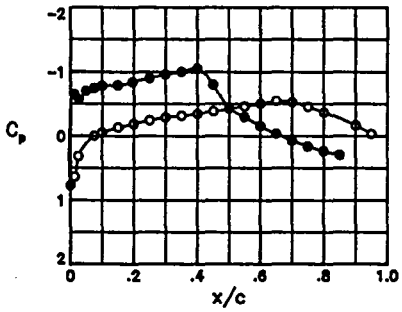

α=-4.02

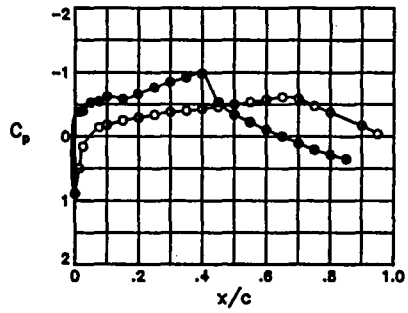

α=-3.00

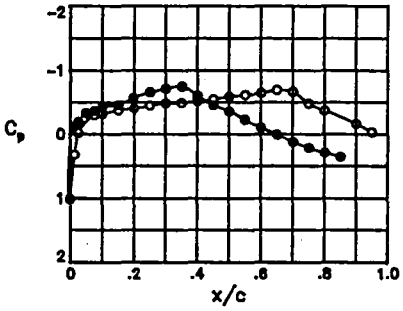

α=-2.00

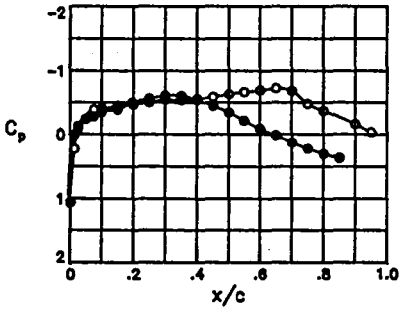

α=-1.49

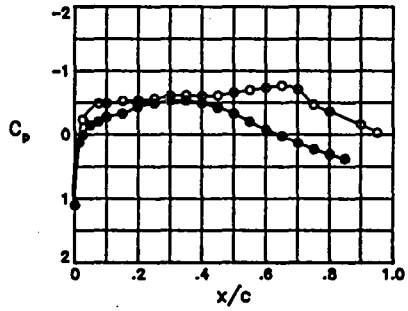

α=-1.00

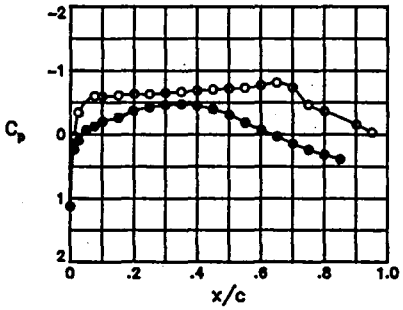

α=-.48

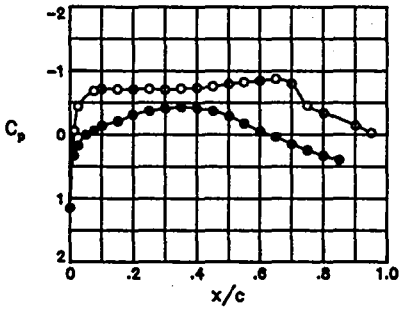

α=.03

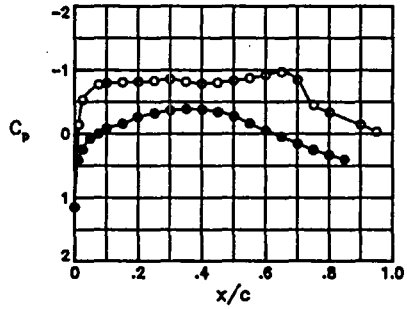

α=.52

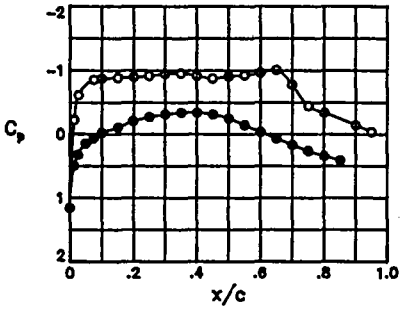

α=1.03

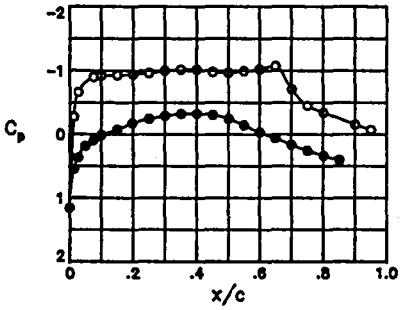

α=1.52

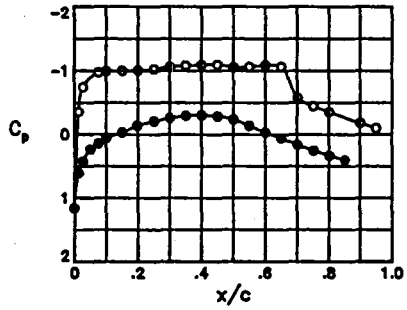

α=2.03

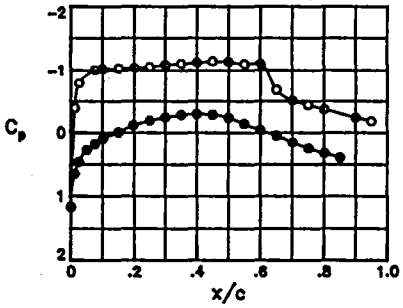

α=2.53

TEST	167
RUN	30
MACH	.780
R	15.0 x 10^6

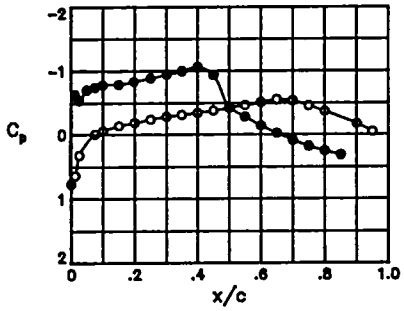

α=-3.98

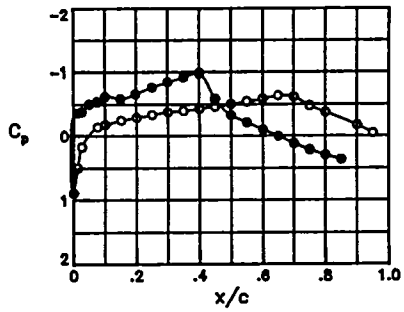

α=-2.99

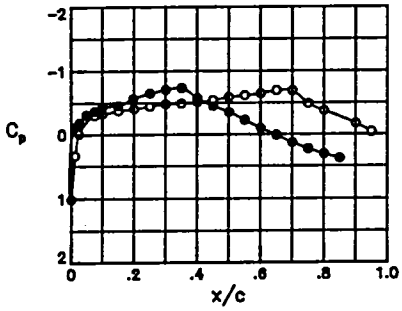

α=-2.00

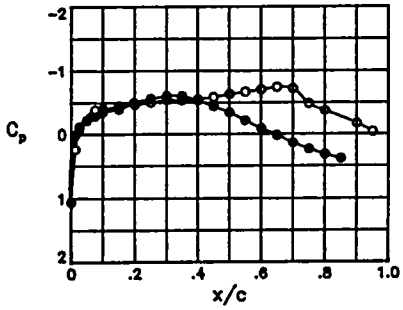

α=-1.50

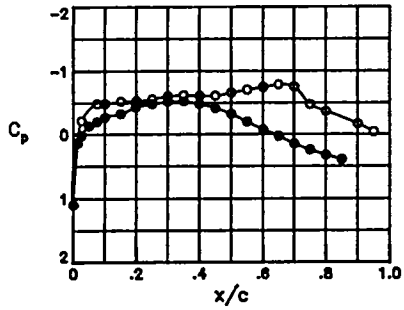

α=-1.00

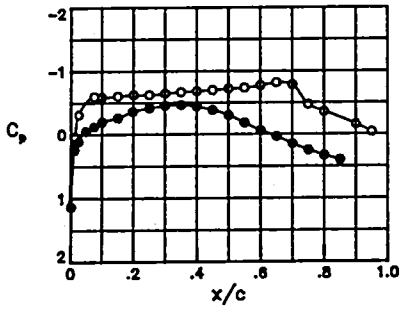

α=-.48

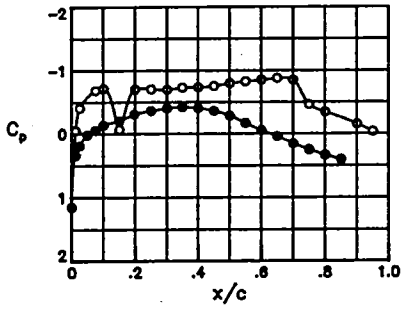

α=.01

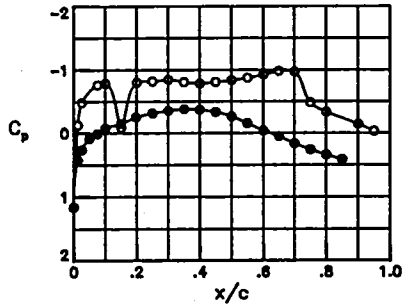

α=.53

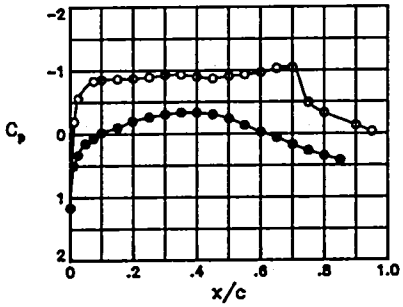

α=1.03

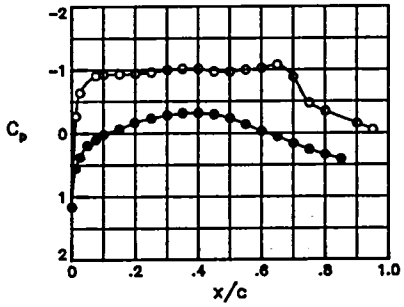

α=1.53

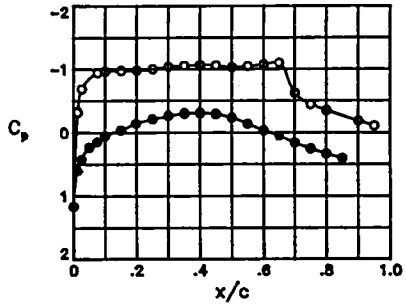

α=2.01

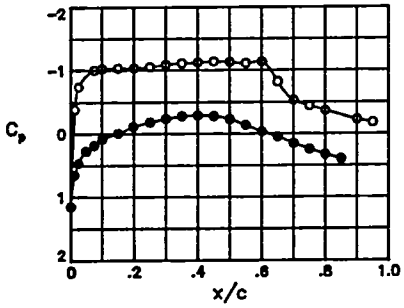

α=2.52

TEST	167
RUN	31
MACH	.780
R	30.0 x 10^6

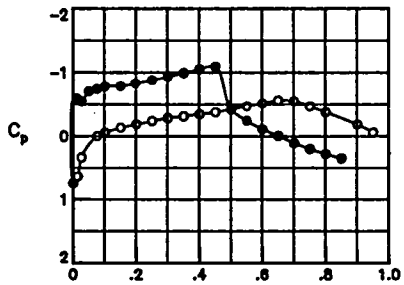

α= -3.98

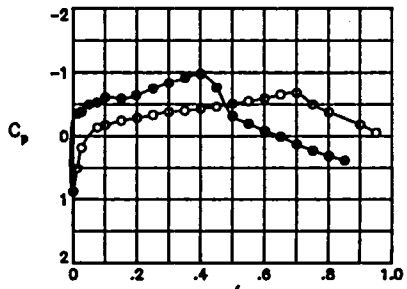

α= -2.99

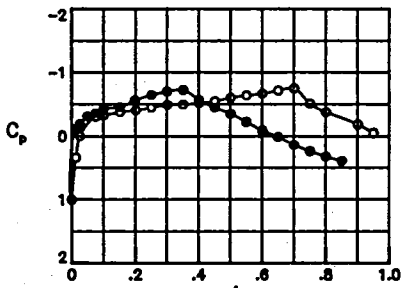

α= -1.99

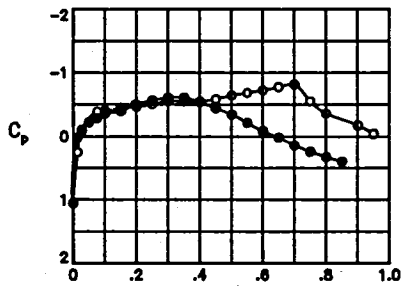

α= -1.50

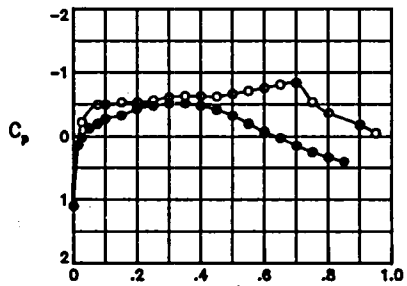

α= -.99

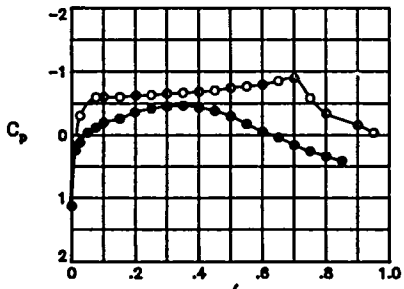

α= -.49

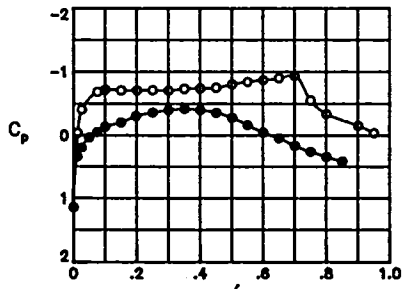

α= .01

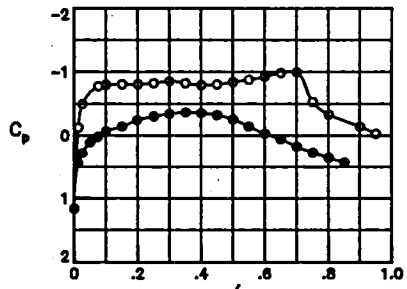

α= .51

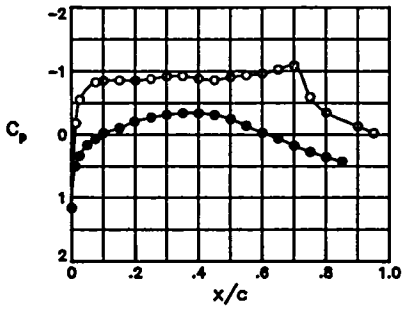

α= 1.00

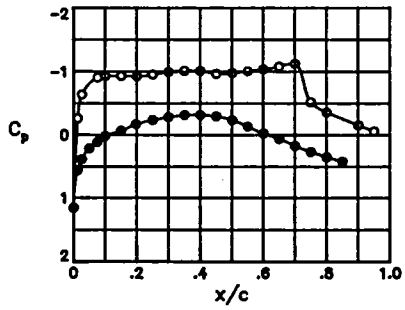

α= 1.51

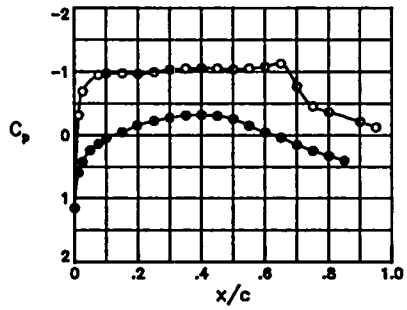

α= 2.02

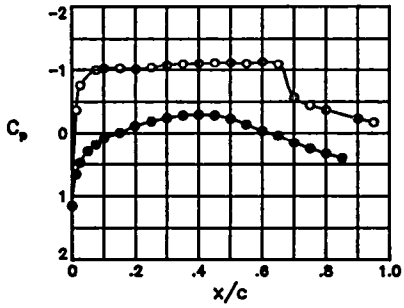

α= 2.52

TEST	167
RUN	32
MACH	.780
R	40.0 x 10^6

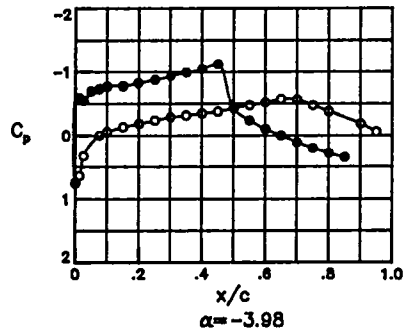

α=-3.98

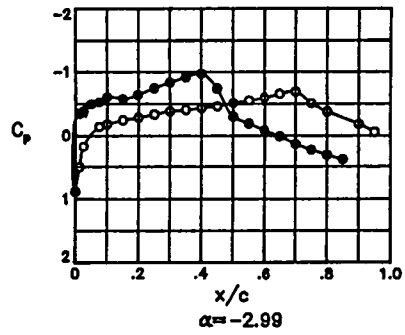

α=-2.99

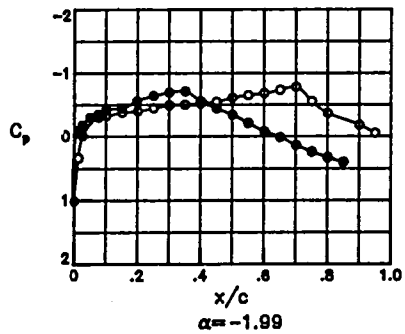

α=-1.99

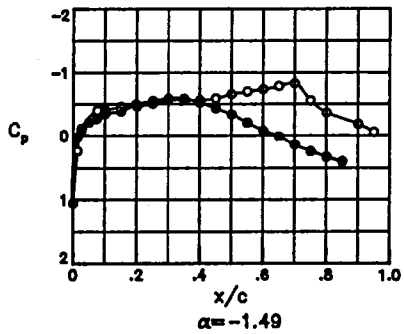

α=-1.49

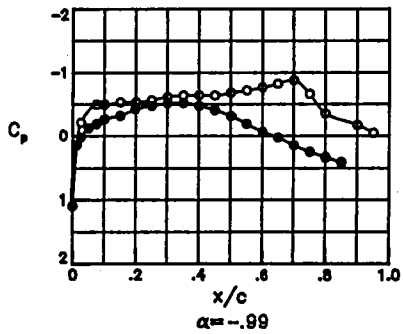

α=-.99

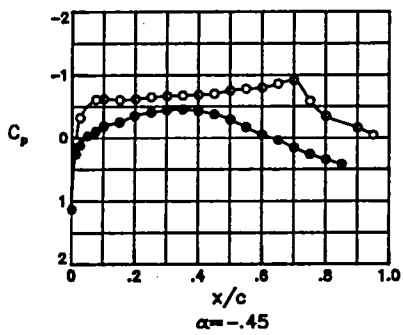

α=-.45

Appendix K

Pressure Data for $M = 0.79$; $R = 10.0 \times 10^6$ and 30.0×10^6; Free Transition

The pressure measurements made on the NASA SC(3)-0712(B) airfoil are presented in coefficient form in graphs in this appendix. The data are for a given Mach number through the Reynolds number range. The pressure data from the upper surface of the airfoil are plotted as open symbols and the lower-surface data are plotted as solid symbols.

TEST	167
RUN	50
MACH	.790
R	10.0×10^6

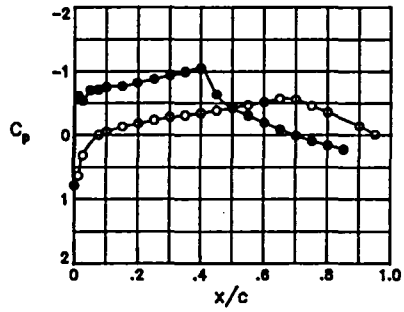

$\alpha = -3.99$

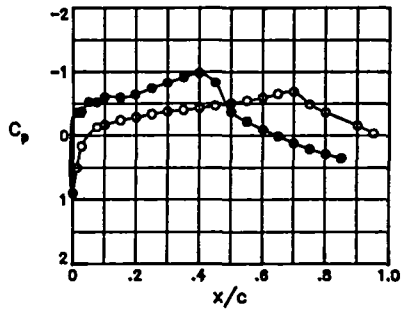

$\alpha = -3.01$

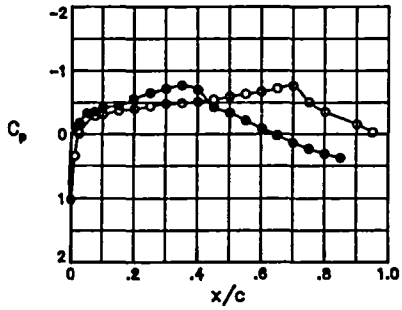

$\alpha = -2.00$

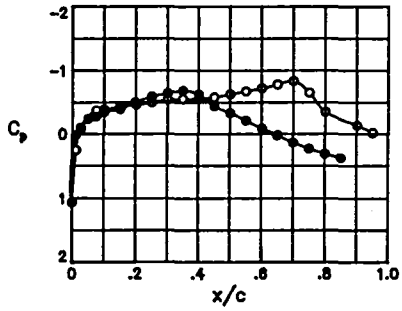

$\alpha = -1.52$

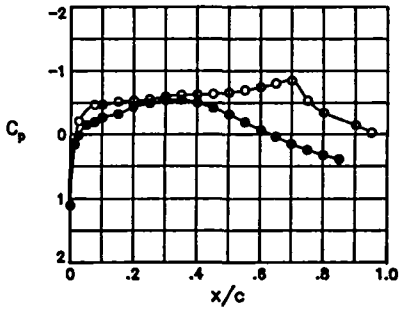

$\alpha = -1.00$

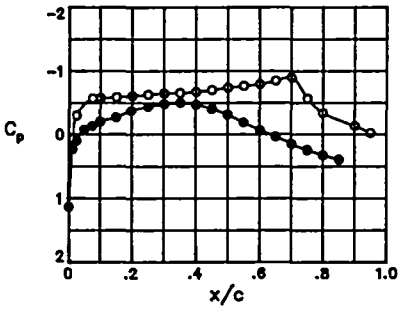

$\alpha = -.51$

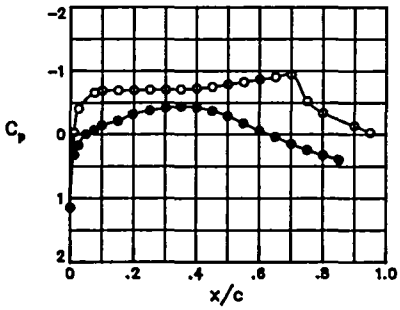

$\alpha = 0.00$

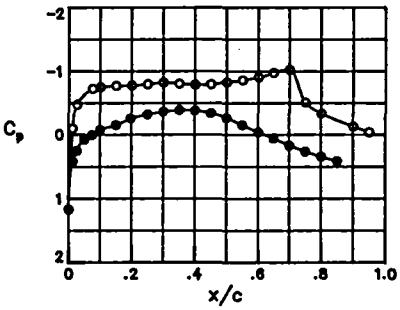

$\alpha = .51$

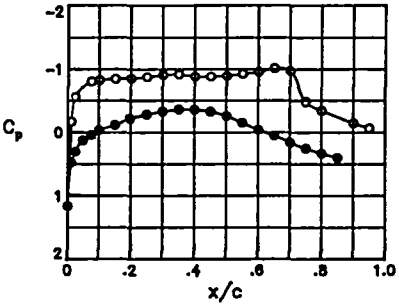

$\alpha = 1.01$

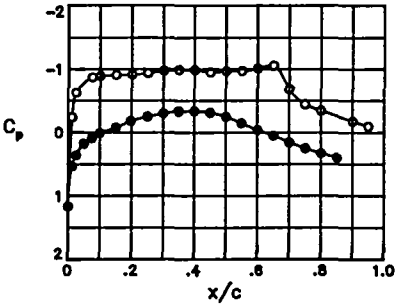

$\alpha = 1.51$

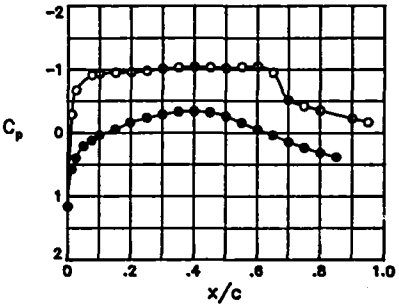

$\alpha = 2.02$

TEST	167
RUN	43
MACH	.790
R	30.0 x 10^6

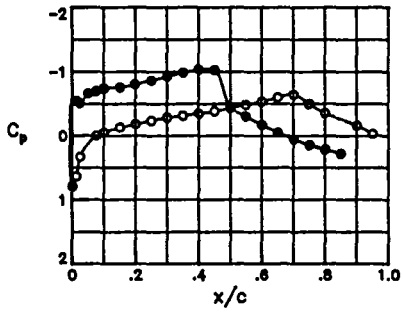

α=-3.99

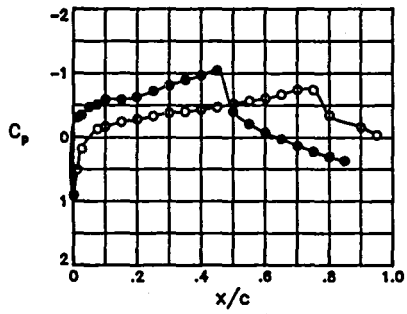

α=-3.00

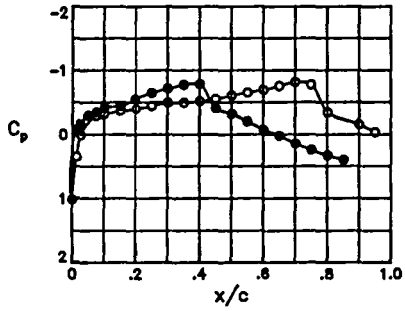

α=-2.00

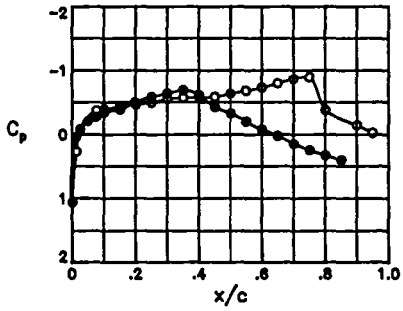

α=-1.49

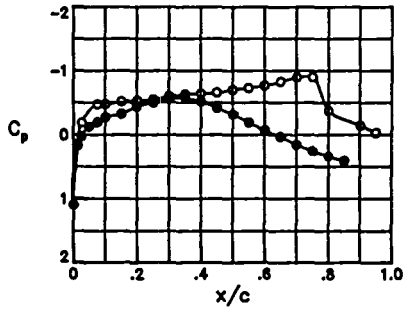

α=-1.00

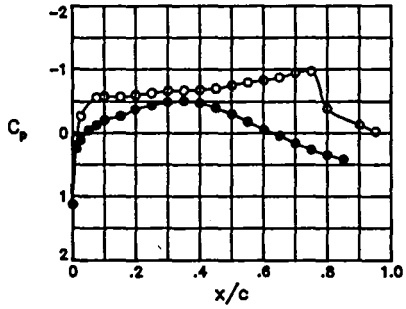

α=-.49

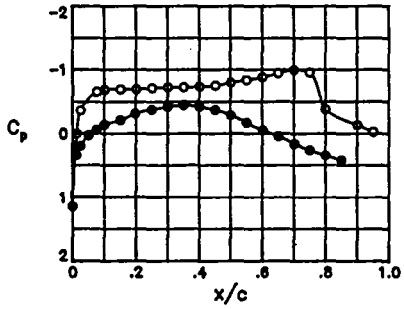

α=.04

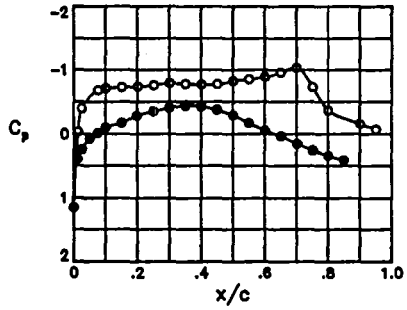

α=.51

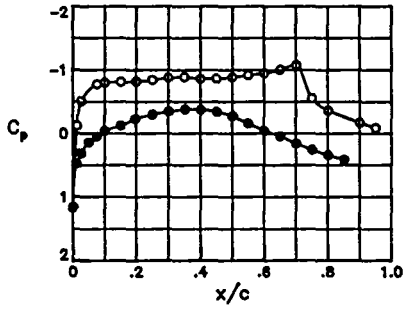

α=1.01

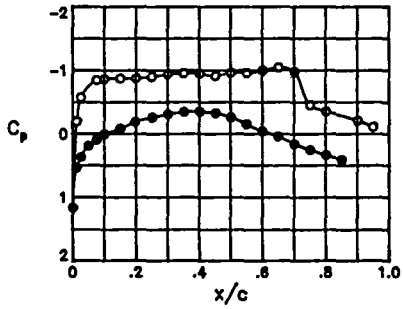

α=1.50

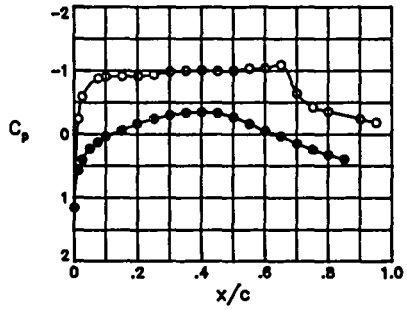

α=2.02

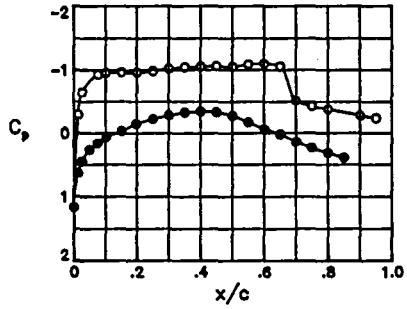

α=2.53

Appendix L

Pressure Data for $M = 0.80$; $R = 4.4 \times 10^6$, 7.0×10^6, 10.0×10^6, 15.0×10^6, and 30.0×10^6; Free Transition

The pressure measurements made on the NASA SC(3)-0712(B) airfoil are presented in coefficient form in graphs in this appendix. The data are for a given Mach number through the Reynolds number range. The pressure data from the upper surface of the airfoil are plotted as open symbols and the lower-surface data are plotted as solid symbols.

TEST	167
RUN	5
MACH	.800
R	4.4 x 10^6

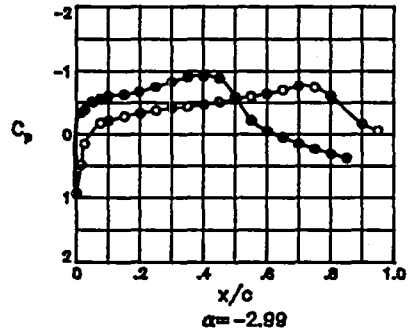

α=-2.99

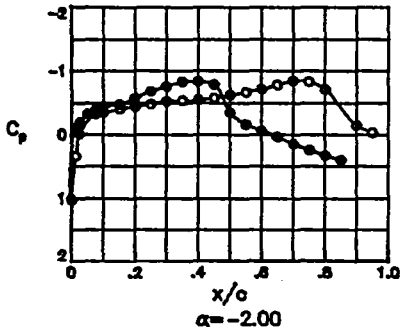

α=-2.00

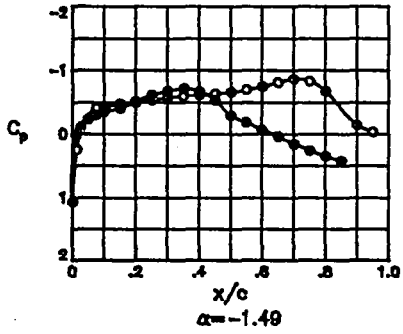

α=-1.49

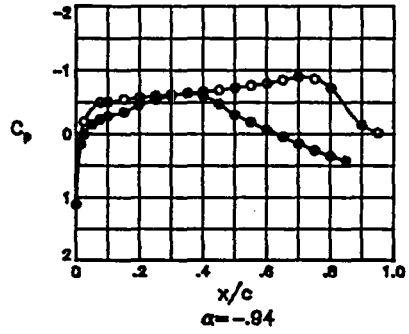

α=-.94

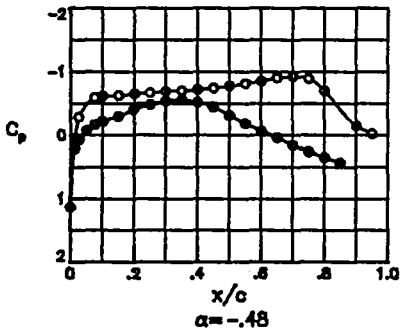

α=-.48

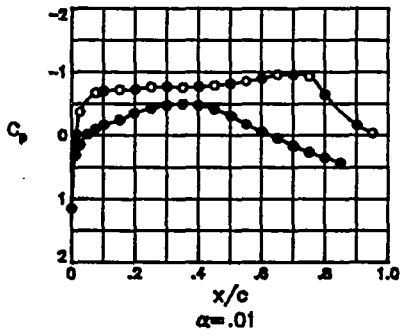

α=.01

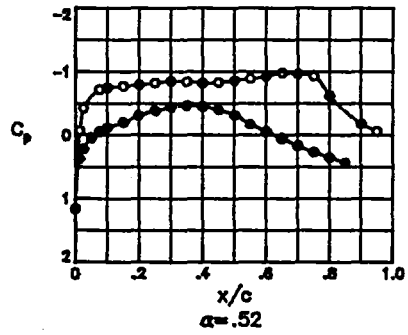

α=.52

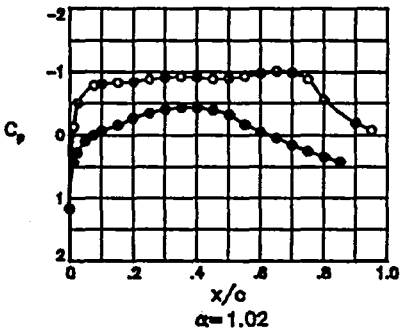

α=1.02

TEST	167
RUN	4
MACH	.800
R	7.0 x 10^6

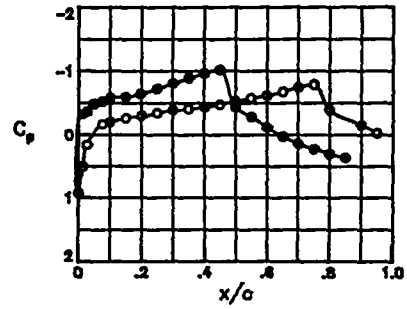

α=-2.96

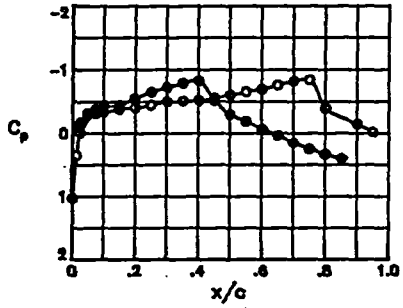

α=-1.98

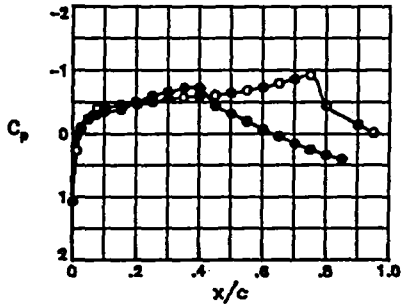

α=-1.49

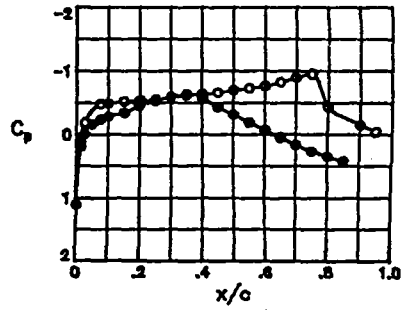

α=-1.03

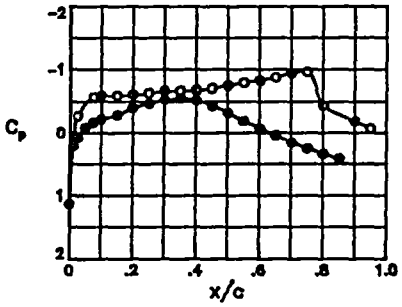

α=-.48

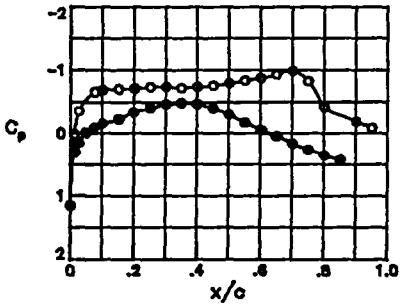

α=.03

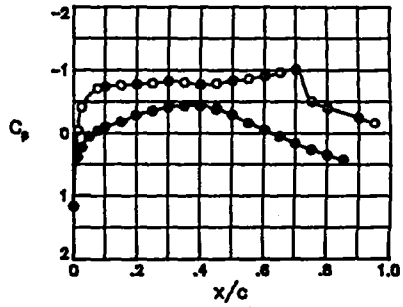

α=.53

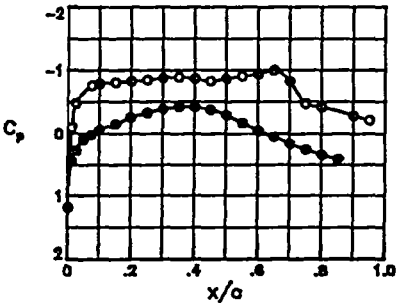

α=1.02

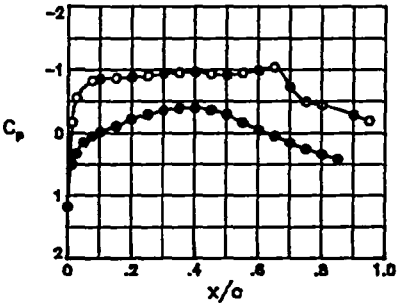

α=1.52

TEST	167
RUN	49
MACH	.800
R	10.0 x 10^6

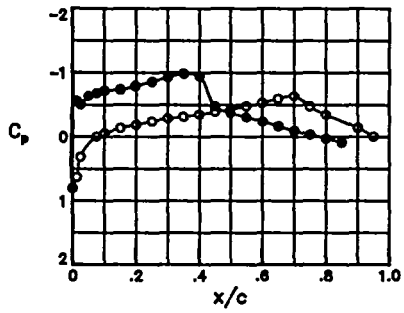

α= -3.99

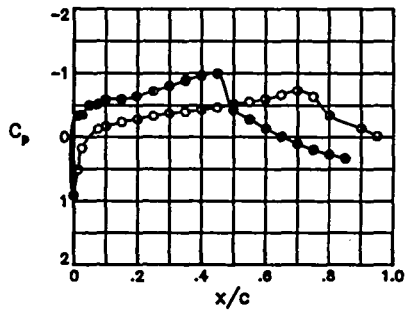

α= -3.01

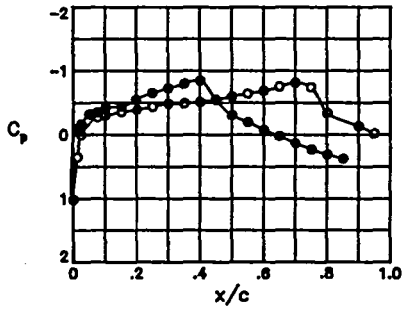

α= -2.00

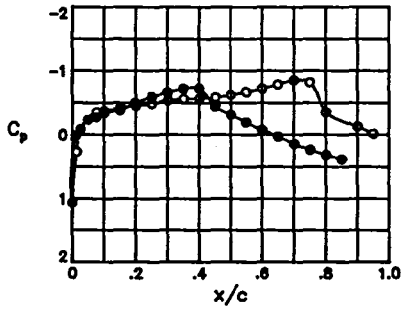

α= -1.51

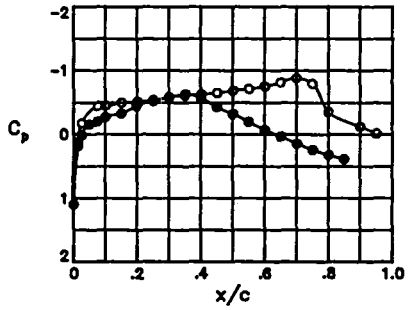

α= -1.00

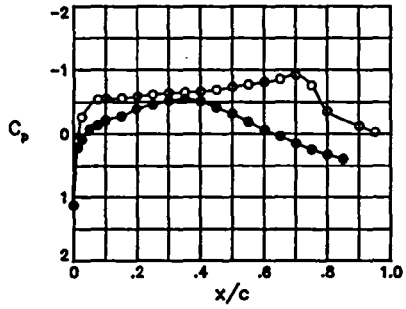

α= -.50

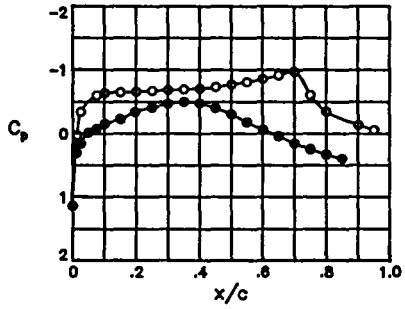

α= 0.00

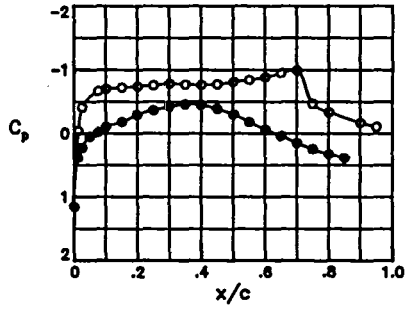

α= .51

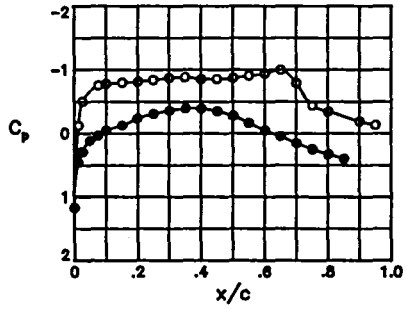

α= 1.01

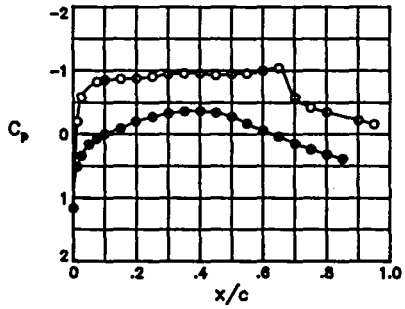

α= 1.51

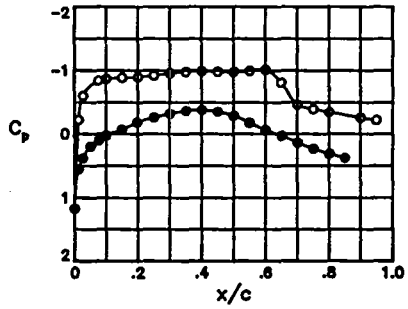

α= 2.02

TEST	167
RUN	35
MACH	.800
R	15.0 x 10^6

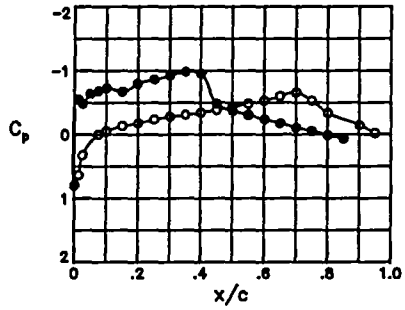

α=-4.00

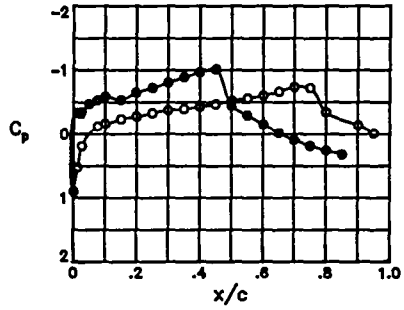

α=-3.01

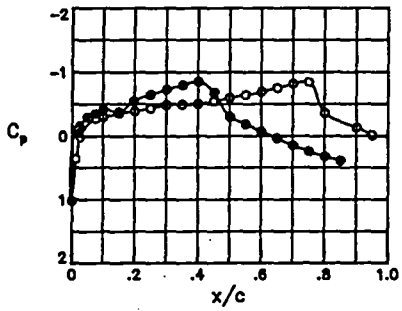

α=-1.98

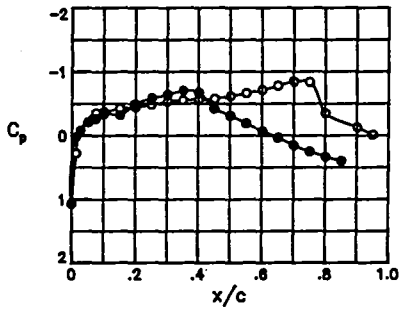

α=-1.48

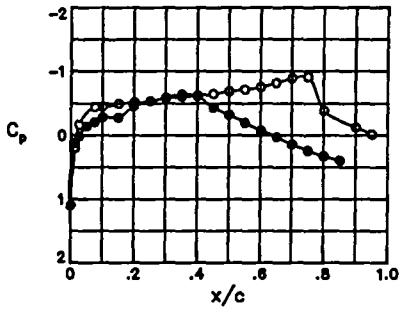

α=-.99

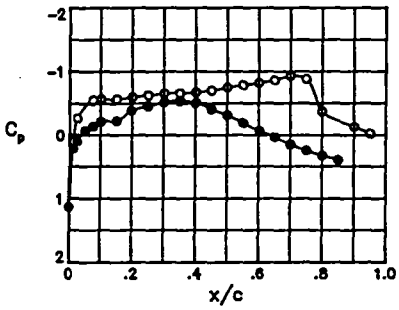

α=-.49

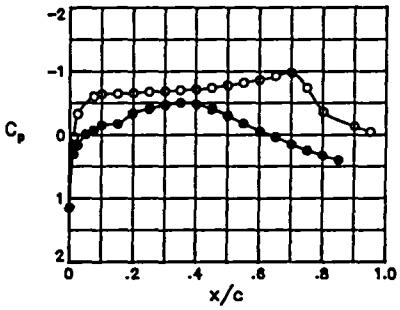

α=.01

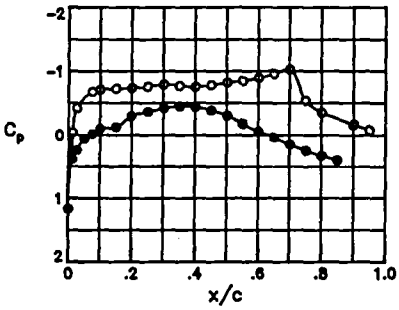

α=.52

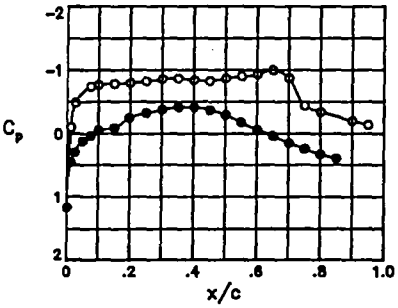

α=1.03

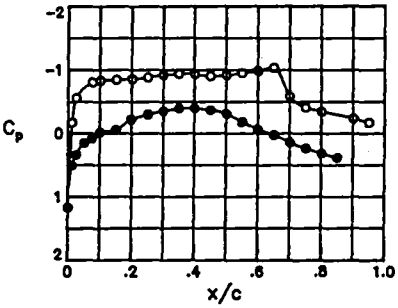

α=1.51

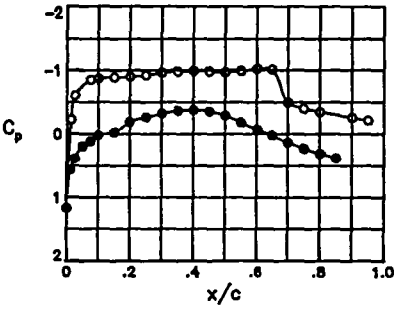

α=2.01

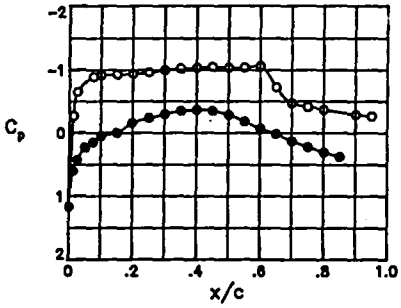

α=2.50

TEST	167
RUN	42
MACH	.800
R	30.0 x 10^6

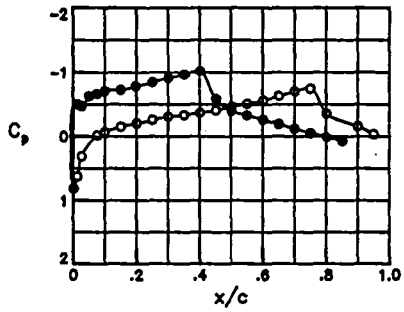

α= -3.94

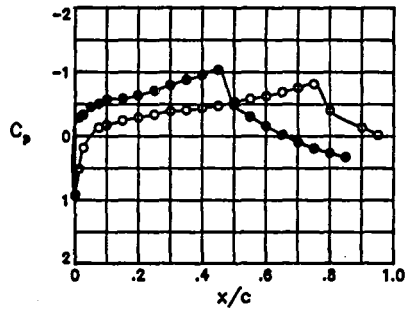

α= -2.97

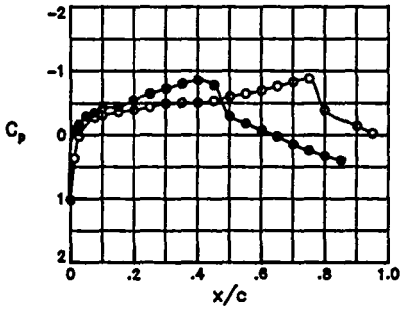

α= -1.99

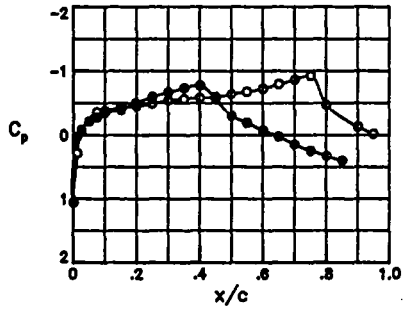

α= -1.48

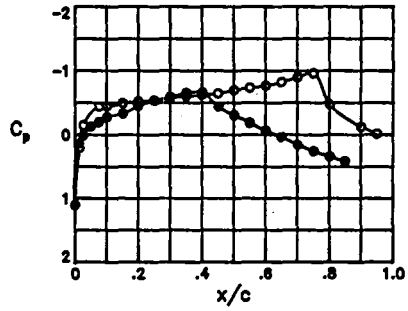

α= -.98

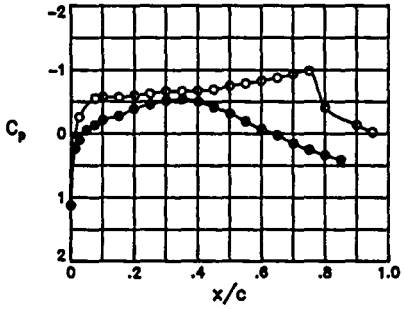

α= -.47

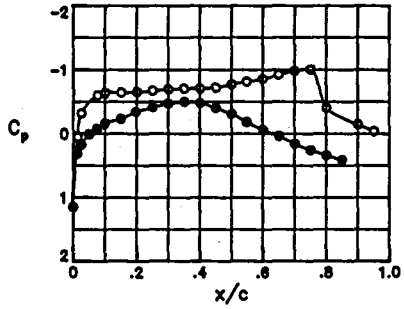

α= 0.00

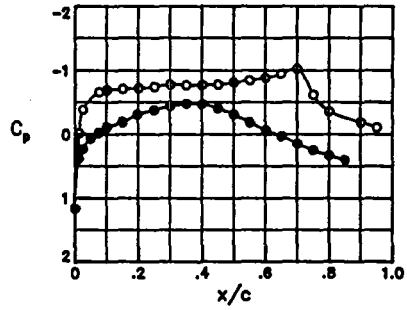

α= .53

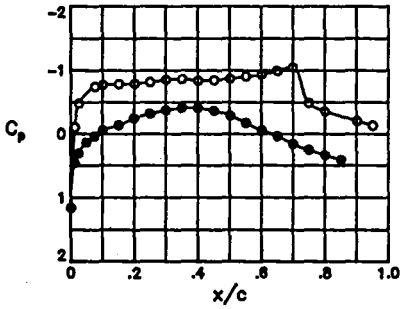

α= 1.02

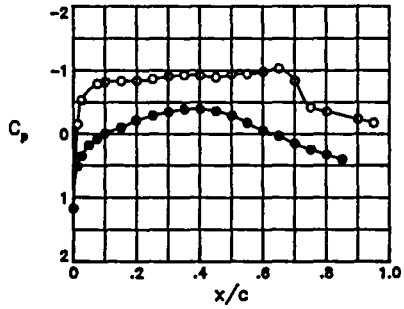

α= 1.54

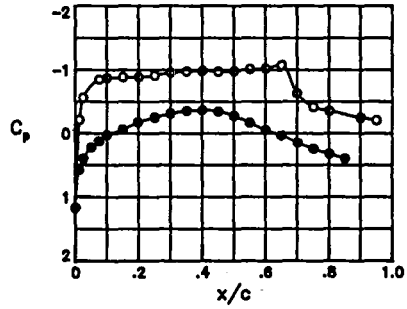

α= 2.01

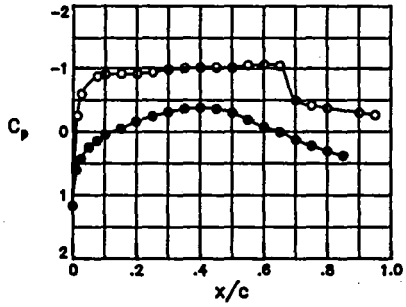

α= 2.51

Appendix M

Pressure Data for $M = 0.50$; $R = 4.4 \times 10^6$ and 7.0×10^6; Fixed Transition

The pressure measurements made on the NASA SC(3)-0712(B) airfoil are presented in coefficient form in graphs in this appendix. The data are for a given Mach number through the Reynolds number range. The pressure data from the upper surface of the airfoil are plotted as open symbols and the lower-surface data are plotted as solid symbols.

TEST	167
RUN	59
MACH	.500
R	4.4 x 10^6

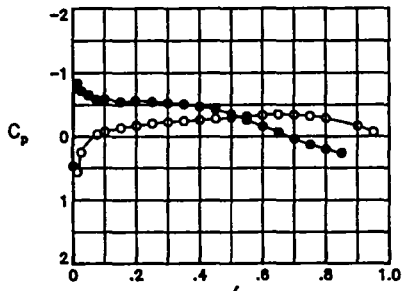

α=-4.00

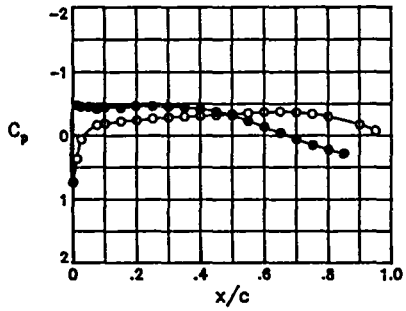

α=-2.99

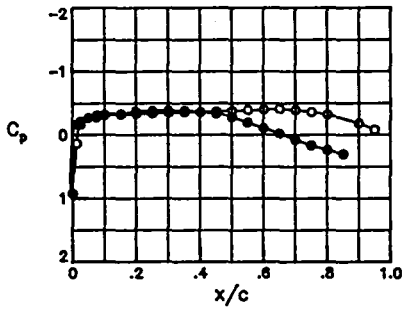

α=-1.99

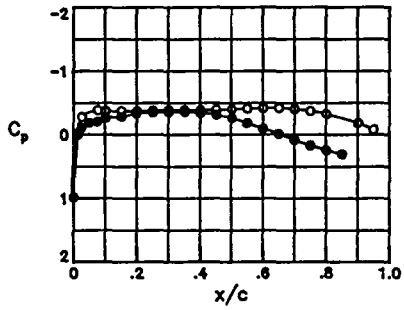

α=-1.49

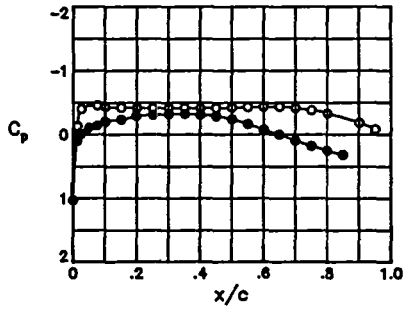

α=-1.00

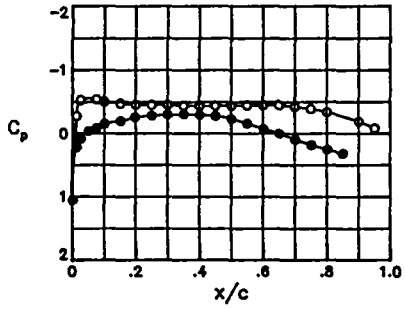

α=-.49

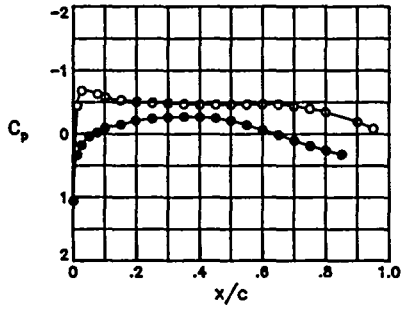

α=.02

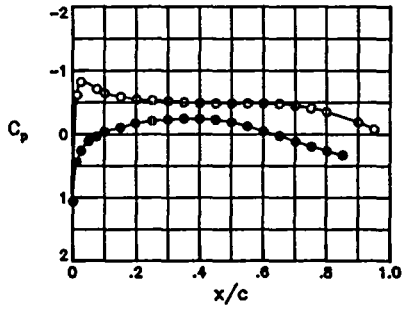

α=.51

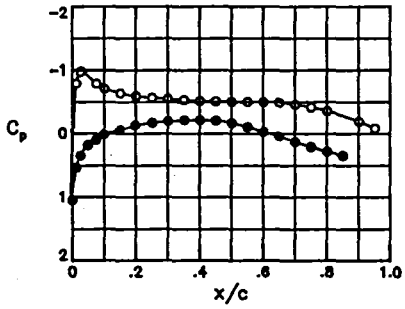

α=1.01

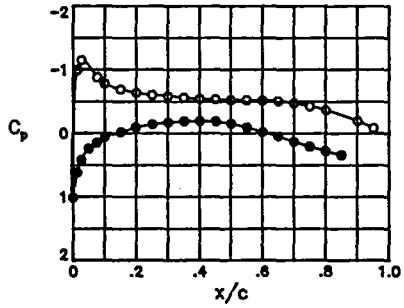

α=1.52

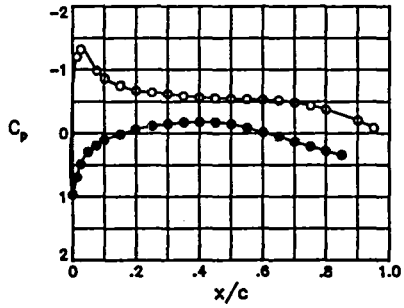

α=2.01

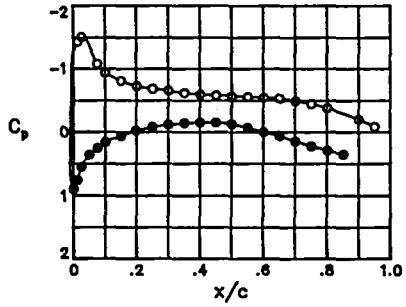

α=2.52

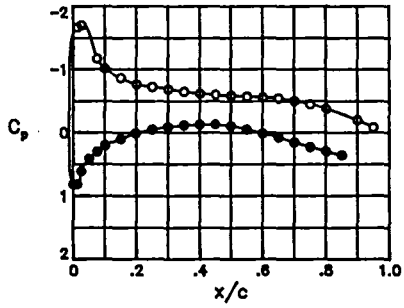

α=3.01

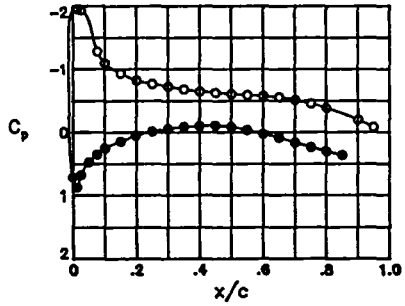

α=3.55

TEST	167
RUN	67
MACH	.500
R	7.0 x 10^6

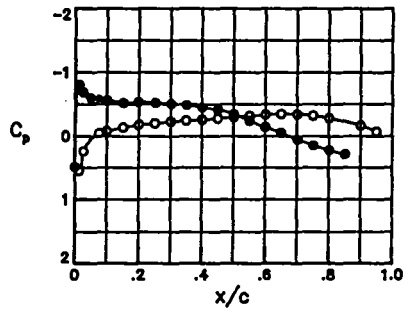

α=-3.98

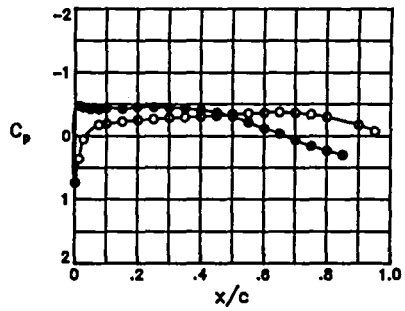

α=-3.01

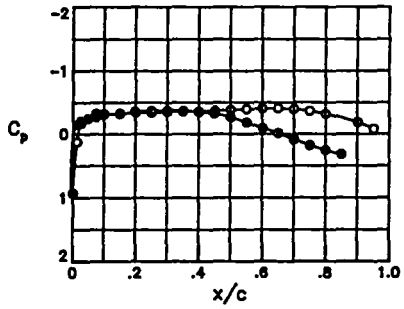

α=-2.00

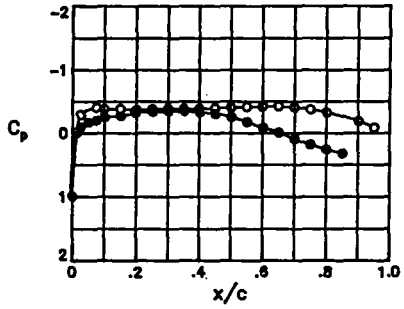

α=-1.50

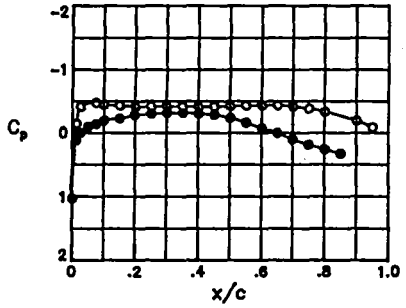

α=-1.01

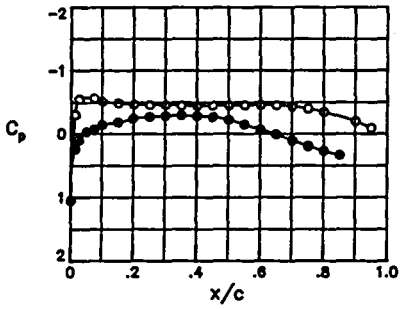

α=-.50

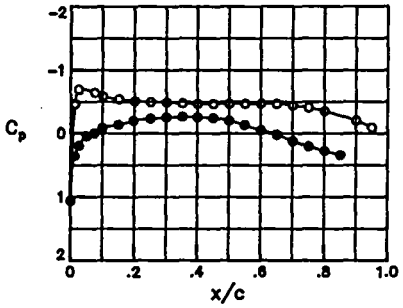

α=.01

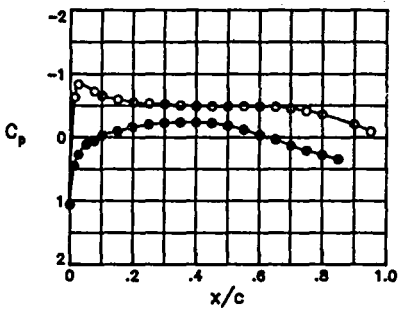

α=.50

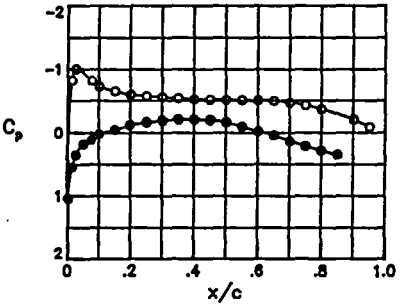

α=1.01

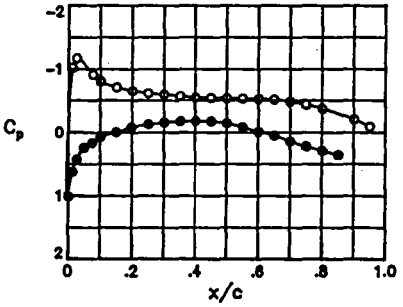

α=1.50

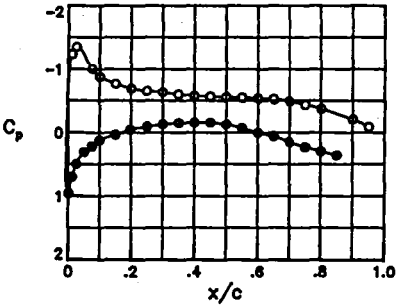

α=2.00

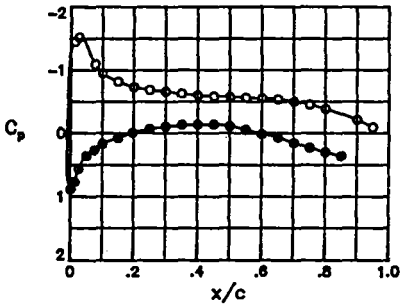

α=2.49

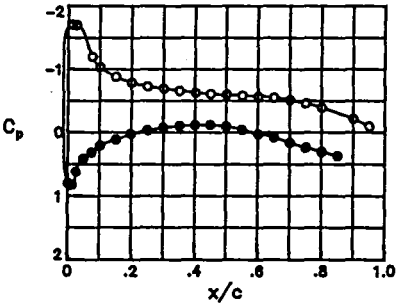

α=2.99

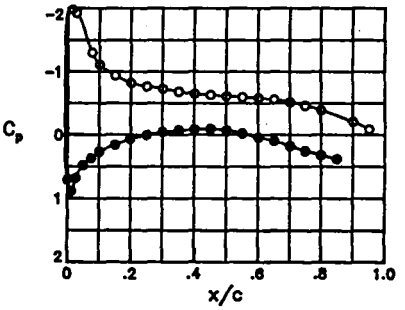

α=3.53

Appendix N

Pressure Data for $M = 0.65$; $R = 7.0 \times 10^6$ and 30.0×10^6; Fixed Transition

The pressure measurements made on the NASA SC(3)-0712(B) airfoil are presented in coefficient form in graphs in this appendix. The data are for a given Mach number through the Reynolds number range. The pressure data from the upper surface of the airfoil are plotted as open symbols and the lower-surface data are plotted as solid symbols.

TEST	167
RUN	62
MACH	.650
R.	7.0 x 10^6

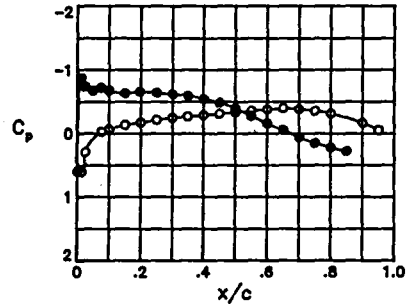

α=-4.00

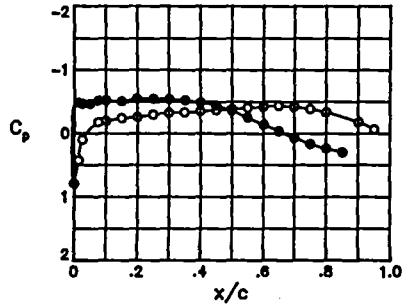

α=-2.98

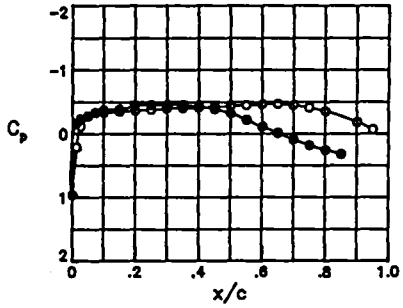

α=-2.00

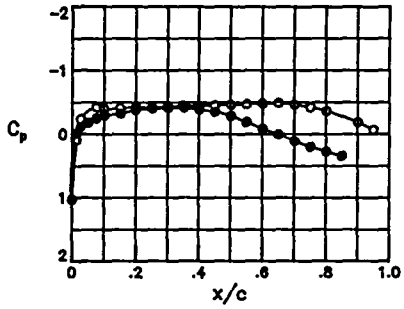

α=-1.50

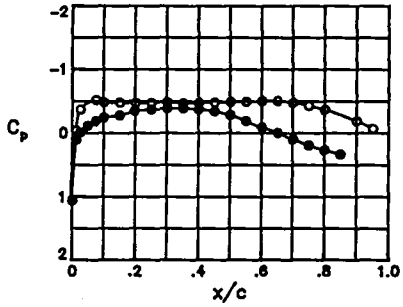

α=-1.00

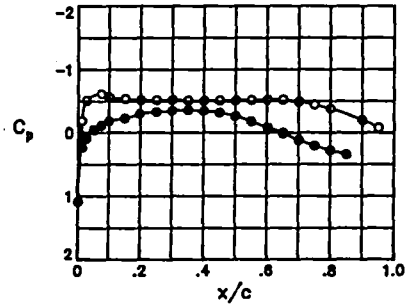

α=-.50

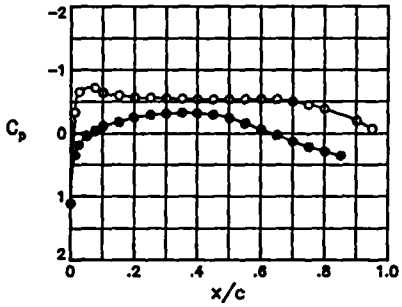

α=-.01

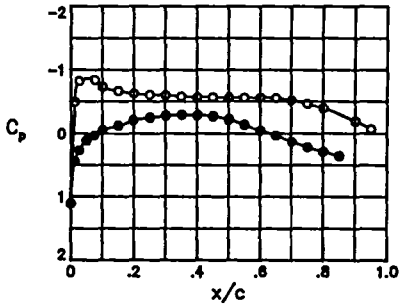

α=.50

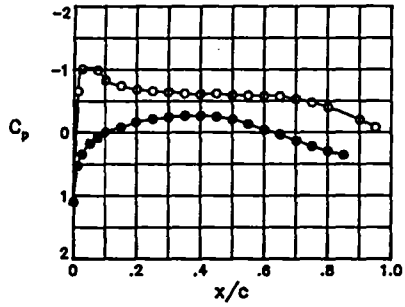

α=1.00

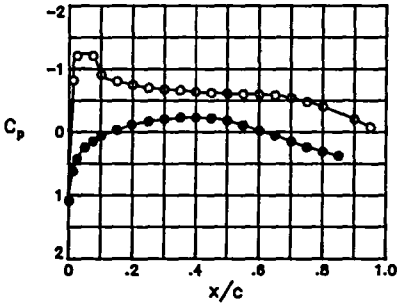

α=1.51

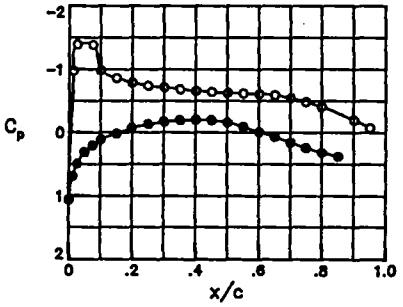

α=2.00

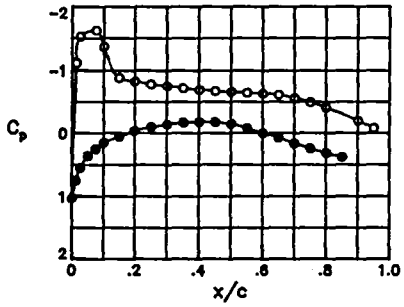

α=2.49

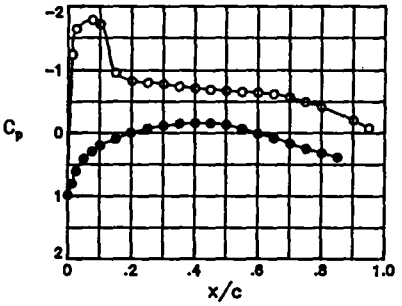

α=3.00

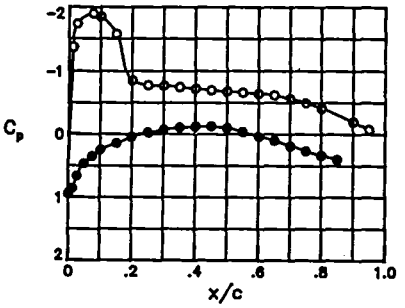

α=3.50

TEST	167
RUN	72
MACH	.650
R	30.0 x 10^6

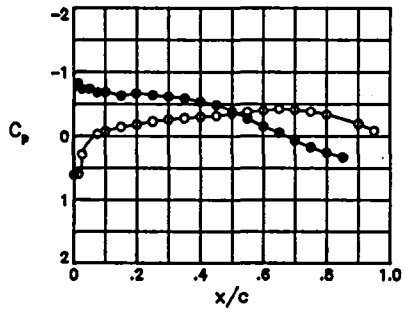

α=-4.06

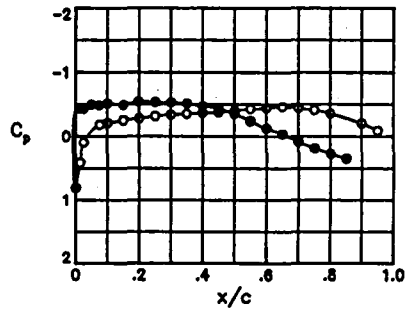

α=-2.99

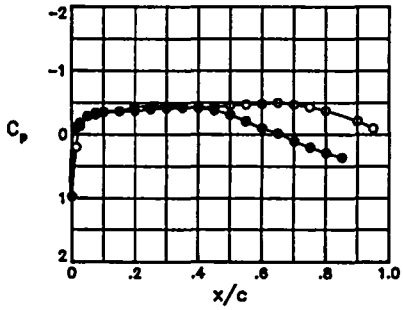

α=-2.01

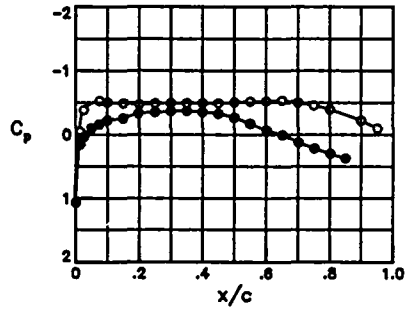

α=-1.01

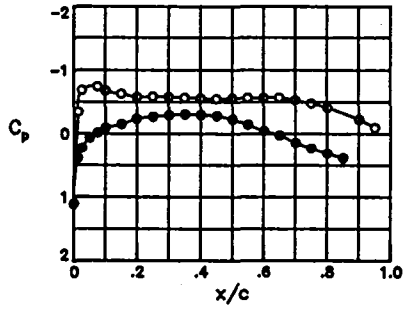

α=.02

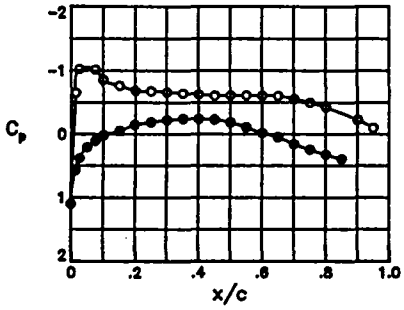

α=1.01

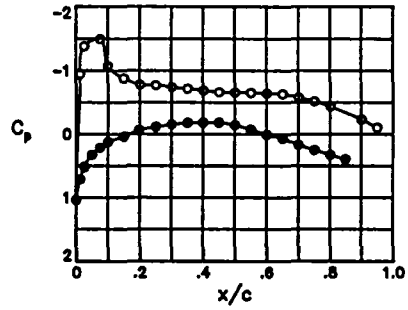

α=2.01

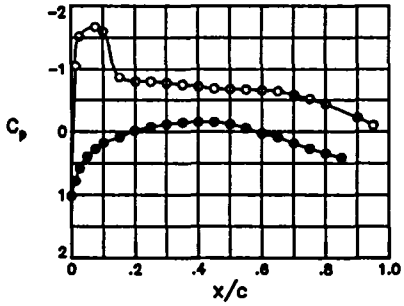

α=2.51

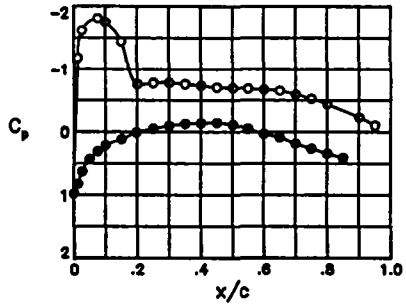

α=3.01

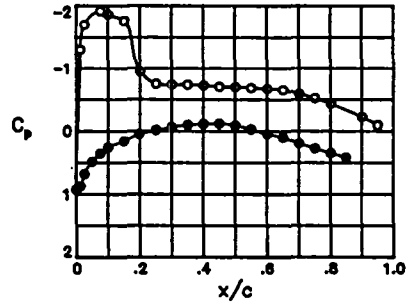

α=3.49

Appendix O

Pressure Data for $M = 0.76$; $R = 4.4 \times 10^6$, 7.0×10^6, 10.0×10^6, 15.0×10^6, 30.0×10^6, and 40.0×10^6; Fixed Transition

The pressure measurements made on the NASA SC(3)-0712(B) airfoil are presented in coefficient form in graphs in this appendix. The data are for a given Mach number through the Reynolds number range. The pressure data from the upper surface of the airfoil are plotted as open symbols and the lower-surface data are plotted as solid symbols.

TEST	167
RUN	58
MACH	.760
R	4.4 x 10^6

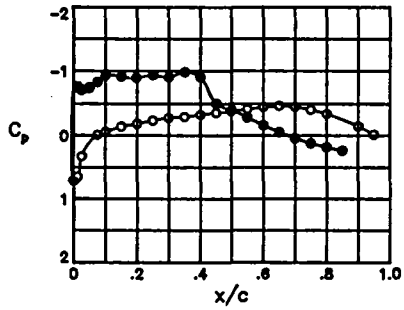

α=-4.03

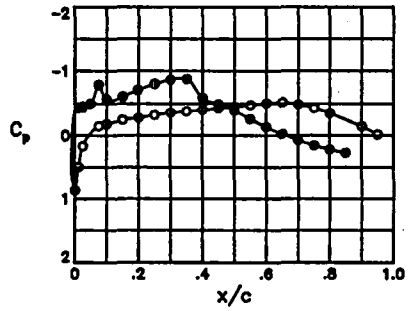

α=-2.98

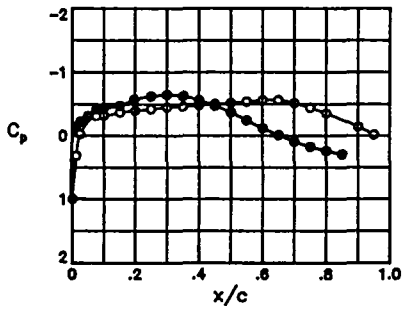

α=-1.98

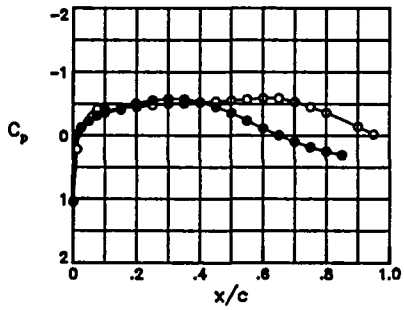

α=-1.49

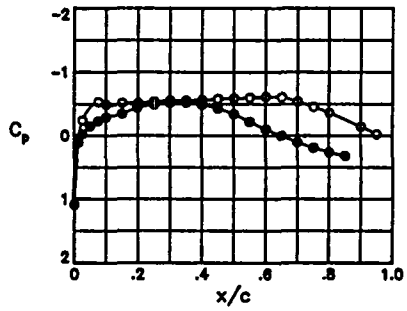

α=-.98

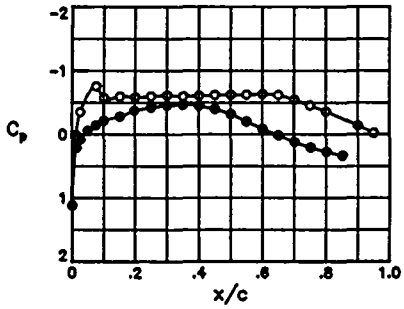

α=-.48

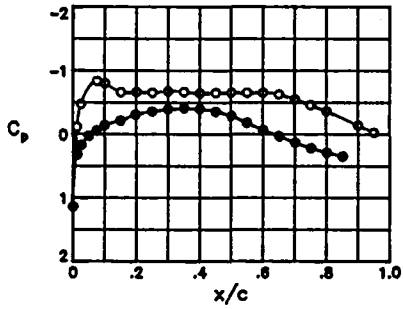

α=.03

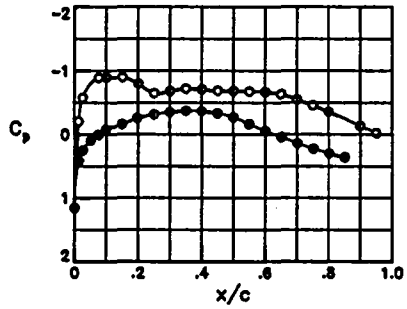

α=.52

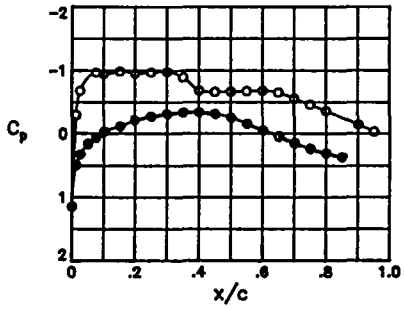

α=1.01

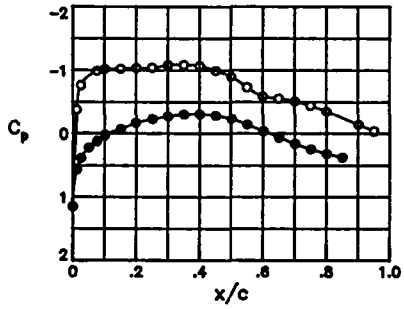

α=1.53

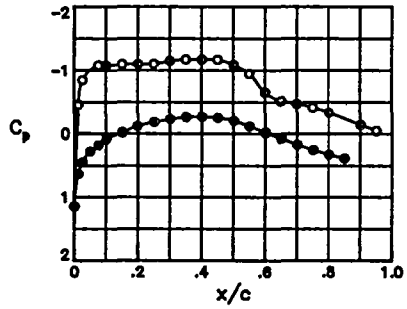

α=2.03

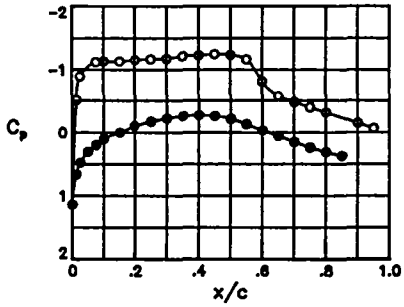

α=2.54

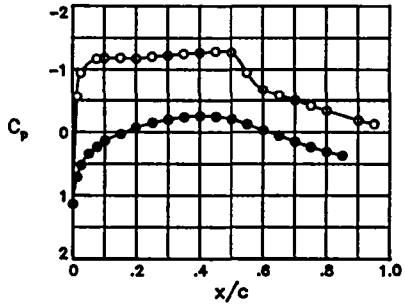

α=3.02

TEST	167
RUN	61
MACH	.760
R	7.0 x 10^6

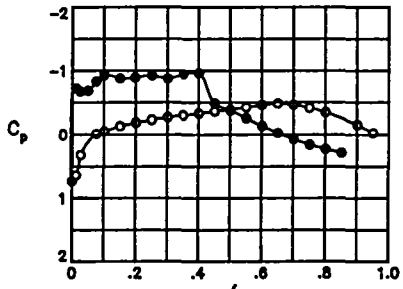

α=-3.99

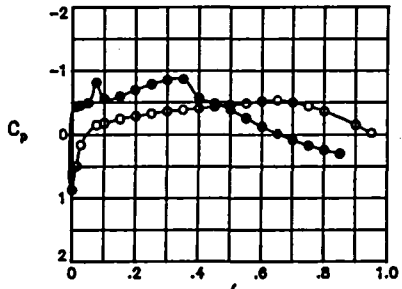

α=-3.01

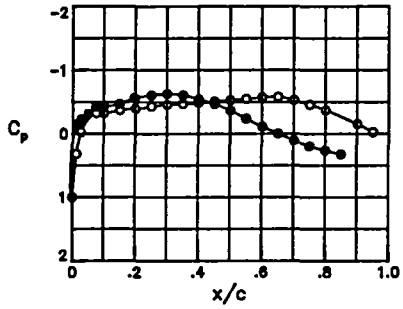

α=-2.00

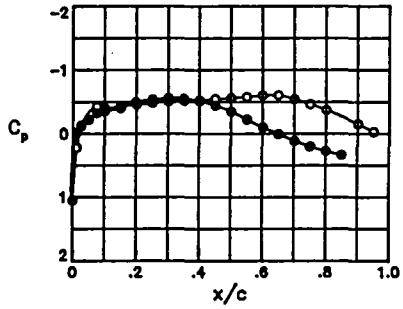

α=-1.51

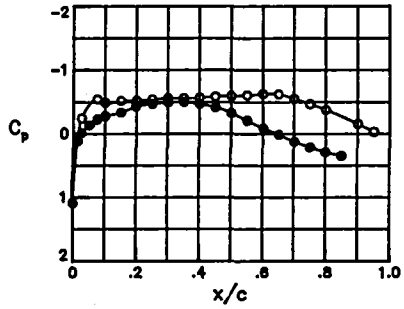

α=-1.01

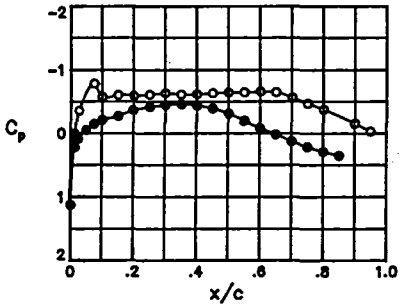

α=-.50

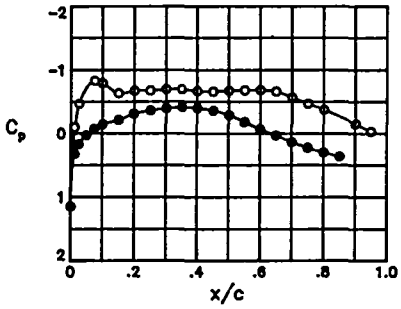

α=0.00

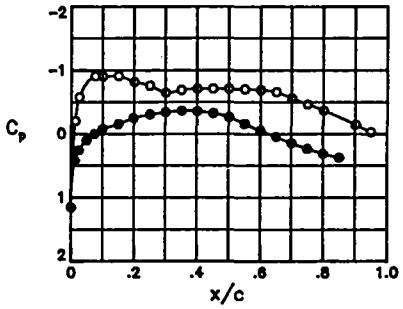

α=.50

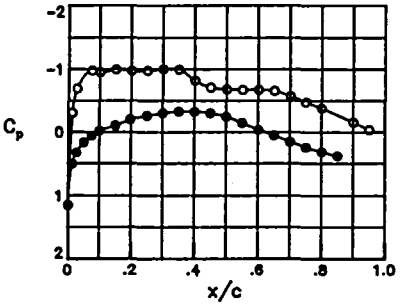

α=1.01

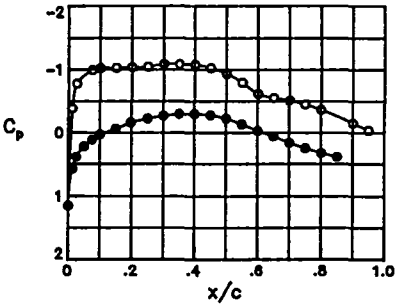

α=1.50

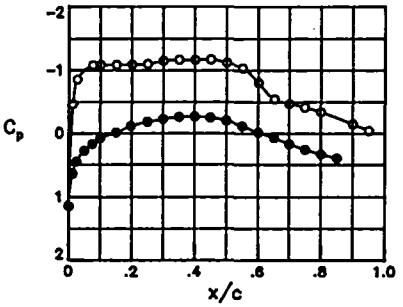

α=2.01

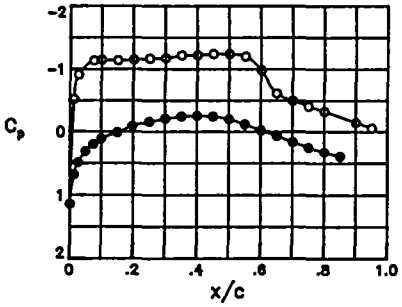

α=2.51

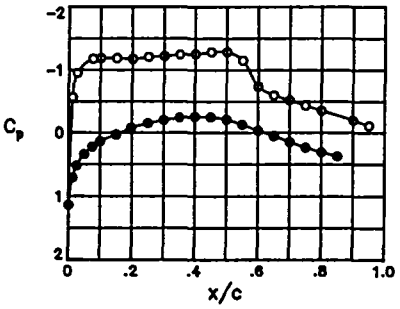

α=3.02

TEST 167
RUN 61
MACH .760
R 7.0 x 10^6

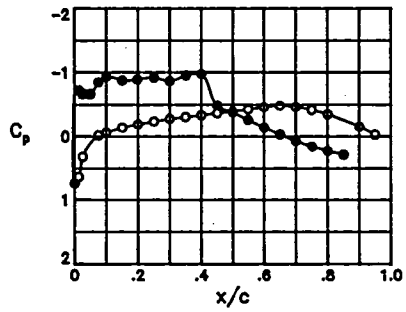

α=-3.98

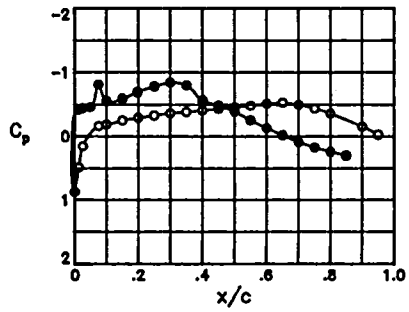

α=-2.98

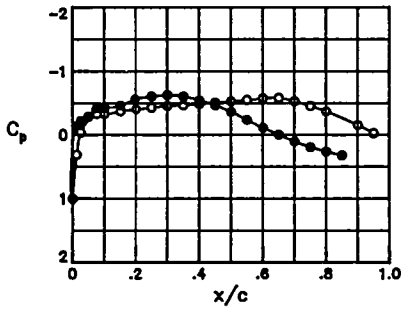

α=-1.99

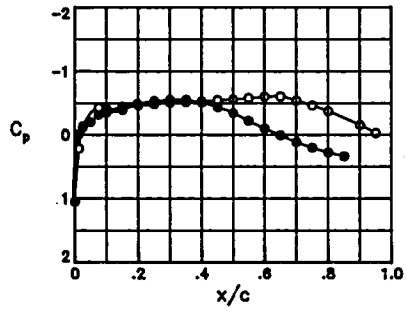

α=-1.49

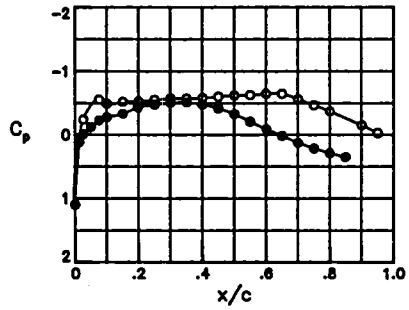

α=-.99

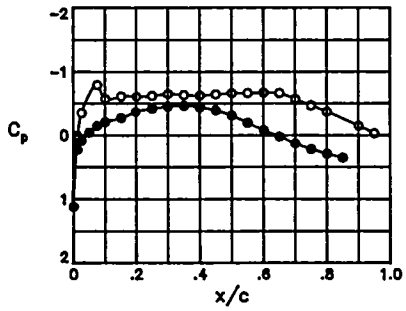

α=-.49

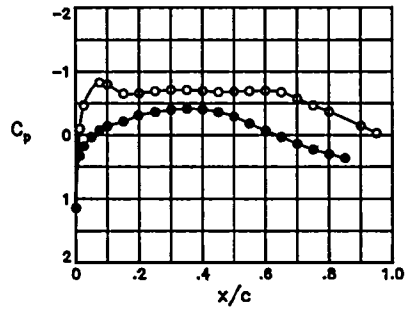

α=.02

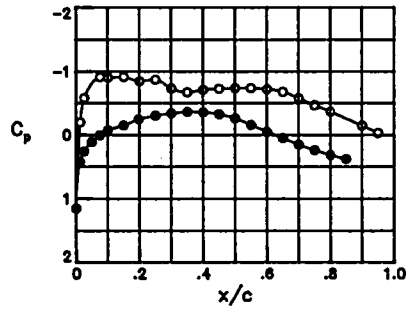

α=.52

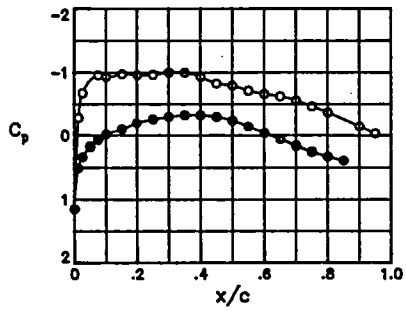

α=1.03

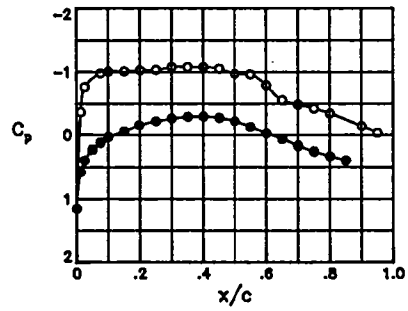

α=1.52

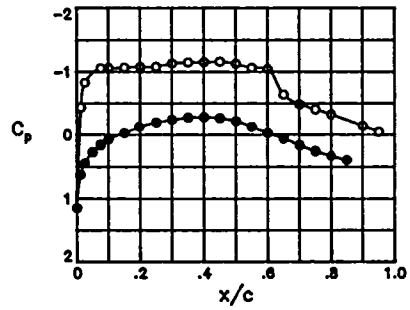

α=2.02

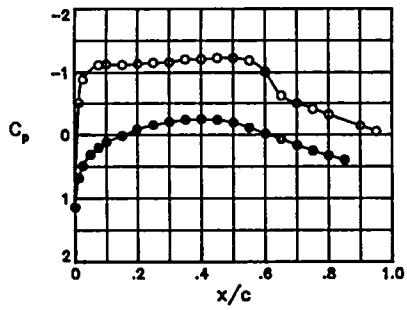

α=2.50

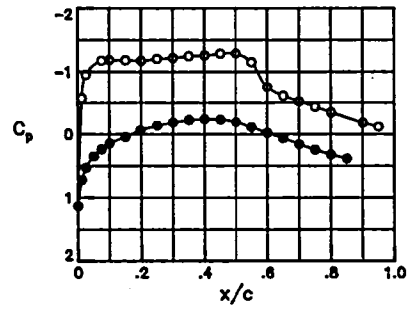

α=3.02

TEST	167
RUN	65
MACH	.760
R	10.0 x 10^6

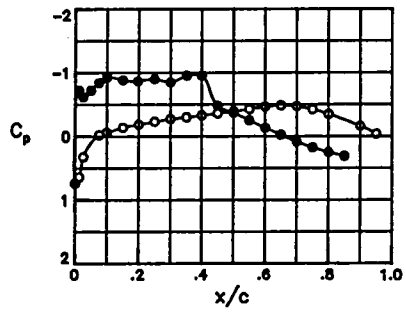

α=-3.98

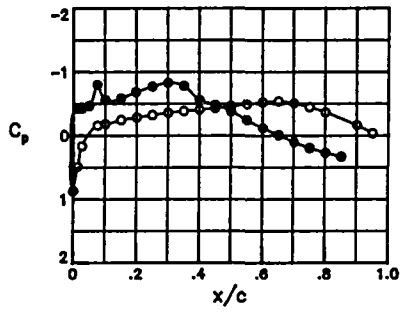

α=-3.01

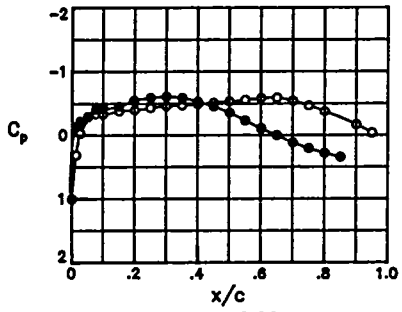

α=-2.00

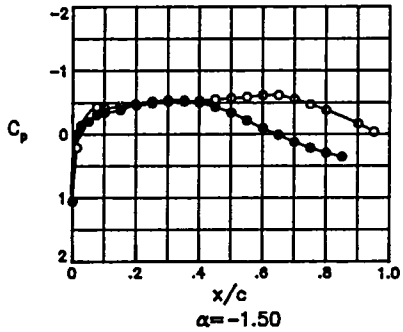

α=-1.50

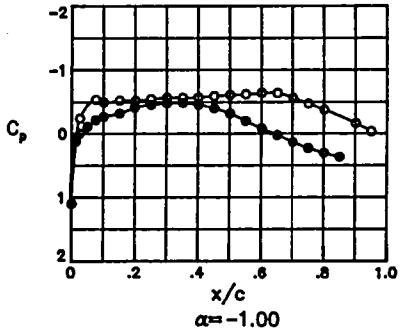

α=-1.00

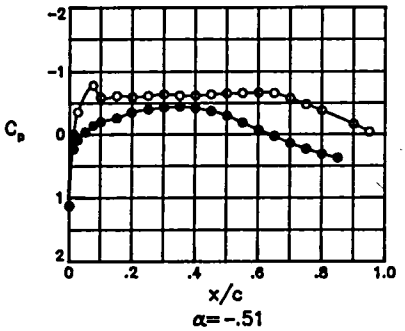

α=-.51

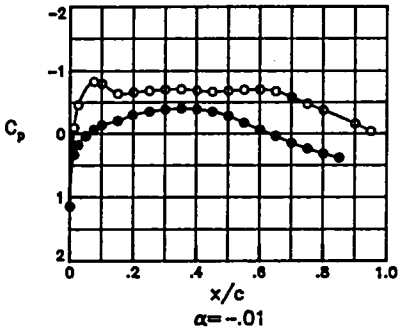

α=-.01

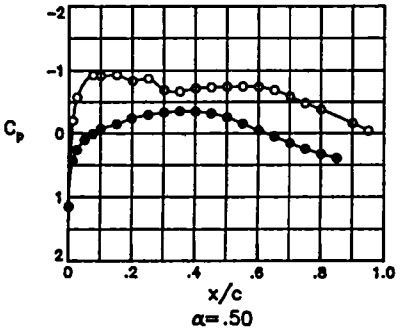

α=.50

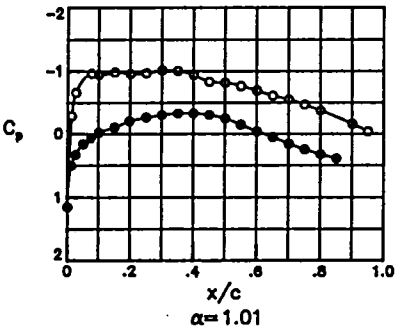

α=1.01

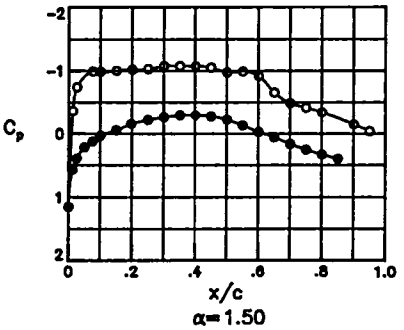

α=1.50

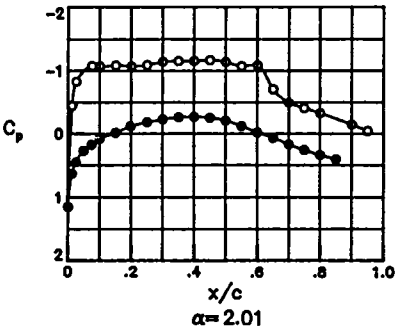

α=2.01

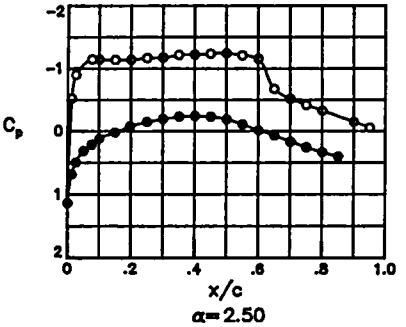

α=2.50

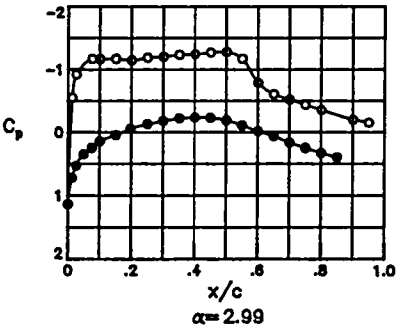

α=2.99

TEST 167
RUN 64
MACH .760
R 15.0 x 10^6

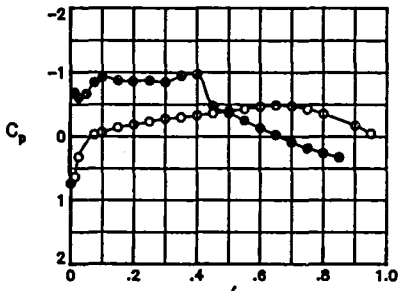

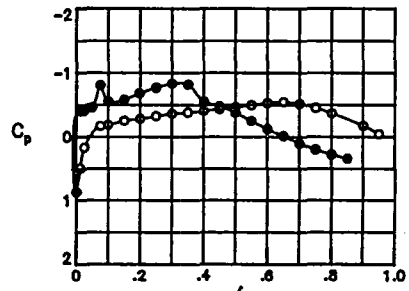

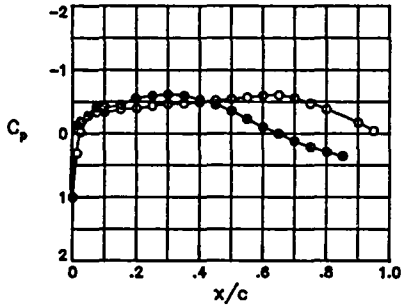

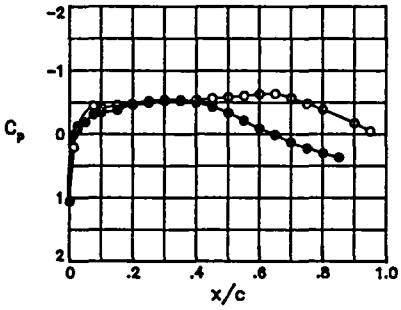

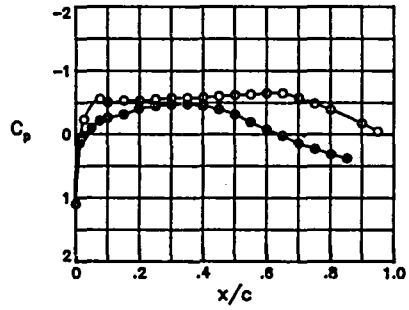

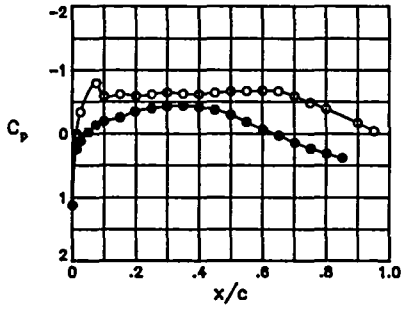

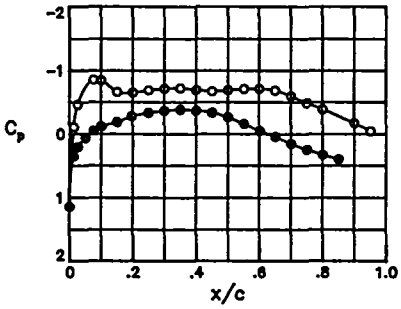

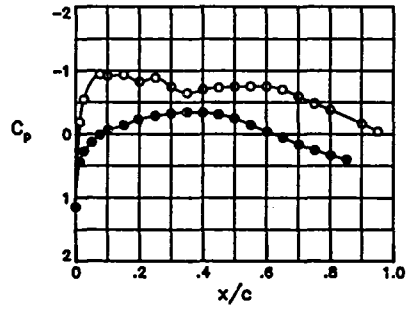

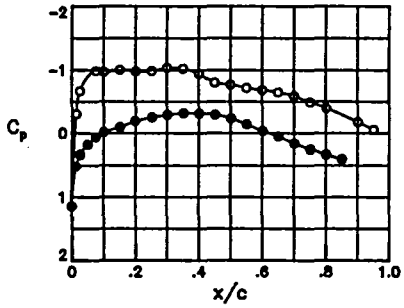

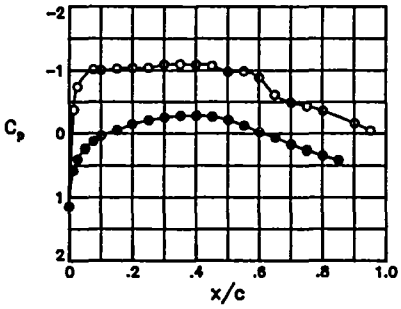

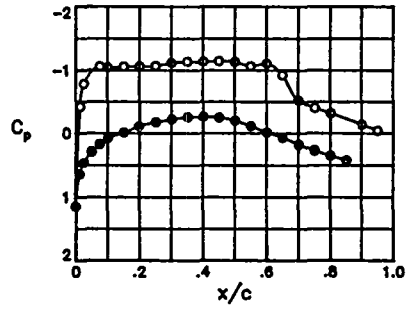

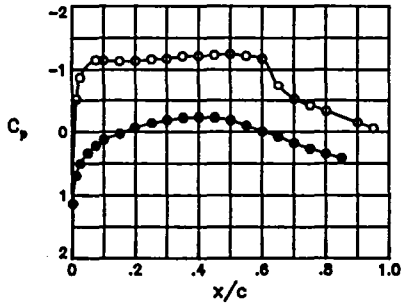

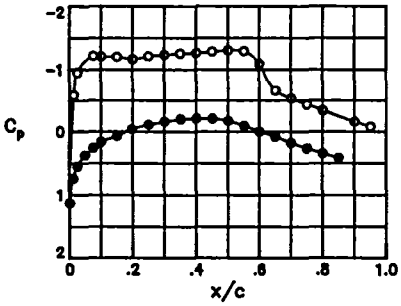

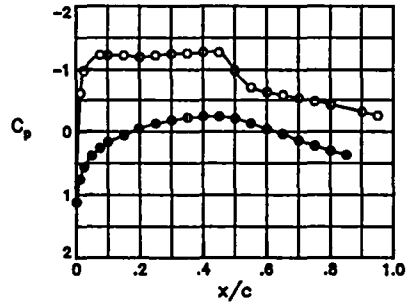

TEST	167
RUN	69
MACH	.760
R	30.0 x 10^6

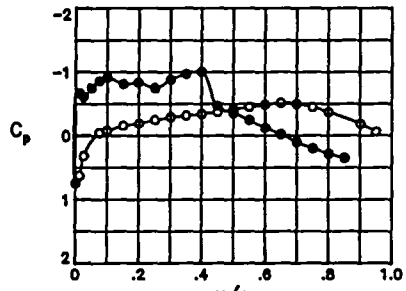

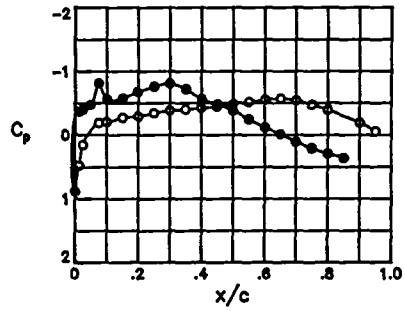

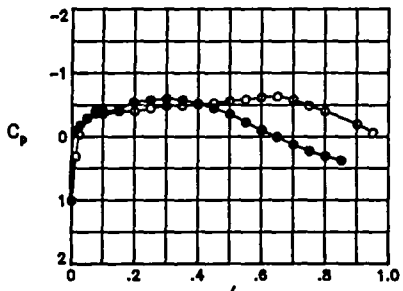

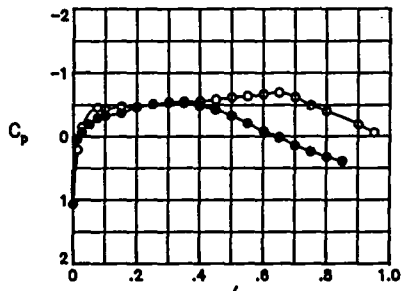

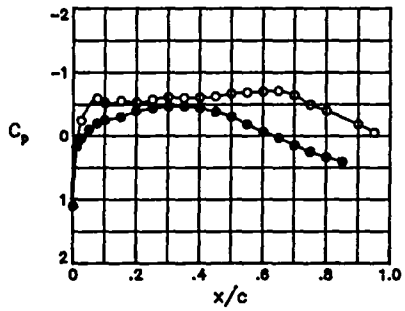

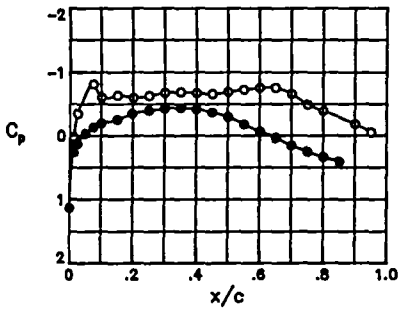

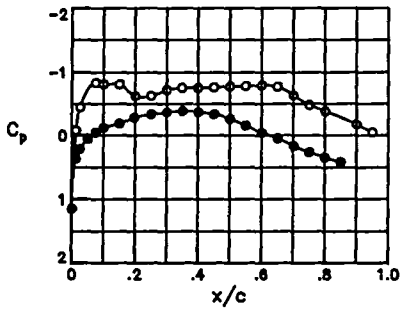

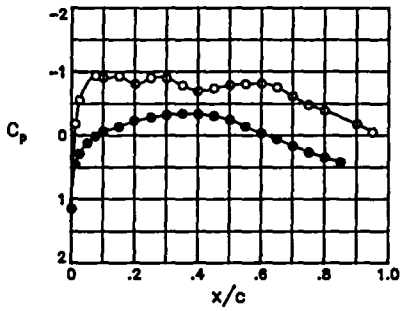

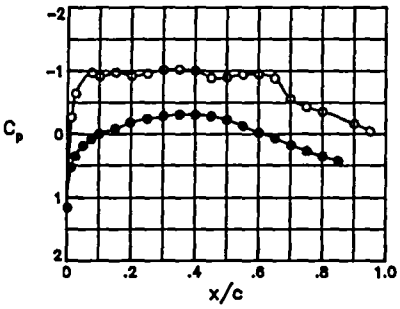

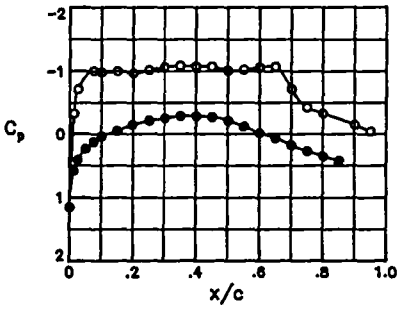

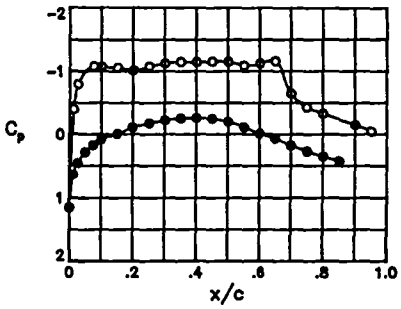

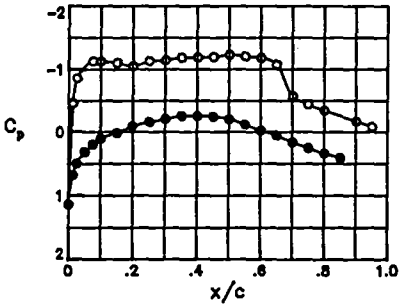

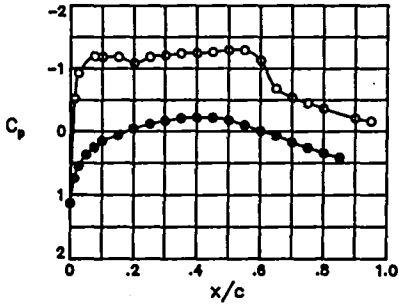

TEST	167
RUN	69
MACH	.760
R	30.0 x 10^6

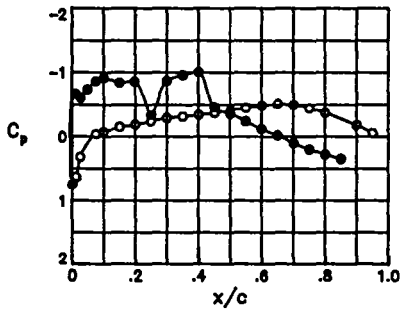

α= -3.98

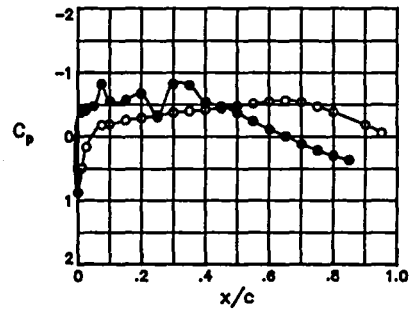

α= -3.00

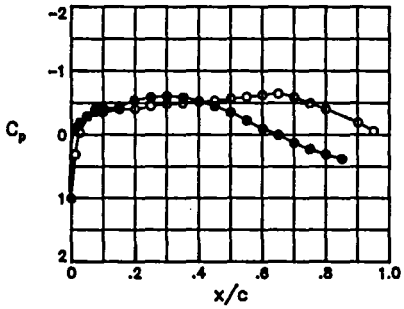

α= -2.00

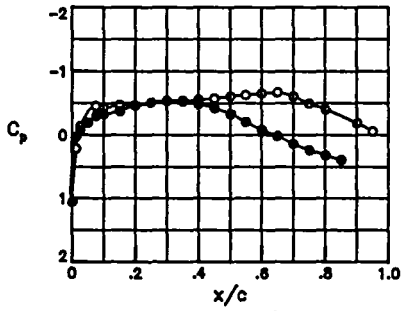

α= -1.50

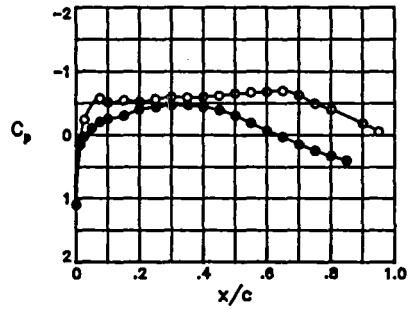

α= -1.01

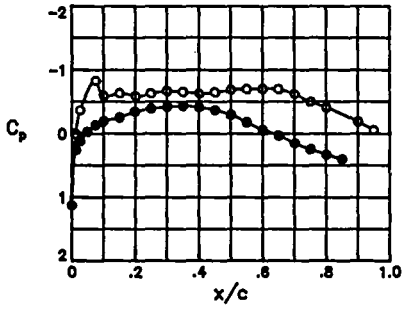

α= -.50

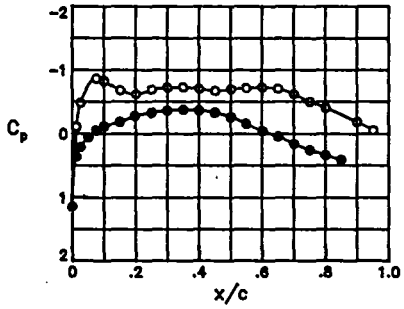

α= 0.00

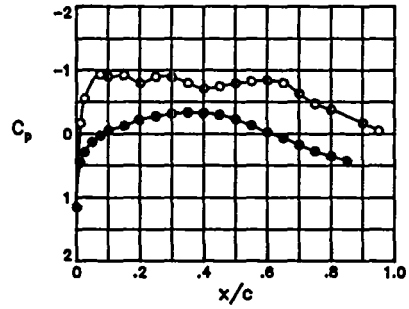

α= .50

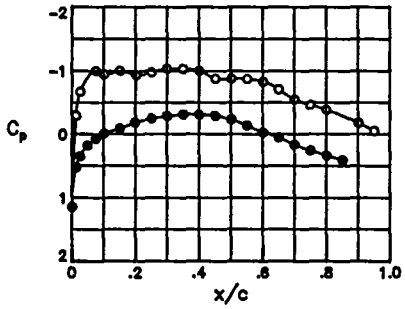

α= 1.02

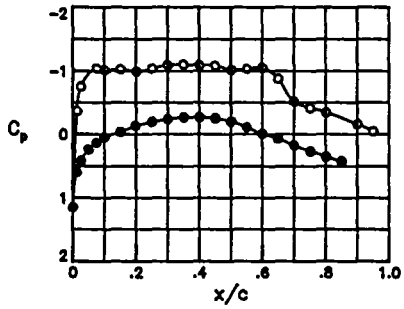

α= 1.51

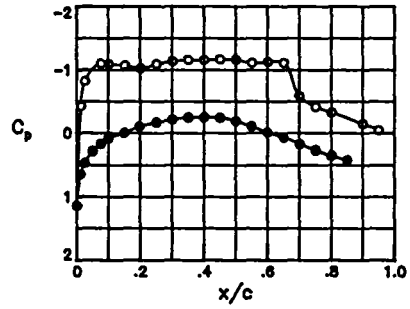

α= 2.02

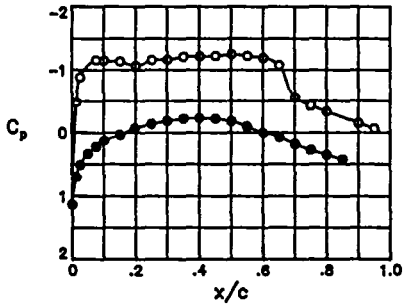

α= 2.52

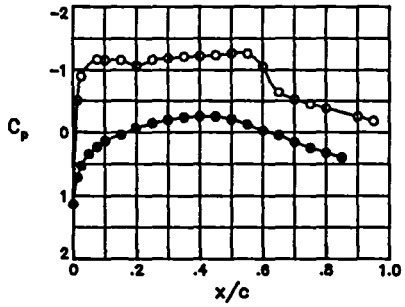

α= 3.03

TEST	167
RUN	71
MACH	.760
R	30.0 x 10^6

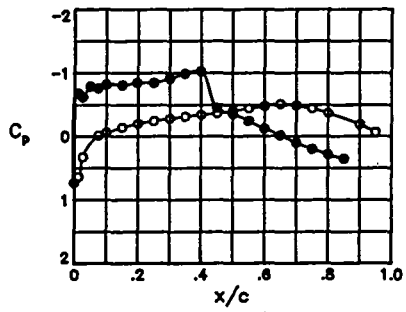

α=-4.04

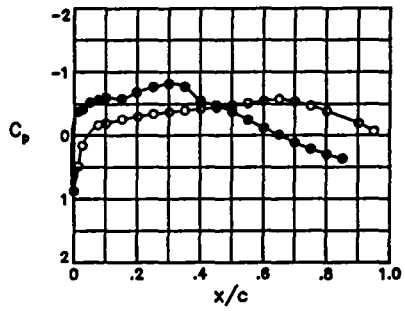

α=-3.00

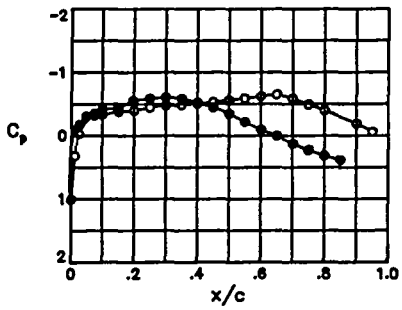

α=-2.01

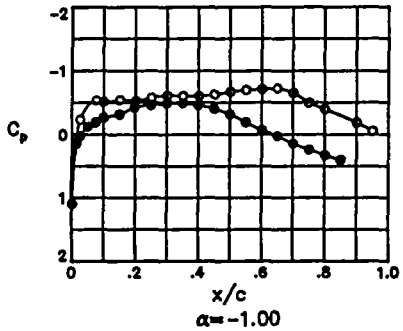

α=-1.00

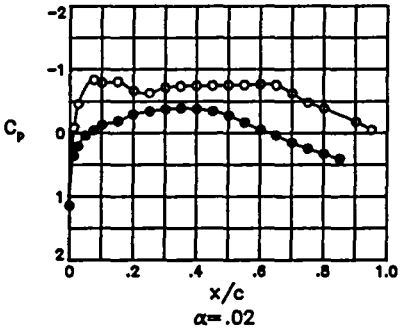

α=.02

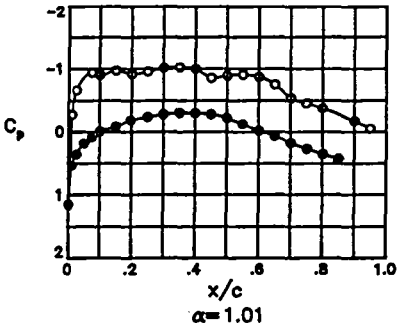

α=1.01

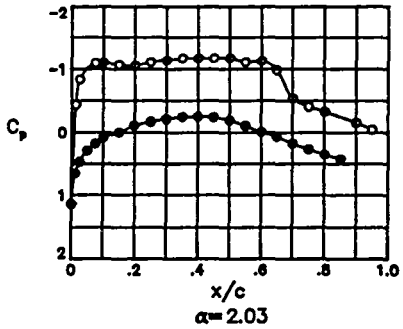

α=2.03

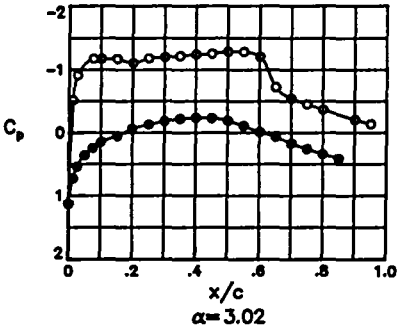

α=3.02

TEST	167
RUN	70
MACH	.760
R	40.0 x 10^6

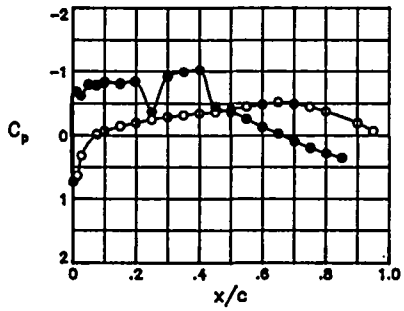

α=-3.97

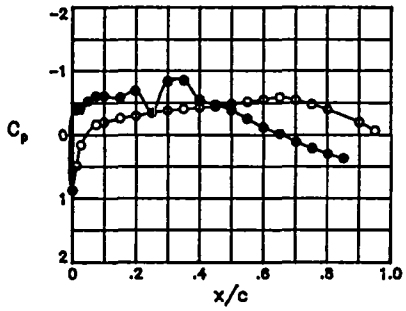

α=-3.00

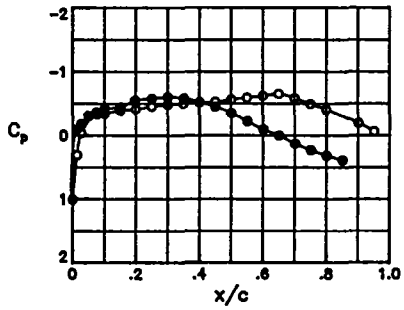

α=-1.97

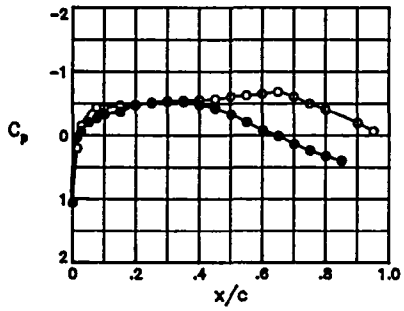

α=-1.46

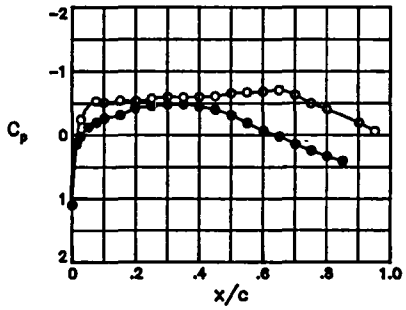

α=-1.03

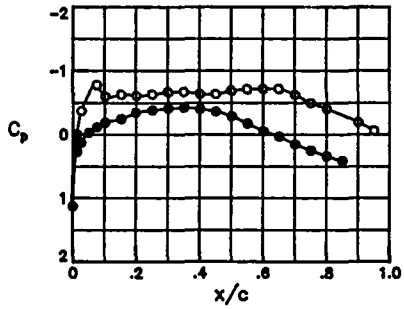

α=-.47

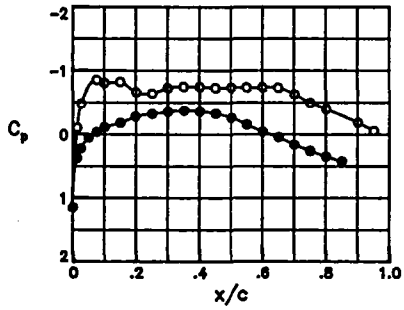

α=.05

Appendix P

Pressure Data for $M = 0.78$; $R = 4.4 \times 10^6$, 7.0×10^6, 10.0×10^6, 15.0×10^6, and 30.0×10^6; Fixed Transition

The pressure measurements made on the NASA SC(3)-0712(B) airfoil are presented in coefficient form in graphs in this appendix. The data are for a given Mach number through the Reynolds number range. The pressure data from the upper surface of the airfoil are plotted as open symbols and the lower-surface data are plotted as solid symbols.

TEST	167
RUN	57
MACH	.780
R	4.4 x 10^6

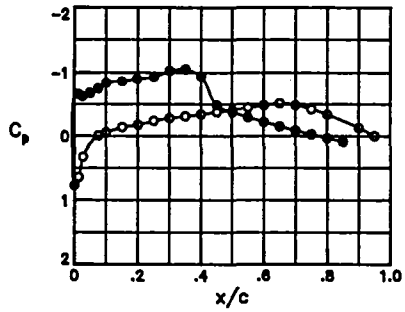

α=-3.98

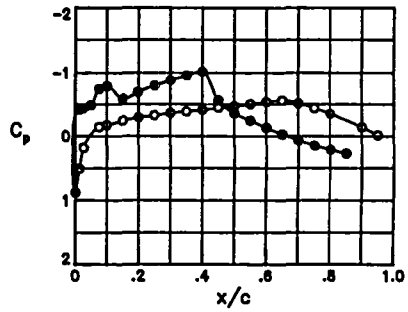

α=-2.99

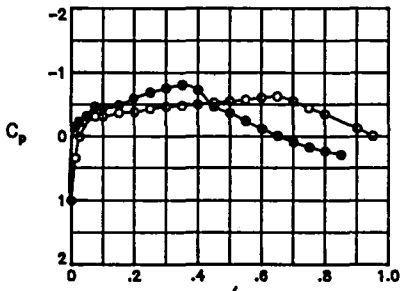

α=-1.99

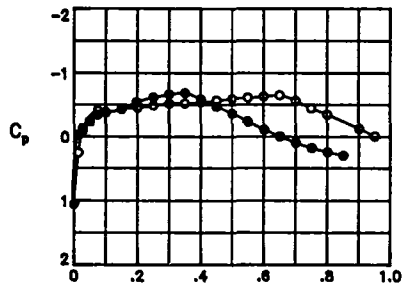

α=-1.50

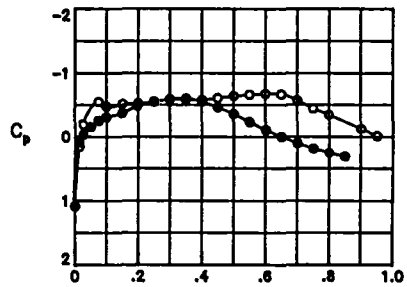

α=-1.00

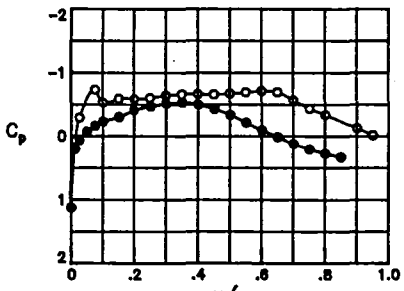

α=-.49

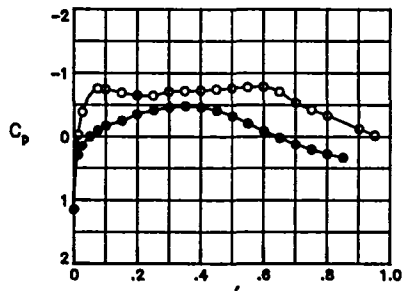

α=.03

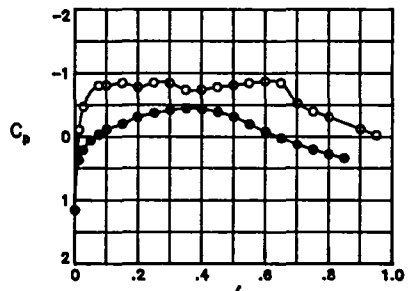

α=.52

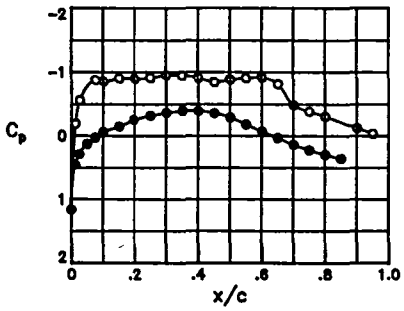

α=1.01

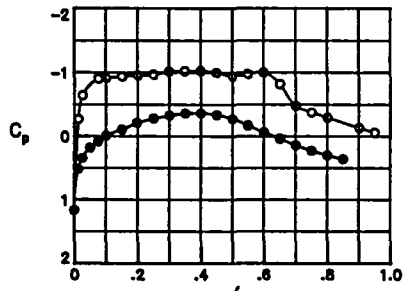

α=1.52

TEST	167
RUN	60
MACH	.780
R	7.0 x 10^6

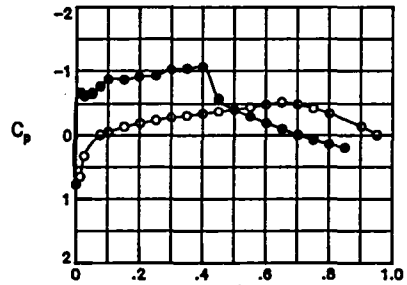

α=-4.01

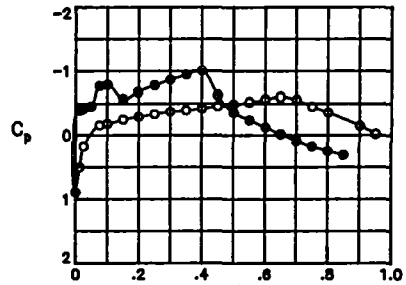

α=-3.00

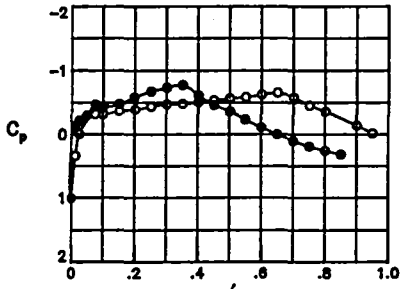

α=-2.00

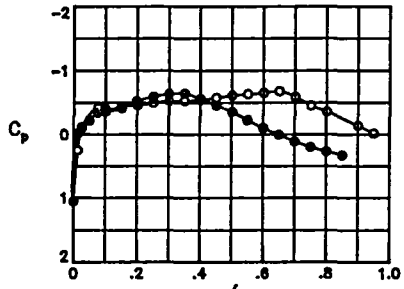

α=-1.51

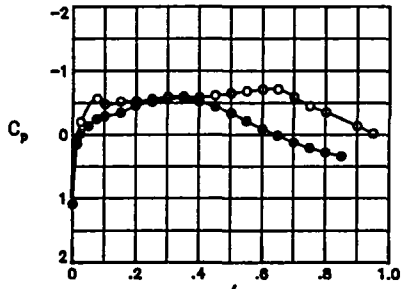

α=-1.01

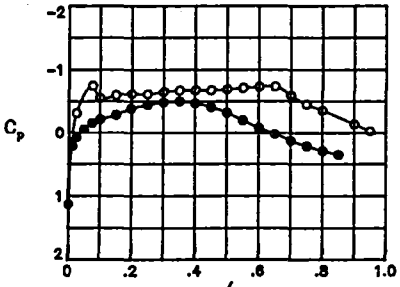

α=-.50

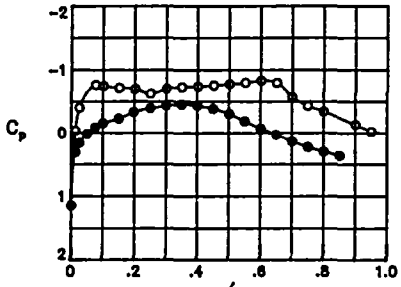

α=-.01

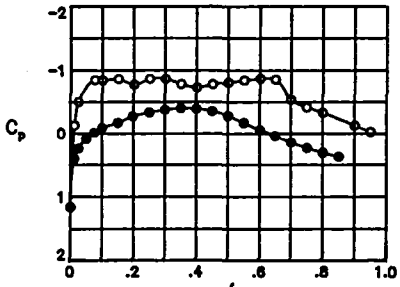

α=.50

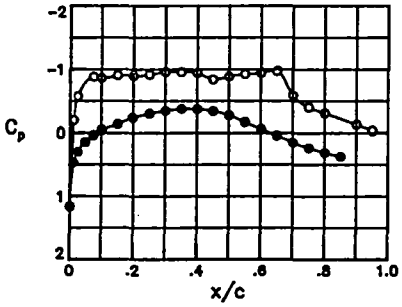

α=1.00

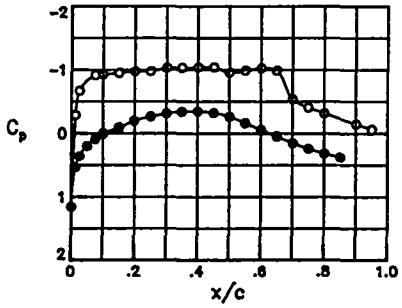

α=1.51

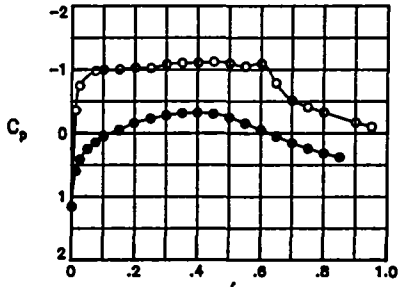

α=2.02

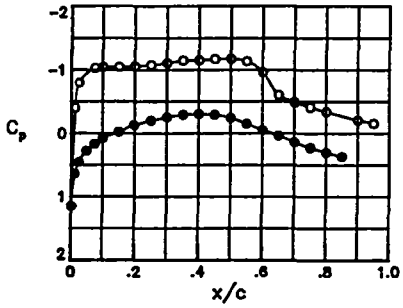

α=2.52

TEST	167
RUN	66
MACH	.780
R	10.0 x 10^6

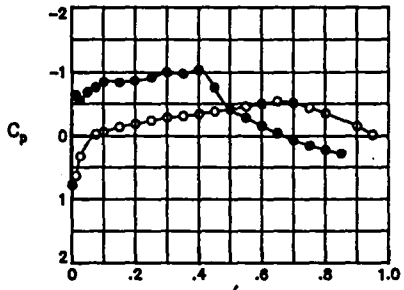

α=-3.98

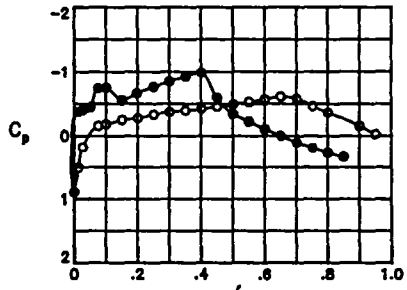

α=-3.01

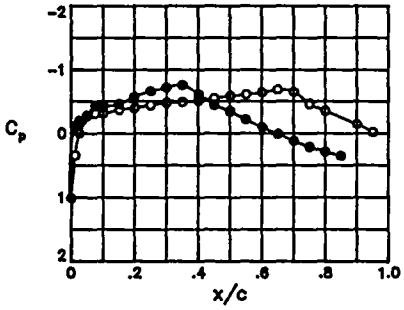

α=-2.00

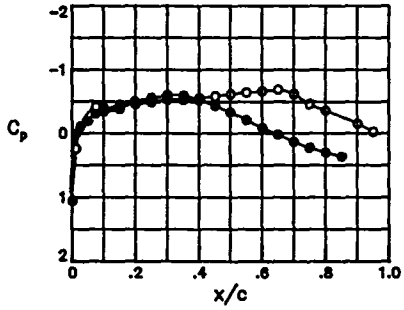

α=-1.50

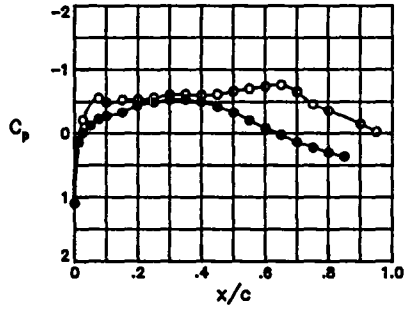

α=-1.00

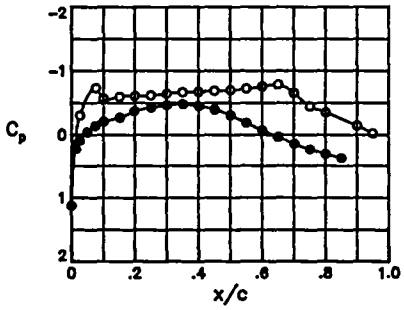

α=-.50

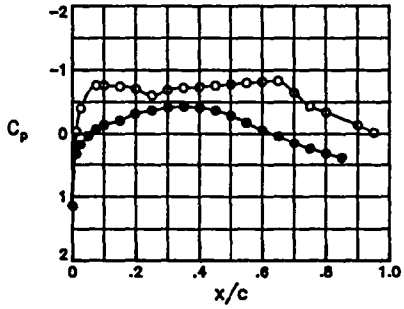

α=-.01

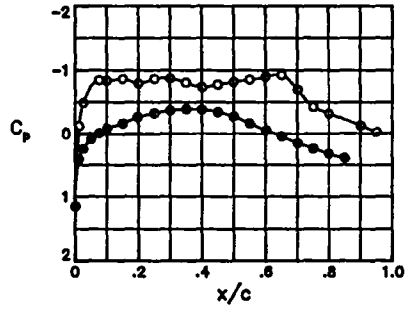

α=.50

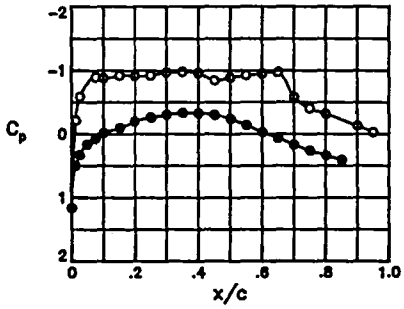

α=1.00

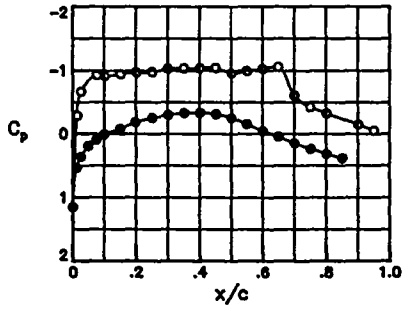

α=1.50

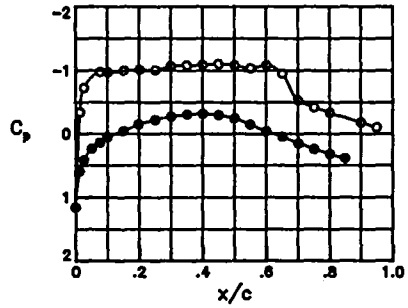

α=2.01

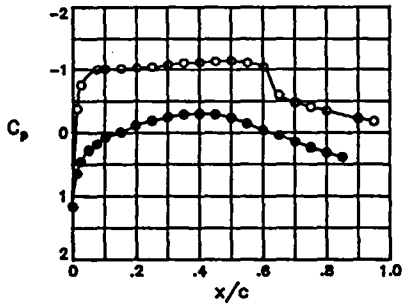

α=2.50

TEST	167
RUN	63
MACH	.780
R	15.0 x 10^6

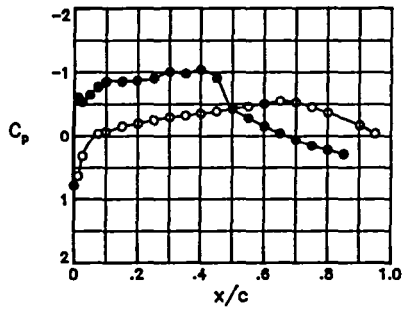

α=-3.97

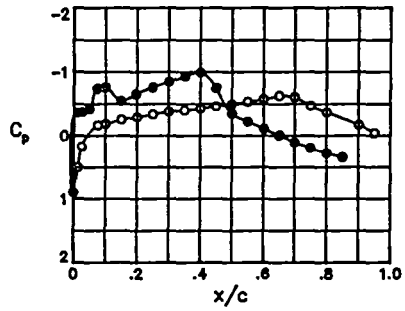

α=-2.99

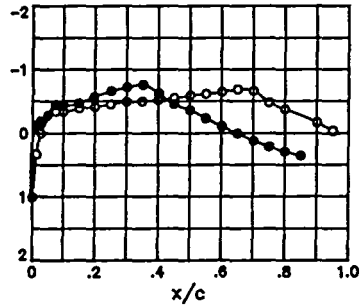

α=-1.99

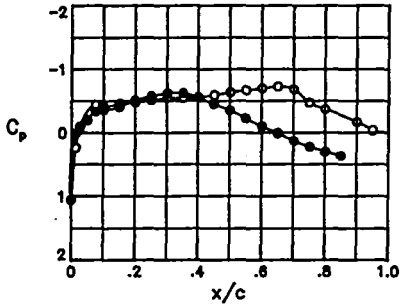

α=-1.48

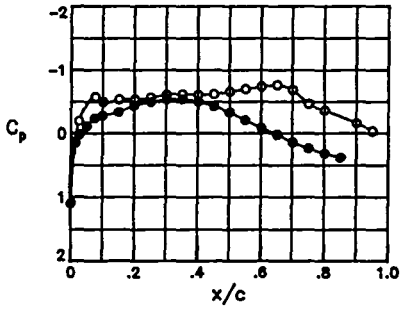

α=-.98

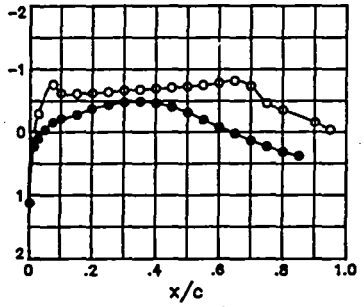

α=-.47

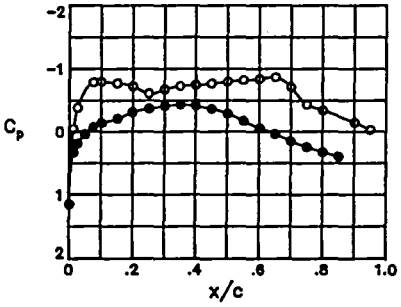

α=.03

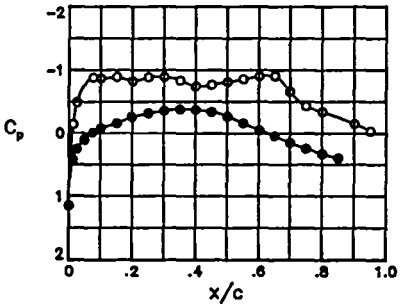

α=.52

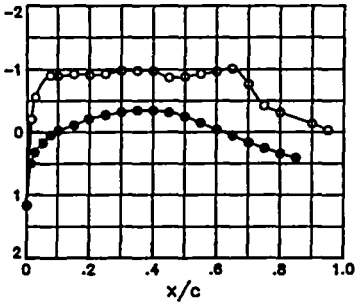

α=1.02

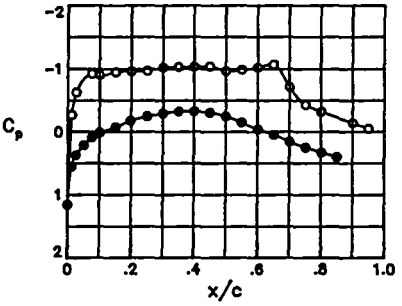

α=1.53

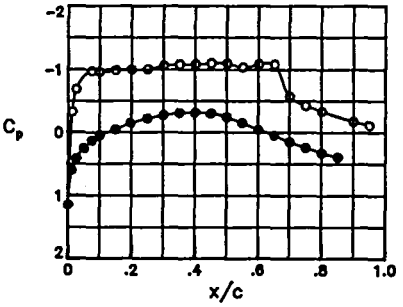

α=2.01

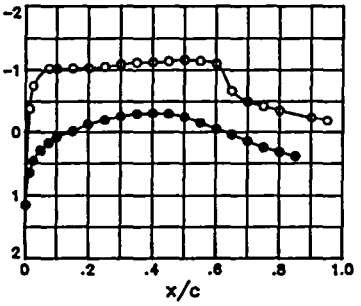

α=2.54

TEST	167
RUN	68
MACH	.780
R	30.0 x 10^6

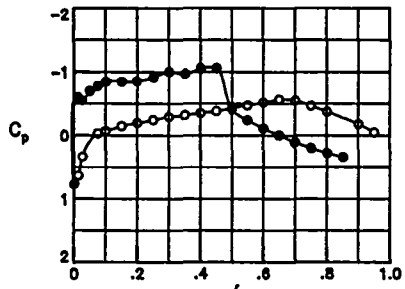

α=-3.99

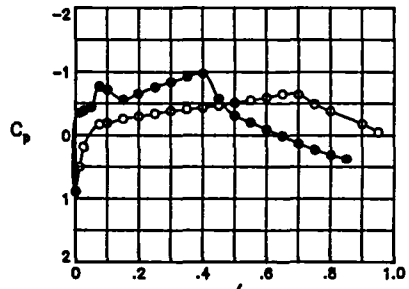

α=-2.99

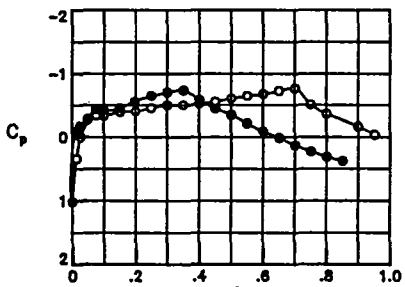

α=-1.99

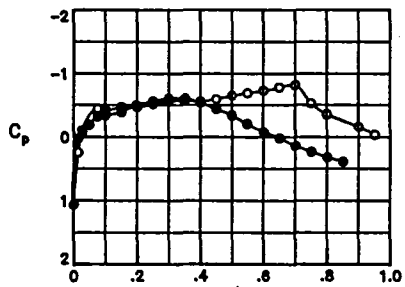

α=-1.49

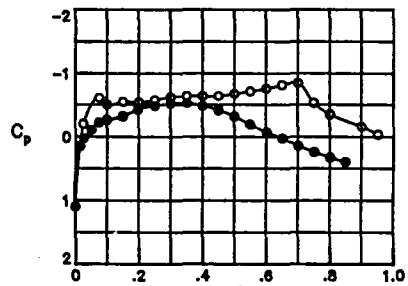

α=-.99

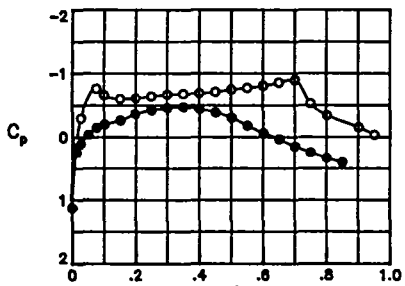

α=-.49

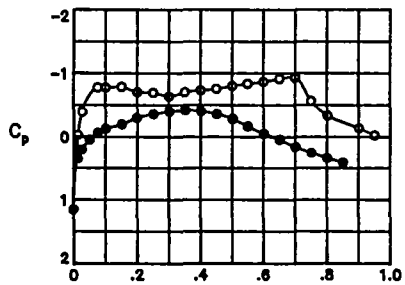

α=.04

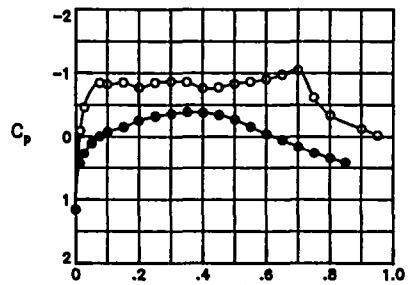

α=.54

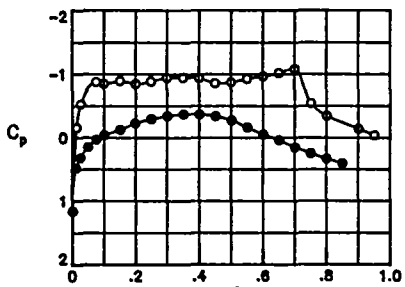

α=1.01

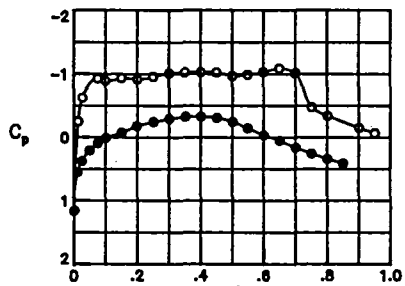

α=1.51

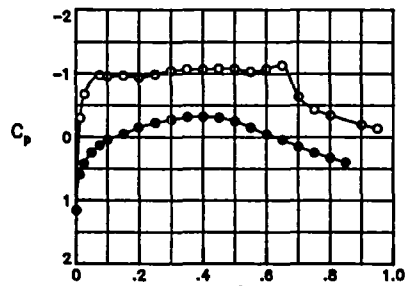

α=2.01

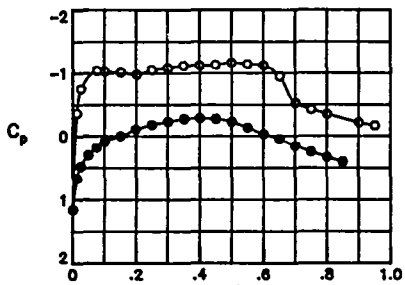

α=2.51

References

1. Ladson, Charles L.; and Ray, Edward J.: Status of Advanced Airfoil Tests in the Langley 0.3-Meter Transonic Cryogenic Tunnel. *Advanced Aerodynamics—Selected NASA Research,* NASA CP-2208, 1981, pp. 37–53.
2. Ray, Edward J.; Ladson, Charles L.; Adcock, Jerry B.; Lawing, Pierce L.; and Hall, Robert M.: *Review of Design and Operational Characteristics of the 0.3-Meter Transonic Cryogenic Tunnel.* NASA TM-80123, 1979.
3. Johnson, William G., Jr.; Hill, Acquilla S.; and Eichmann, Otto: *Pressure Distributions From High Reynolds Number Tests of a NASA SC(3)-0712(B) Airfoil in the Langley 0.3-Meter Transonic Cryogenic Tunnel.* NASA TM-86370, 1985.
4. Mechtly, E. A.: *The International System of Units—Physical Constants and Conversion Factors (Second Revision).* NASA SP-7012, 1973.
5. Kilgore, Robert A.; Adcock, Jerry B.; and Ray, Edward J.: The Cryogenic Transonic Wind Tunnel for High Reynolds Number Research. *Windtunnel Design and Testing Techniques,* AGARD-CP-174, 1976, pp. 1-1—1-20.
6. Kilgore, Robert A.: *Design Features and Operational Characteristics of the Langley 0.3-Meter Transonic Cryogenic Tunnel.* NASA TN D-8304, 1976.
7. Ladson, Charles L.; and Kilgore, Robert A.: *Instrumentation for Calibration and Control of a Continuous-Flow Cryogenic Tunnel.* NASA TM-81825, 1980.
8. Baals, Donald D.; and Mourhess, Mary J.: *Numerical Evaluation of the Wake-Survey Equations for Subsonic Flow Including the Effect of Energy Addition.* NACA WR L-5, 1945. (Formerly NACA ARR L5H27.)
9. Hall, Robert M.; and Adcock, Jerry B.: *Simulation of Ideal-Gas Flow by Nitrogen and Other Selected Gases at Cryogenic Temperatures.* NASA TP-1901, 1981.
10. Adcock, Jerry B.: *Real-Gas Effects Associated With One-Dimensional Transonic Flow of Cryogenic Nitrogen.* NASA TN D-8274, 1976.
11. Adcock, Jerry B.; and Johnson, Charles B.: *A Theoretical Analysis of Simulated Transonic Boundary Layers in Cryogenic-Nitrogen Wind Tunnels.* NASA TP-1631, 1980.

TABLE I. PRESSURE ORIFICE LOCATIONS

Upper surface			
Orifice no.	x/c	$y/(b/2)$	z/c
1	0.0000	0.0000	0.0000
2	.0132	.0924	.0206
3	.0259	.0626	.0274
[a]4	.0514	.0326	.0353
5	.0759	.0326	.0407
6	.1003	.0326	.0445
7	.1507	.0326	.0504
8	.2003	.0326	.0543
9	.2503	.0326	.0572
10	.3001	.0326	.0589
11	.3502	.0326	.0599
12	.4003	.0326	.0601
13	.4501	.0326	.0596
14	.5002	.0326	.0583
15	.5502	.0326	.0564
16	.6002	.0326	.0536
17	.6500	.0326	.0499
18	.7000	.0326	.0450
19	.7500	.0326	.0389
20	.8002	.0326	.0315
[a,b]21	.8500	.0326	.0228
[b]22	.9002	.0326	.0129
[c]23	.9501	.0976	.0016
[a,c]24	1.0000	.0000	−.0025

Spanwise			
Orifice no.	x/c	$y/(b/2)$	z/c
25	0.1507	0.7476	0.0504
26	.1507	.4976	.0504
27	.1507	.2476	.0504
28	.1507	−.2524	.0504
29	.1507	−.5024	.0503
30	.1507	−.7524	.0503
31	.5002	.7476	.0583
32	.5002	.4976	.0583
33	.5002	.2476	.0583
34	.5002	−.2524	.0583
35	.5002	−.5024	.0583
36	.5002	−.7524	.0584
37	.8002	.7476	.0315
38	.8002	.4976	.0315
39	.8002	.2476	.0315
[a]40	.8002	−.2524	.0315
41	.8002	−.5024	.0315
42	.8002	−.7524	.0315

Lower surface			
Orifice no.	x/c	$y/(b/2)$	z/c
43	0.0126	−0.0324	−0.0127
44	.0255	−.0624	−.0185
45	.0495	−.0924	−.0263
46	.0753	−.0924	−.0326
47	.1002	−.0324	−.0376
48	.1503	−.0324	−.0457
49	.1976	−.0324	−.0517
50	.2503	−.0324	−.0566
51	.3001	−.0324	−.0594
52	.3507	−.0324	−.0608
53	.4001	−.0324	−.0607
54	.4501	−.0324	−.0591
55	.5001	−.0324	−.0558
56	.5497	−.0324	−.0508
57	.6003	−.0324	−.0446
58	.6500	−.0324	−.0375
59	.7000	−.0324	−.0299
60	.7501	−.0324	−.0220
61	.8001	−.0324	−.0148
[b]62	.8501	−.0324	−.0086
[a,b]63	.8986	−.0324	−.0047
[a,c]64	.9489	−.0974	−.0068

[a]These tubes blocked or had high leak rates.

[b]Used 0.102-cm (0.040-in.) o.d. and 0.051-cm (0.020-in.) i.d. tubing.

[c]Used 0.051-cm (0.020-in.) o.d. and 0.025-cm (0.010-in.) i.d. tubing.

TABLE II. DESIGN AND MEASURED AIRFOIL COORDINATES

Upper surface		
x/c	z_{design}/c	z_{meas}/c
0.002	0.0092	0.0074
.005	.0141	.0131
.010	.0190	.0181
.020	.0252	.0247
.030	.0294	.0291
.040	.0327	.0325
.050	.0354	.0352
.070	.0397	.0397
.080	.0415	.0415
.100	.0446	.0445
.120	.0471	.0471
.150	.0504	.0504
.180	.0530	.0529
.200	.0544	.0544
.220	.0557	.0556
.250	.0572	.0572
.280	.0584	.0584
.300	.0590	.0589
.330	.0596	.0596
.350	.0599	.0599
.370	.0601	.0600
.400	.0601	.0601
.420	.0600	.0600
.450	.0596	.0596
.480	.0590	.0589
.500	.0584	.0583
.530	.0573	.0572
.550	.0564	.0563
.580	.0549	.0548
.600	.0537	.0536
.630	.0516	.0515
.650	.0500	.0499
.670	.0482	.0481
.700	.0451	.0450
.730	.0416	.0415
.750	.0390	.0389
.770	.0362	.0360
.800	.0316	.0315
.830	.0266	.0264
.850	.0230	.0228
.870	.0192	.0190
.900	.0131	.0129
.920	.0088	.0086
.940	.0042	.0040
.950	.0018	.0016
.960	−.0007	−.0009
.970	−.0033	−.0035
.980	−.0060	−.0062
.990	−.0088	−.0090
1.000	−.0117	−.0118

Lower surface		
x/c	z_{design}/c	z_{meas}/c
0.002	−0.0051	−.0039
.005	−.0081	−.0077
.010	−.0116	−.0113
.020	−.0165	−.0162
.030	−.0204	−.0202
.040	−.0238	−.0235
.050	−.0266	−.0264
.070	−.0316	−.0314
.080	−.0338	−.0336
.100	−.0377	−.0375
.120	−.0412	−.0410
.150	−.0458	−.0456
.180	−.0498	−.0496
.200	−.0521	−.0520
.230	−.0550	−.0549
.250	−.0566	−.0565
.280	−.0585	−.0584
.300	−.0595	−.0594
.330	−.0605	−.0604
.350	−.0609	−.0608
.380	−.0610	−.0609
.400	−.0608	−.0607
.430	−.0600	−.0599
.450	−.0591	−.0591
.480	−.0573	−.0572
.500	−.0558	−.0557
.530	−.0530	−.0529
.550	−.0509	−.0508
.580	−.0472	−.0471
.600	−.0446	−.0445
.620	−.0419	−.0418
.650	−.0376	−.0375
.680	−.0331	−.0329
.700	−.0299	−.0298
.720	−.0267	−.0266
.750	−.0221	−.0220
.770	−.0191	−.0190
.800	−.0149	−.0147
.820	−.0123	−.0121
.850	−.0088	−.0086
.880	−.0059	−.0057
.900	−.0049	−.0046
.930	−.0055	−.0051
.950	−.0074	−.0069
.960	−.0088	−.0082
.970	−.0105	−.0099
.980	−.0126	−.0120
.990	−.0150	−.0143
1.000	−.0177	−.0167

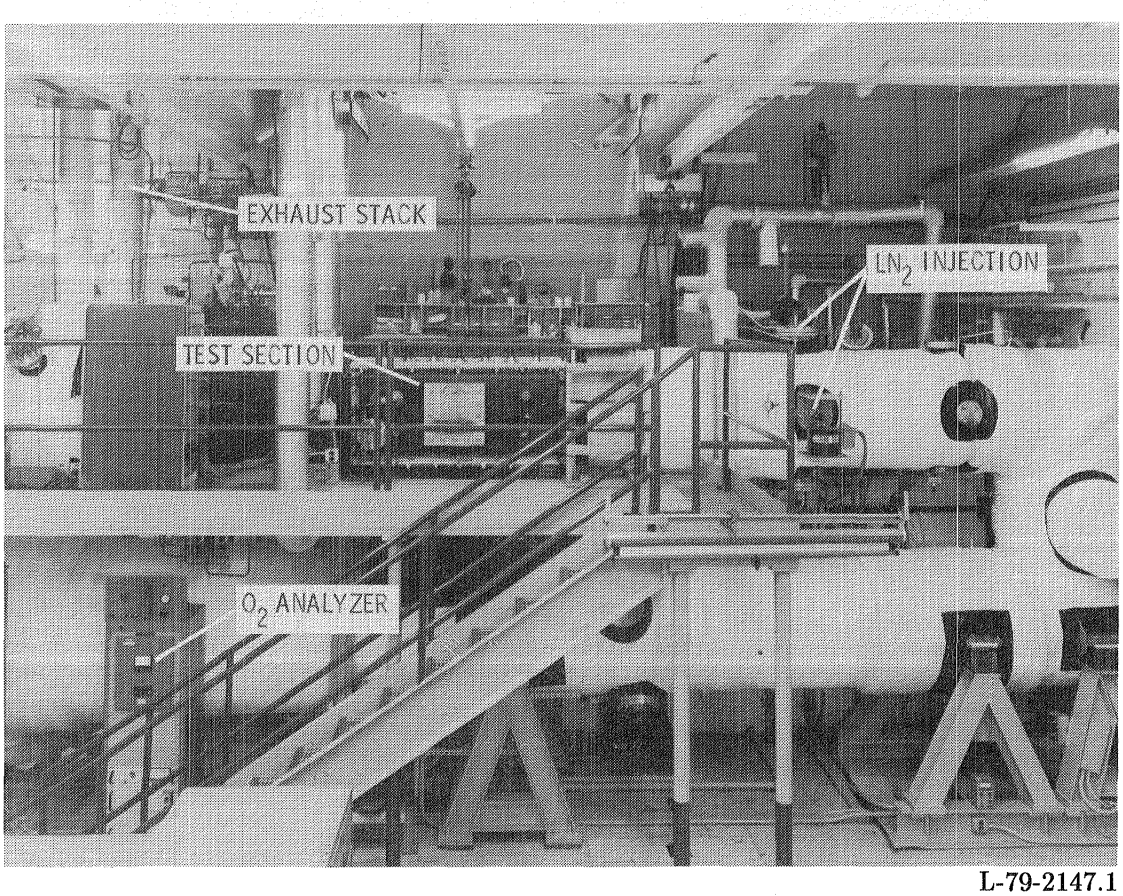

L-79-2147.1

(a) Photograph.

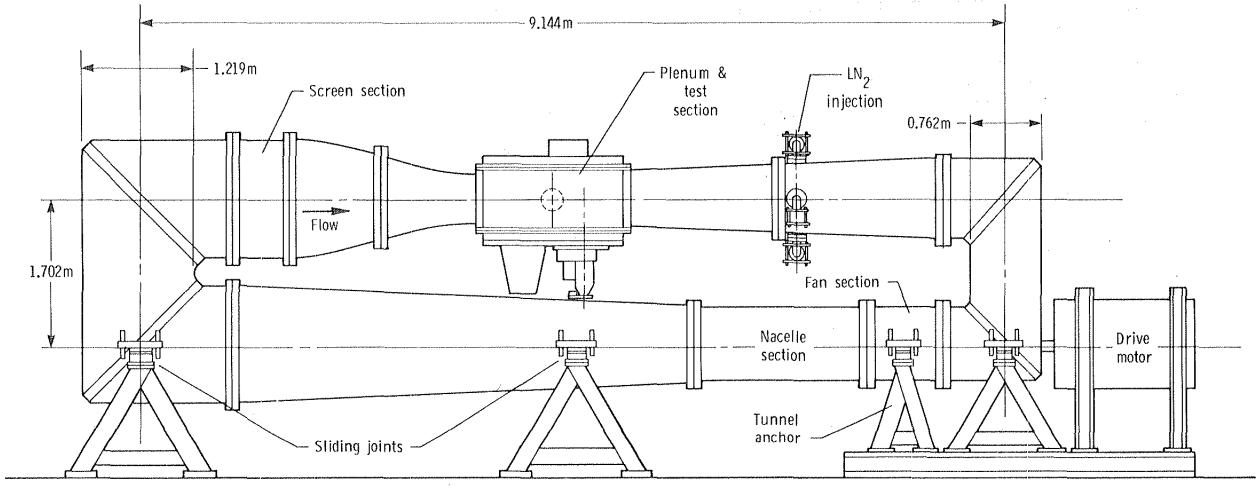

(b) Schematic drawing.

Figure 1. Langley 0.3-Meter Transonic Cryogenic Tunnel with two-dimensional test section installed.

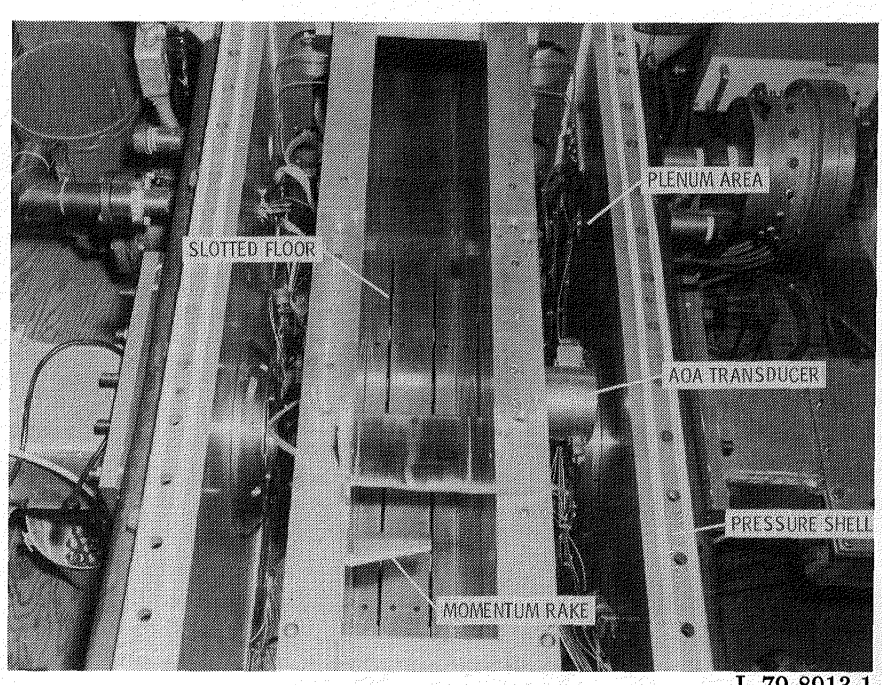

L-79-8913.1

(a) Top-view photograph.

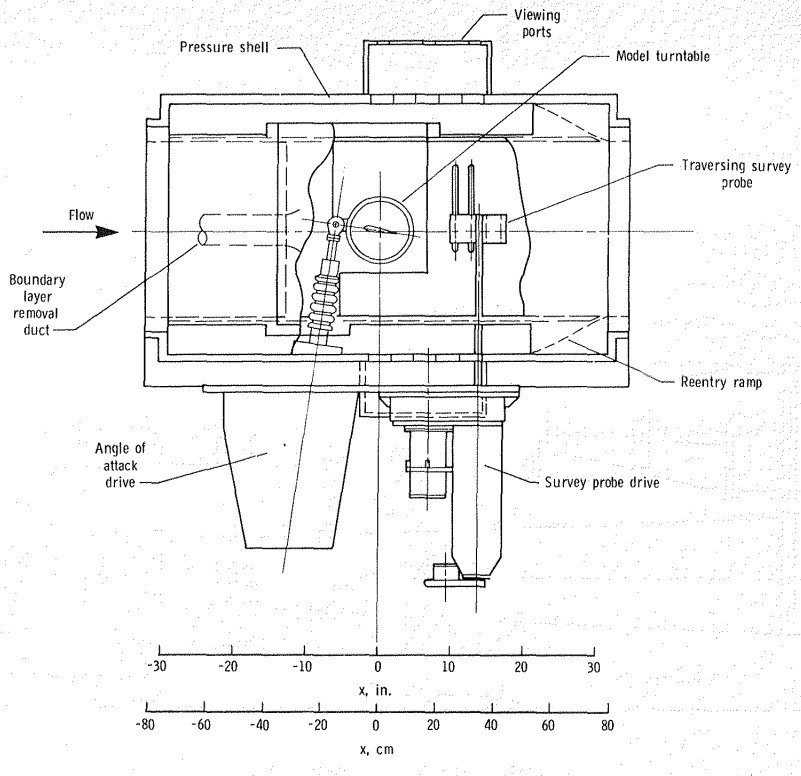

(b) Schematic drawing showing major components.

Figure 2. Two-dimensional test section of 0.3-m TCT.

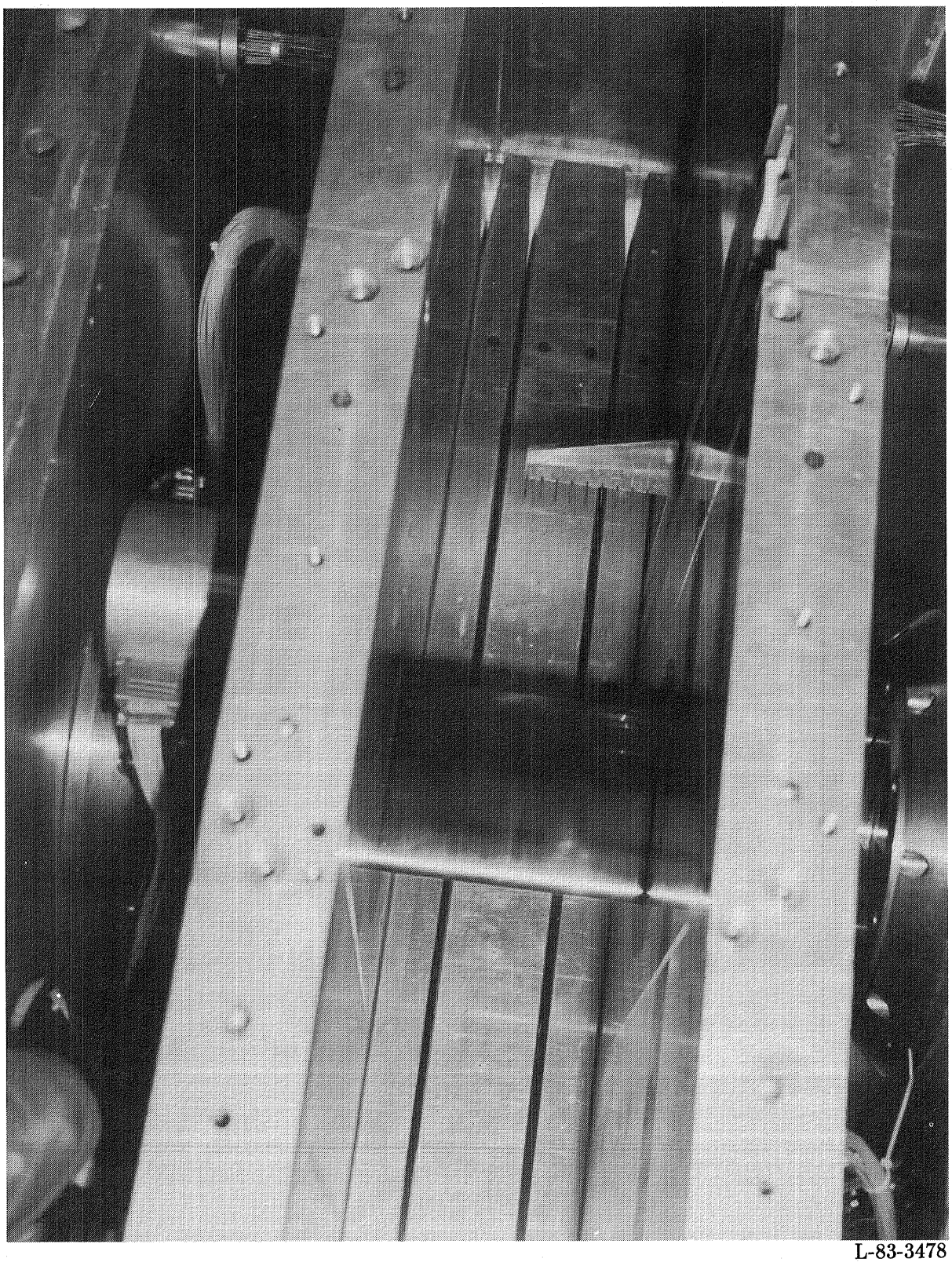

L-83-3478

Figure 3. Model installed in test section of 0.3-m TCT.

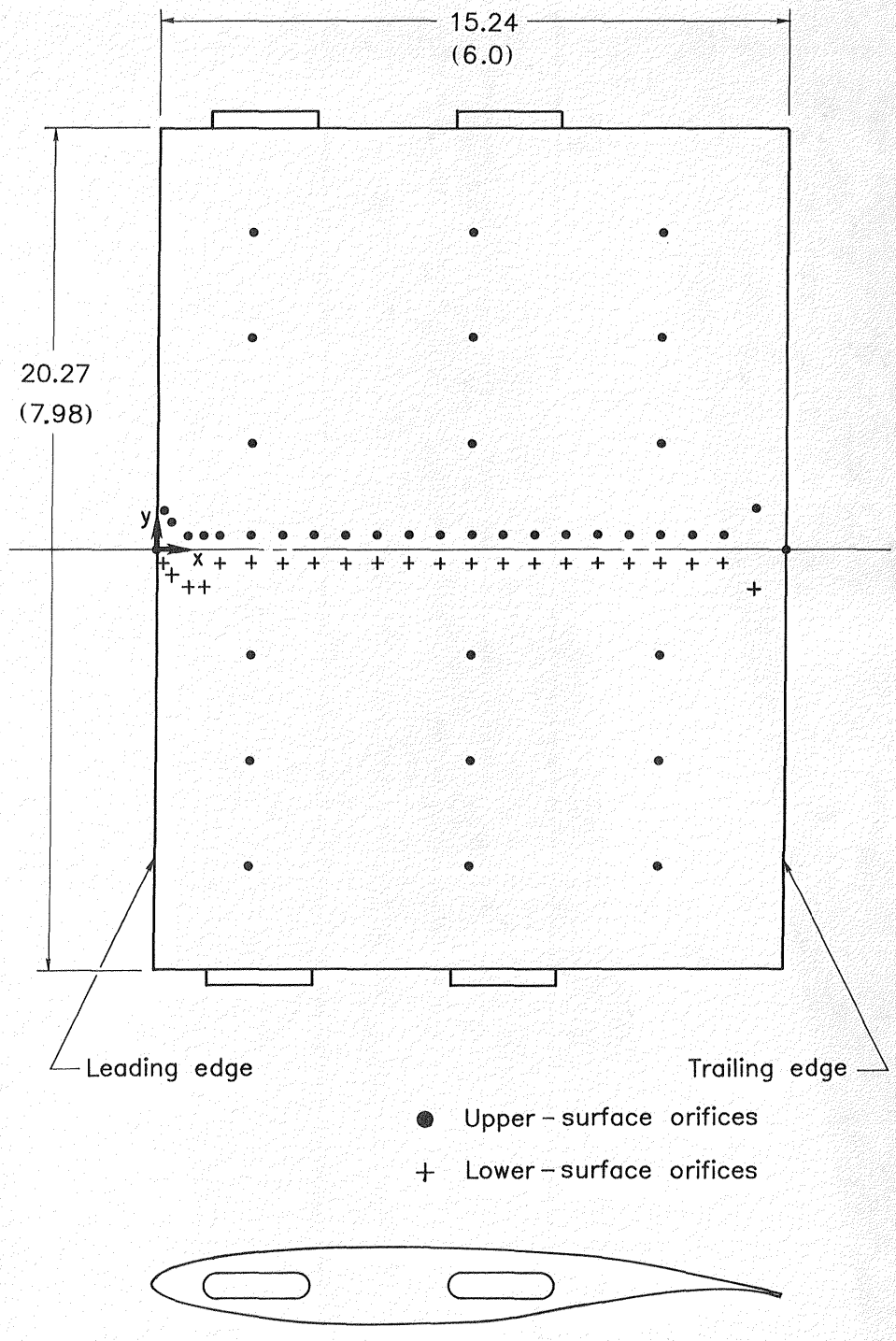

Figure 4. Schematic drawing of model showing orifice arrangement. All dimensions are in cm (in.).

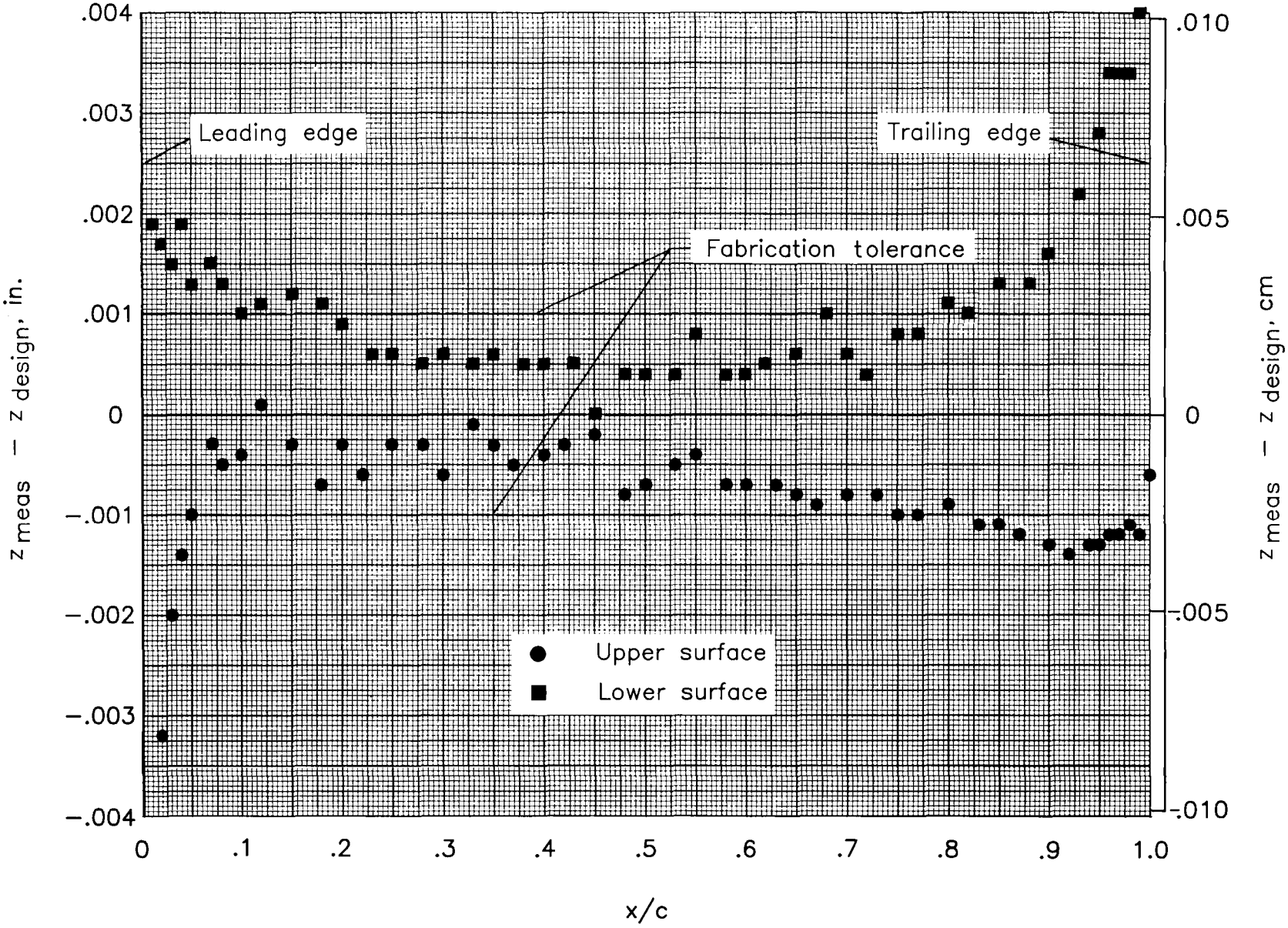

Figure 5. Measured airfoil coordinate error at centerline station.

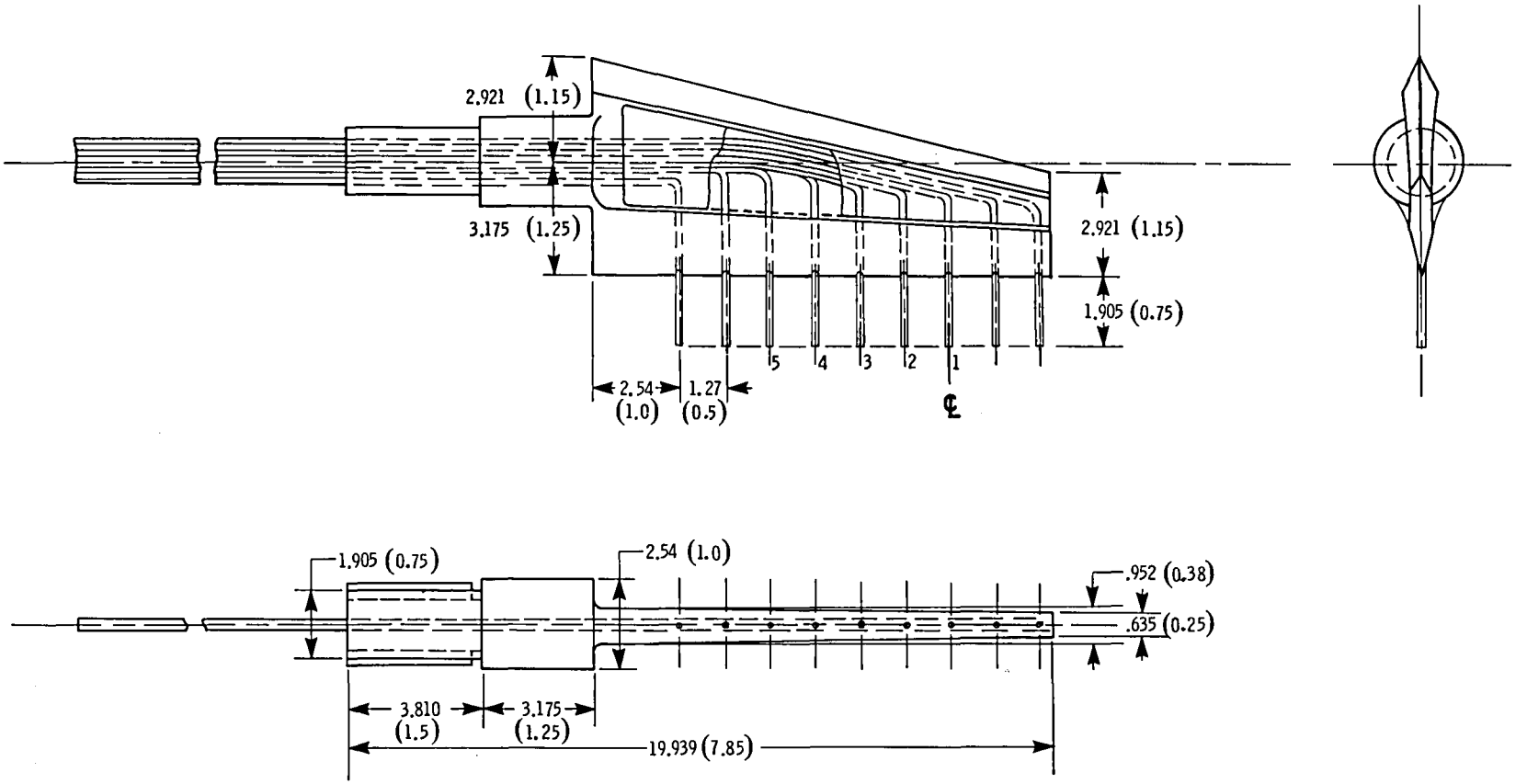

Figure 6. Details of wake survey probe. All dimensions are in cm (in.).

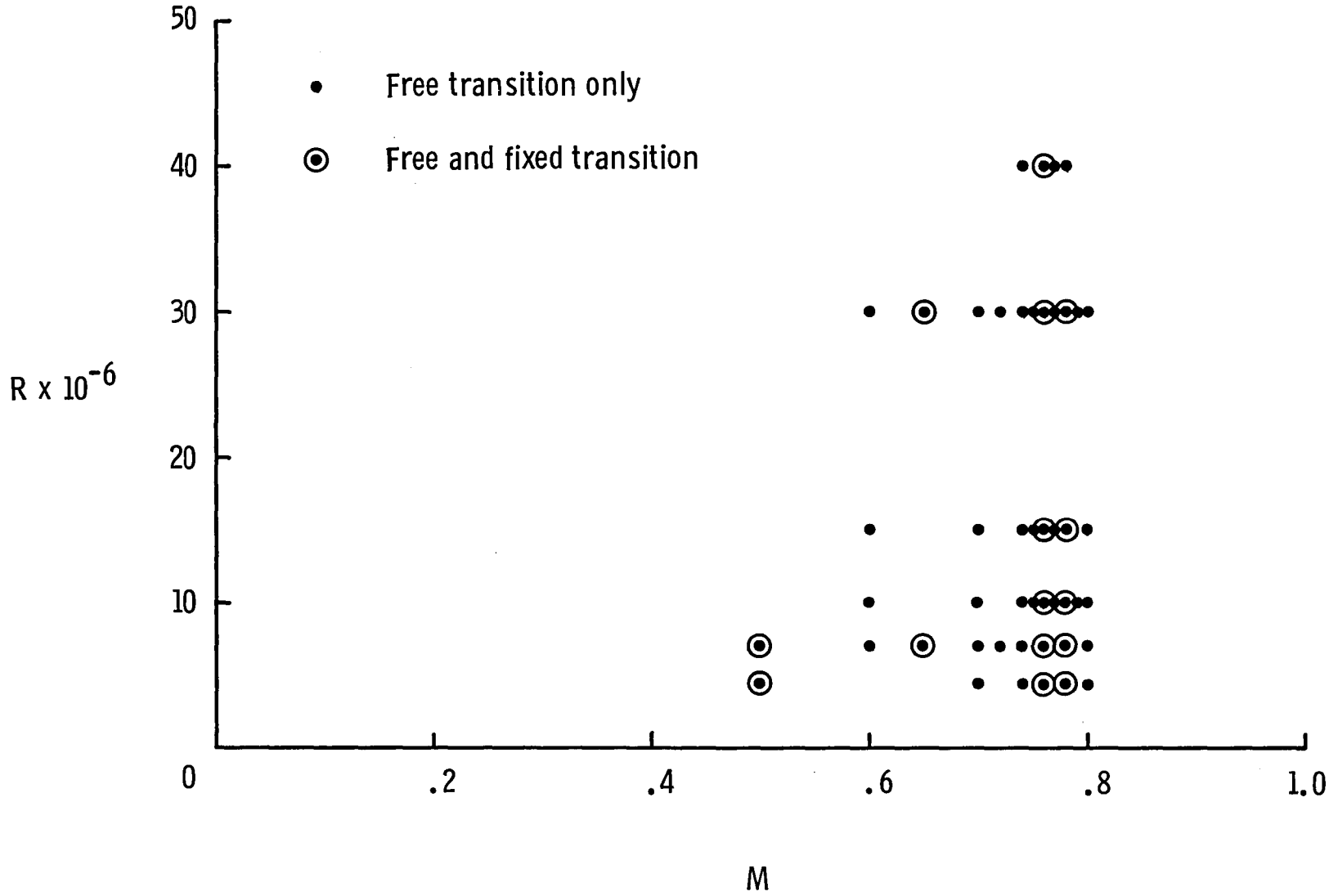

Figure 7. Range of Reynolds number and Mach number used in test program.

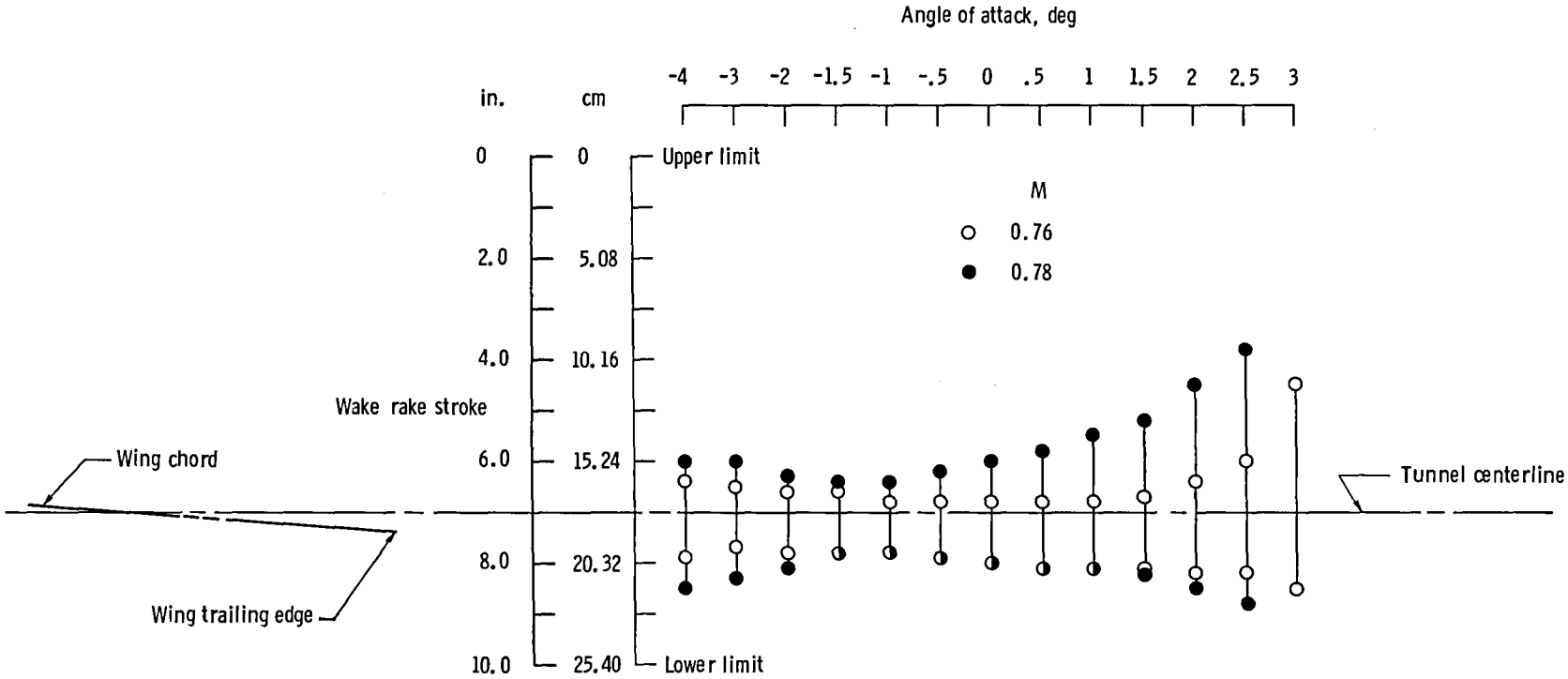

Figure 8. Variation of stroke length used to define wake at $M = 0.76$ and $M = 0.78$.

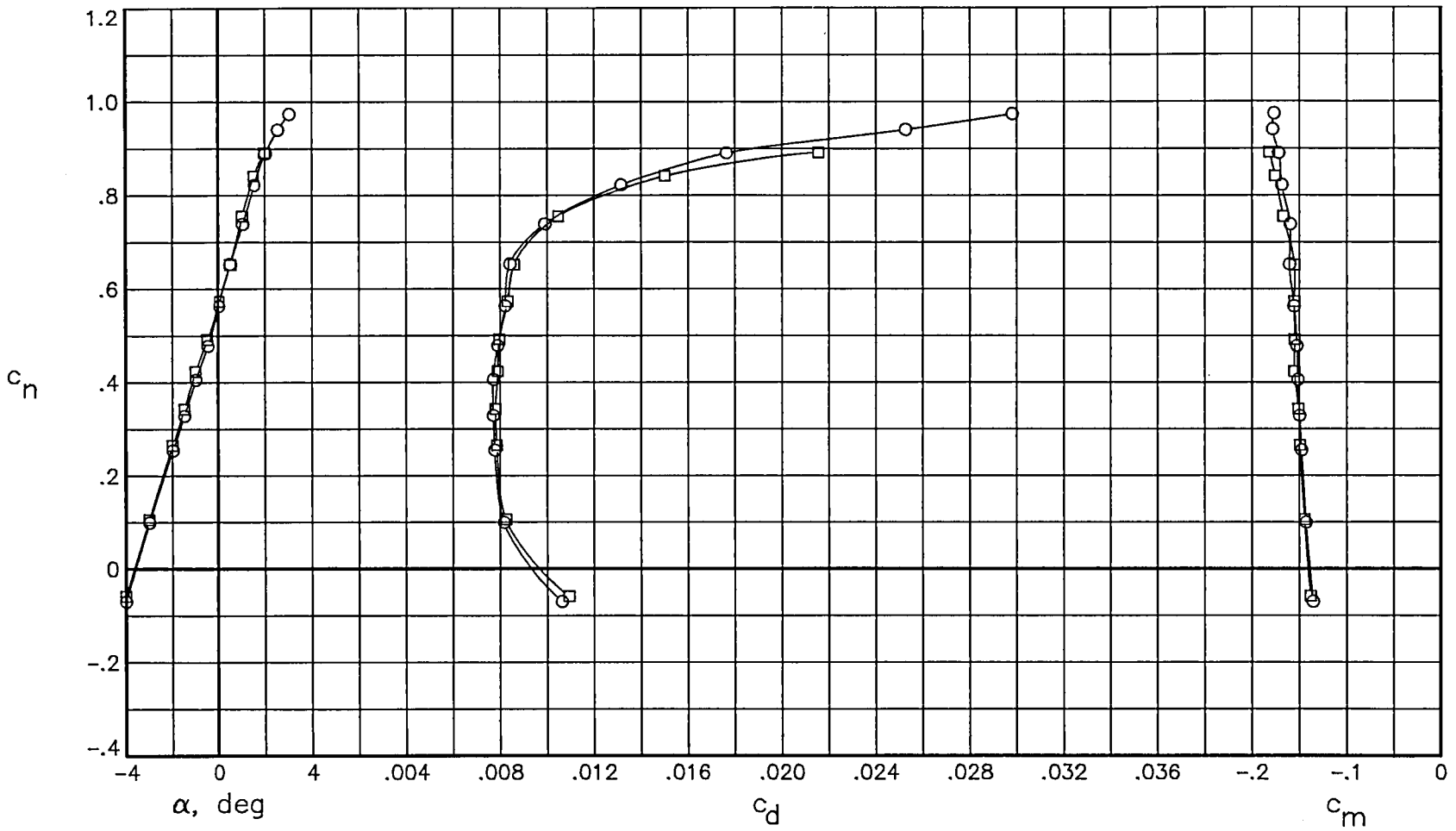

Figure 9. Repeatability of two sets of data (○,□) with free transition at $M = 0.76$ and $R = 30.0 \times 10^6$.

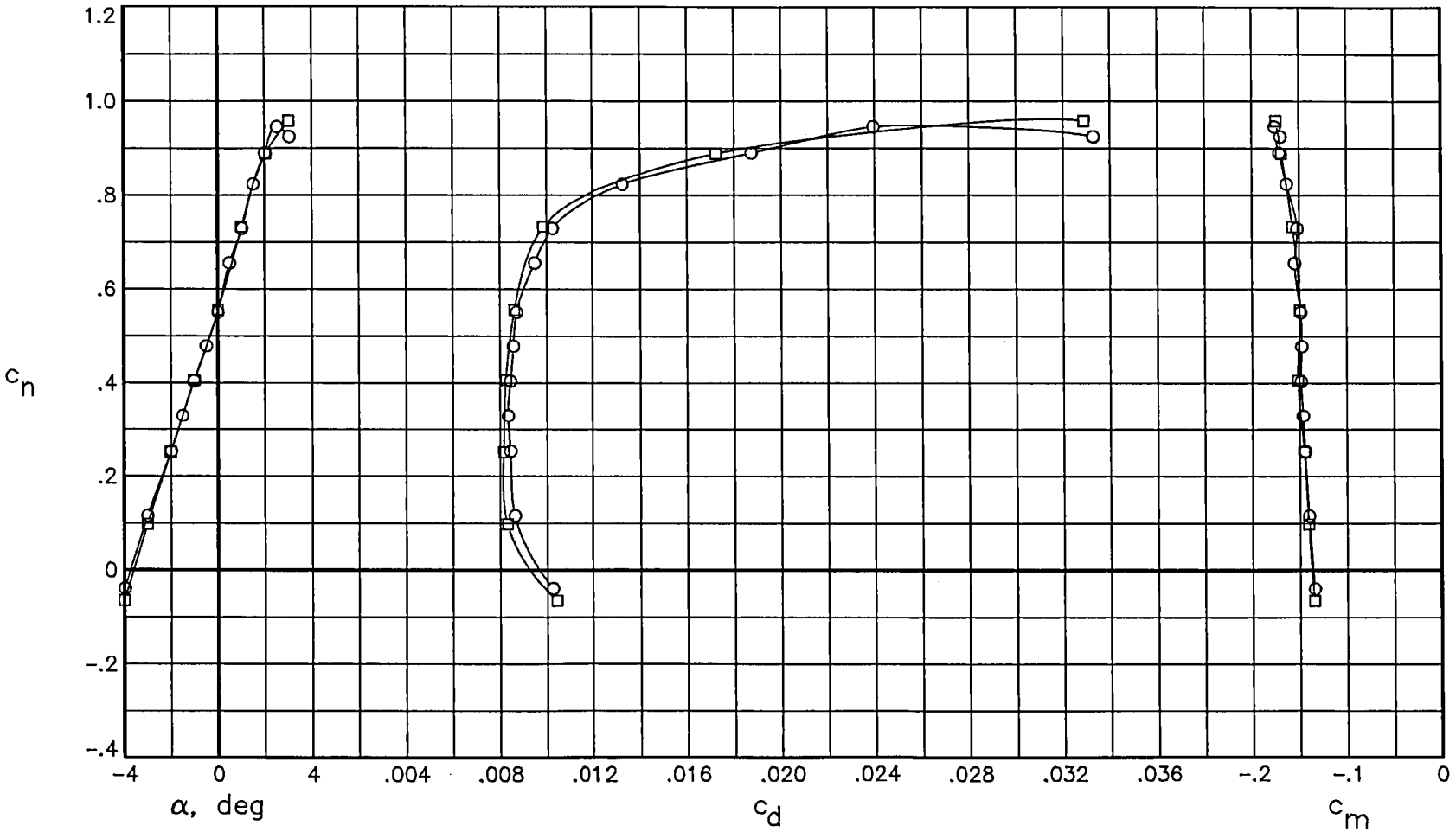

Figure 10. Repeatability of two sets of data (○,□) with fixed transition at $M = 0.76$ and $R = 30.0 \times 10^6$.

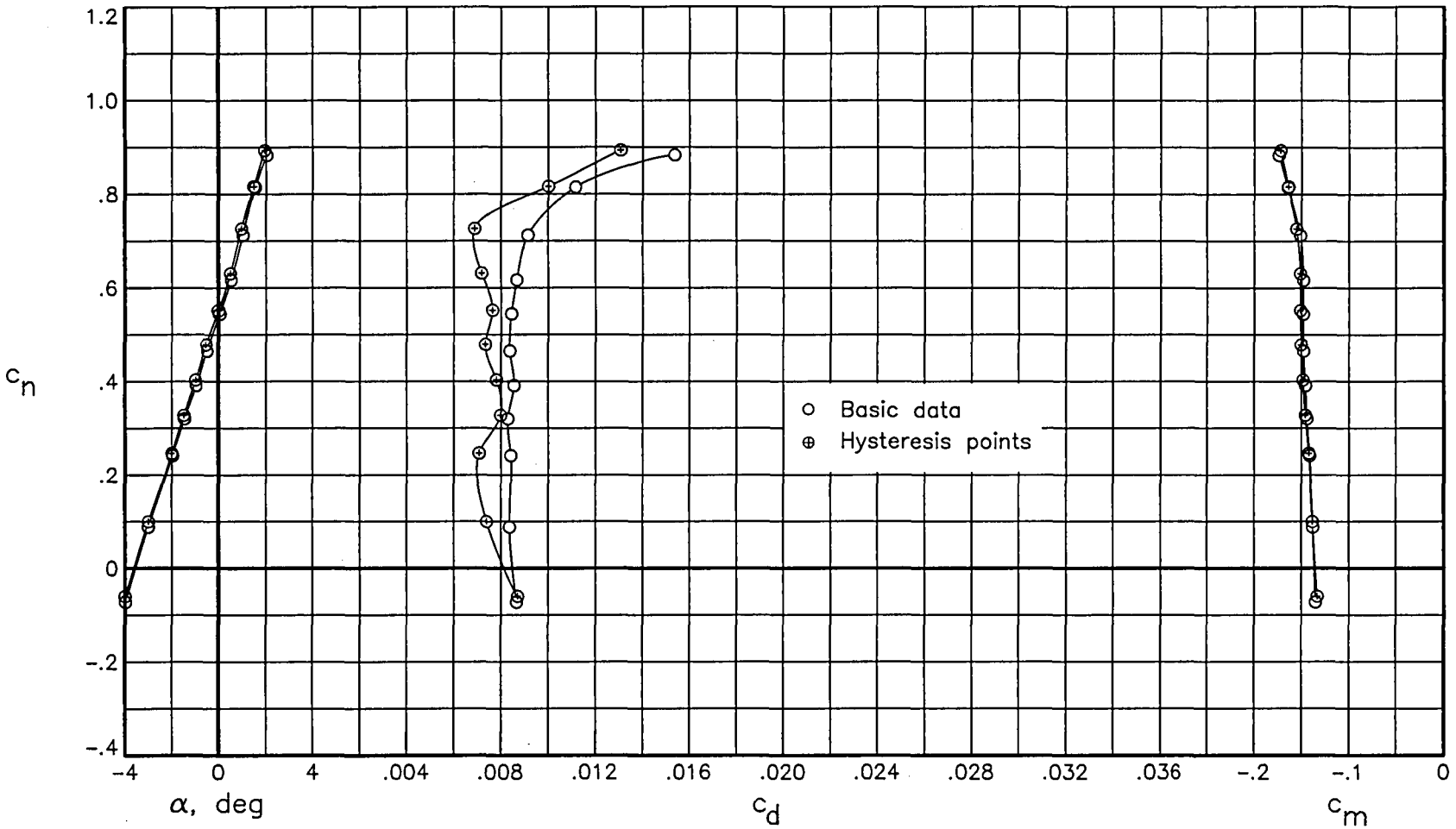

Figure 11. Hysteresis characteristics of data with free transition at $M = 0.76$ and $R = 7.0 \times 10^6$.

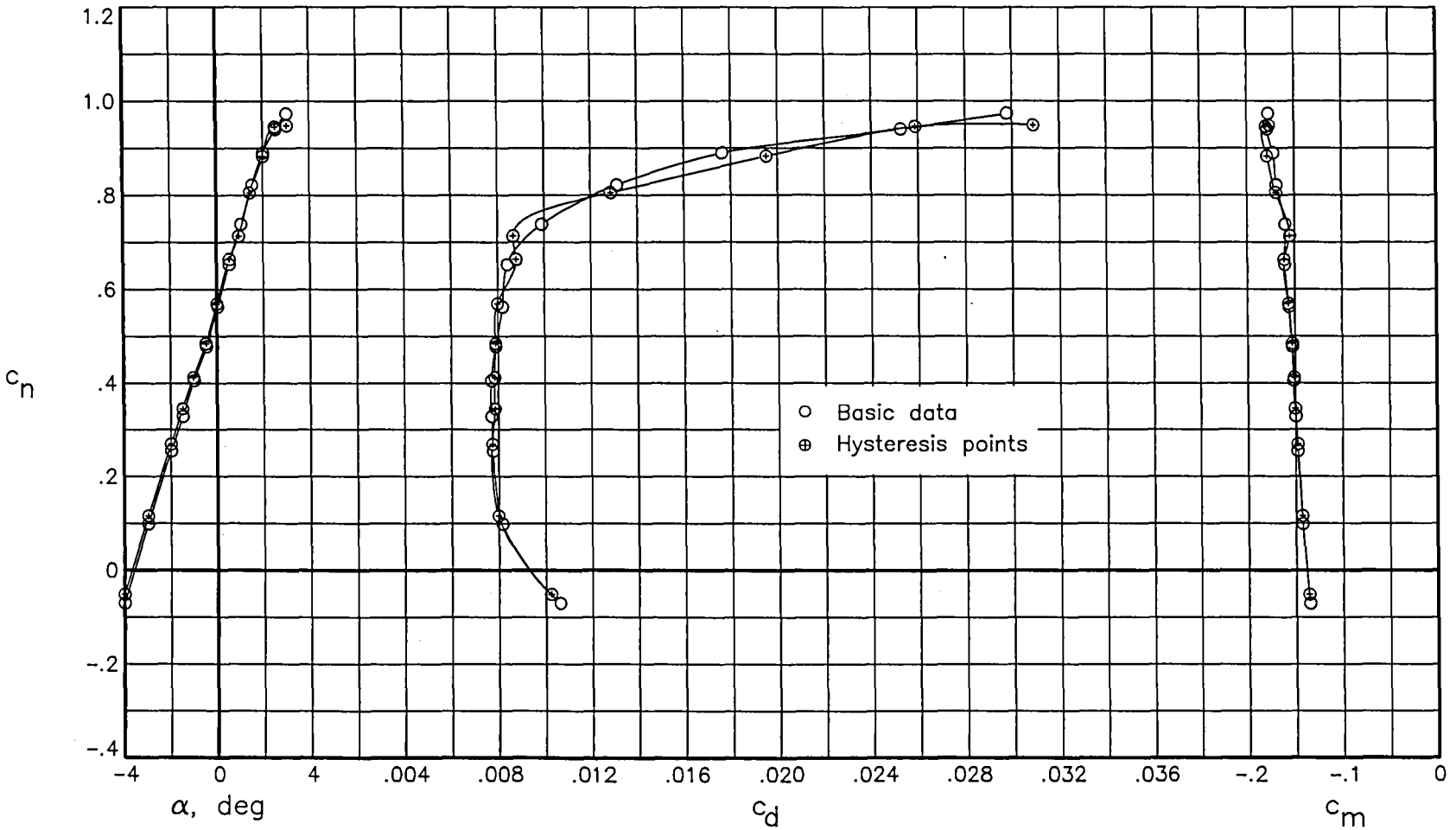

Figure 12. Hysteresis characteristics of data with free transition at $M = 0.76$ and $R = 30.0 \times 10^6$.

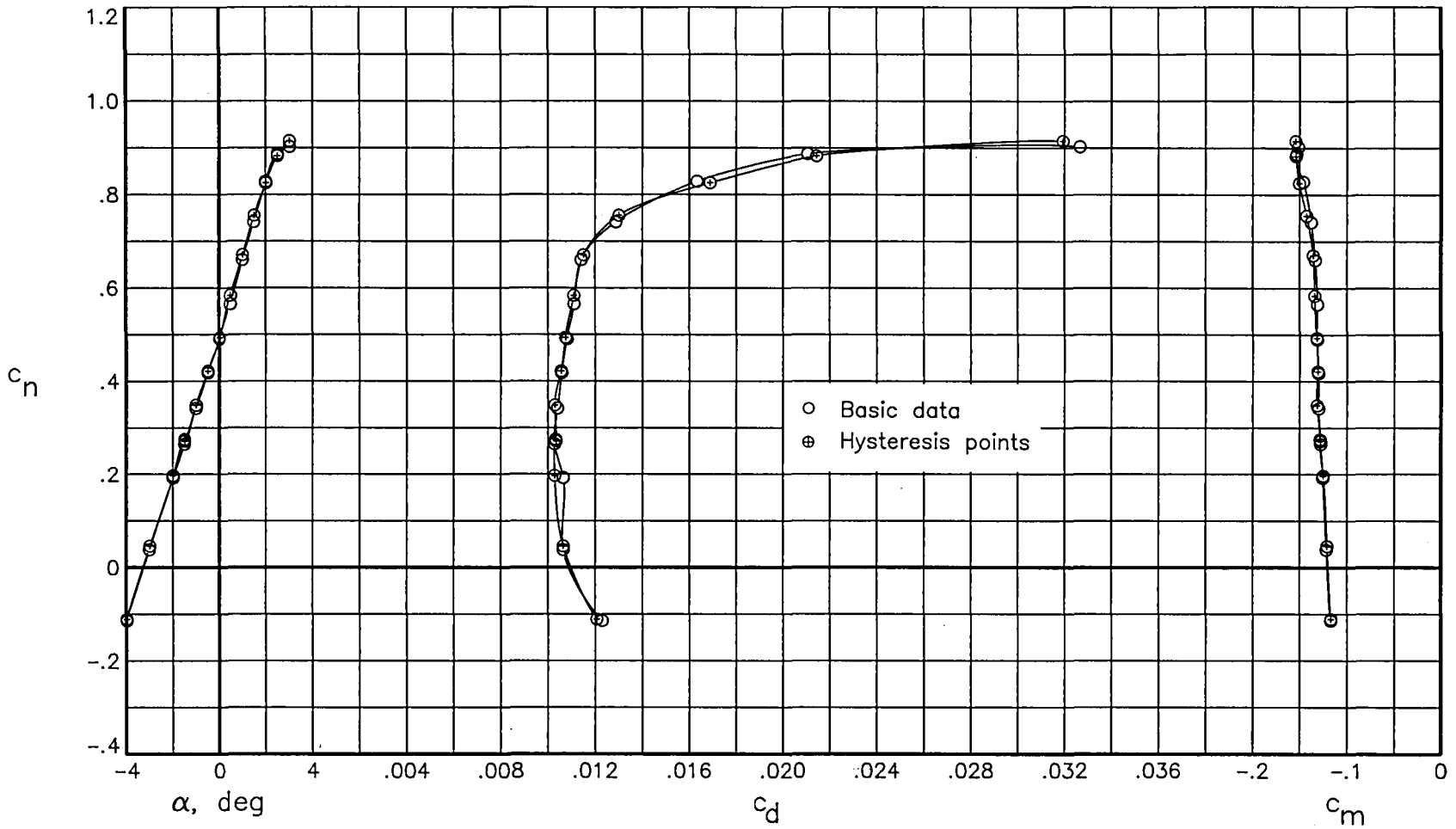

Figure 13. Hysteresis characteristics of data with fixed transition at $M = 0.76$ and $R = 7.0 \times 10^6$.

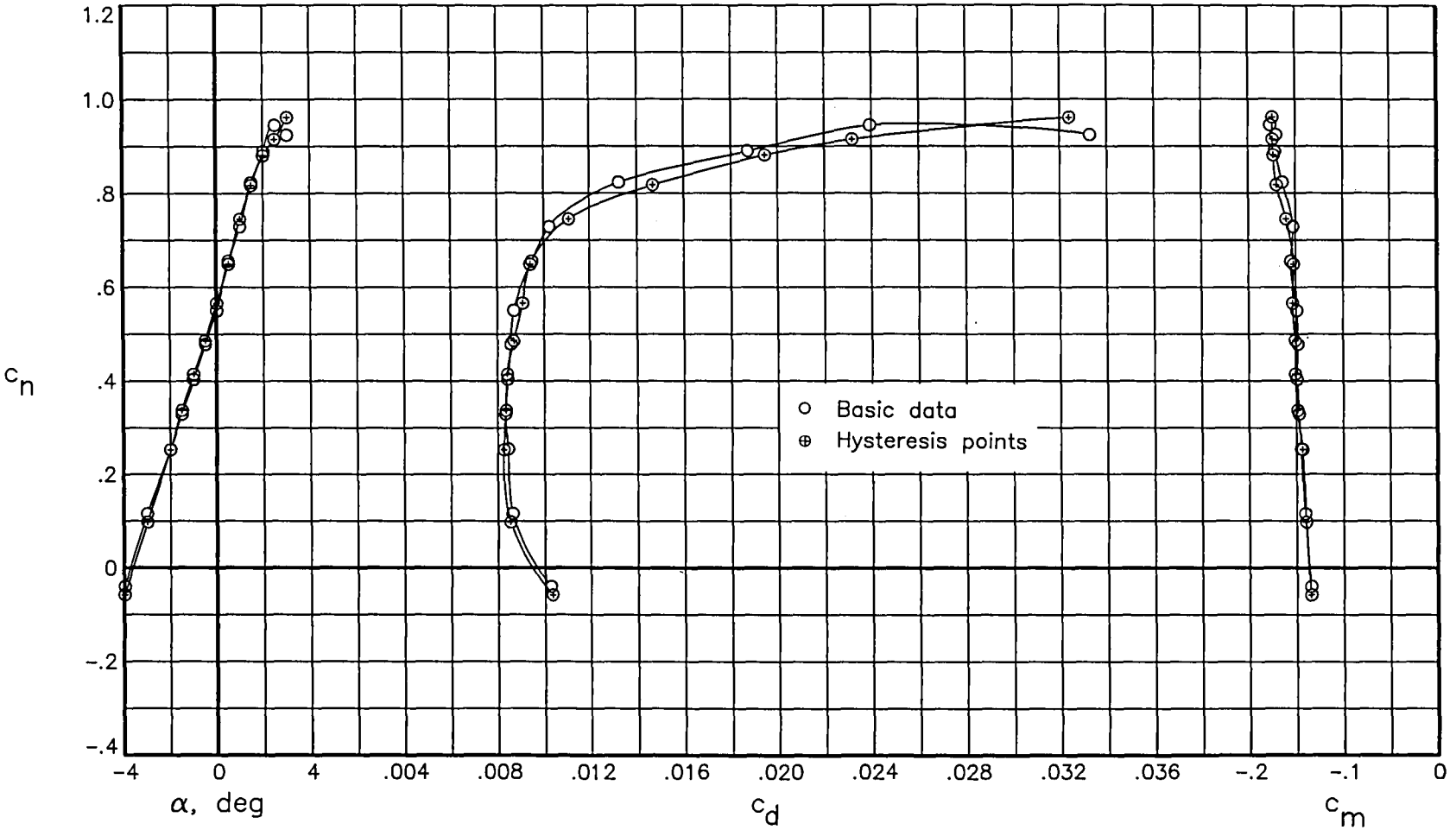

Figure 14. Hysteresis characteristics of data with fixed transition at $M = 0.76$ and $R = 30.0 \times 10^6$.

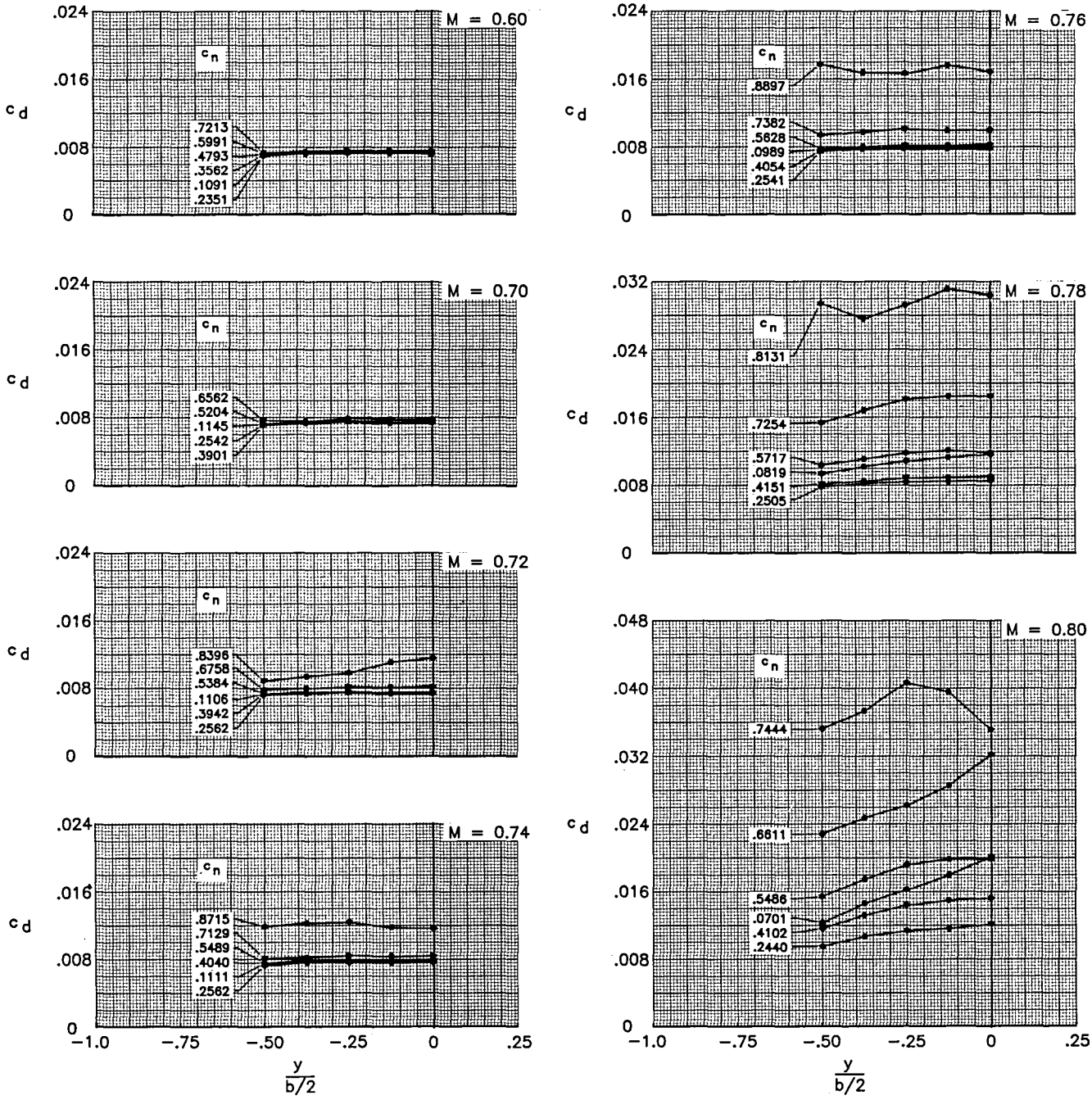

Figure 15. Spanwise drag of airfoil with free transition for several Mach numbers at $R = 30.0 \times 10^6$.

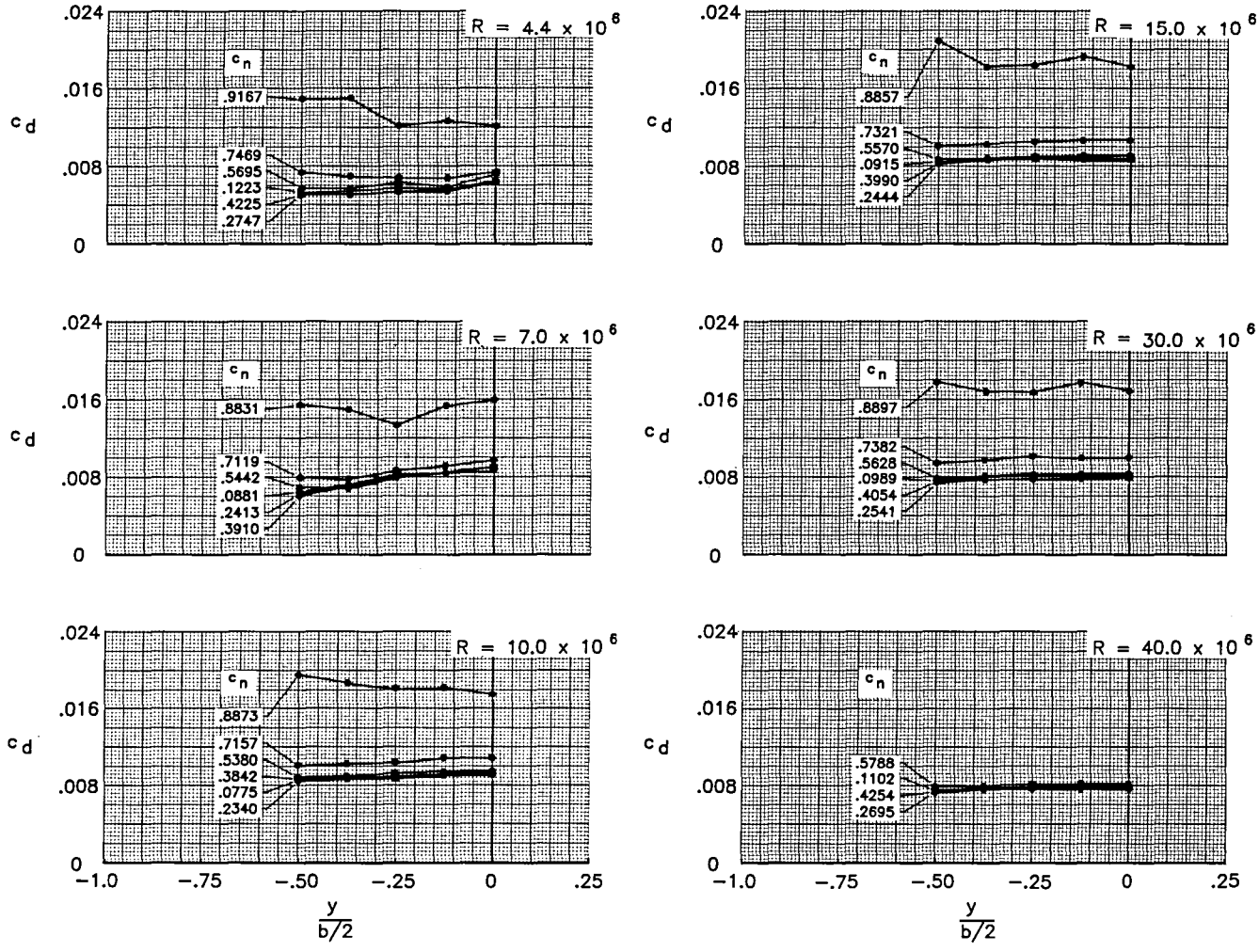

Figure 16. Spanwise drag of airfoil with free transition for several Reynolds numbers at $M = 0.76$.

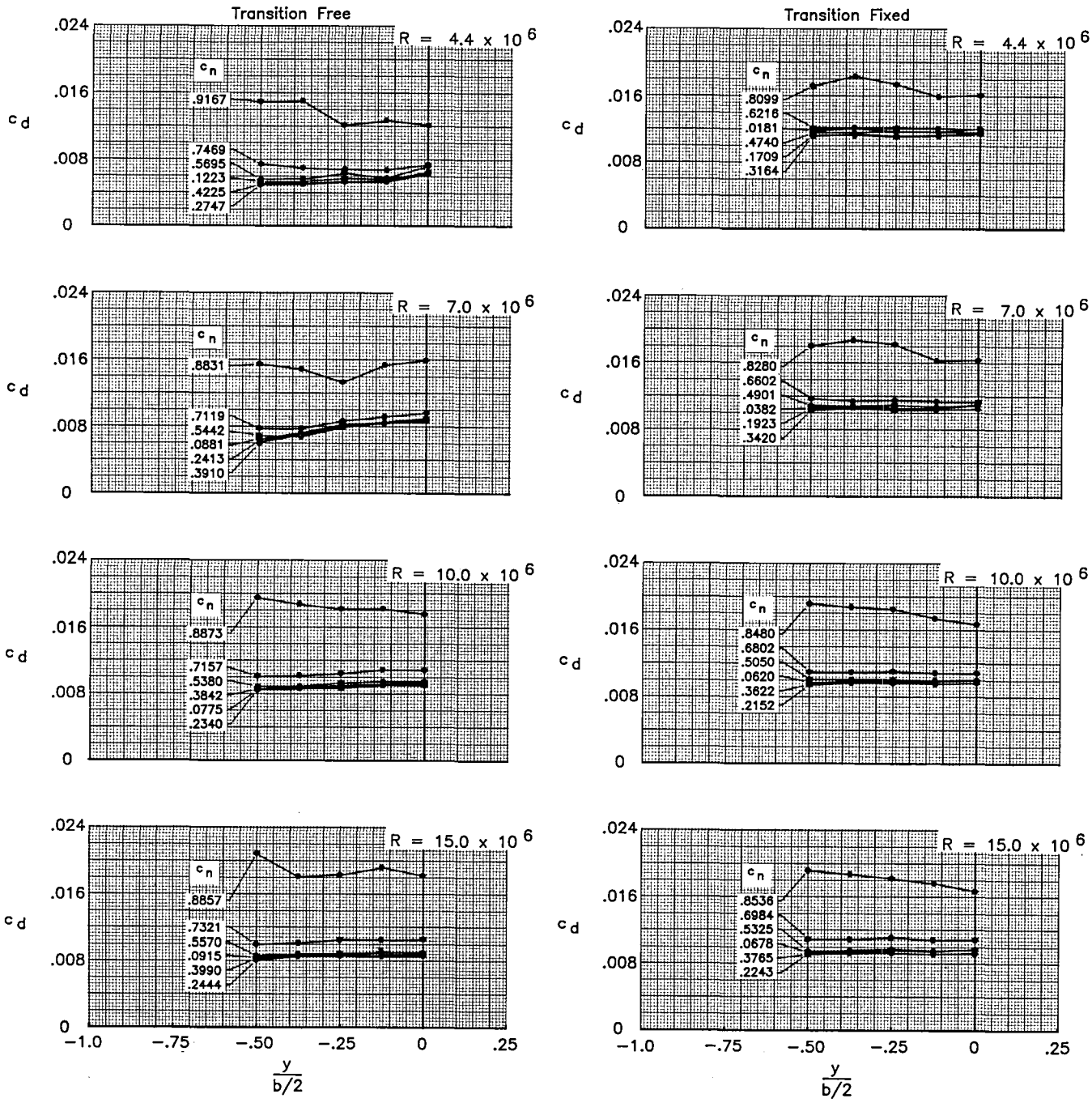

Figure 17. Comparison of spanwise drag of airfoil with free and fixed transition for several Reynolds numbers at $M = 0.76$.

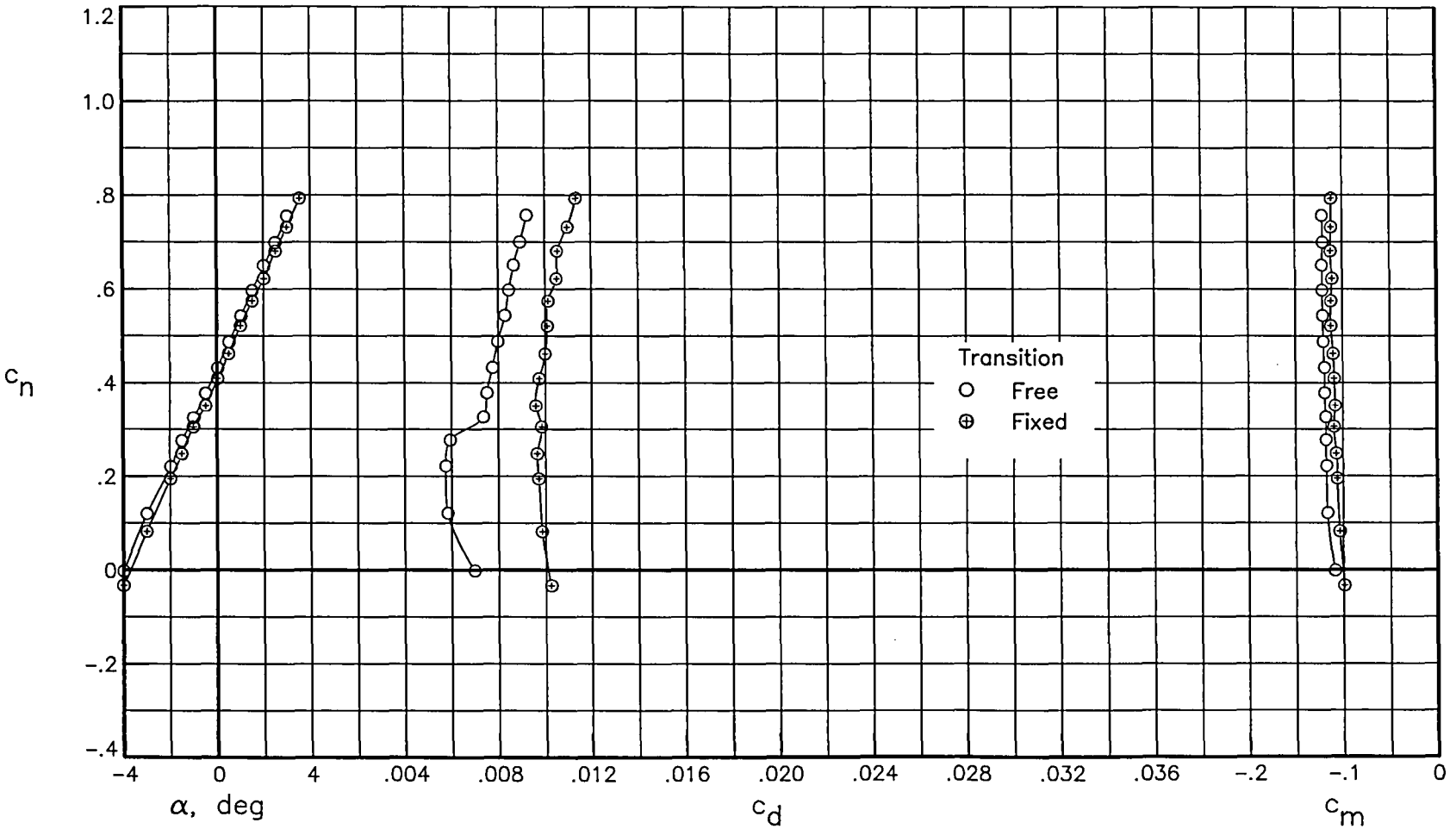

Figure 18. Effect of fixing transition on aerodynamic characteristics of airfoil at $M = 0.50$ and $R = 4.4 \times 10^6$.

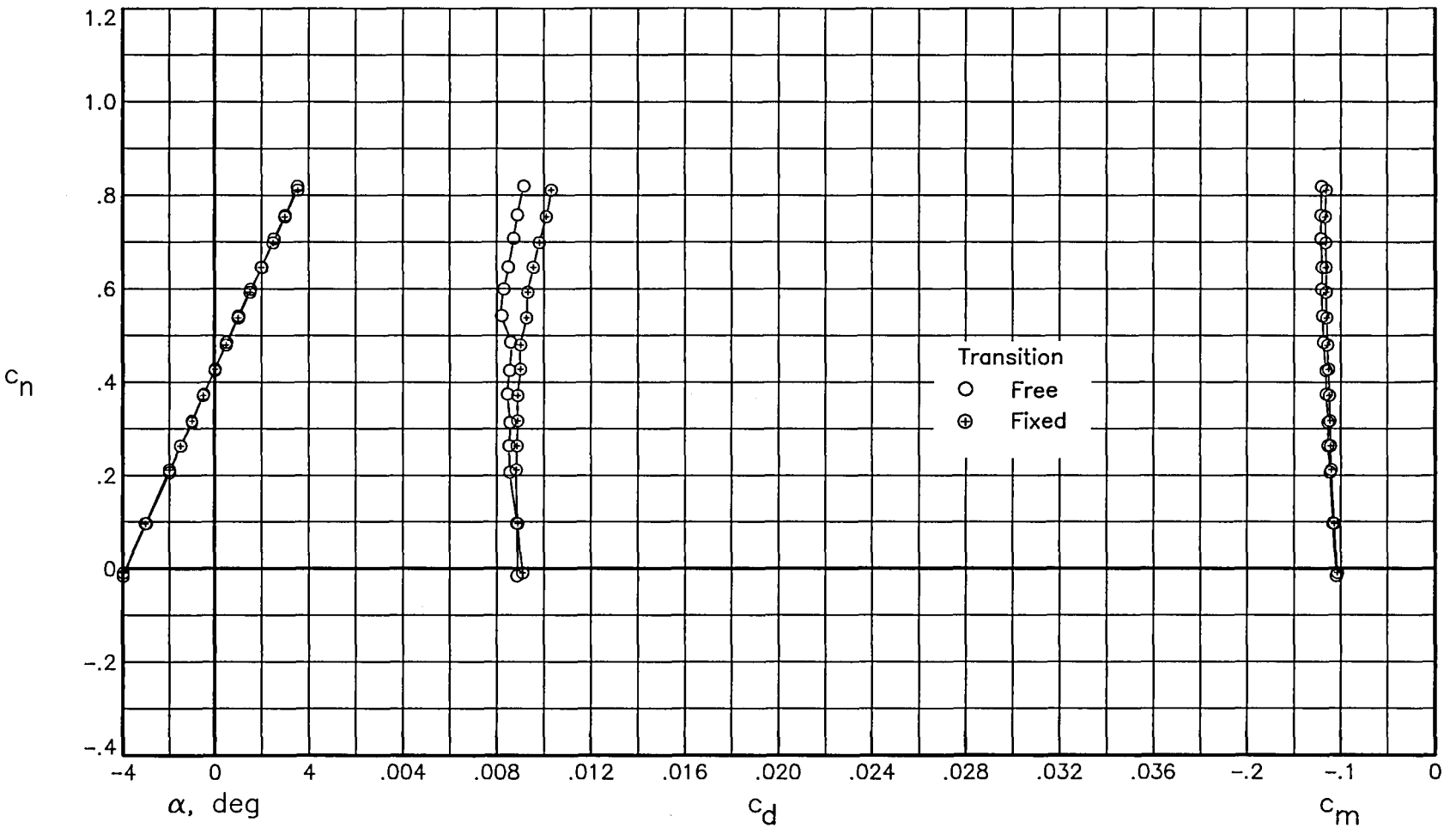

Figure 19. Effect of fixing transition on aerodynamic characteristics of airfoil at $M = 0.50$ and $R = 7.0 \times 10^6$.

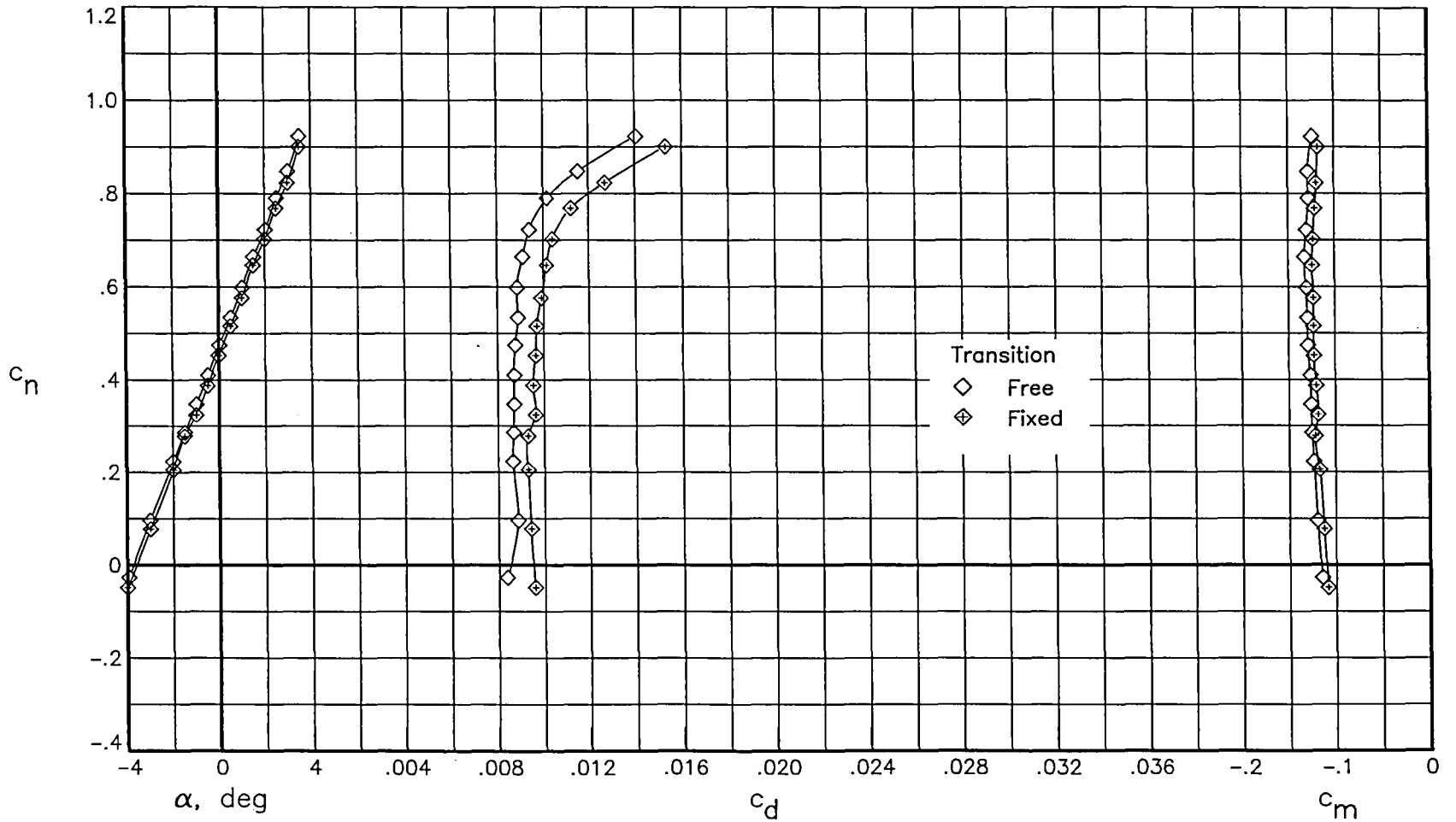

Figure 20. Effect of fixing transition on aerodynamic characteristics of airfoil at $M = 0.65$ and $R = 7.0 \times 10^6$.

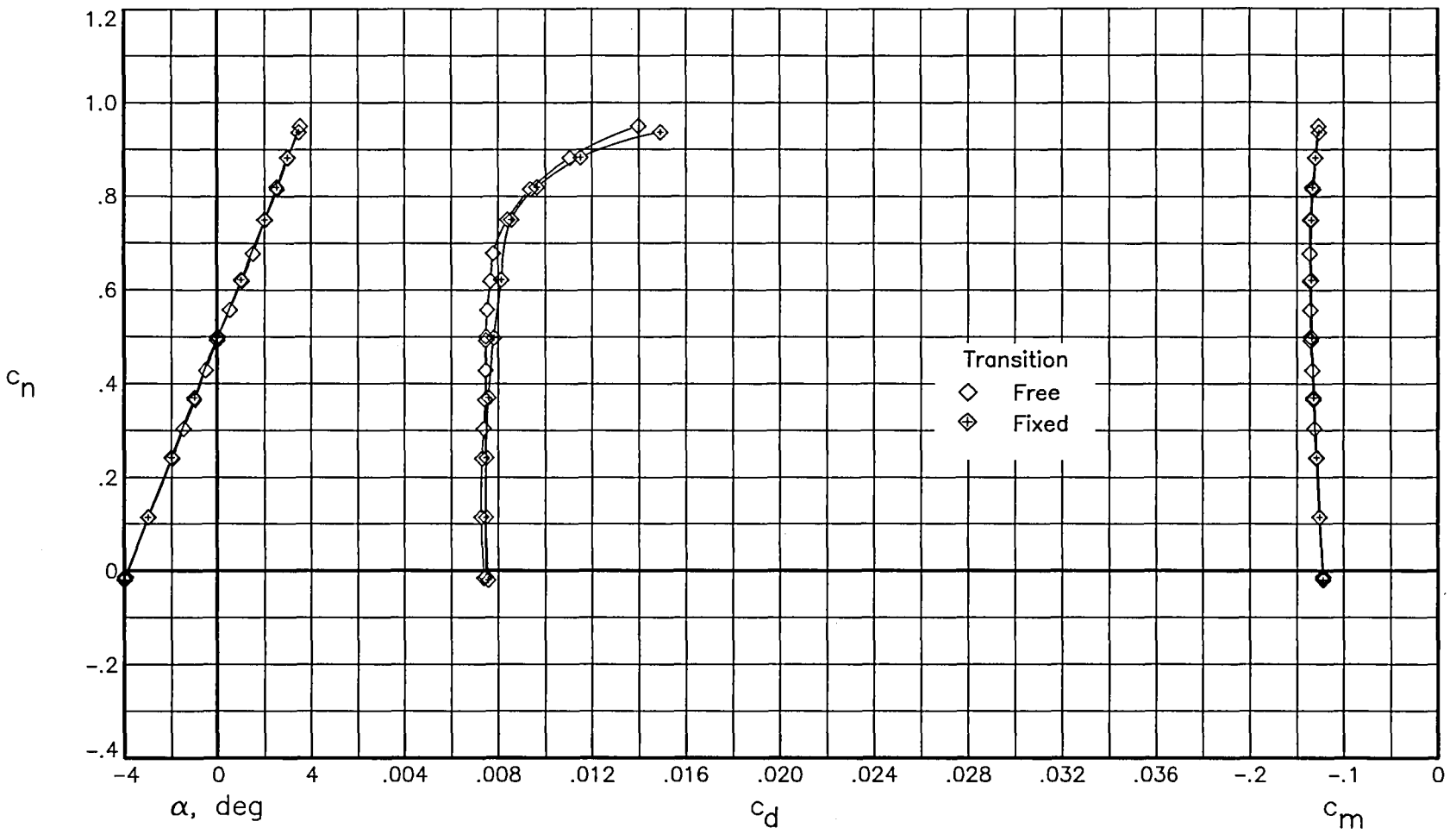

Figure 21. Effect of fixing transition on aerodynamic characteristics of airfoil at $M = 0.65$ and $R = 30.0 \times 10^6$.

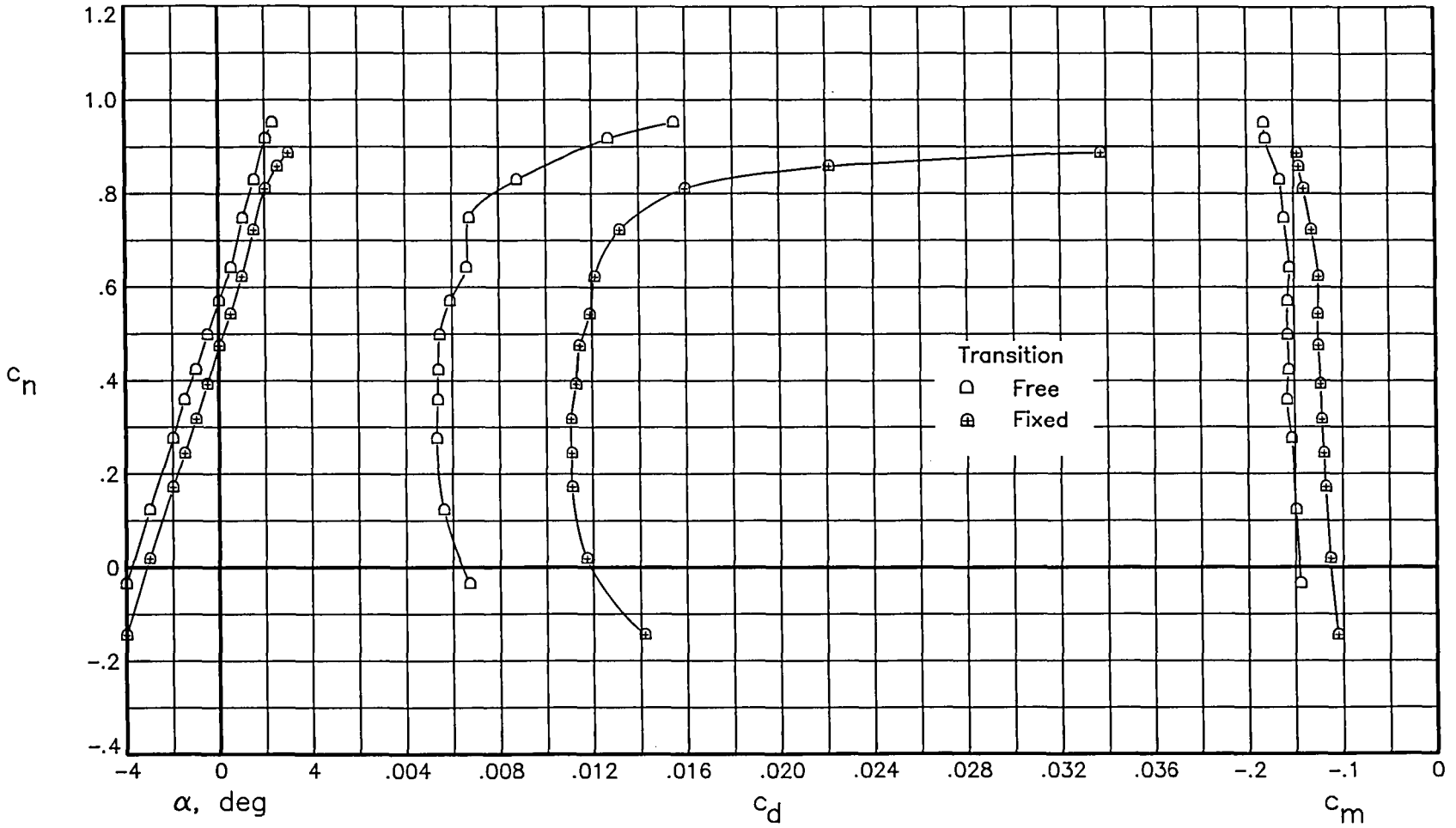

Figure 22. Effect of fixing transition on aerodynamic characteristics of airfoil at $M = 0.76$ and $R = 4.4 \times 10^6$.

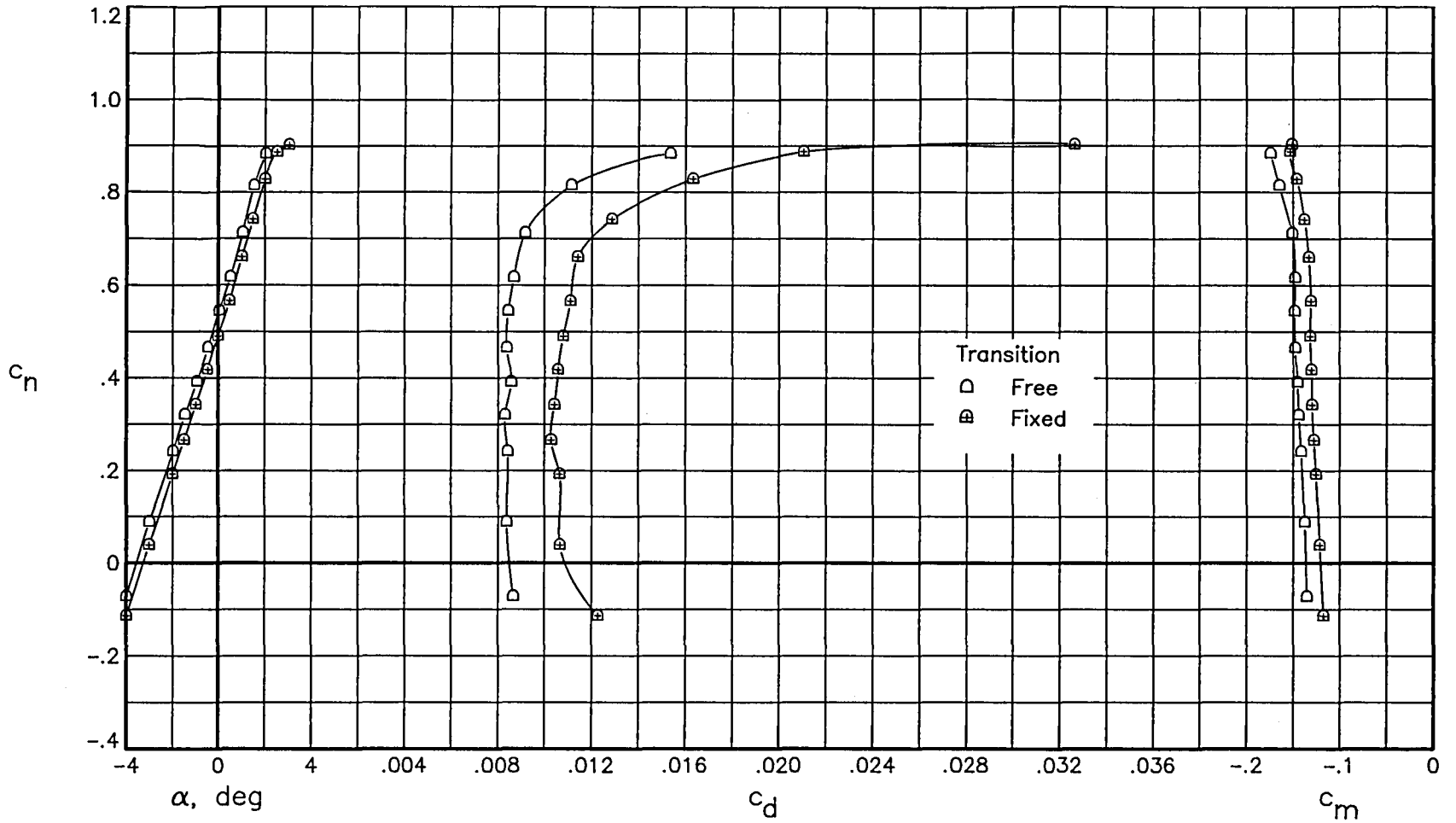

Figure 23. Effect of fixing transition on aerodynamic characteristics of airfoil at $M = 0.76$ and $R = 7.0 \times 10^6$.

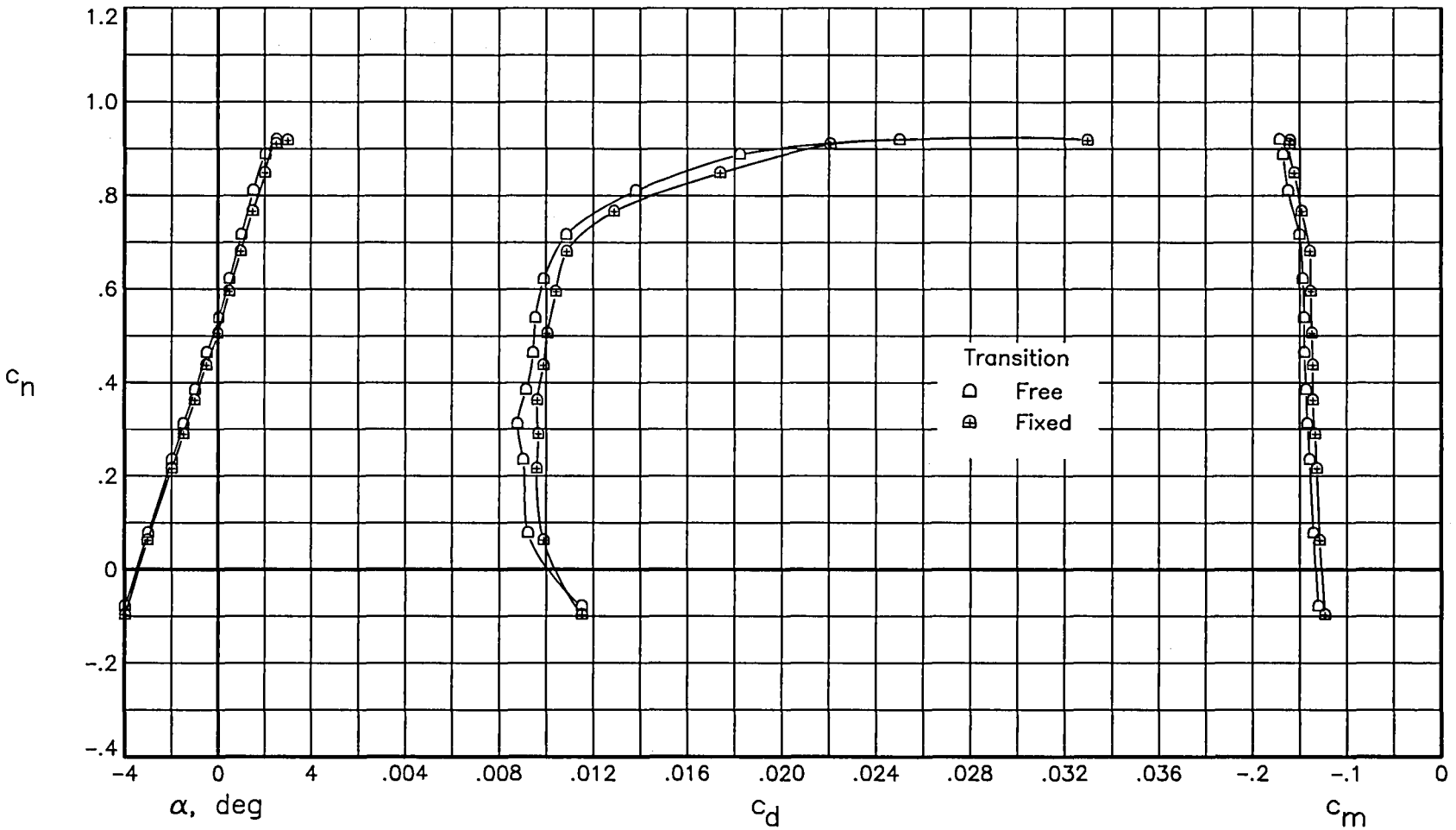

Figure 24. Effect of fixing transition on aerodynamic characteristics of airfoil at $M = 0.76$ and $R = 10.0 \times 10^6$.

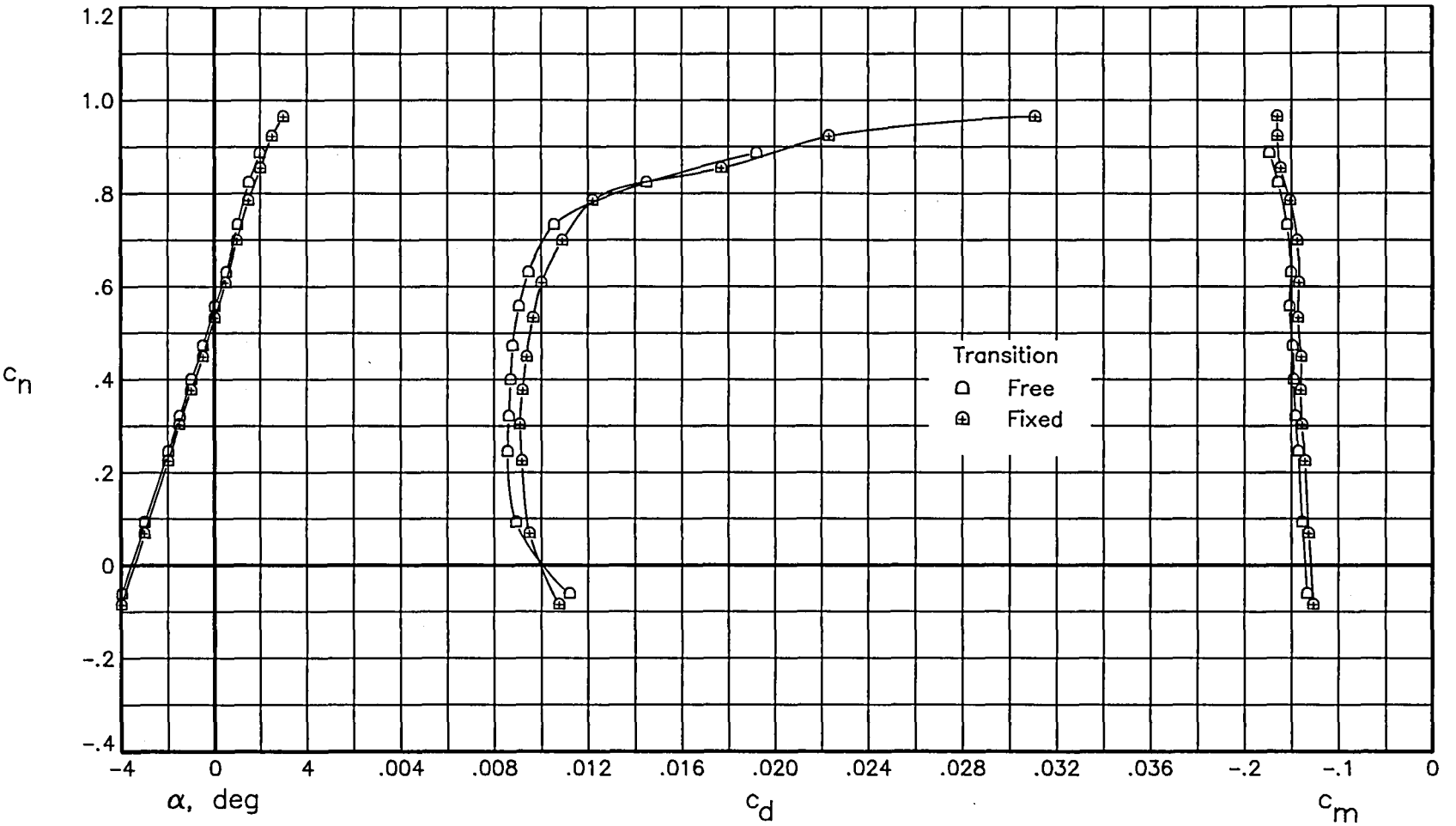

Figure 25. Effect of fixing transition on aerodynamic characteristics of airfoil at $M = 0.76$ and $R = 15.0 \times 10^6$.

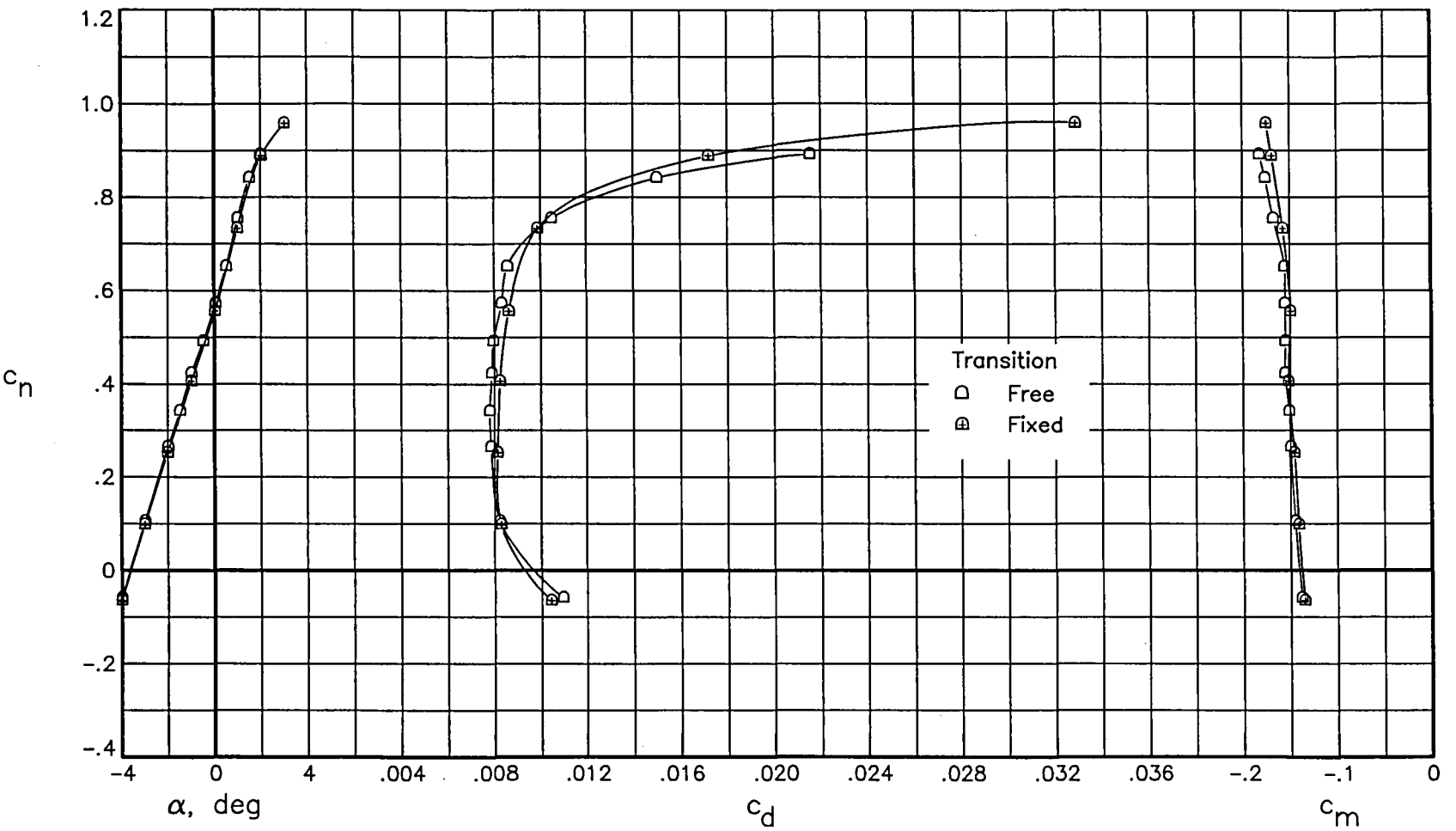

Figure 26. Effect of fixing transition on aerodynamic characteristics of airfoil at $M = 0.76$ and $R = 30.0 \times 10^6$.

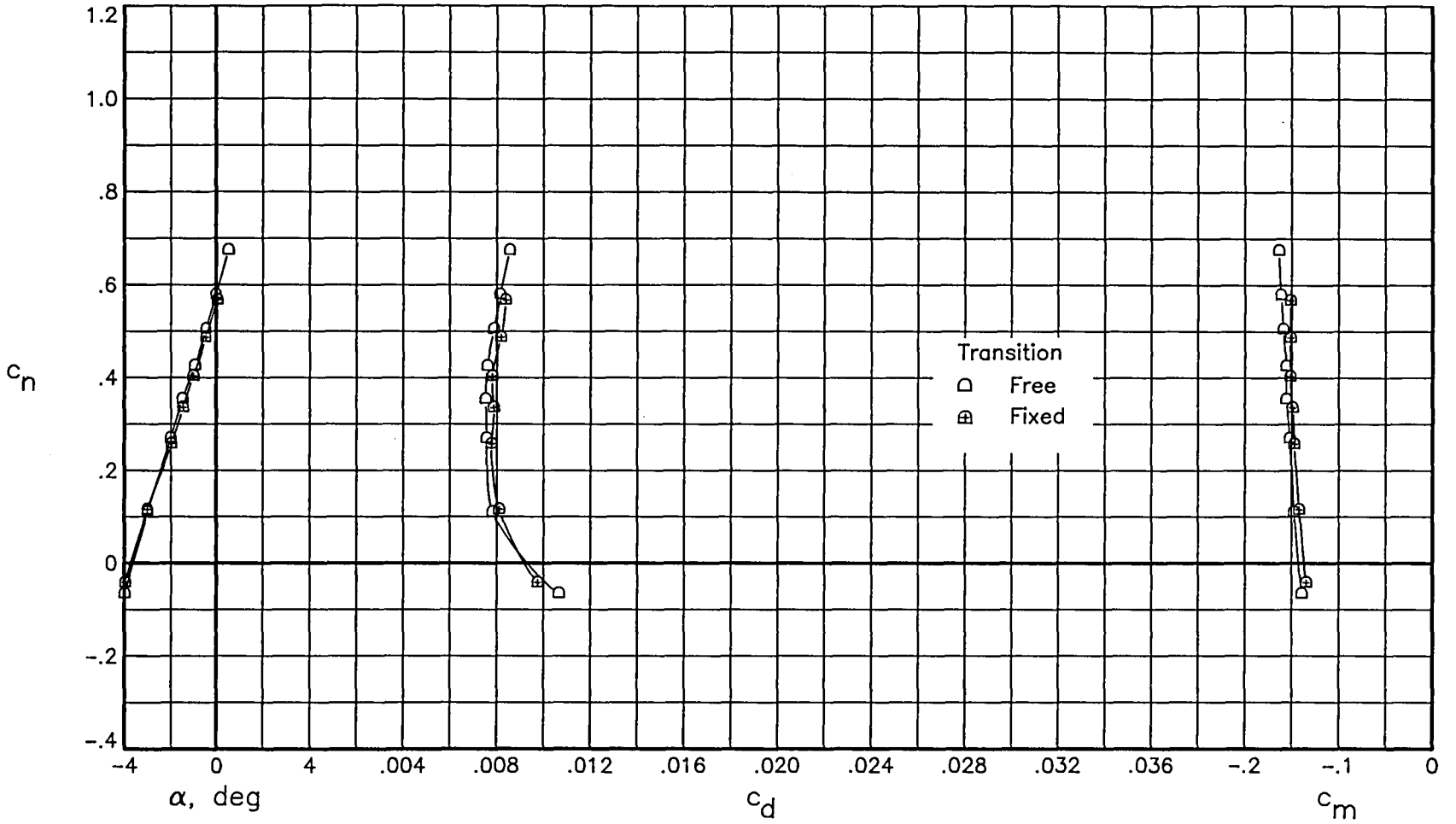

Figure 27. Effect of fixing transition on aerodynamic characteristics of airfoil at $M = 0.76$ and $R = 40.0 \times 10^6$.

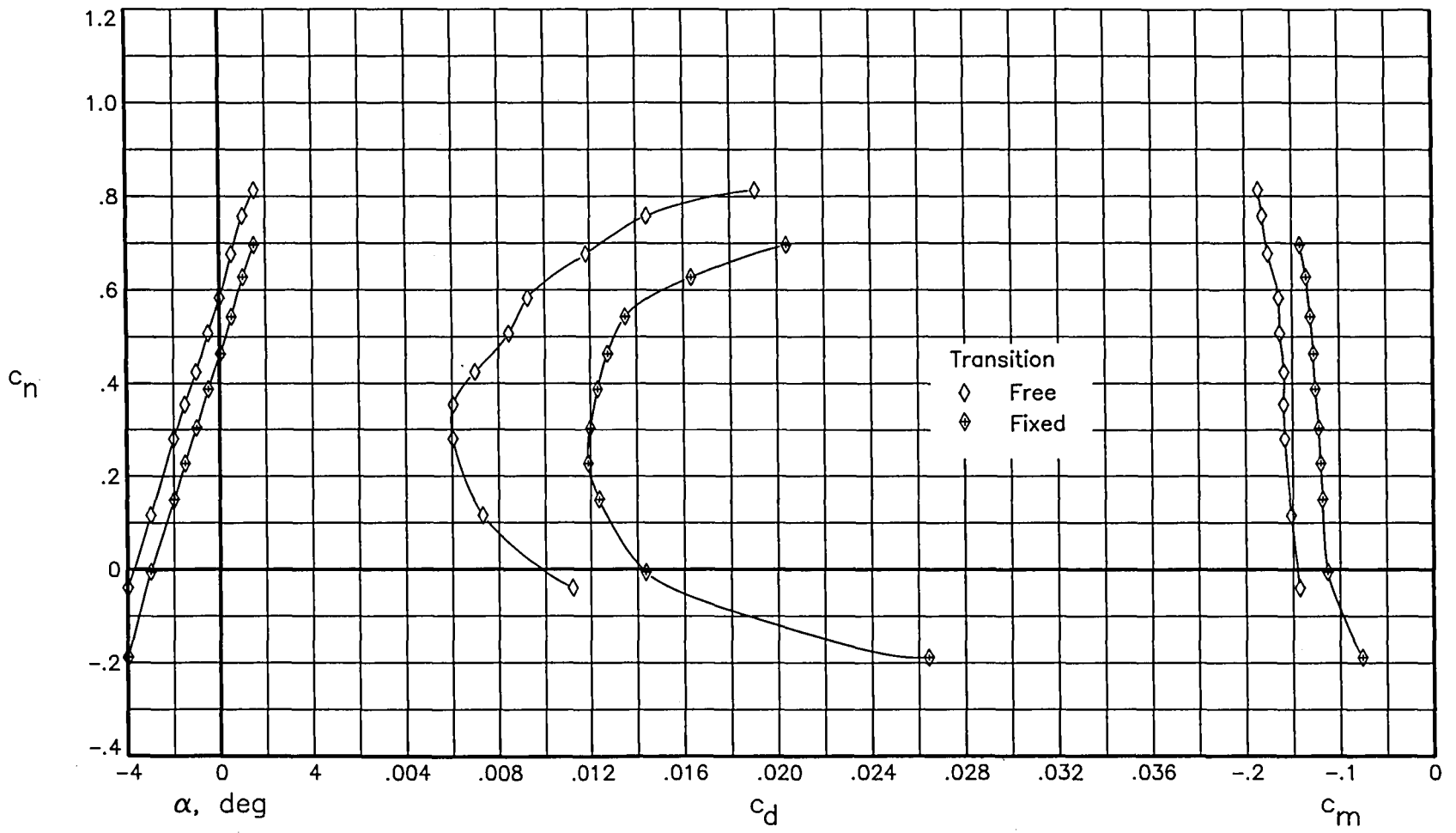

Figure 28. Effect of fixing transition on aerodynamic characteristics of airfoil at $M = 0.78$ and $R = 4.4 \times 10^6$.

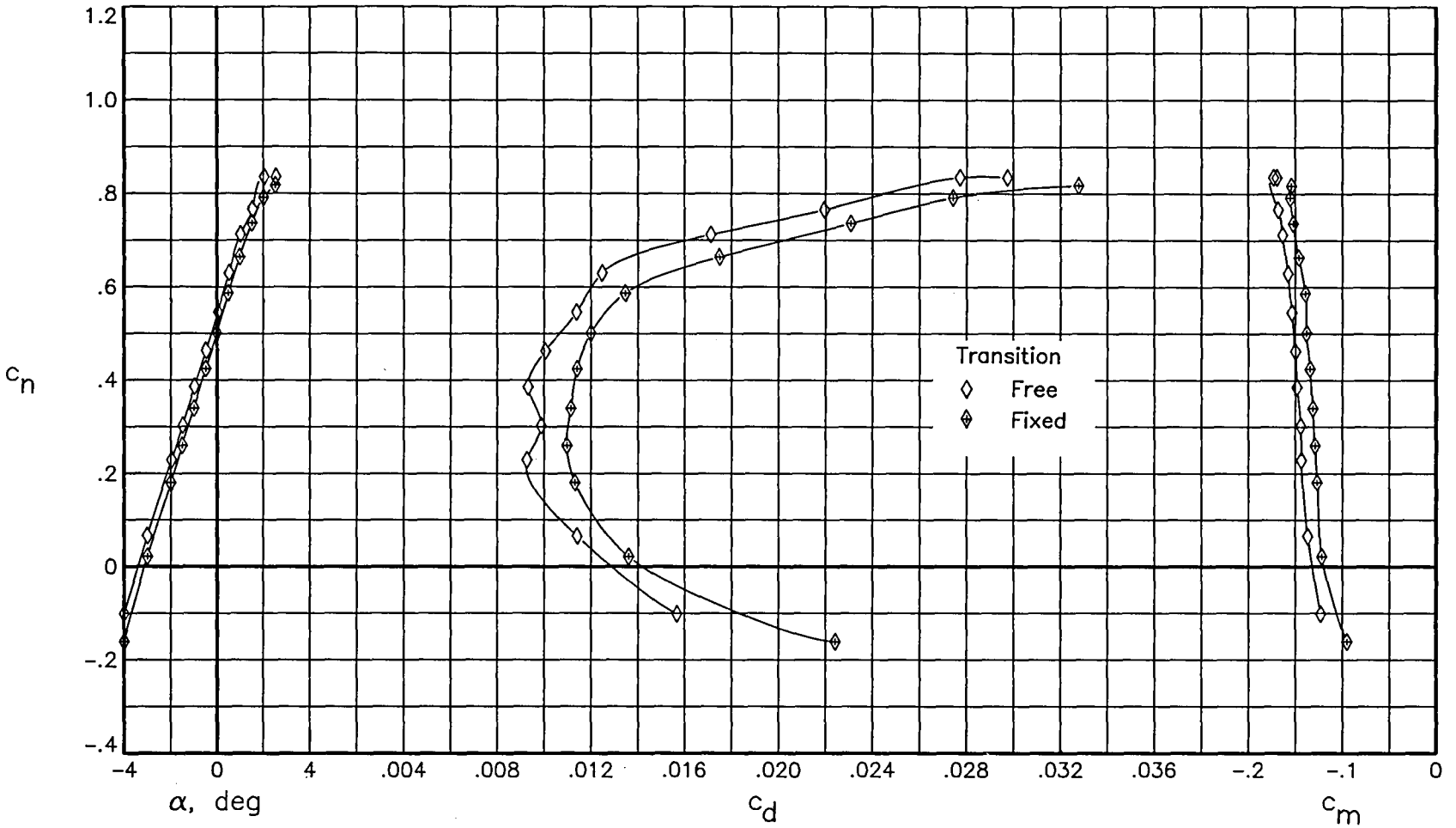

Figure 29. Effect of fixing transition on aerodynamic characteristics of airfoil at $M = 0.78$ and $R = 7.0 \times 10^6$.

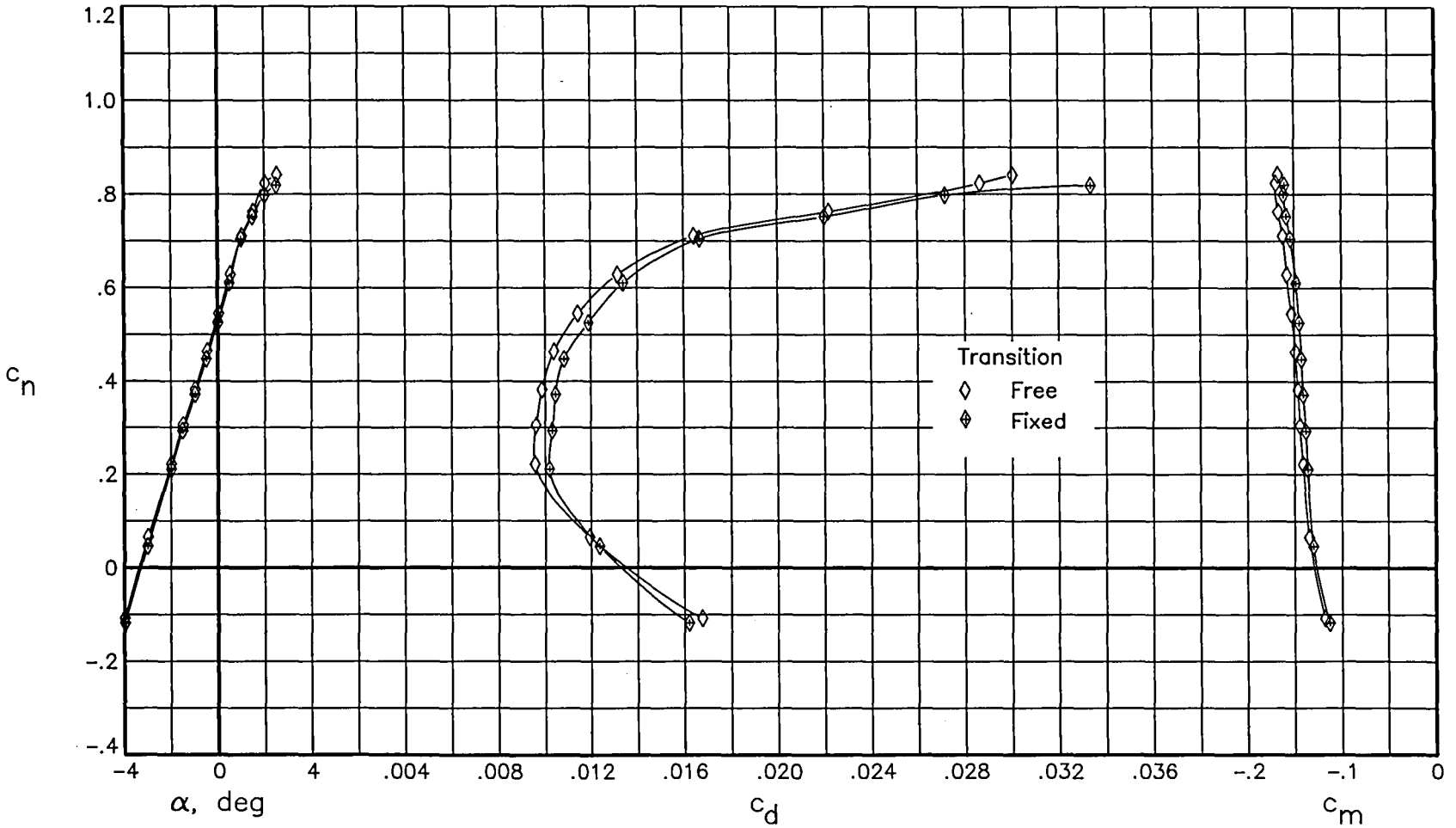

Figure 30. Effect of fixing transition on aerodynamic characteristics of airfoil at $M = 0.78$ and $R = 10.0 \times 10^6$.

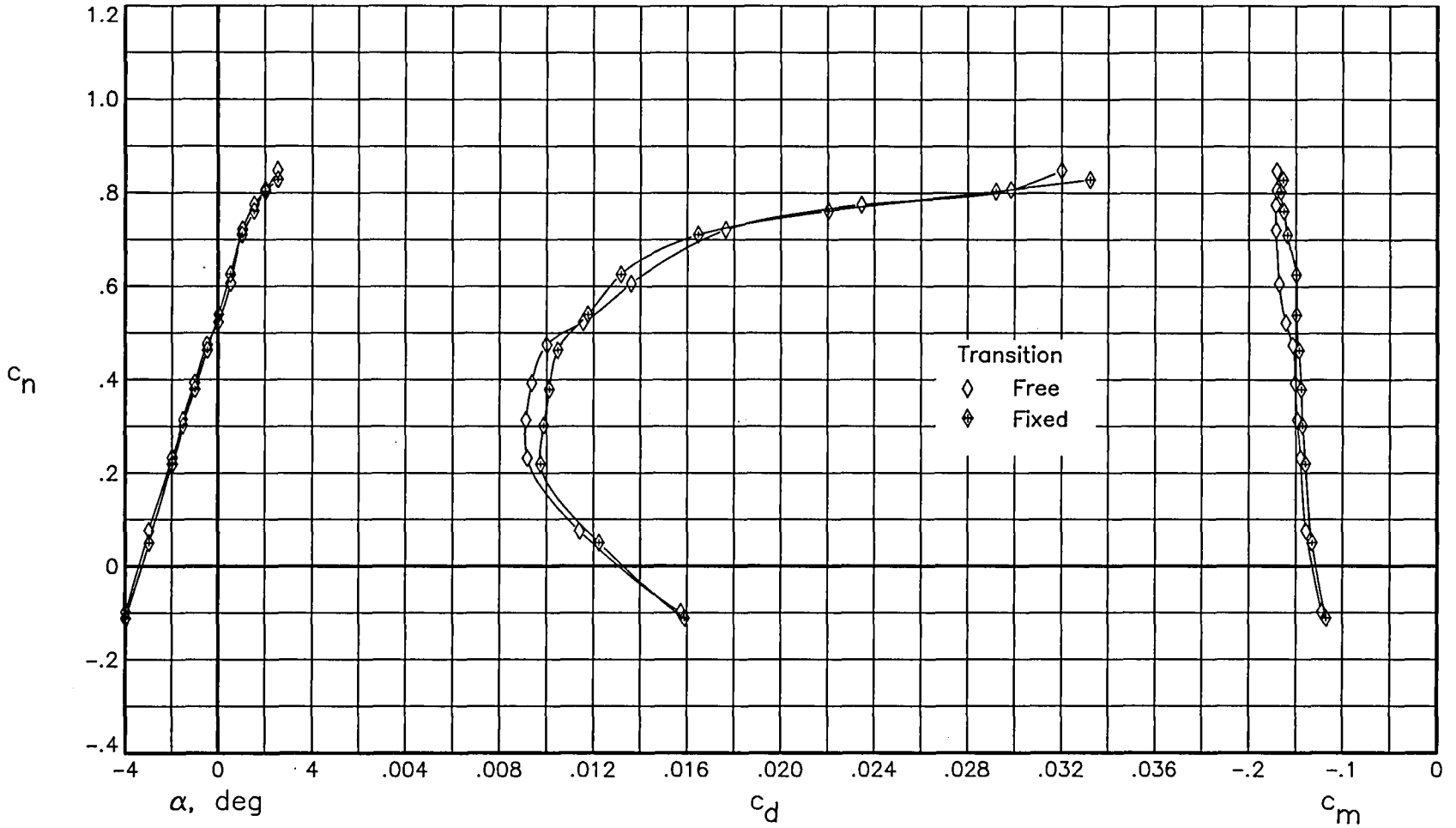

Figure 31. Effect of fixing transition on aerodynamic characteristics of airfoil at $M = 0.78$ and $R = 15.0 \times 10^6$.

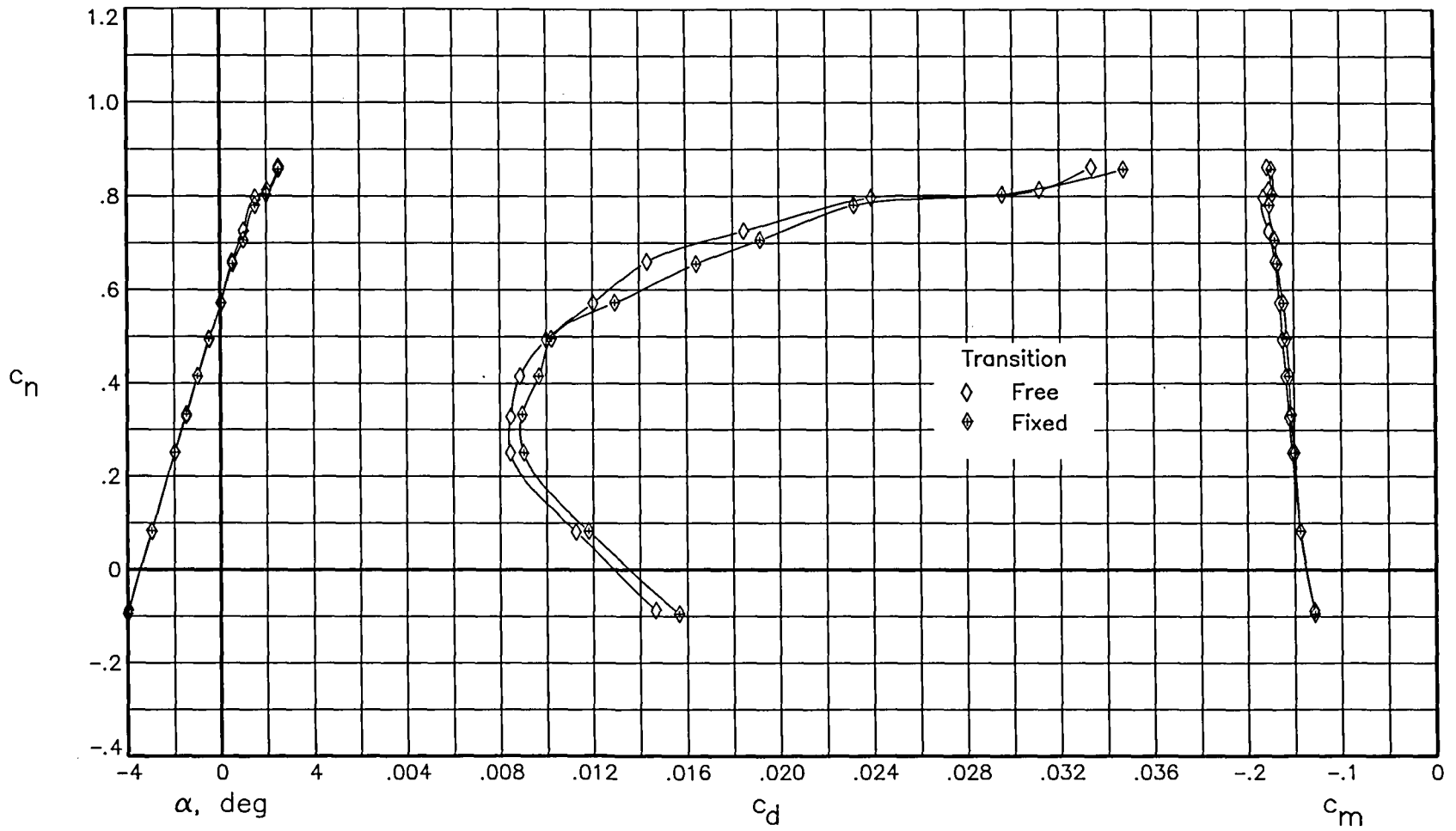

Figure 32. Effect of fixing transition on aerodynamic characteristics of airfoil at $M = 0.78$ and $R = 30.0 \times 10^6$.

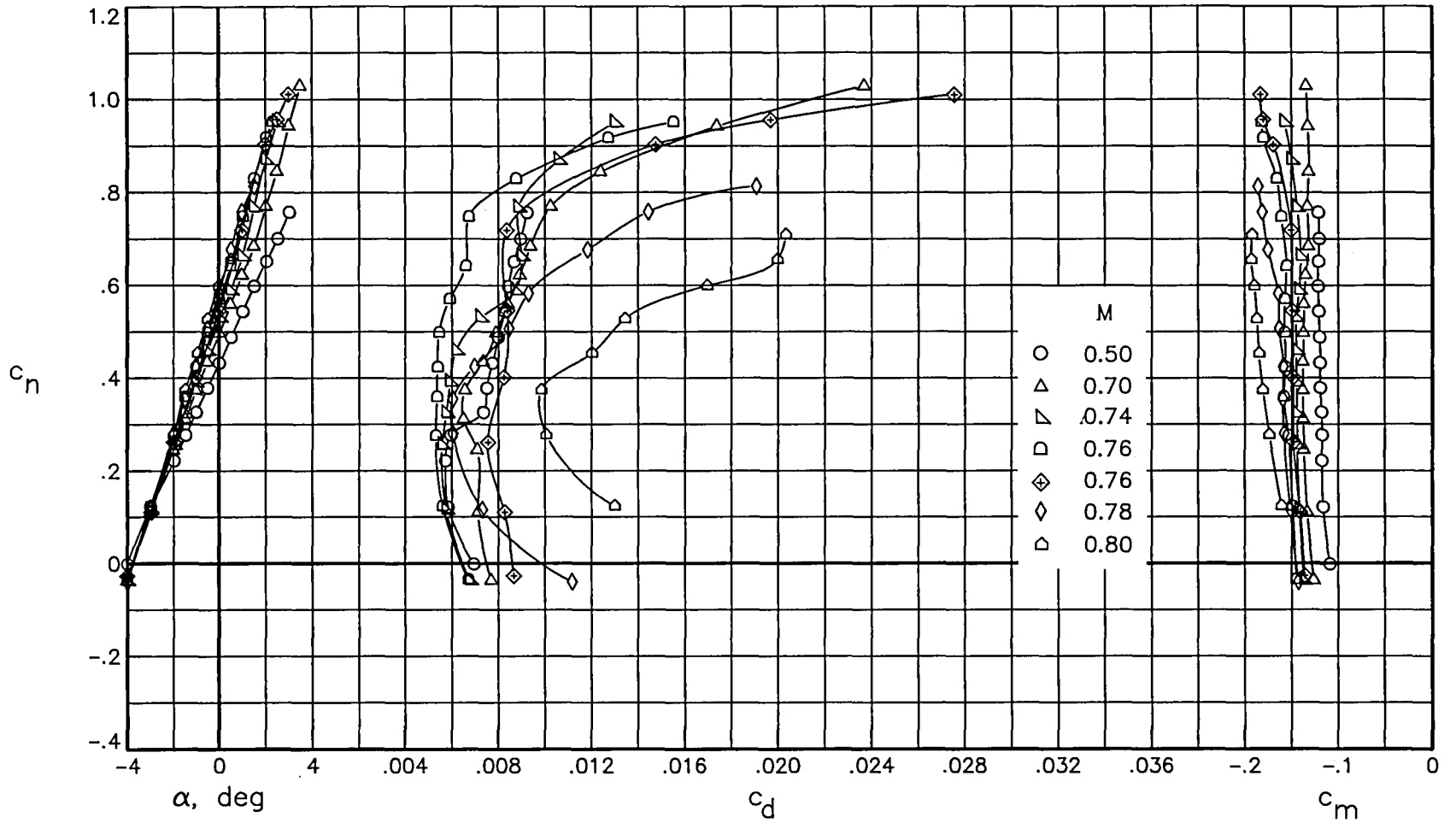

Figure 33. Effect of Mach number on aerodynamic characteristics of airfoil with free transition at $R \approx 4.4 \times 10^6$.

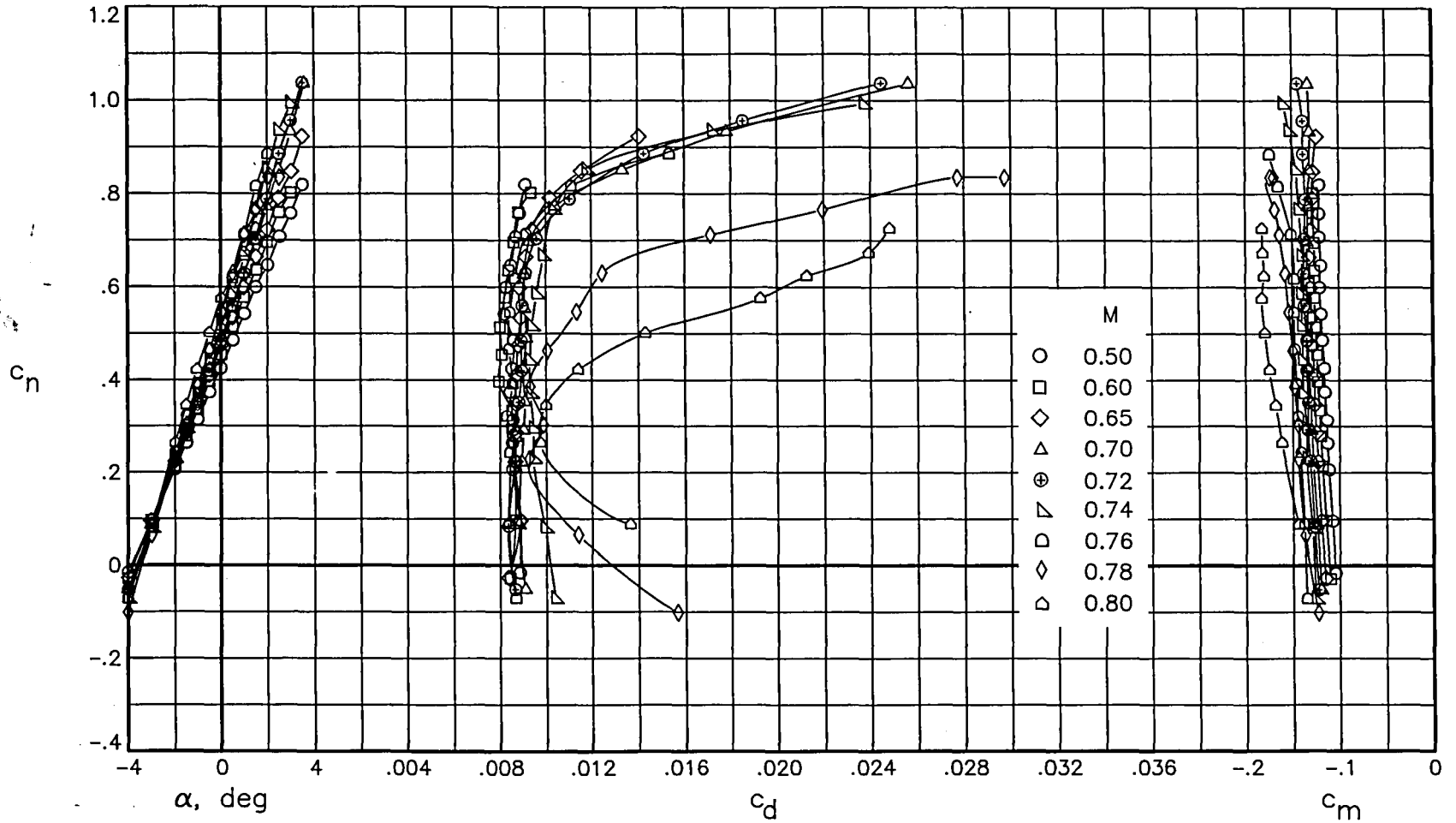

Figure 34. Effect of Mach number on aerodynamic characteristics of airfoil with free transition at $R \approx 7.0 \times 10^6$.

$m = .76 \quad \alpha = 1$

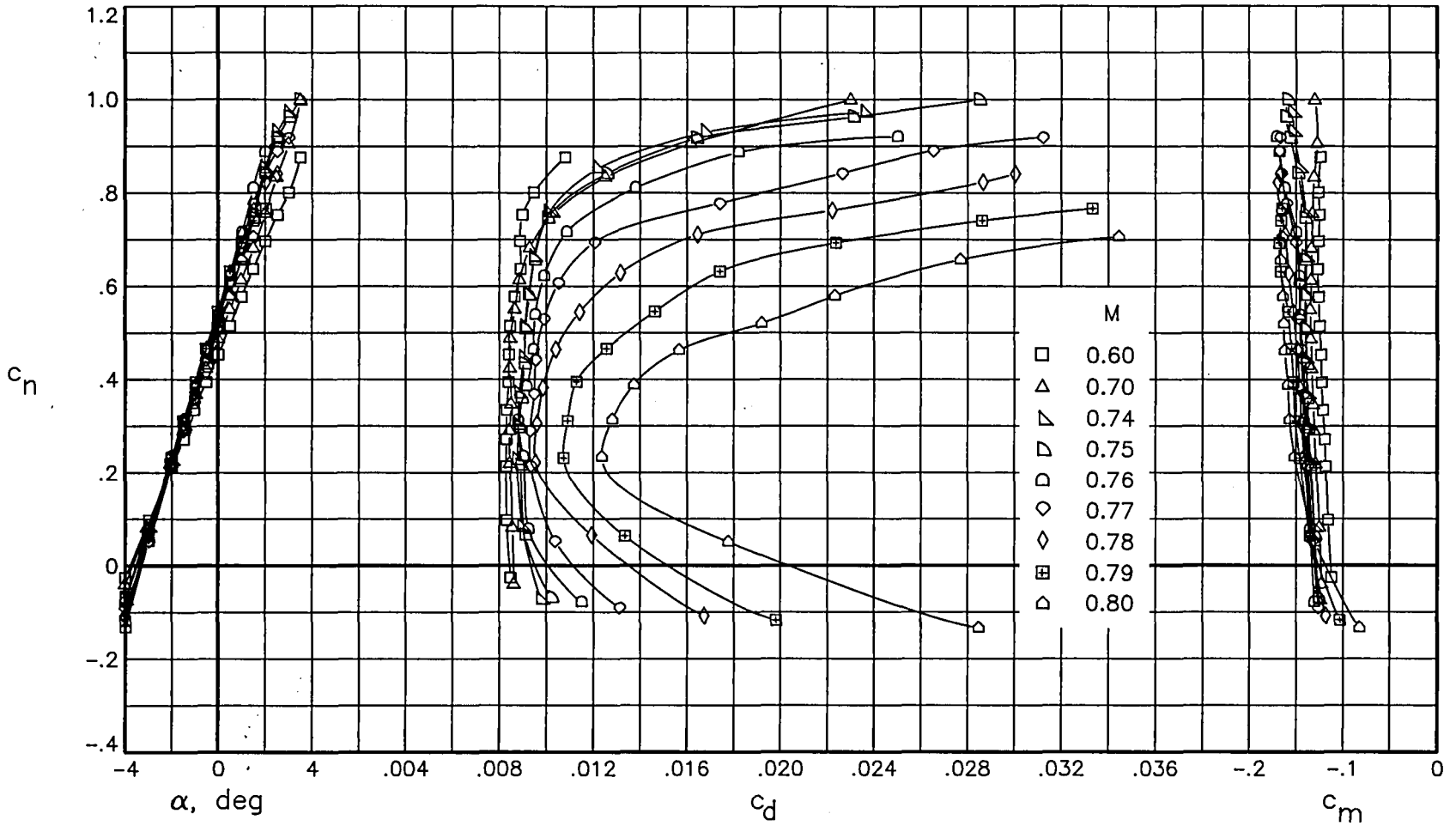

Figure 35. Effect of Mach number on aerodynamic characteristics of airfoil with free transition at $R \approx 10.0 \times 10^6$.

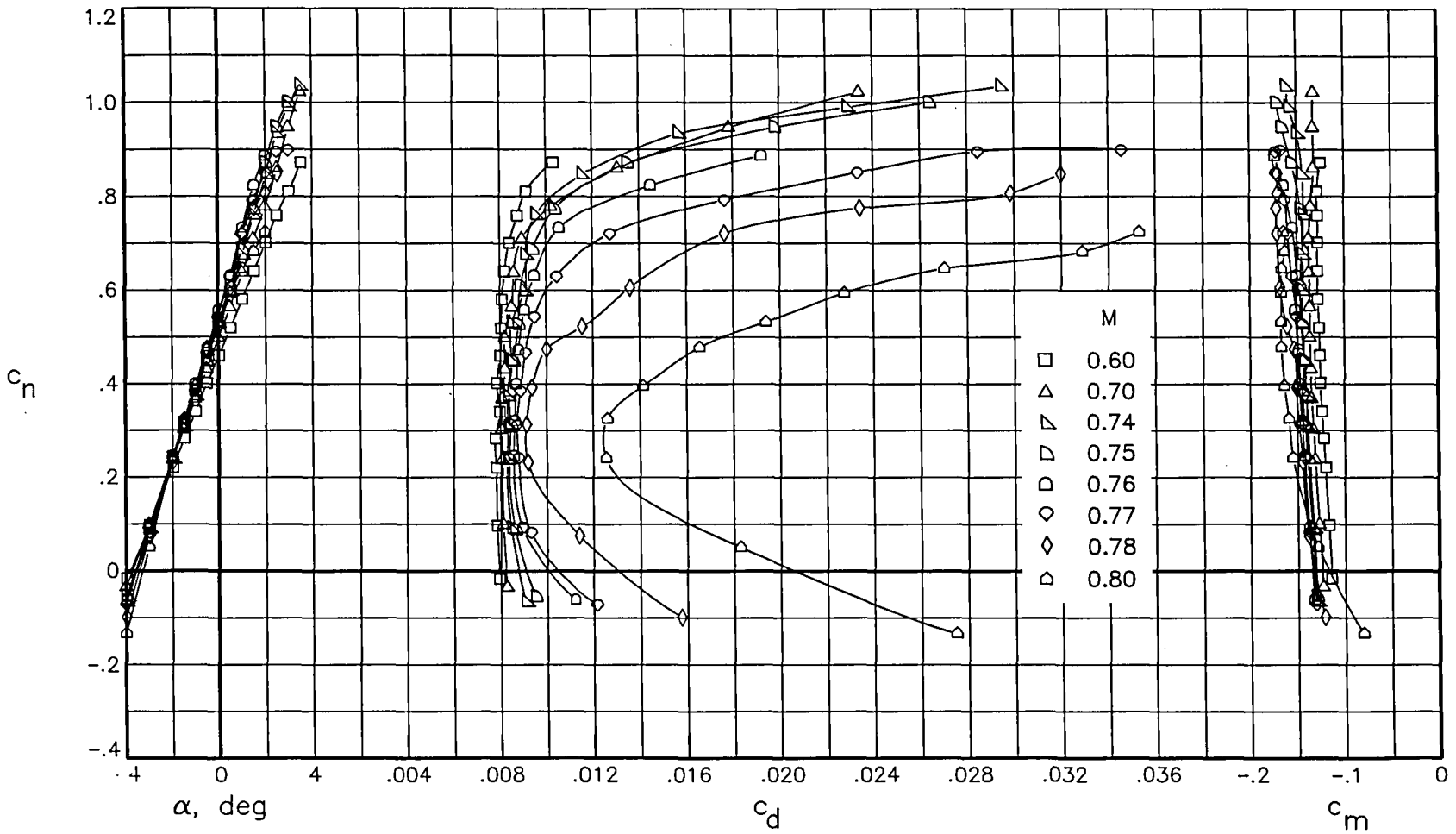

Figure 36. Effect of Mach number on aerodynamic characteristics of airfoil with free transition at $R \approx 15.0 \times 10^6$.

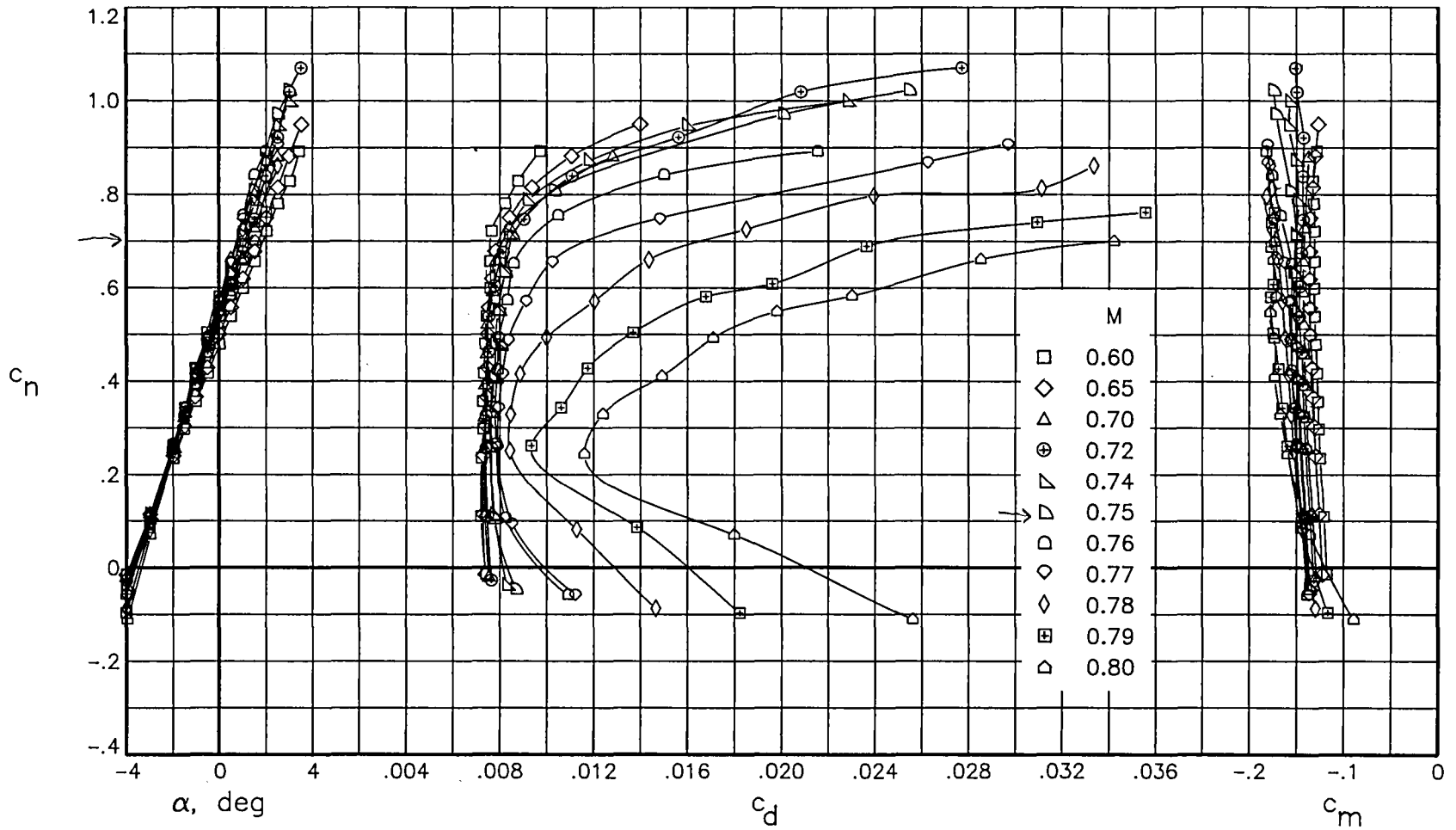

Figure 37. Effect of Mach number on aerodynamic characteristics of airfoil with free transition at $R \approx 30.0 \times 10^6$.

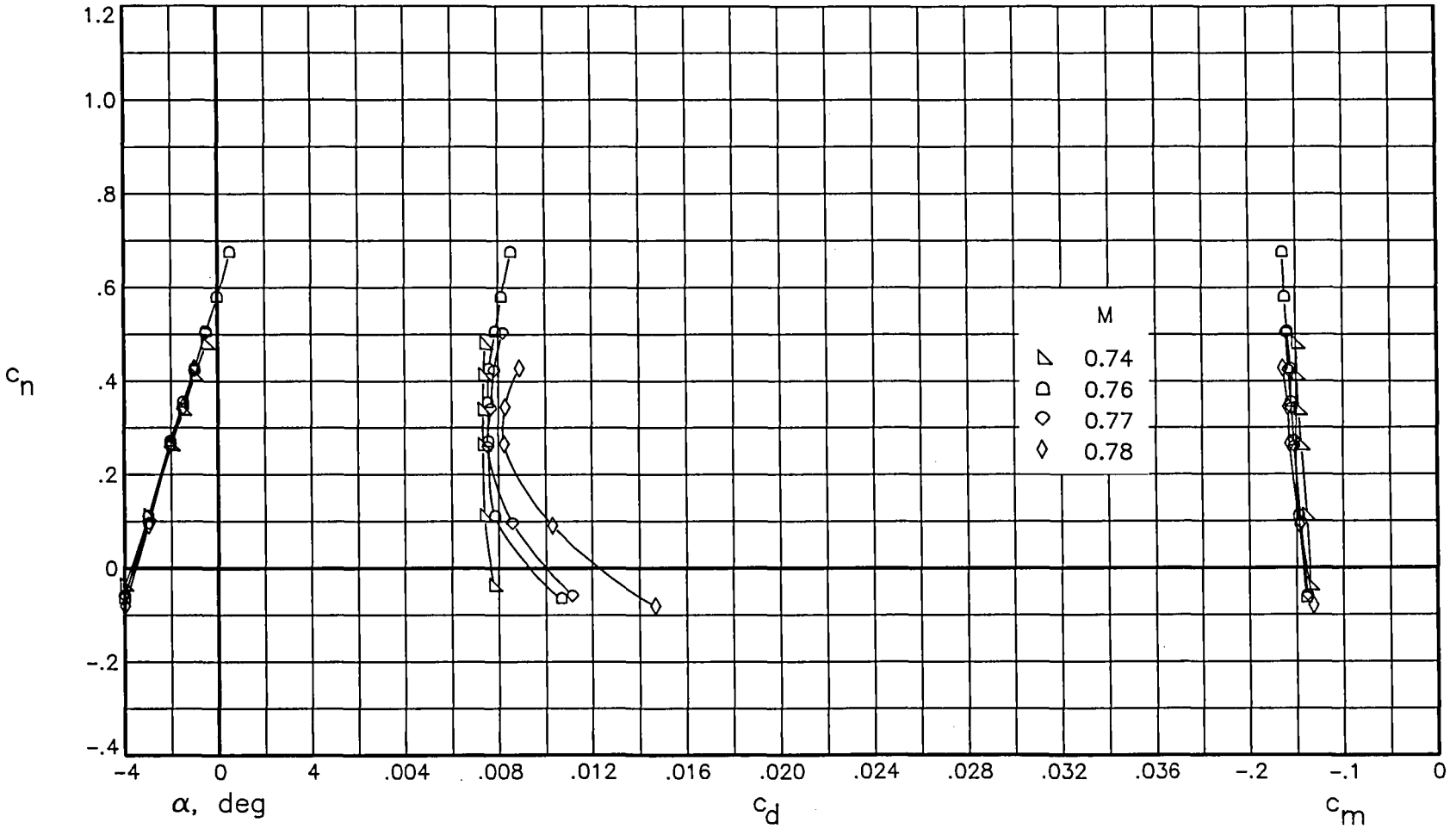

Figure 38. Effect of Mach number on aerodynamic characteristics of airfoil with free transition at $R \approx 40.0 \times 10^6$.

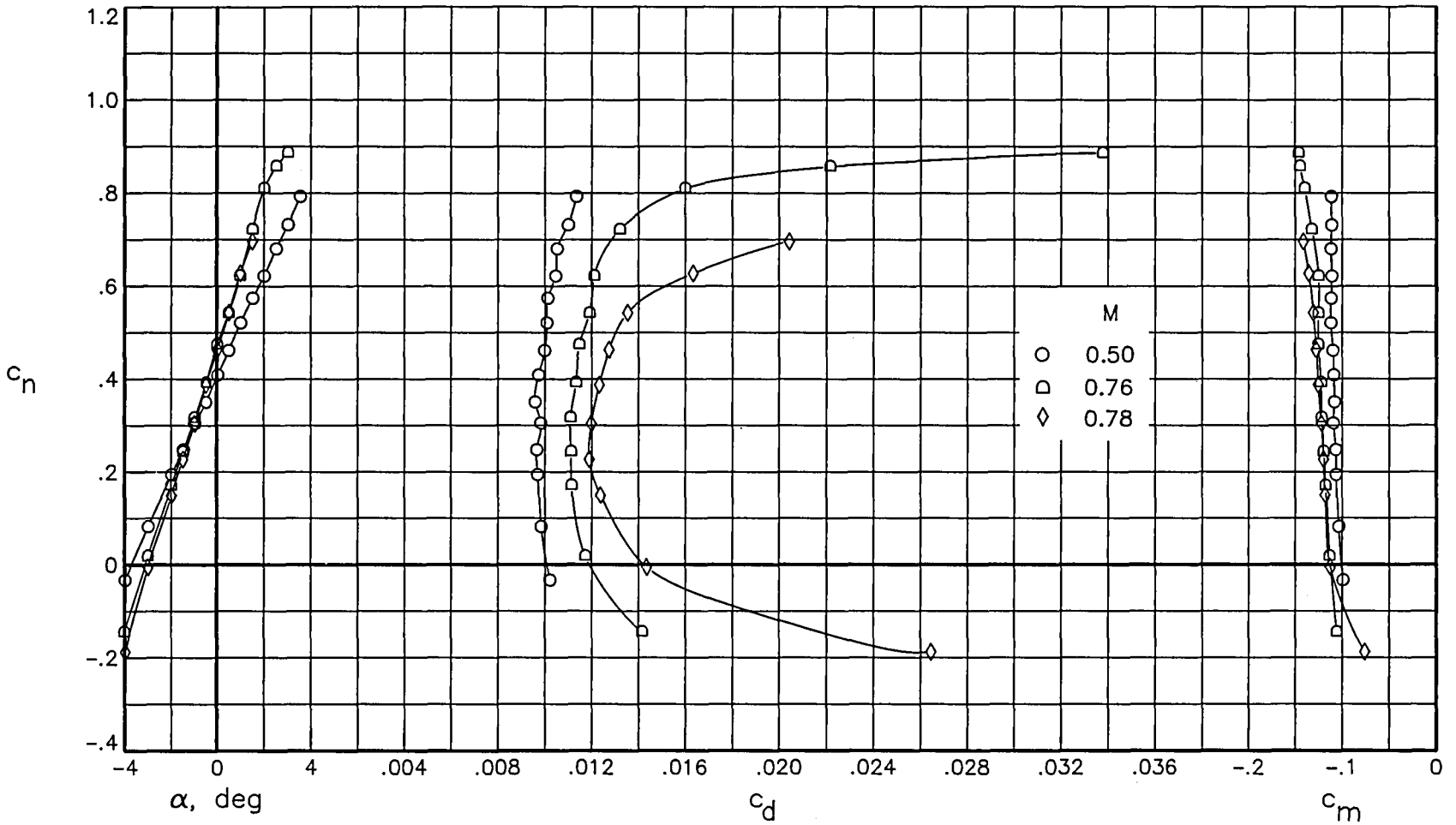

Figure 39. Effect of Mach number on aerodynamic characteristics of airfoil with fixed transition at $R \approx 4.4 \times 10^6$.

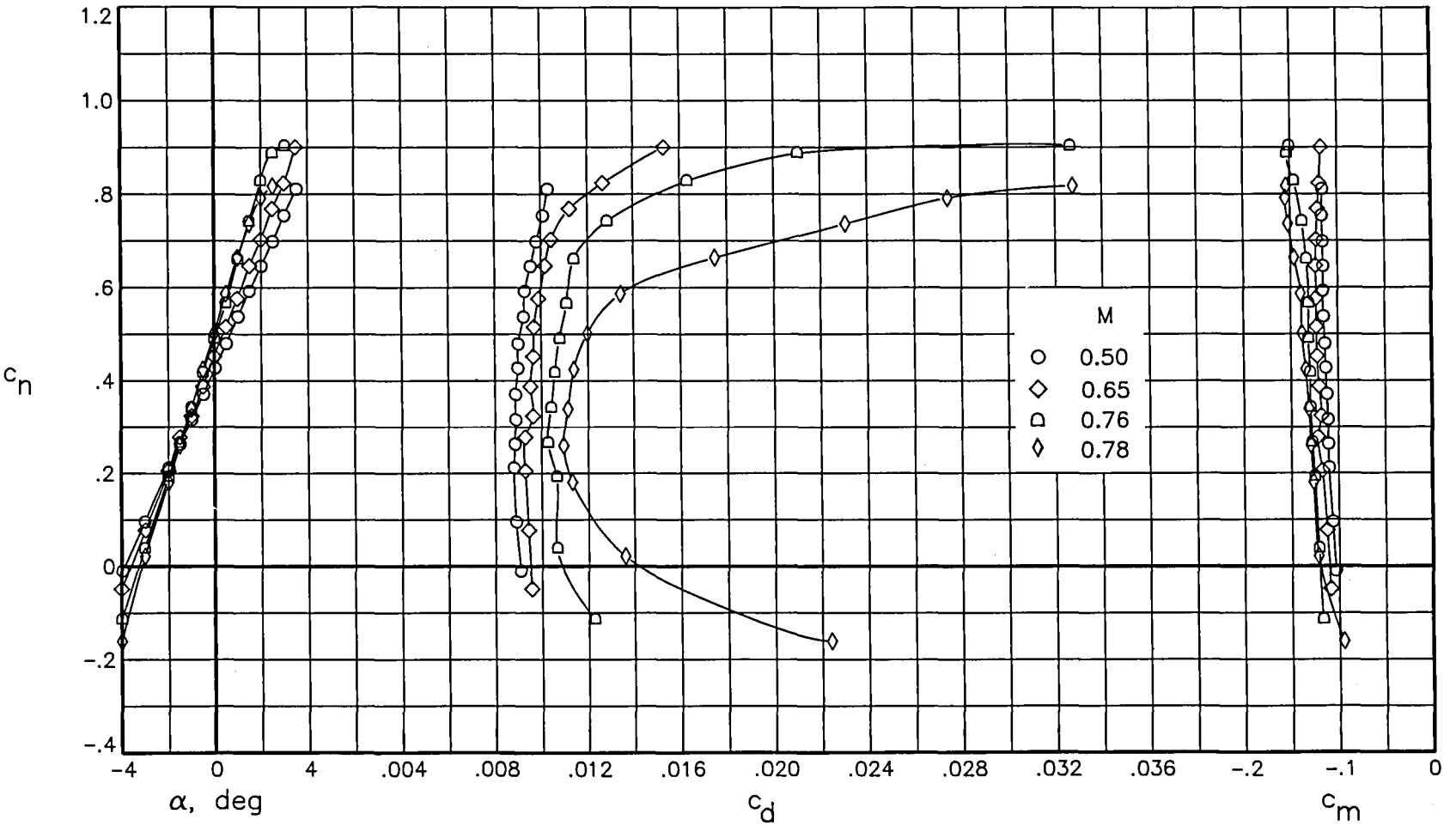

Figure 40. Effect of Mach number on aerodynamic characteristics of airfoil with fixed transition at $R \approx 7.0 \times 10^6$.

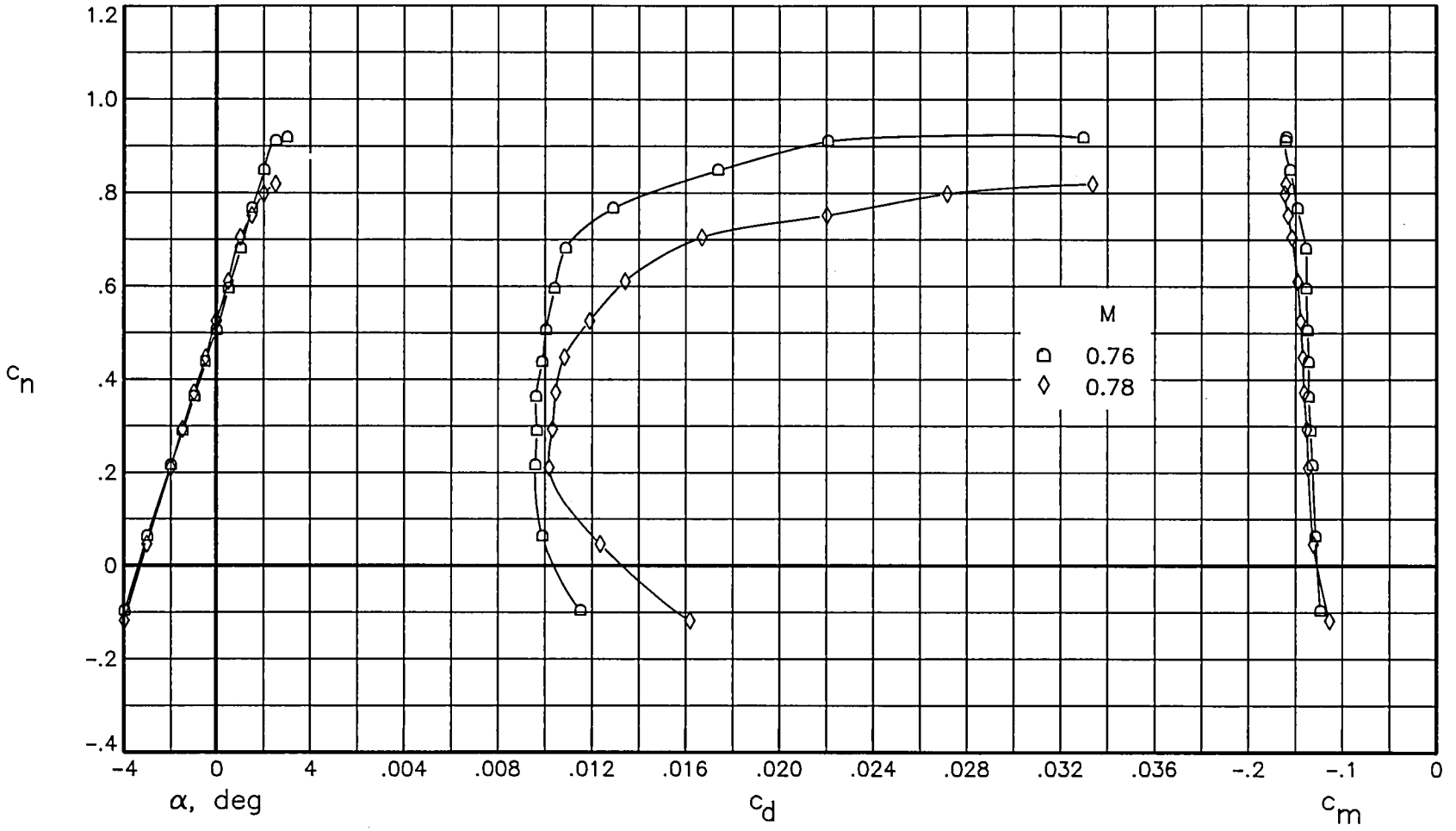

Figure 41. Effect of Mach number on aerodynamic characteristics of airfoil with fixed transition at $R \approx 10.0 \times 10^6$.

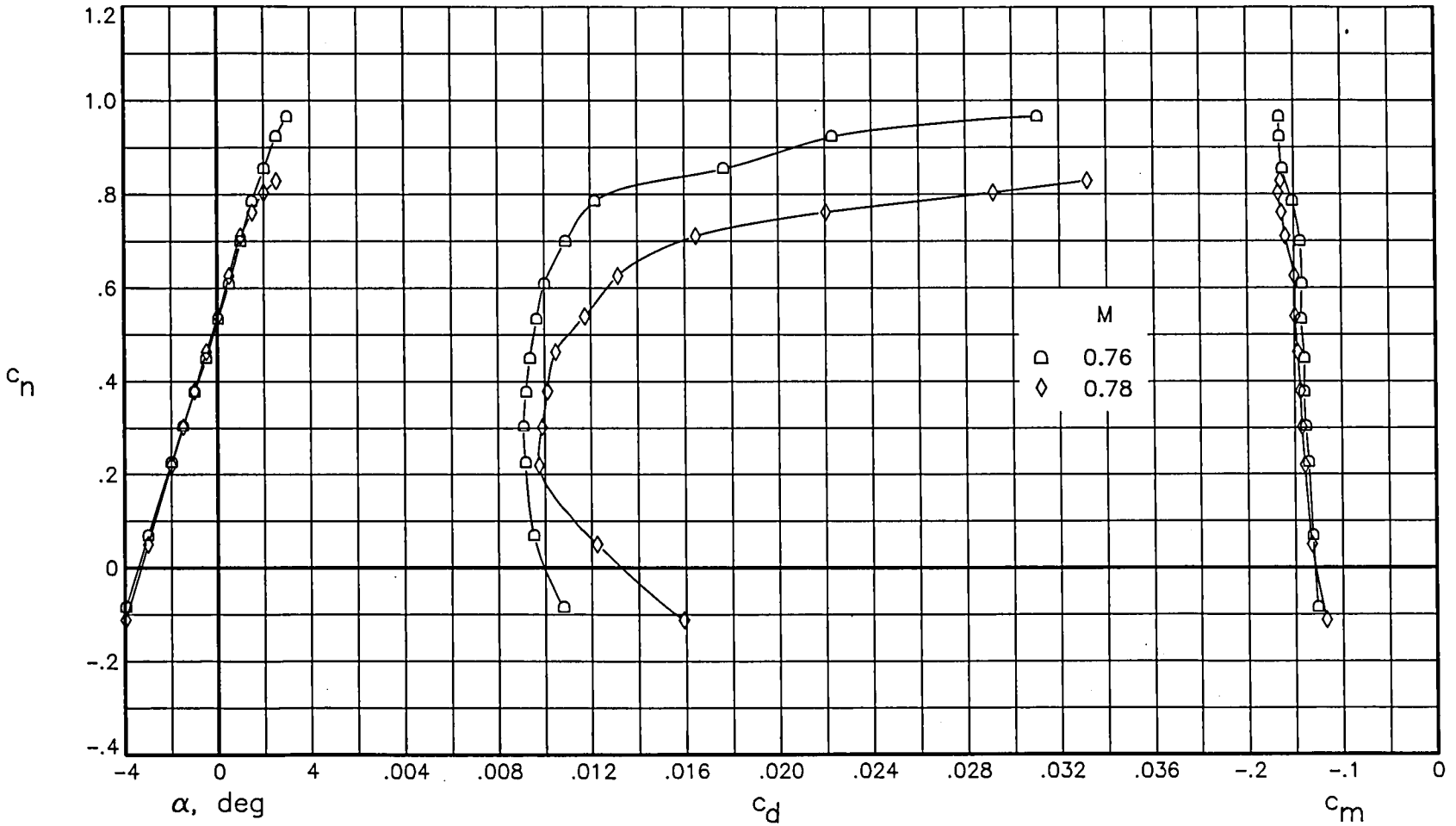

Figure 42. Effect of Mach number on aerodynamic characteristics of airfoil with fixed transition at $R \approx 15.0 \times 10^6$.

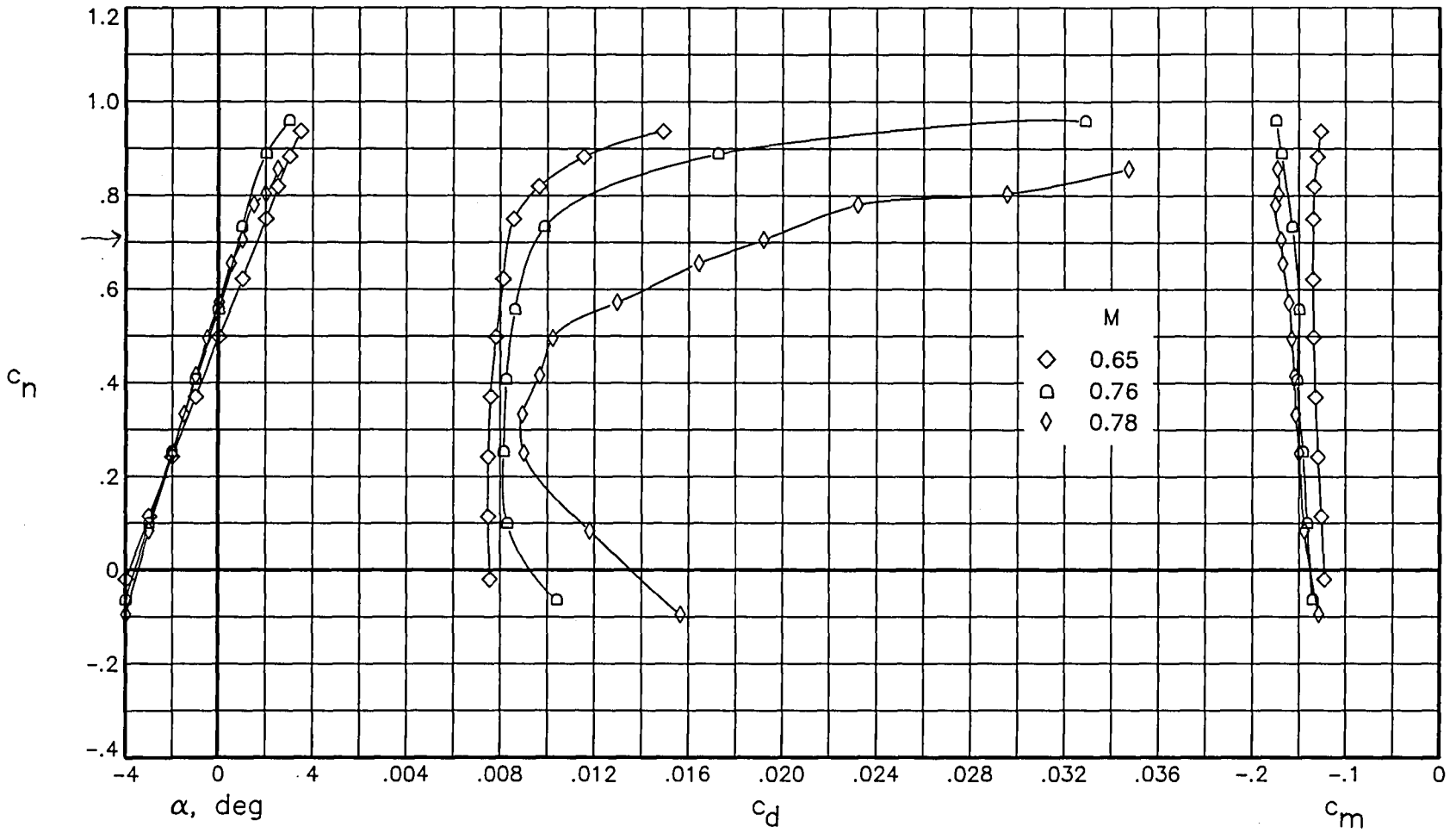

Figure 43. Effect of Mach number on aerodynamic characteristics of airfoil with fixed transition at $R \approx 30.0 \times 10^6$.

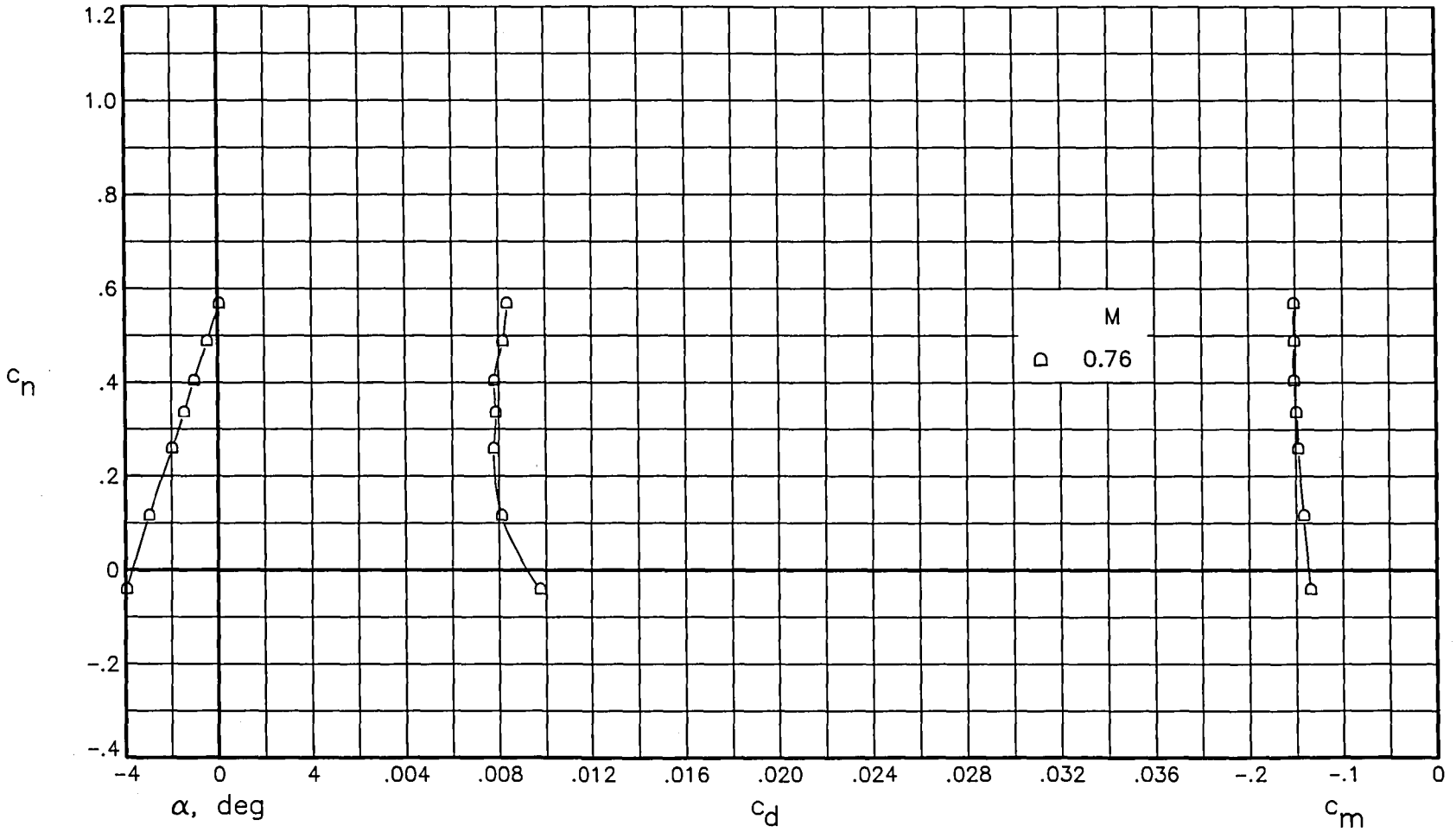

Figure 44. Effect of Mach number on aerodynamic characteristics of airfoil with fixed transition at $R \approx 40.0 \times 10^6$.

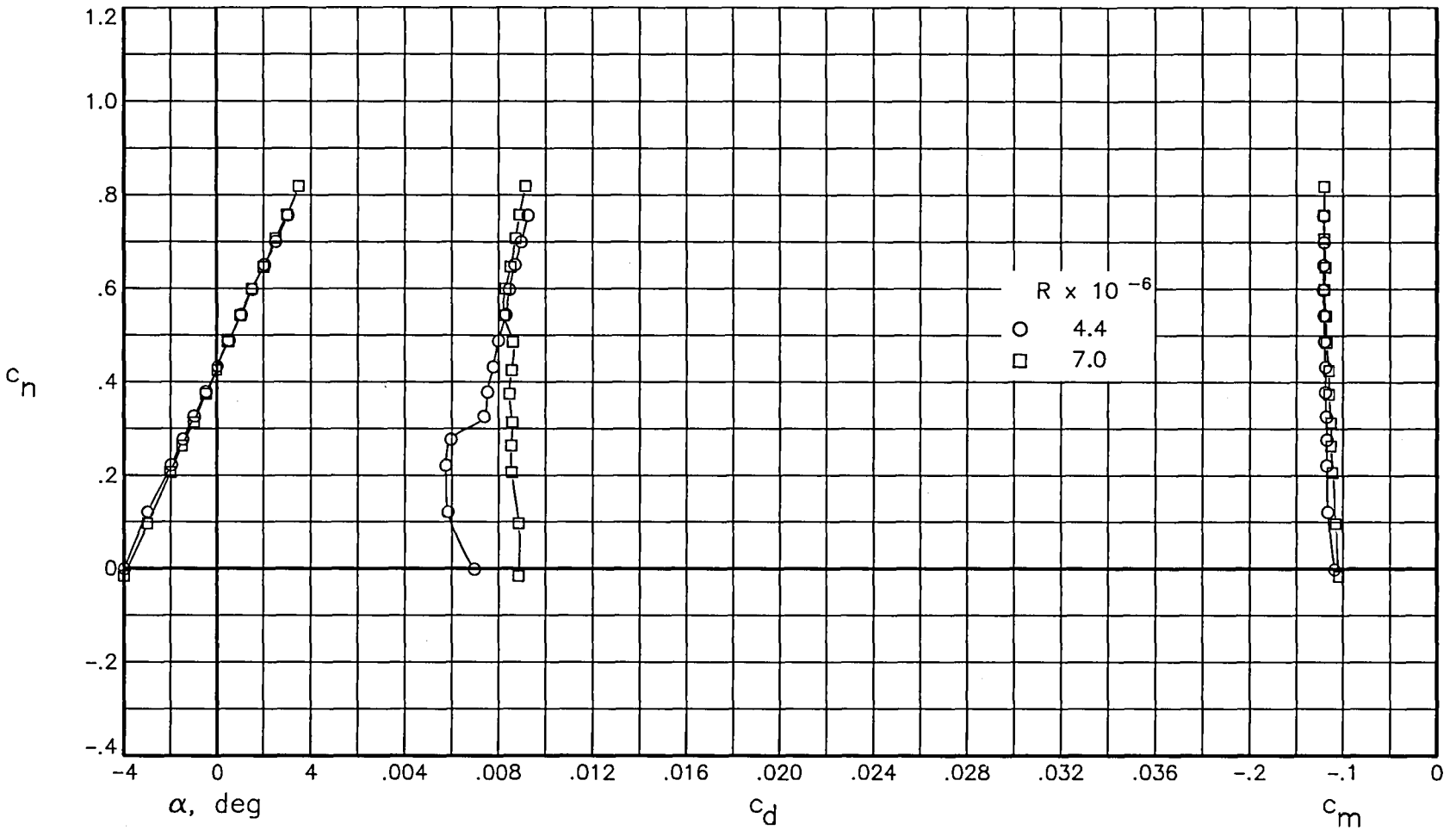

Figure 45. Effect of Reynolds number on aerodynamic characteristics of airfoil with free transition at $M \approx 0.50$.

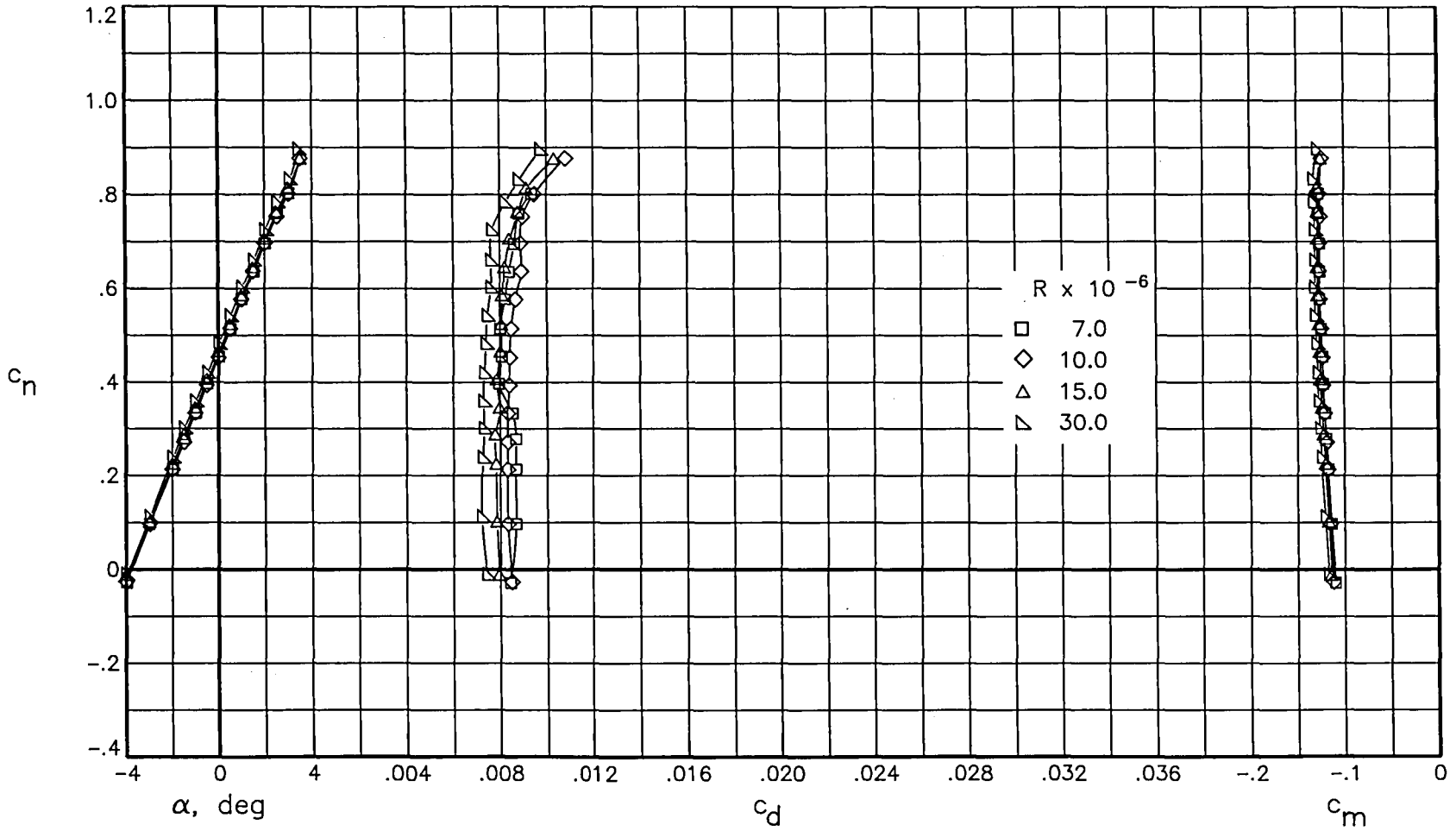

Figure 46. Effect of Reynolds number on aerodynamic characteristics of airfoil with free transition at $M \approx 0.60$.

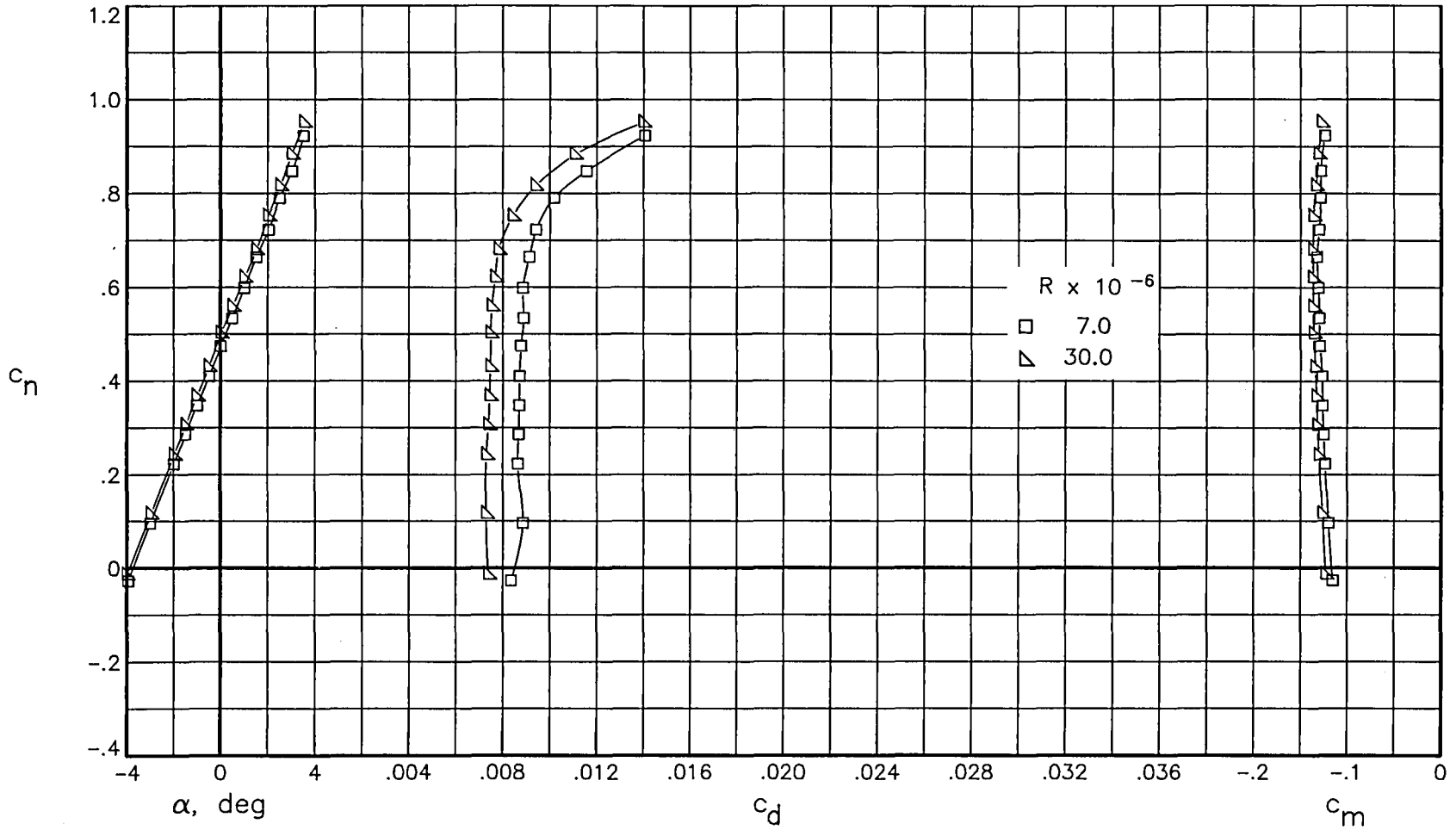

Figure 47. Effect of Reynolds number on aerodynamic characteristics of airfoil with free transition at $M \approx 0.65$.

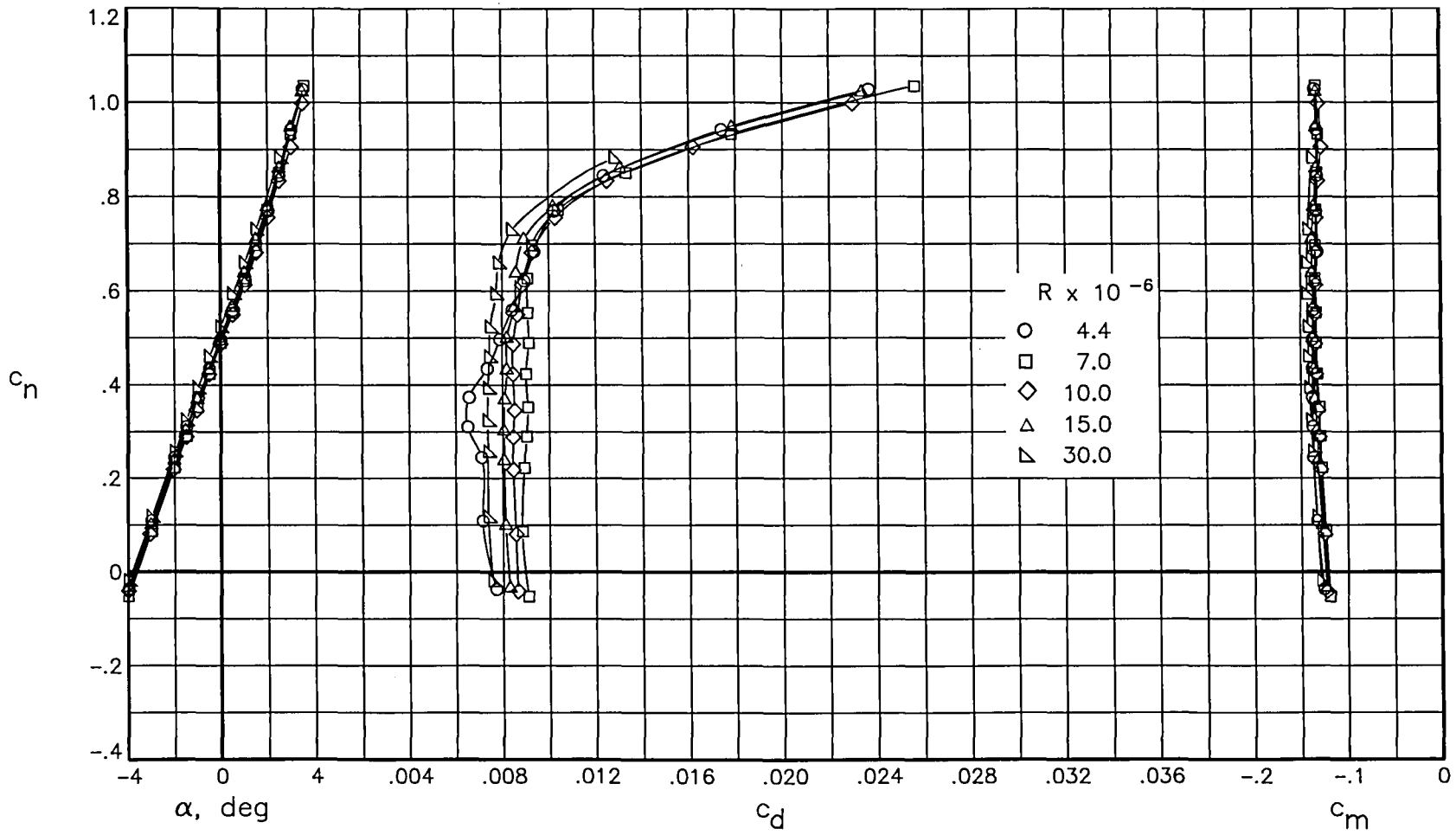

Figure 48. Effect of Reynolds number on aerodynamic characteristics of airfoil with free transition at $M \approx 0.70$.

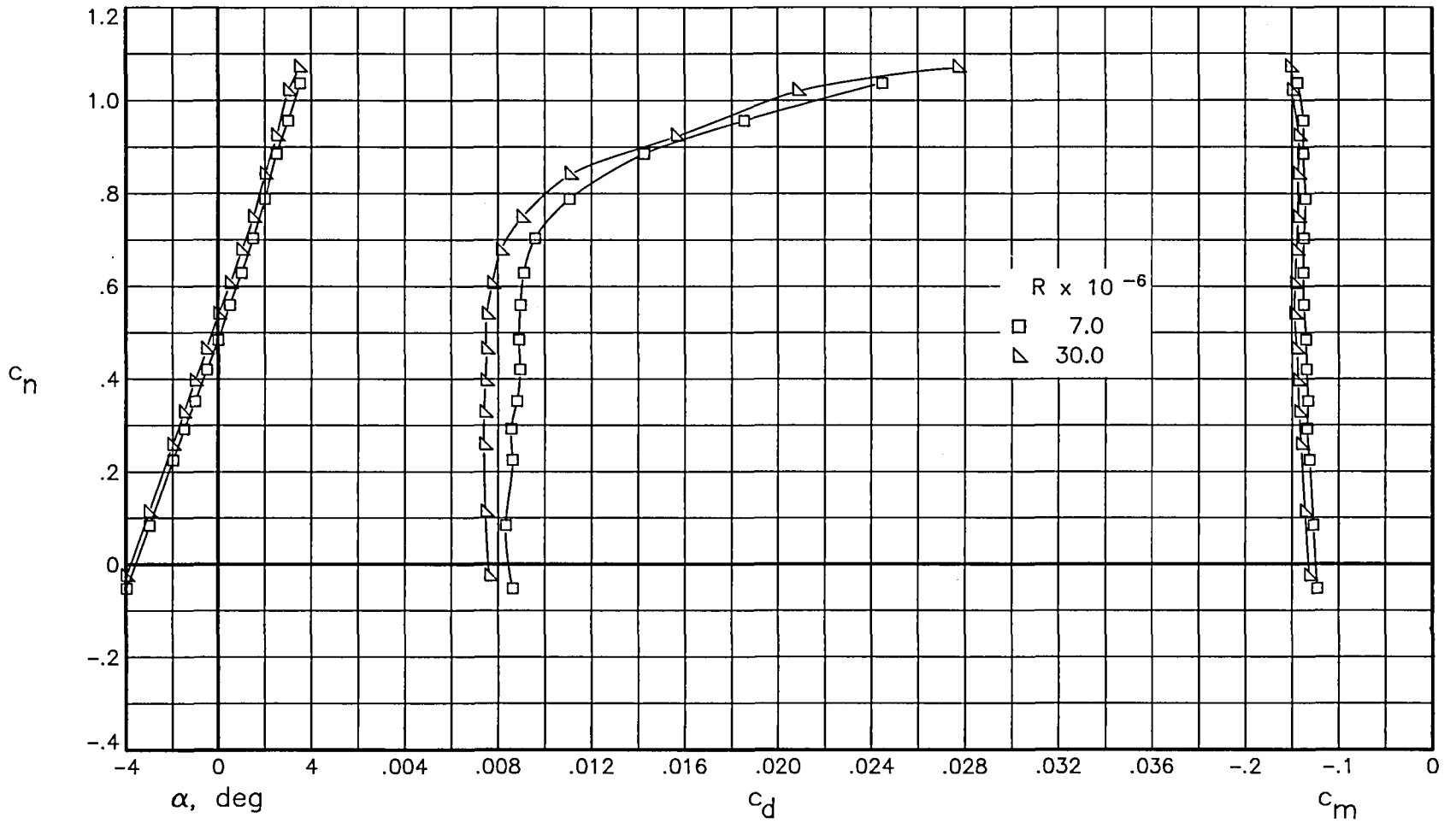

Figure 49. Effect of Reynolds number on aerodynamic characteristics of airfoil with free transition at $M \approx 0.72$.

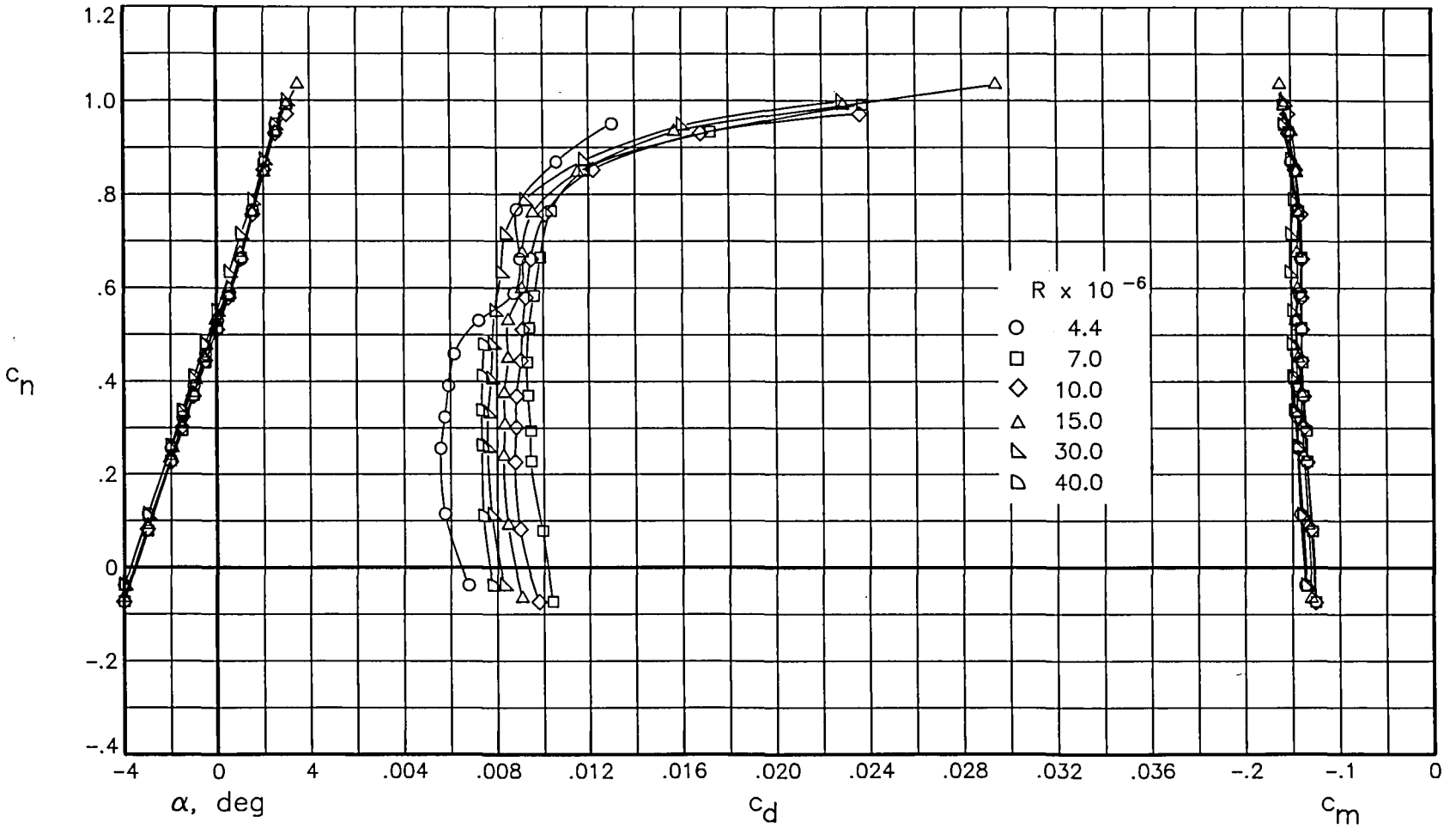

Figure 50. Effect of Reynolds number on aerodynamic characteristics of airfoil with free transition at $M \approx 0.74$.

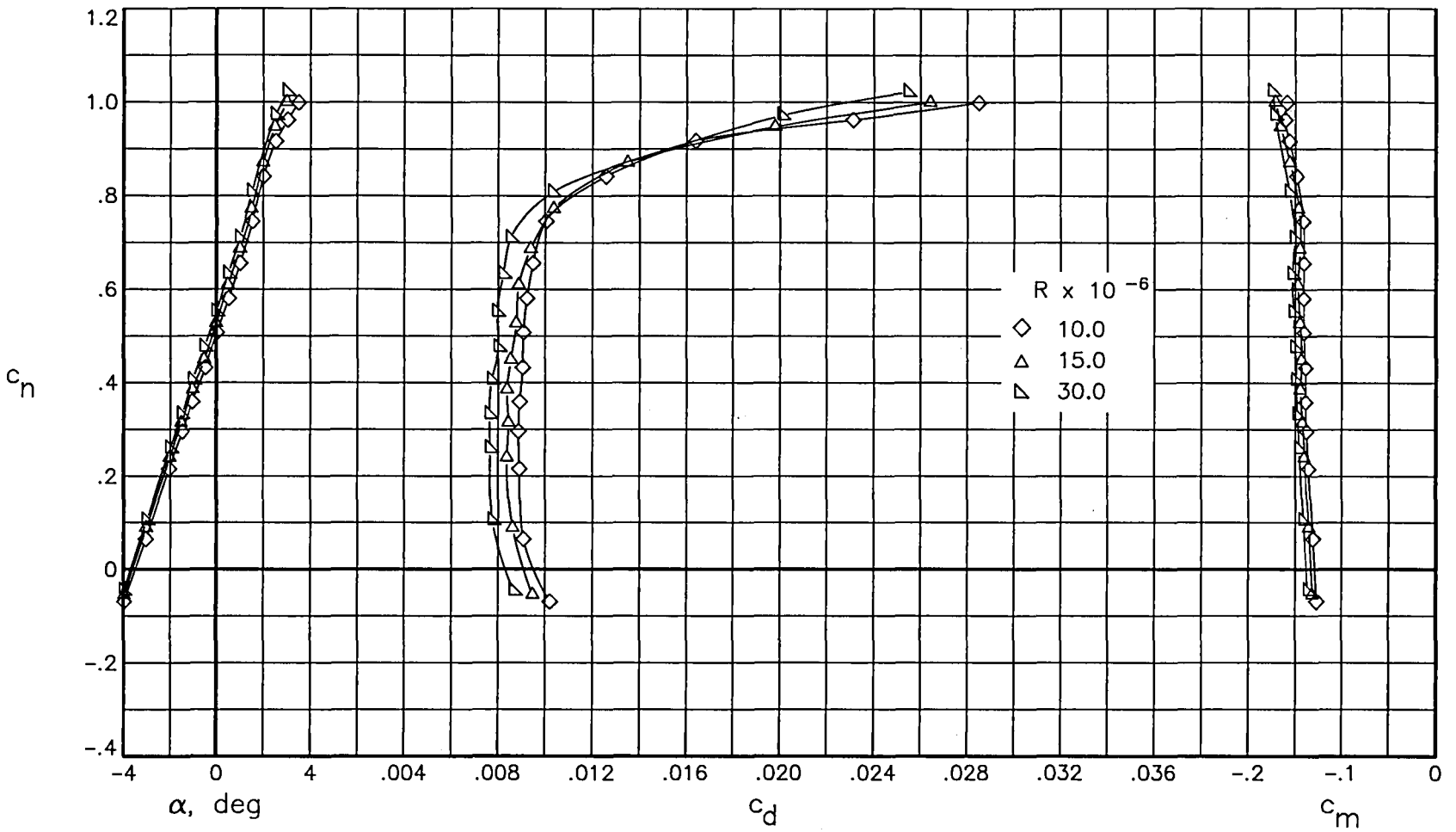

Figure 51. Effect of Reynolds number on aerodynamic characteristics of airfoil with free transition at $M \approx 0.75$.

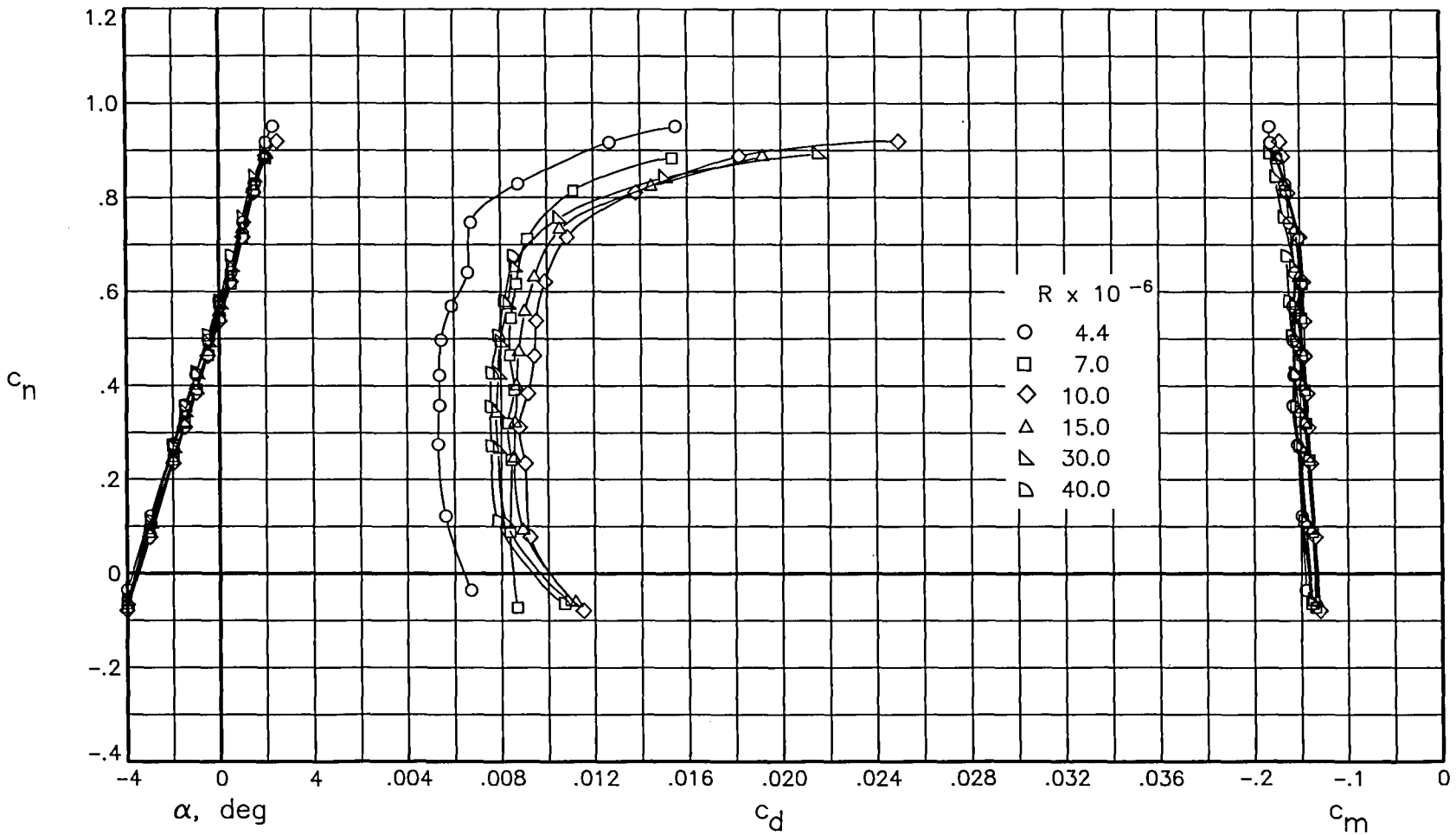

Figure 52. Effect of Reynolds number on aerodynamic characteristics of airfoil with free transition at $M \approx 0.76$.

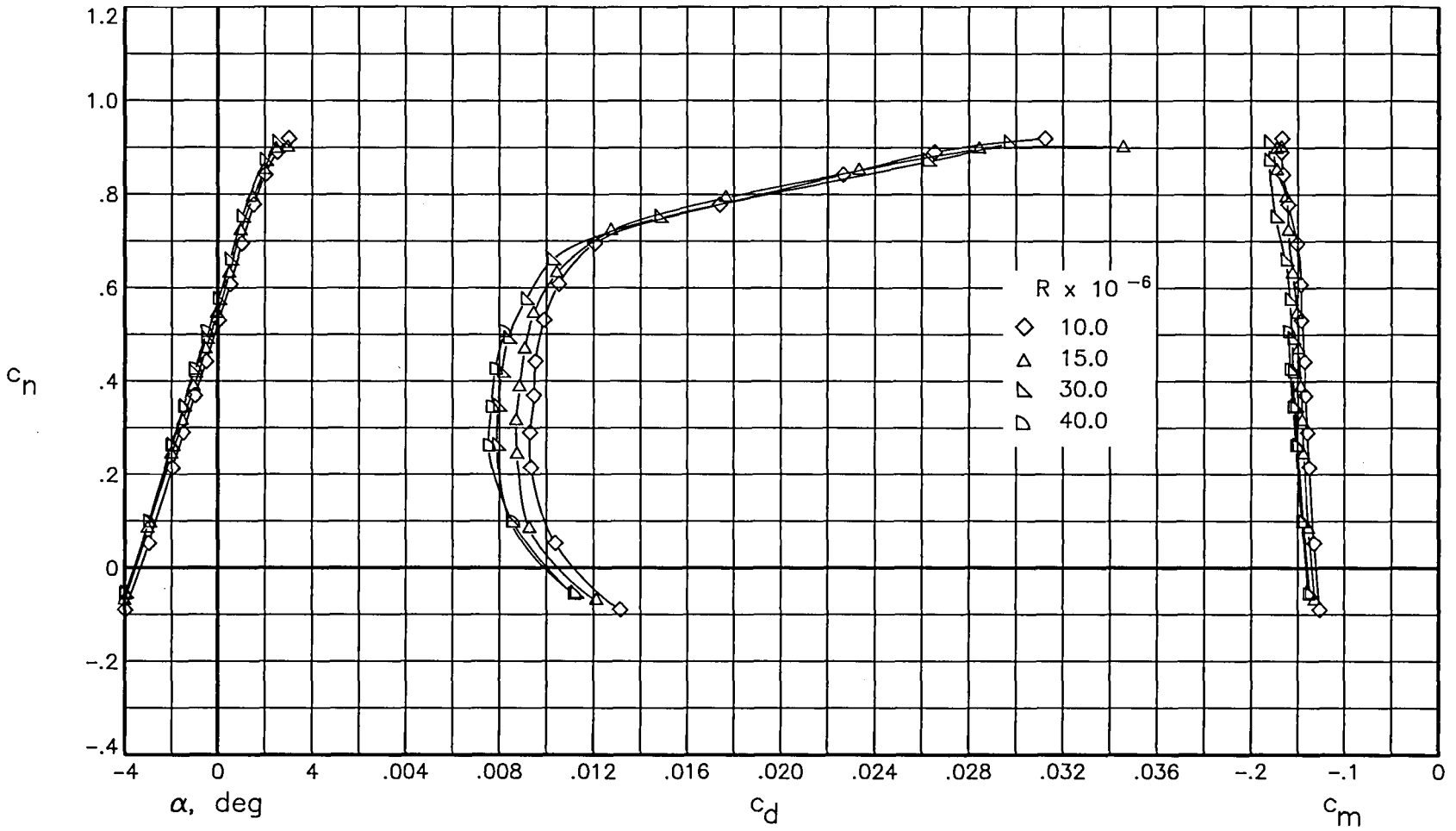

Figure 53. Effect of Reynolds number on aerodynamic characteristics of airfoil with free transition at $M \approx 0.77$.

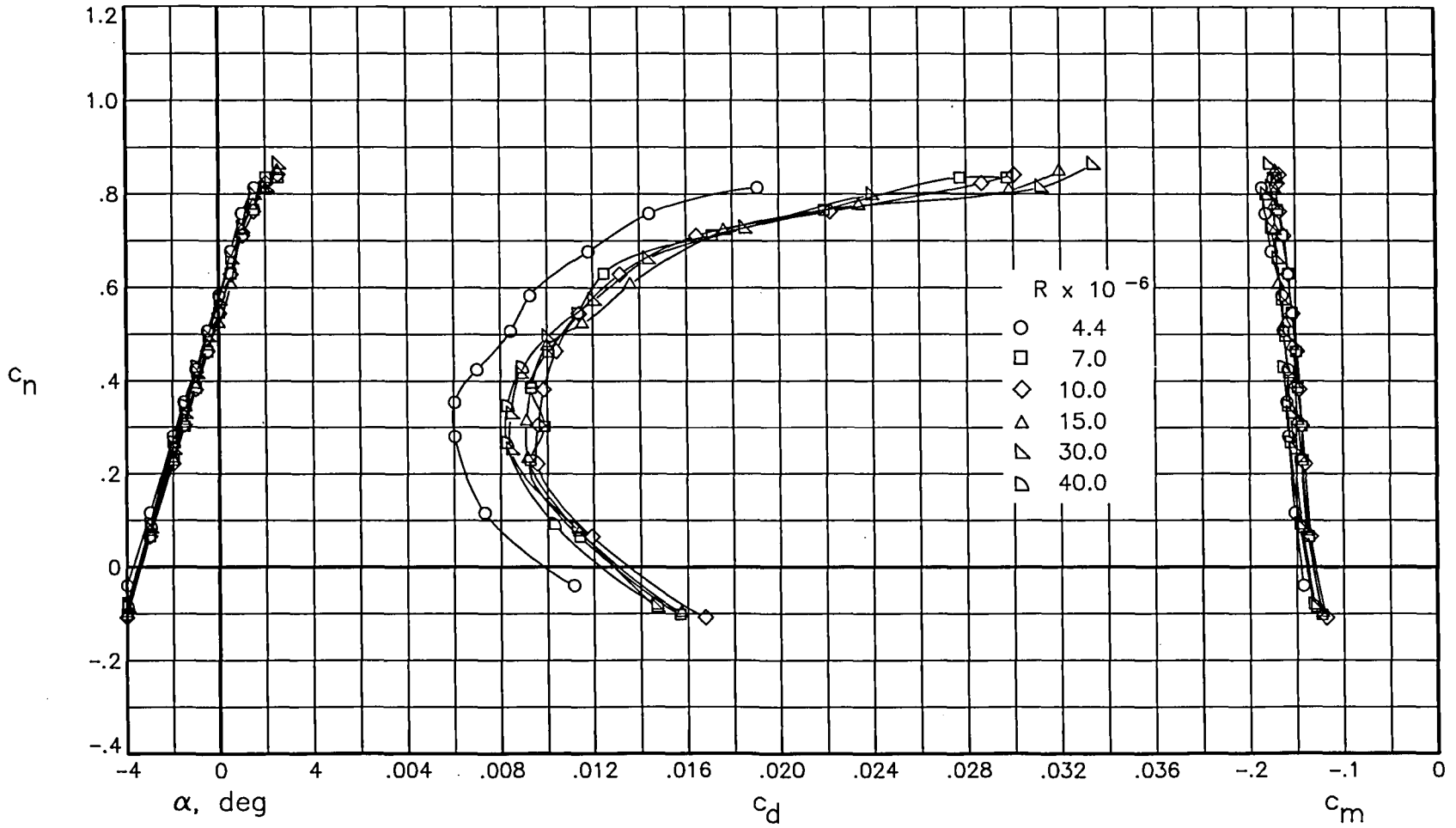

Figure 54. Effect of Reynolds number on aerodynamic characteristics of airfoil with free transition at $M \approx 0.78$.

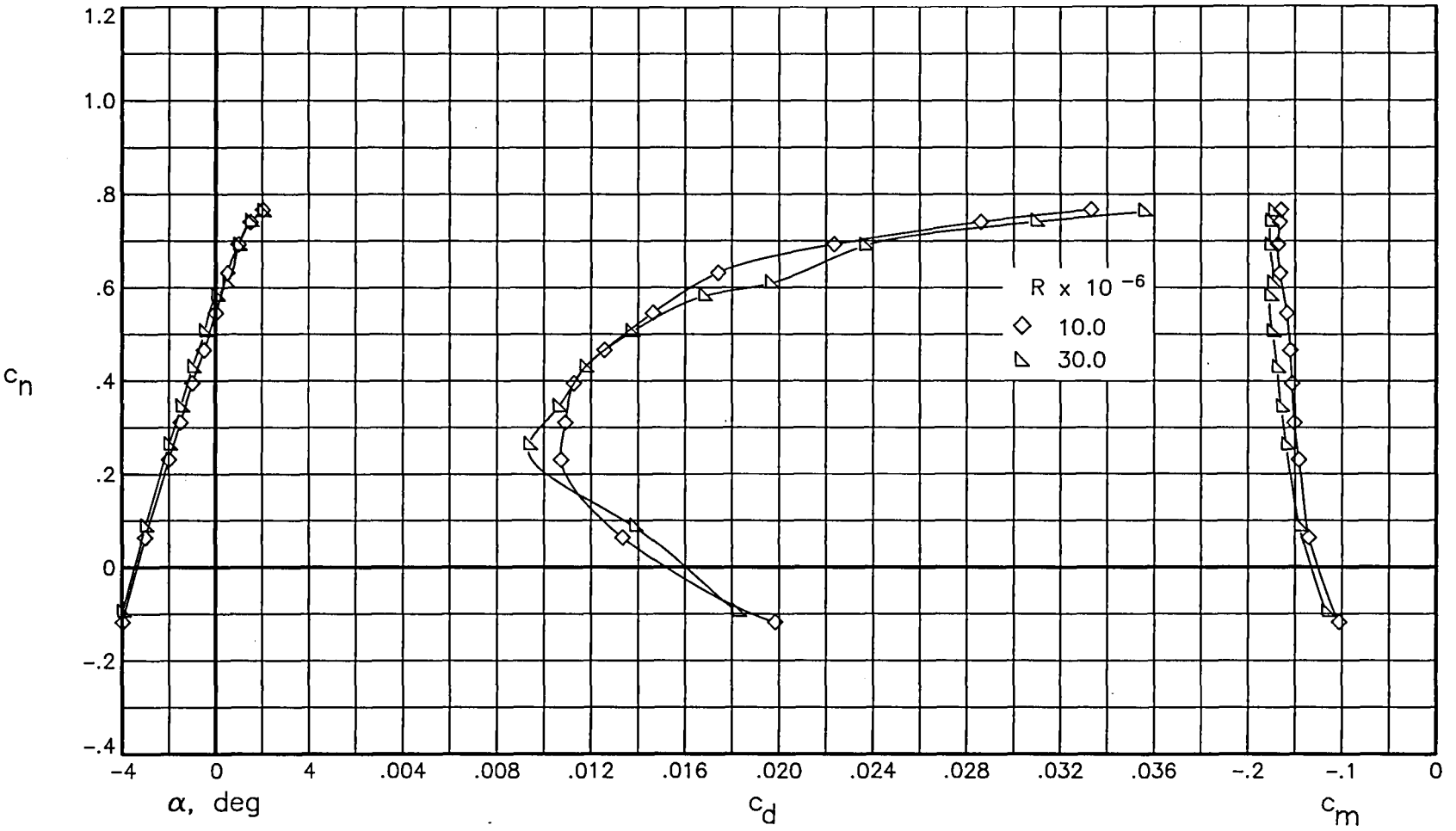

Figure 55. Effect of Reynolds number on aerodynamic characteristics of airfoil with free transition at $M \approx 0.79$.

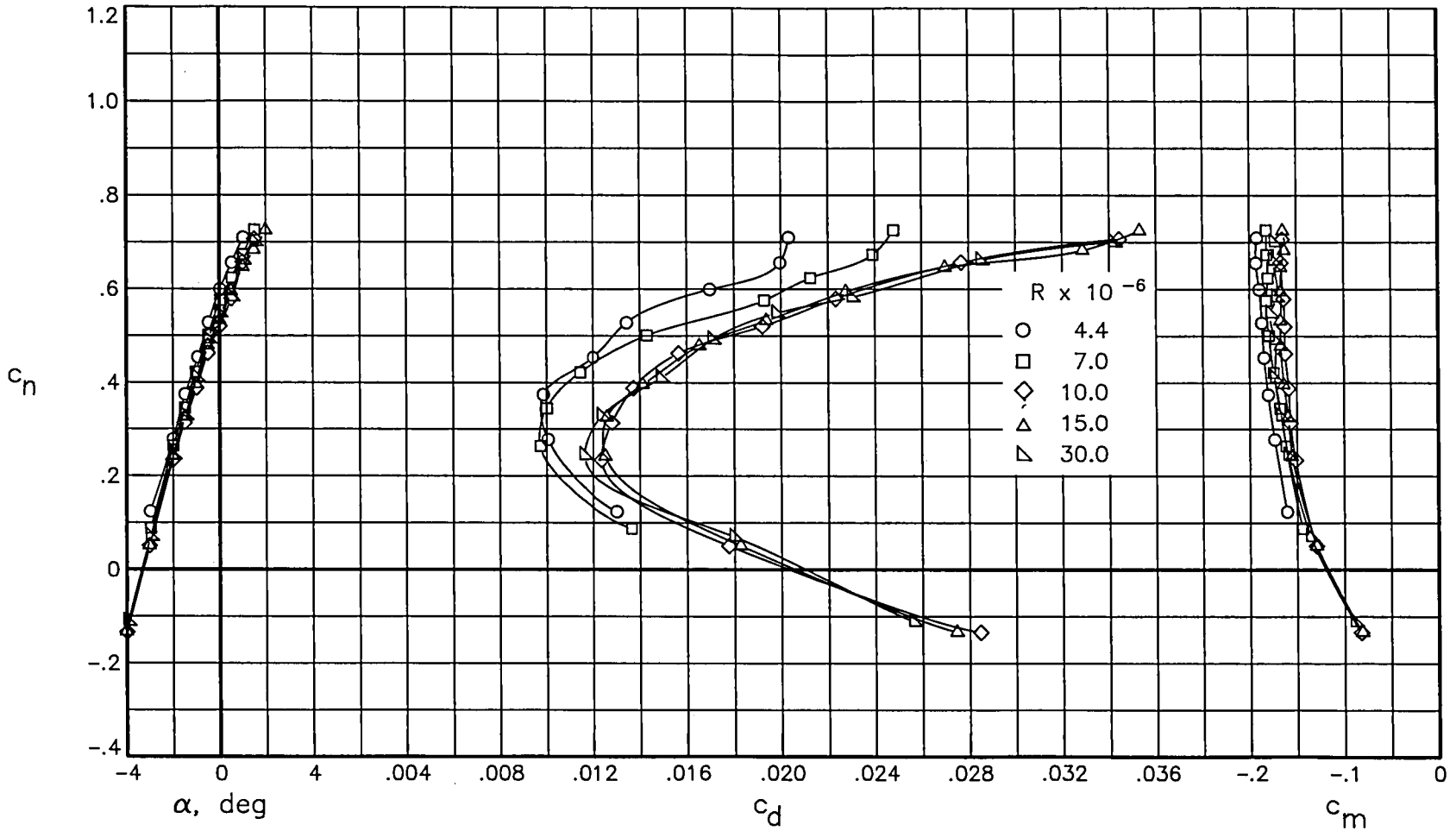

Figure 56. Effect of Reynolds number on aerodynamic characteristics of airfoil with free transition at $M \approx 0.80$.

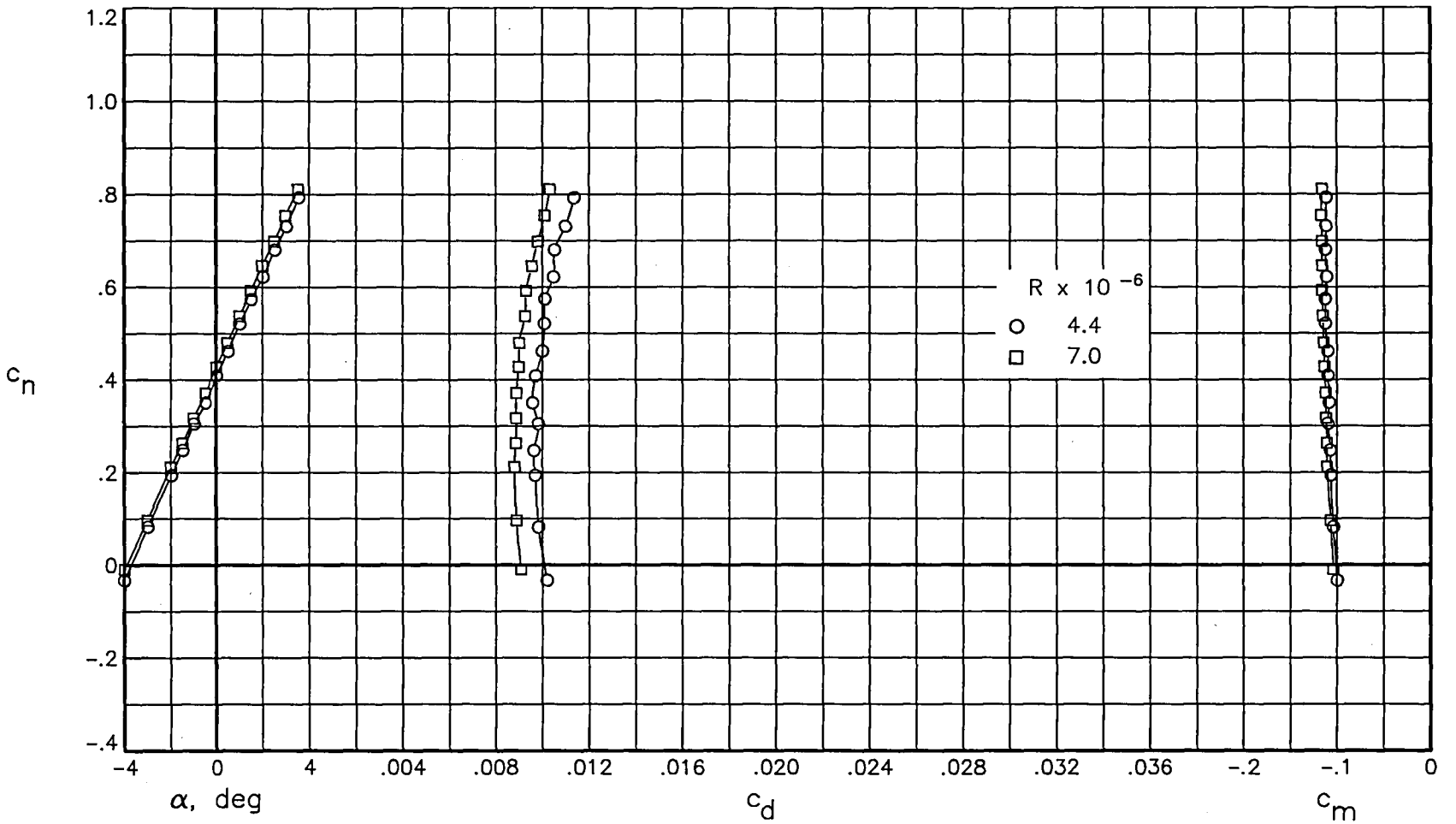

Figure 57. Effect of Reynolds number on aerodynamic characteristics of airfoil with fixed transition at $M \approx 0.50$.

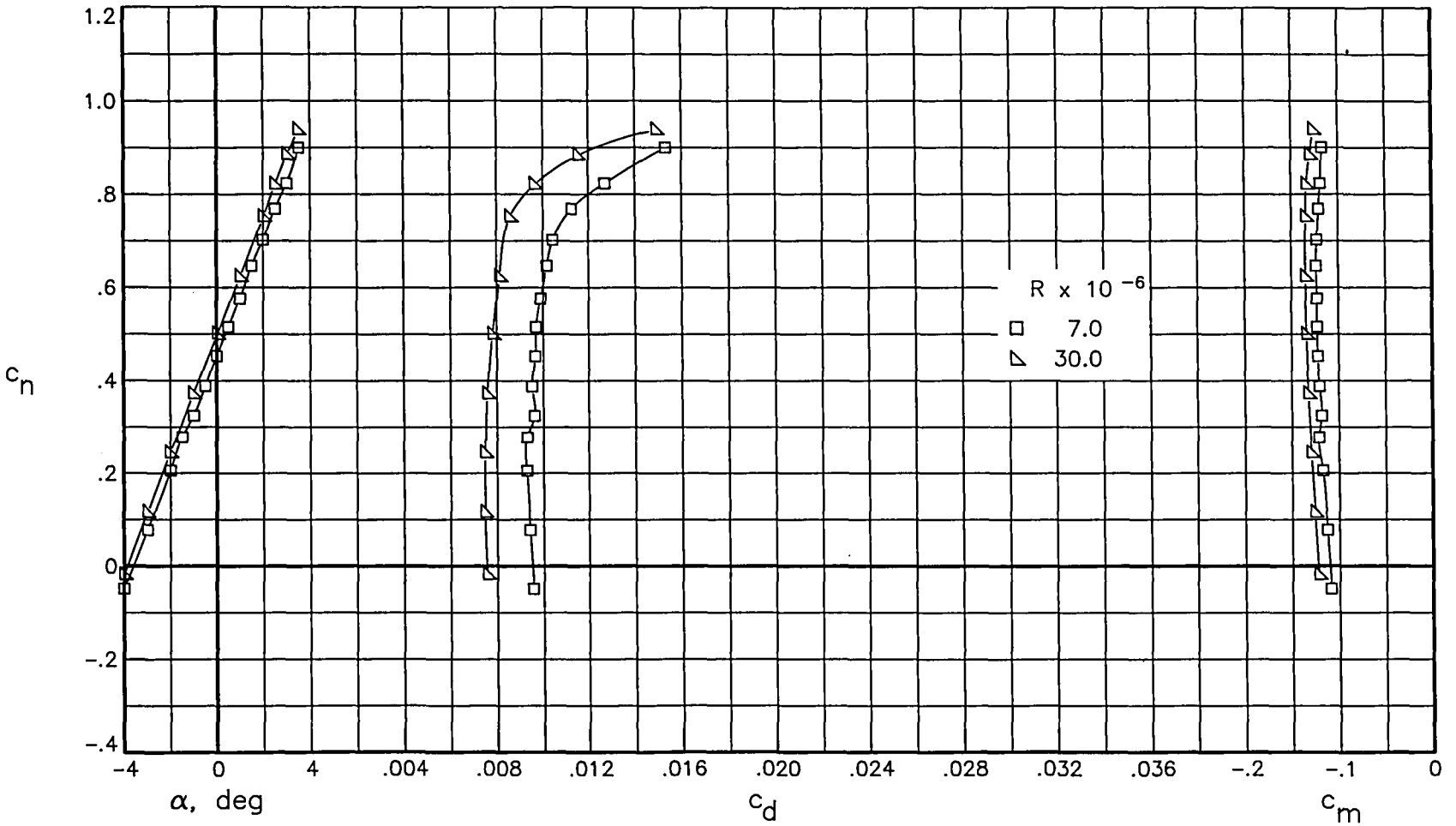

Figure 58. Effect of Reynolds number on aerodynamic characteristics of airfoil with fixed transition at $M \approx 0.65$.

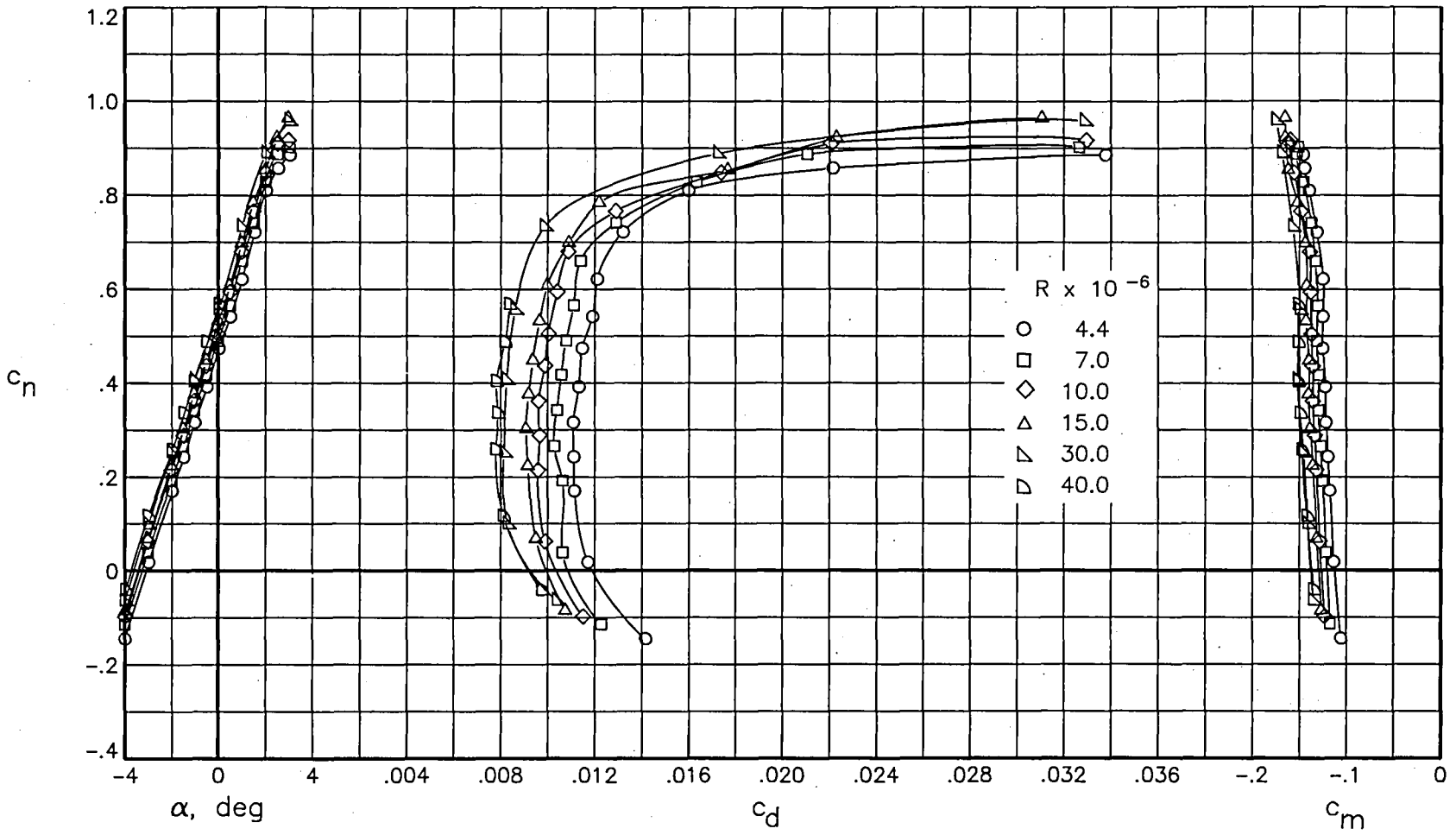

Figure 59. Effect of Reynolds number on aerodynamic characteristics of airfoil with fixed transition at $M \approx 0.76$.

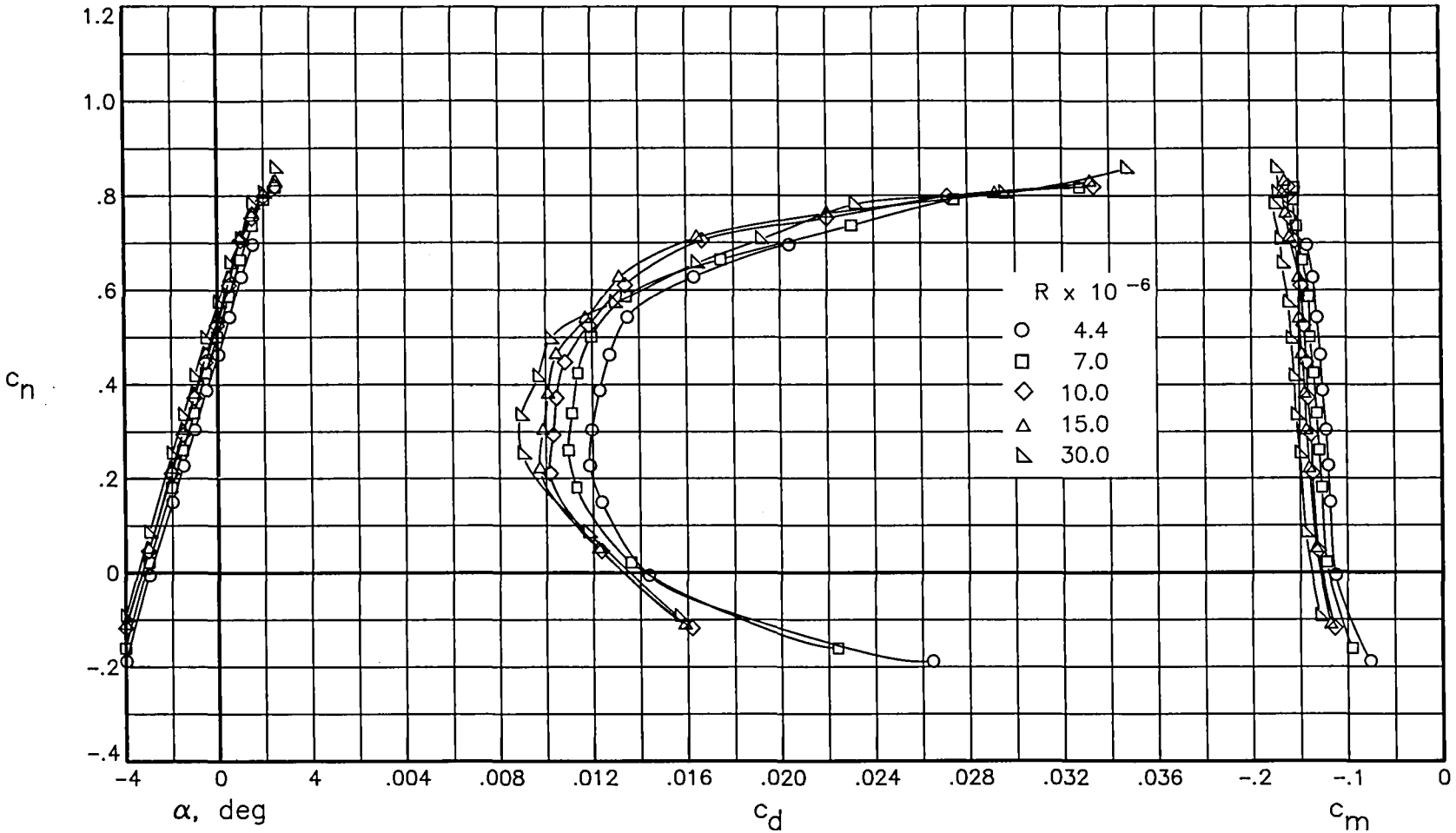

Figure 60. Effect of Reynolds number on aerodynamic characteristics of airfoil with fixed transition at $M \approx 0.78$.

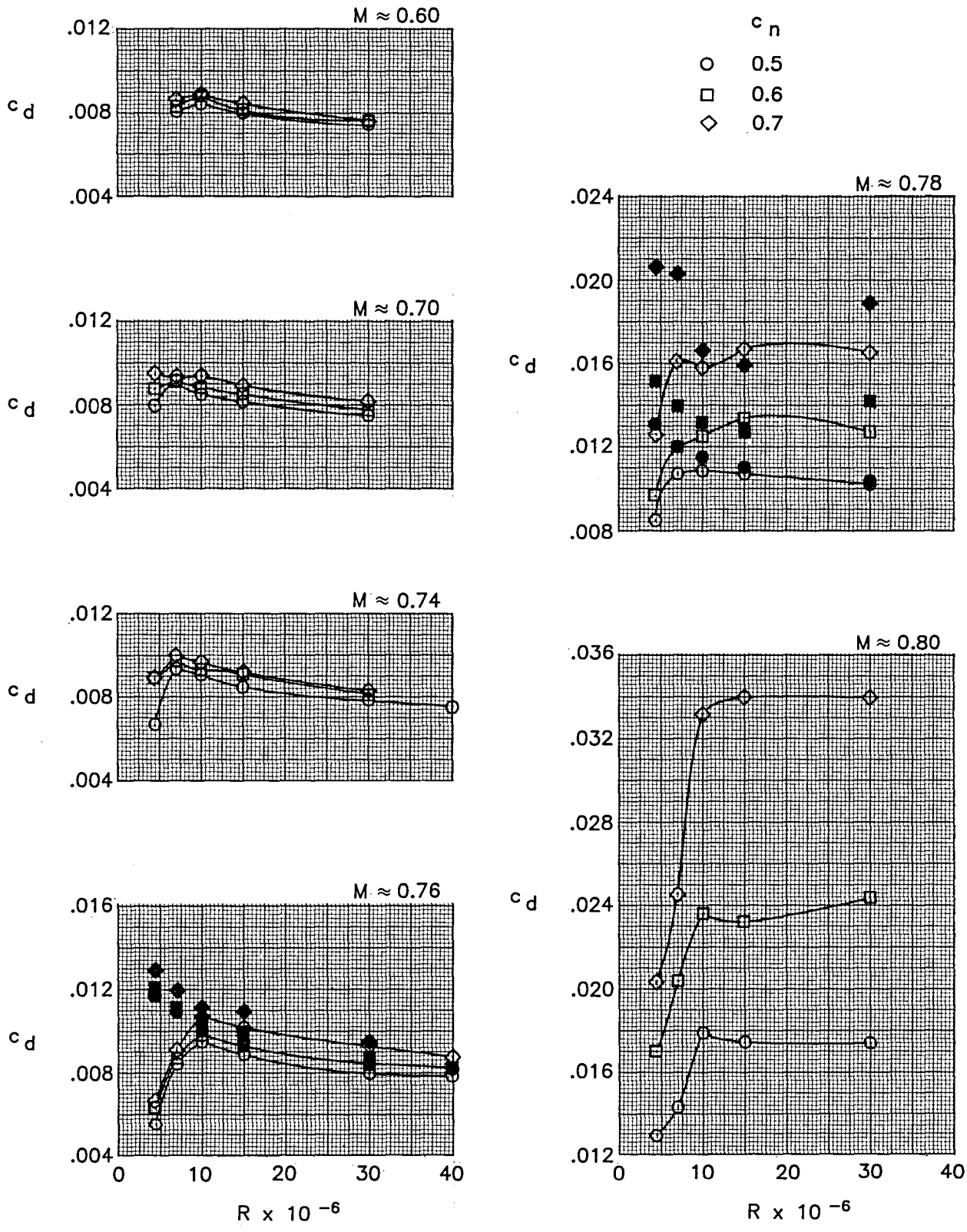

Figure 61. Effect of Mach number on variation of section drag coefficient with Reynolds number. Solid symbols indicate fixed transition.

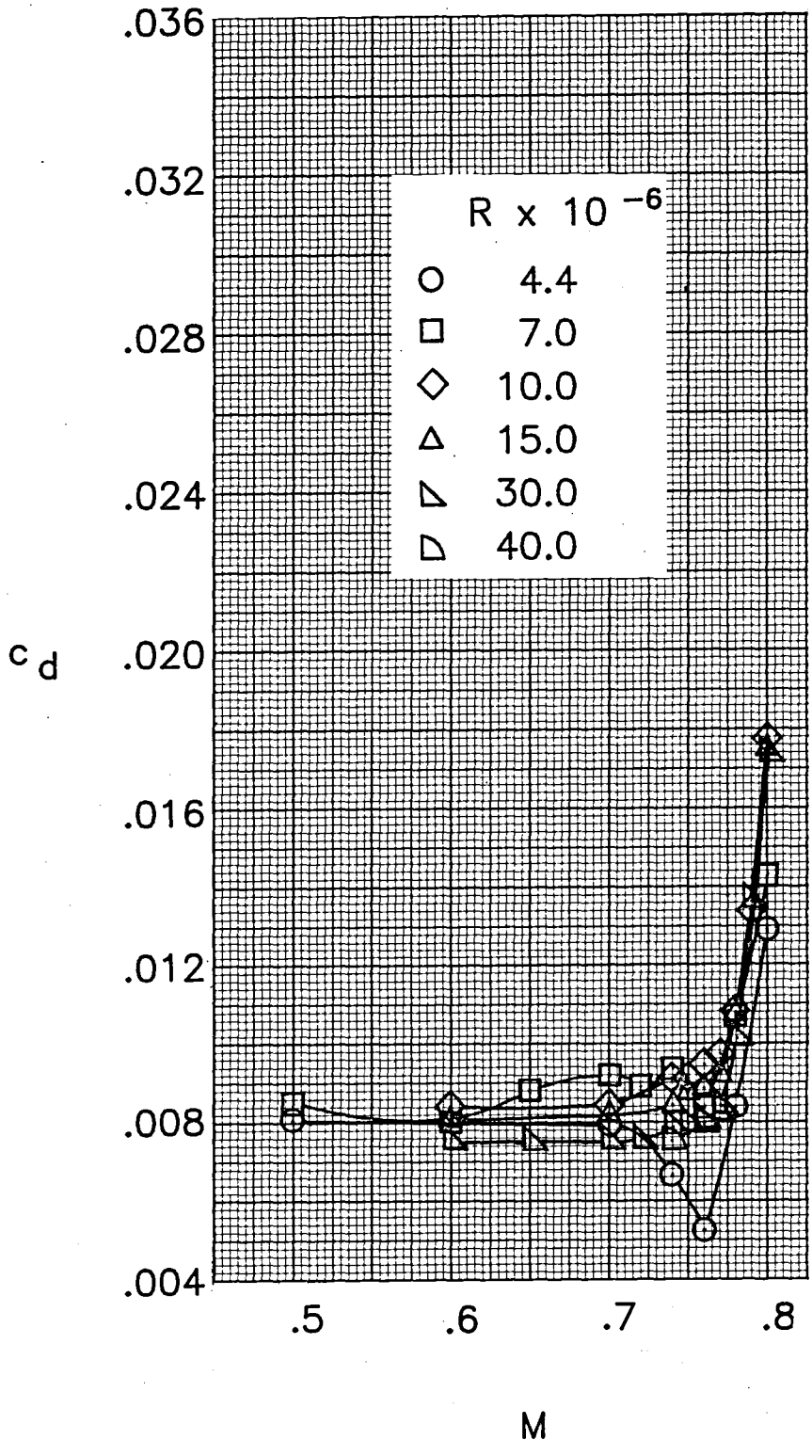

(a) $c_n = 0.5$.

Figure 62. Effect of Reynolds number on variation of section drag coefficient with Mach number. Free transition.

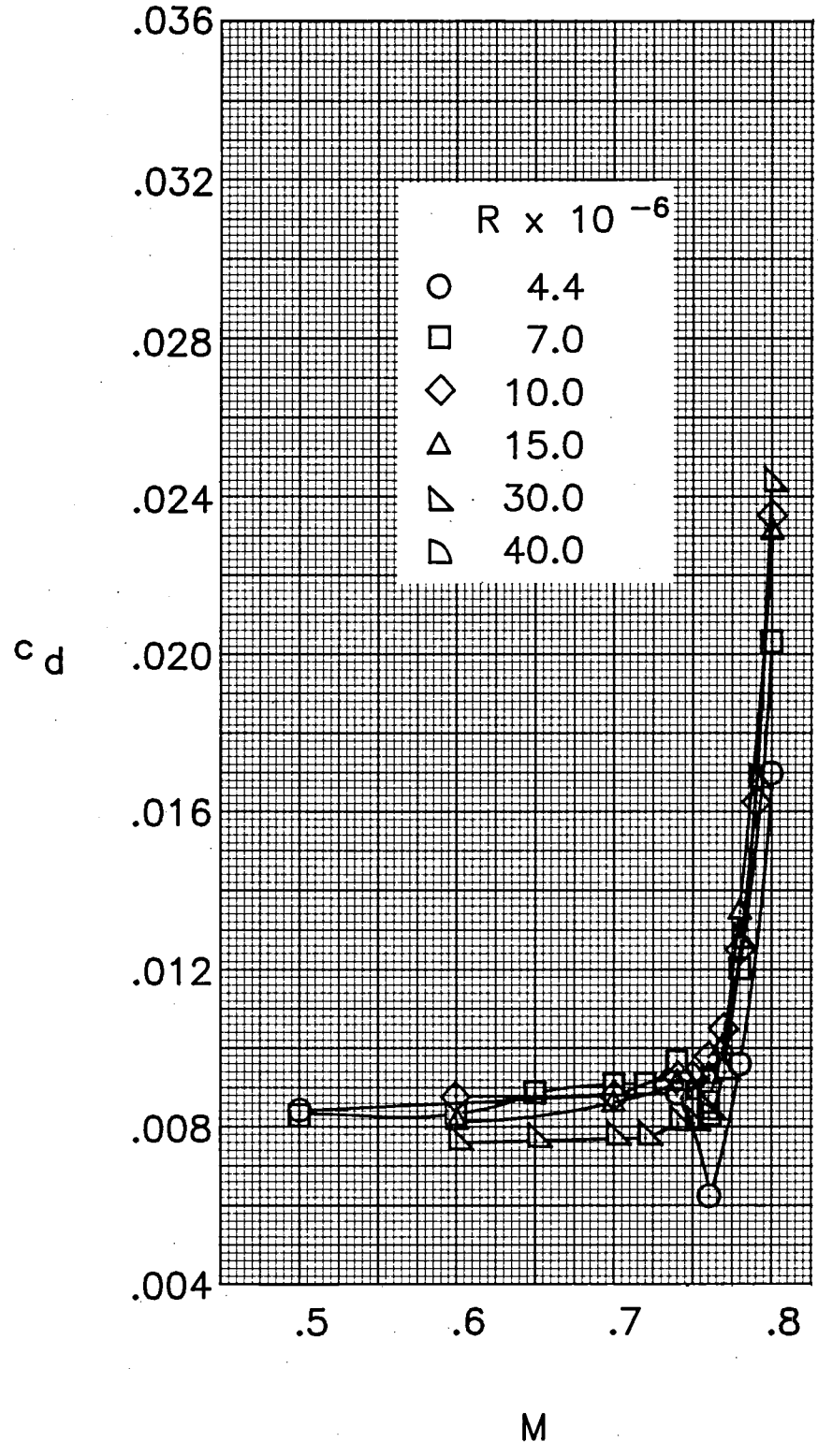

(b) $c_n = 0.6$.

Figure 62. Continued.

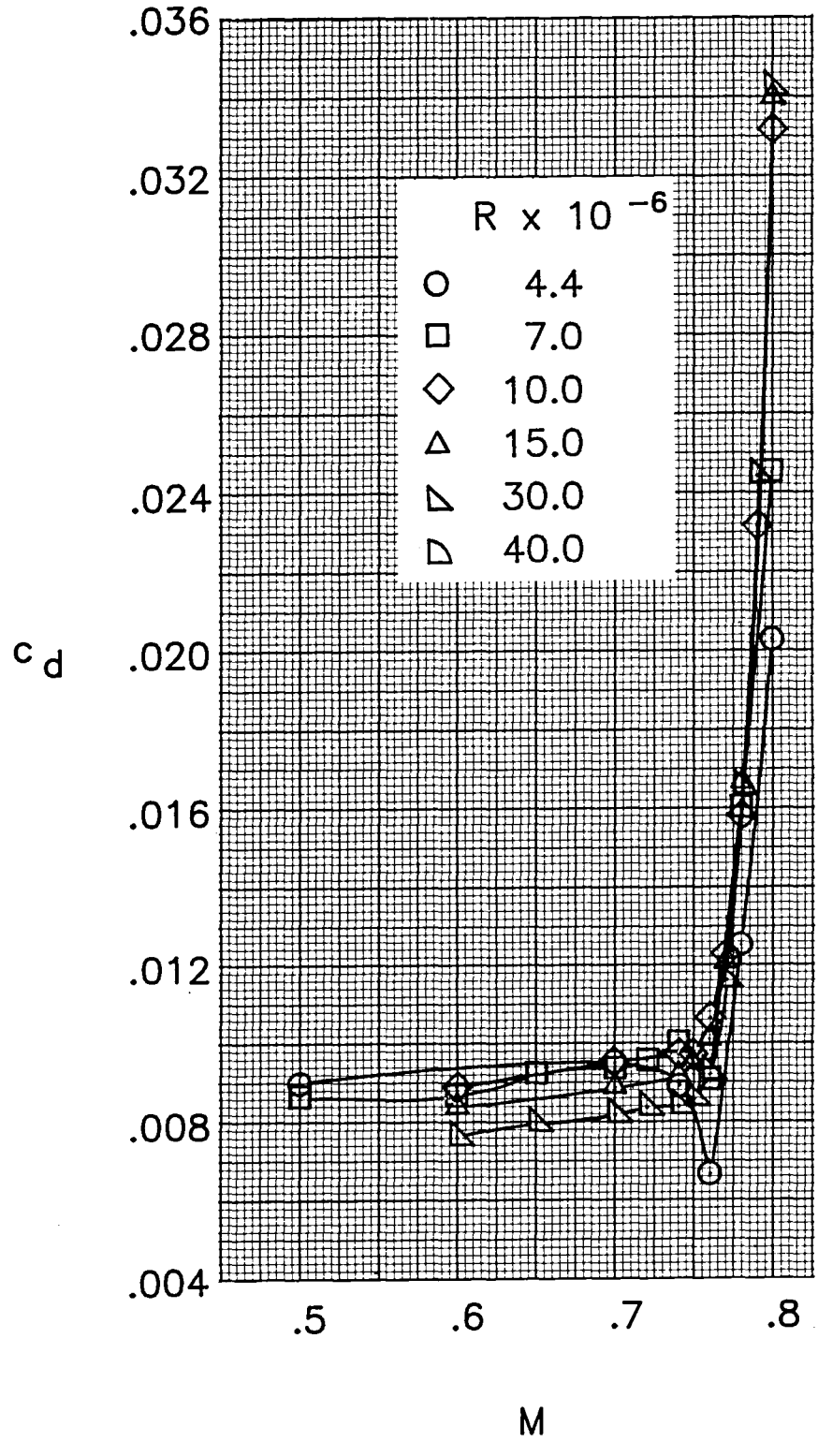

(c) $c_n = 0.7$.

Figure 62. Concluded.

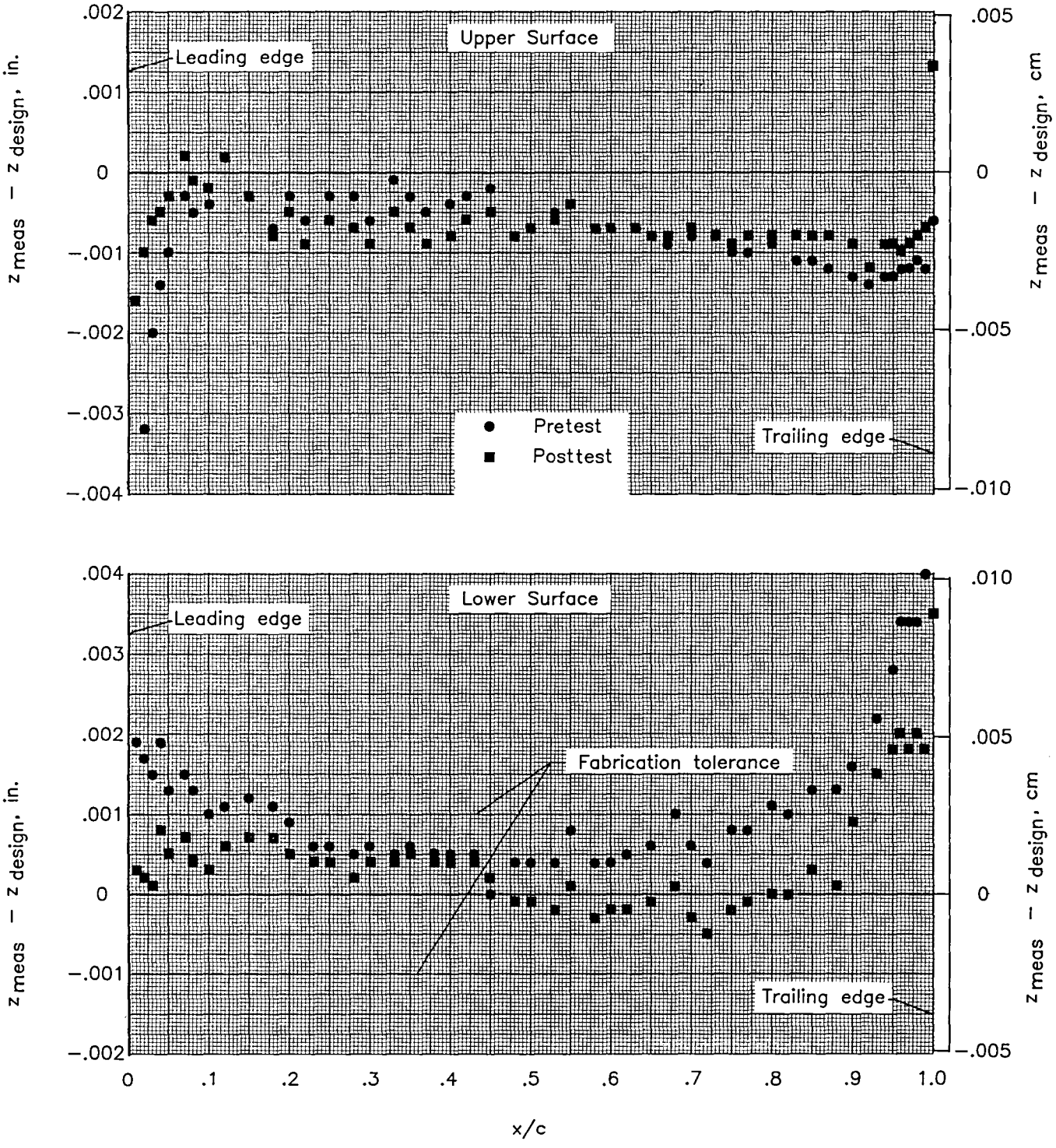

Figure 63. Pretest and posttest coordinate validations.

1. Report No.	2. Government Accession No.	3. Recipient's Catalog No.
NASA TM-86371		

4. Title and Subtitle	5. Report Date
High Reynolds Number Tests of a NASA SC(3)-0712(B) Airfoil in the Langley 0.3-Meter Transonic Cryogenic Tunnel	June 1985
	6. Performing Organization Code: 505-31-53-10
7. Author(s): William G. Johnson, Jr., Acquilla S. Hill, and Otto Eichmann	8. Performing Organization Report No.: L-15909
9. Performing Organization Name and Address: NASA Langley Research Center, Hampton, VA 23665	10. Work Unit No.
	11. Contract or Grant No.
12. Sponsoring Agency Name and Address: National Aeronautics and Space Administration, Washington, DC 20546	13. Type of Report and Period Covered: Technical Memorandum
	14. Sponsoring Agency Code

15. Supplementary Notes

16. Abstract

A wind tunnel investigation of a NASA 12-percent-thick, advanced-technology supercritical airfoil was conducted in the Langley 0.3-Meter Transonic Cryogenic Tunnel (TCT). This investigation represents another in the series of NASA/U.S. industry two-dimensional airfoil studies to be completed in the Advanced Technology Airfoil Tests program. Test temperature was varied from 220 K to 96 K at pressures ranging from 1.2 to 4.3 atm. Mach number was varied from 0.60 to 0.80. These variables provided a Reynolds number range from 4.4×10^6 to 40.0×10^6 based on a 15.24-cm (6.0-in.) airfoil chord. This investigation was designed to (1) test a NASA advanced-technology airfoil from low to flight-equivalent Reynolds numbers, (2) provide experience in cryogenic wind tunnel model design and testing techniques, and (3) demonstrate the suitability of the 0.3-m TCT as an airfoil test facility. The aerodynamic results are presented as integrated force and moment coefficients and pressure distributions. (The same pressure data are also published in plotted and tabulated formats in a separate companion report, NASA TM-86370.) Data are included which demonstrate the effects of fixed transition, Mach number, and Reynolds number on the aerodynamic characteristics. Also included are remarks on the model design, the model structural integrity, and the overall test experience.

17. Key Words (Suggested by Authors(s))	18. Distribution Statement
Supercritical airfoil Two-dimensional airfoil Cryogenic wind tunnel High Reynolds number	Unclassified—Unlimited Subject Category 02

19. Security Classif.(of this report)	20. Security Classif.(of this page)	21. No. of Pages	22. Price
Unclassified	Unclassified	167	A08

For sale by the National Technical Information Service, Springfield, Virginia 22161

NASA-Langley, 1985

End of Document